ATMOSPHERIC PARTICULATE MATTER AND HISTORIC BUILDINGS

KEITH JOHN VINCENT

A thesis submitted in partial fulfilment of the requirements of Middlesex University for the degree of Doctor of Philosophy

September 1993

Middlesex University in collaboration with the Building Research Establishment

ABSTRACT

Atmospheric particulate matter, along with gaseous and precipitation pollutants, were collected close to three historic buildings; Lincoln Cathedral, Bolsover Castle and Wells Cathedral, in order to estimate the amount of sulphur and nitrogen deposited onto each. Results obtained showed that the gaseous dry deposition of both sulphur and nitrogen was the main deposition pathway at Lincoln and Bolsover, whereas as a result of high precipitation amounts the wet deposition pathway was the most significant at Wells. At each sampling site the amount of sulphur and nitrogen deposited as dry particulate matter was relatively insignificant.

Estimated washout values for both SO_2 and SO_4^{2-}, indicated that the former provided approximately 80% of the sulphur in precipitation arriving at the building surfaces. The important role of the gas was reinforced by the significant correlation between the sulphur level in precipitation and sulphur dioxide. The concentration of sulphur in precipitation was found to decrease at high precipitation volumes, whereas the nitrogen concentration was unaffected by precipitation volume.

A high sulphate to sulphur dioxide concentration ratio during the summer months was indicative of photochemical oxidation processes. Conversely, during the winter months the relatively low sulphate to sulphur dioxide concentration ratio suggested that sulphate and sulphur dioxide were released from common sources.

Multivariate statistical techniques, comprising principal component analysis and multiple regression analysis, were used to infer characteristics about the origin of the constituent parts of the collected particulate matter. In general, three sources of material; secondarily formed particulate matter, sea-salt and crustal material, were estimated to contribute to the collected particulate matter.

CONTENTS

PAGE

SECTION TITLES

TABLES

CHAPTER 2

CHAPTER 3

CHAPTER 4

CHAPTER 5

CHAPTER 6

CHAPTER 7

FIGURES

PLATES

CHAPTER 2

CHAPTER 4

ABBREVIATIONS AND SYMBOLS

A,	Cross-sectional area
A,	Factor loading matrix
APCS,	Absolute principal component score
A_Q,	Factor loading matrix in FANTASIA
B,	Factor score coefficients
b,	Regression coefficient
$\boldsymbol{B}$,	Scaled factor loading matrix in FANTASIA
BERG,	Building Effects Review Group
c,	Concentration of ion in precipitation
C_A,	Concentration of pollutant in air
C_j,	Contribution from sampling source
COV,	Coefficient of variation
cum dep.,	Cumulative dry deposition
cum prec.,	Total rain deposition
d_{50},	Collection efficiency for cascade impactor
df,	Degrees of freedom
DDDW,	Doubled distilled deionised water
ESCA,	Electron spectroscopy for chemical analysis
δ_{ij},	Kronecker Delta
e^t,	Transpose matrix of eigenvectors
η,	Fluid viscosity
$\bar{f}$,	Mean contribution from a source
f,	Contribution from a source
f_s,	Standard deviation of mean from source
$\acute{F}$,	Interception factor
F,	Dry deposition flux
FANTASIA,	Factor analysis to apportion sources in aerosols
G,	Standardised source contribution
h,	Regression coefficient obtained in FANPART2
H,	Mixing layer height
I,	Identity Matrix
ICP-AES,	Inductively coupled plasma-atomic emission spectrometry
IR	Induction zone
IRZ	Initial radiation zone
J,	Photodissociative constant
K_H,	Henry's Law constant
k_1,	Rate constant
K,	Hydraulic permeability
L,	Liquid water content of a cloud
λ,	Eigenvalue
m,	Regression coefficient in FANPART2
M,	"Third body" involved in photochemical reaction
MR,	Multiple regression
MSE,	Error mean square
NAZ	Normal analytical zone
NMEP,	National Material Exposure Programme

LIST OF ABBREVIATIONS AND SYMBOLS (continued)

PC,	Principal components
PCA,	Principal component analysis
PORG,	Photochemical Oxidant Review Group
v_g	Deposition velocity
φ,	Photochemical state number
PHZ	Preheating zone
PMT,	Photomultiplier tube
NAPAP,	National Acid Precipitation Assessment Programme
Q,	Sum of the squared deviations
Q_Q,	Matrix of eigenvectors in FANTASIA
QUARG,	Quality of Urban Air Review Group
q_x,	Velocity of water flow in rock
r,	Correlation coefficient
r_a,	Aerodynamic resistance
r_b,	Laminar layer resistance
r_s,	Surface resistance
r_t,	Total resistance
R	Correlation matrix
R^2,	Coefficient of Determination
$\mathbb{R}$,	Rotation matrix in FANTASIA
R_i,	Rainout efficiency
RAGR.	Review Group on Acid Rain
RI,	Rain intensity
RAPCS	Regression on absolute principal component scores
ρ,	Density
ϕ,	Porosity
σ_g,	Geometric mean
s^2,	Estimated variance of regression coefficient
SSE,	Error sum of squares
S(IV),	Sulphur, oxidation state four
S(VI),	Sulphur, oxidation state six
TSP,	Total Suspended Particulate matter
u,	Concentrations of constituent parts for a collected sample
v,	Test vector matrix in FANTASIA
V_{dN},	Dry deposition for nitric acid
V_{dS},	Dry dposition for sulphur dioxide
VWM,	Volume weighted mean
W,	Weighting factor in FANTASIA
W_m,	Mass mixing ratio
W_v,	Volume mixing ratio
X,	Independent variable
y,	Dependent variable
$\hat{y}$,	Predicted dependent variable
Z,	Standardised variable

ACKNOWLEDGEMENTS

I would like to take this opportunity to thank the many people who assisted in completion of this research project.

First, I must acknowledge the encouragement and constructive criticism from Professor Ron Hamilton and Professor Mike Revitt, my research supervisors, whose guidance especially in the latter stages was invaluable.

Next, I am grateful to the Building Research Establishment and the Department of the Environment, for providing the necessary research funding (Contract Number PECD7/12/06).

Particular thanks also to colleagues and technical staff at the Urban Pollution Research Centre for providing a collaborative and dynamic atmosphere under which the work was conducted.

Finally, I must thank my wife, Sarah, for her continual support and understanding throughout the entire duration of the project.

This thesis is dedicated to my mother, Yvonne.

CHAPTER 1: INTRODUCTION

1.1 Background

This thesis describes the research work carried out between January 1989 and January 1992 at Middlesex University, within the Urban Pollution Research Centre, and in conjunction with the Building Research Establishment through the National Material Exposure Programme. The research provides an important contribution to this programme which is currently monitoring and quantifying changes in building materials placed at various sites throughout the United Kingdom. The role of the atmosphere in bringing about possible changes to building materials is evaluated in the context of meteorological data, together with gaseous pollutant and particulate matter concentrations which have been monitored throughout the sampling period.

Deterioration in the building fabric of historic buildings has increased in recent times due to the presence in the atmosphere of damaging pollutants released as a consequence of industrial activity. Methods of arresting the decline in stone surfaces can range from replacement with fresh stone blocks to cleaning by various sand or water blasting techniques. Alternatively, the actual fabric surface may be given a degree of protection using synthetic polymers. Preventative measures to reduce deterioration would involve reducing the levels of pollutants to such an extent that the stone surface would be exposed to levels that can be shown not to affect the stone surface. However, due to the complex interactions between a stone surface and the immediate environment, establishing a cause-effect response is difficult and not easily quantified. Parameters which have to be taken into consideration include stone type, presence of water, temperature and pollutant levels.

The National Material Exposure Programme (NEMP), started in 1988, and coordinated for the U.K. Department of the Environment by the Building Research Establishment, will provide insight into the stone deterioration process. Field tests using specially prepared building materials are being conducted at twenty nine sites located throughout the United Kingdom. These tests include monitoring weight loss from stone tablets placed in sheltered and unsheltered locations, measuring the ion concentration in run-off water from the surface of the historic monument and measuring the time of "wetness"

of exposed electrochemical cells. Alongside the exposed samples, gaseous pollutant and meteorological parameters are also monitored. Preliminary results have shown that the two main factors affecting stone loss are rainfall volume and sulphur dioxide concentration (Butlin *et al.*, 1992). An additional factor that may be causing stone deterioration is the presence of atmospheric particulate matter arising from sources such as combustion and wind erosion processes. The Queen's University, Belfast, has been assigned by the Building Research Establishment to elucidate possible reaction mechanisms occurring on the stone surface as a consequence of deposited particulate matter by using scanning electron microscopy to observe structural changes on the stone surface.

Parallel research into the alteration of building materials by air pollution is being conducted in the United States and Europe. In the United States, the research is coordinated by the United States National Acid Precipitation Assessment Programme. In Europe, a significant proportion of the current work is conducted under the auspices of the European Communities' Environment Programme, part of which specifically investigates the relationship between environmental factors and damage to cultural property. The results from this on-going research are published in a newsletter: *European Cultural Heritage.*

The study presented here is primarily concerned with the composition, including sulphur and nitrogen components, of atmospheric particulate matter and estimating the amounts depositing on the stone surface. These sulphur and nitrogen deposition rates will be compared to the amounts of each element depositing both in the gaseous dry form and in the incident precipitation. Interaction between each of the depositing pathways will also be assessed. This particulate matter may originate from a variety of different sources. For example, the oxides of sulphur and nitrogen released into the air from combustion processes will form particulate matter that may have an acidic component and may consequently react with the limestone. Other components of atmospheric particulate matter such as transition metals, arising from naturally occurring or anthropogenic sources have been shown to increase the rate of oxidation of sulphur dioxide to sulphate, and thus may also be involved in the deterioration process.

Previous work carried out at Middlesex University has investigated the role of the

carbon component of the atmospheric particulate matter on the rate of soiling of building materials. Future work will measure the deposition flux of the carbon component of particulate matter directly on to the surface of historic buildings using scanning electron microscopy and automated particle analysis.

1.2 Aims and objectives

The main aim of this project is to provide quantitative information on the deposition flux of sulphur and nitrogen, in particulate form, on to historic buildings and to compare this with the relative magnitudes of sulphur and nitrogen deposition in gaseous and wet forms. Additionally, the contribution of particulate matter from postulated sources is estimated using receptor modelling techniques.

In order to calculate each deposition flux the following procedures were followed:

- Atmospheric particulate matter was collected using a high volume sampler at three of the NEMP sampling sites; Lincoln Cathedral, Bolsover Castle and Wells Cathedral. Sulphate and nitrate ions were subsequently extracted from the filter papers and their respective mass concentration determined. The deposition fluxes were determined by multiplying the mass concentrations by the appropriate deposition velocity, v_g.
- Gaseous fluxes were determined a similar manner. The sulphur dioxide concentrations were determined on a daily basis by collection in hydrogen peroxide and analysis of the resulting sulphate concentration using ion chromatography. The nitrogen dioxide concentrations were determined by using diffusion tubes followed by spectrophotometric analysis. The nitrogen dioxide concentrations were determined weekly.
- Wet deposition was determined as a weighted product of ion concentration and precipitation amount. The precipitation was collected using a "wet-only" sampler, whose sampling inlet was open only during a precipitation event.

The elemental particulate masses originating from the various sources were calculated using a combination of two statistical methods; principal component analysis and multiple regression analysis. Three different combinations of the methods were employed:

- Selection of independent variables using principal component analysis followed by a multi-regression analysis.
- Regression on absolute principal component scores.
- Use of a designated source apportionment software package, FANTASIA.

The source-receptor methodology has the potential to be developed as a pollution control mechanism since once a source is identified to be contributing to collected particulate matter, alleviation measures can be enforced.

1.3 Outline of thesis

Following this introductory section, Chapter 2 describes how the effects of air pollution on buildings and building materials have been assessed. Methods employed to analyse effects of air pollution on stone surfaces are also described. The chemical and physical processes which control the concentrations of sulphur and nitrogen in the atmosphere from point of release to site of deposition are discussed in Chapter 3. The sampling and analytical methods employed in the study are described in Chapter 4. Sampling has involved the collection of atmospheric particulate matter using a high volume sampler. The collected samples were analysed for the major soluble ions and a range of metals. A brief survey of the receptor models used in the literature to calculate the mass contribution from various sources is presented in Chapter 5. The theoretical basis to the three receptor models used in this thesis is also presented in this chapter.

Chapter 6 presents the results of the monitoring programme at each of the sites. The deposition rates of sulphur and nitrogen in their various forms on to the building surface and interactions between the phases are also presented in Chapter 6. The results of the three source-receptor modelling techniques are described in Chapter 7. Source contributions of particulate matter are calculated for each of the three methods with percentage contributions of elements and ions originating from each source given for two of the three methods. Concluding remarks relating to the results obtained and recommendations to alleviate the effect of air pollutants on building surfaces are presented in Chapter 8.

CHAPTER 2: WEATHERING OF BUILDING MATERIALS

2.1 Introduction

Buildings and building materials are continually exposed to weathering elements such as frost, wind and precipitation which, depending on the stone type, cause various degrees of deterioration. In addition, anthropogenic material released into the atmosphere has been shown to cause an increase in the rate of deterioration of the stone quality. This chapter will present the evidence available from the literature confirming and quantifying the role of anthropogenic materials in this process. The building material of interest in this study is mainly calcareous building stone which has been used for centuries due to its durability, availability and aesthetic quality. To provide insight into how stones are altered, the physical and chemical properties of the stones are initially discussed.

2.2 Physical properties of building stones

Building stone sources can be classified as a function of their formation mechanism into three main divisions:

a) Igneous rocks

b) Sedimentary rocks

c) Metamorphic rocks

Igneous rocks are formed by the cooling and consequent solidification of molten material. The extent of crystallisation is dependent on the cooling time. Granite is an example of an igneous rock. Sedimentary rocks are formed from the disintegration of igneous rocks or pre-existing sediments which are consequently compounded by pressure. Sandstone and limestone are examples of sedimentary rocks. Sandstones are composed of the more resistant constituents of the igneous rocks. The weathering quality is determined by the chemical stability and cementing properties of the cement that binds the quartz grains. Limestones consist of calcium carbonate deposited either through evaporation of water from a calcium carbonate solution or from the skeletal tissue of dead sea animals. Metamorphic rocks are formed from either igneous rocks or sedimentary rocks by the addition of pressure and/or heat. Limestones are converted

into marbles, sandstones into quartzite, clays into slates and igneous rocks into gneisses. Slates and marbles are the metamorphic rocks commonly used as building stones.

The actual stone chosen as a building material will depend on a number of factors, such as cost, durability, aesthetic requirements and stone availability. Limestone and sandstones are perhaps the most popular natural building stone materials. This thesis will be primarily concerned with these stone types.

2.2.1 Aggregation properties

Building stones are polycrystalline mineral aggregates. The range in the intergranular bonding and pore shapes are in turn responsible for the differing densities, porosities and permeabilities in stone. Porosity and permeability are probably the most important physical properties of rocks employed in studies of decay and corrosion of building materials). This is because they control the accessibility of water to the interior of the stones. Porosity, ϕ, can be defined technically as the ratio of internal pore volume to bulk volume (Tombach, 1982). The porosity of igneous and metamorphic rocks is low, usually less than 5 percent. Typical values for limestone range from 0.3 to 30%. Stones with low porosities are much more resistant to weathering.

The porosity of a stone can be estimated using the densities, ρ_G and ρ_B:

$$\phi\ (\%) = \frac{(\rho_G - \rho_B)}{\rho_G} \times 100 \quad \text{Equation 2.1}$$

where: ρ_G, is the density of the component grains of the stone.
ρ_B, is the density of the bulk stone.

The total porosity and microporosity values for a range of British limestones are presented in Table 2.1 (Schaffer, 1932), where total porosity was estimated by measuring the volume of water absorbed by each stone type. Microporosity was estimated by subtracting from total porosity, the estimated percentage pore volume corresponding to pores with a diameter greater than 0.005 mm.

Table 2.1 Total and microporosity of limestones (Schaffer, 1932)

Limestone	Total Porosity % by volume	Microporosity % by volume
Portland (Whitbed) Portland (Basebed)	20.5 21.5	8.2 10.1
Clipsham	14.7	12.6
Headington (soft)	37.8	16.4
Box Ground	33.0	17.5
Combe Down	30.4	18.0
Beer	26.0	19.7
Monk's Park	22.5	21.8
Hartham Park	23.4	22.9
Stoke Ground	25.2	24.4
Corsham Down	28.4	26.1
Farleigh Down	32.2	29.5

Portland limestone can be seen to have the lowest microporosity and was chosen as the building stone for St. Paul's Cathedral.

Permeability is the ease with which a fluid will flow through a rock and is defined empirically by Darcy's law (Goodman, 1989):

$$q_x = -\frac{K}{\eta}\frac{dp}{dx}A \quad \text{. . . . . Equation 2.2}$$

Where: q_x is the flow rater of water in the x direction ($m^3\ s^{-1}$)
η is the fluids' viscosity (the viscosity of water is 1.005×10^{-3} N m^{-2} s)
K is the hydraulic permeability (m^2)
dp/dx, the pressure gradient (N m^{-3})
A is the cross-sectional area normal to x (m^2)

Permeability can be determined in the laboratory by measuring the time for a calibrated volume of fluid to pass through a rock specimen when a constant pressure acts over the surface of the fluid (Goodman, 1989). The common unit of measurement for permeability is the Darcy, where one Darcy corresponds to 9.86×10^{-9} cm^2.

2.2.2 Thermal properties

Stone will expand when heated and the consequent thermal gradients will cause stresses. Expansion will also occur when the stone absorbs water; however, there is no evidence to show that the decay of stone is attributed to moisture absorption only (Schaffer, 1932). Heating rock to high temperatures can result in an irreversible reduction of the elastic modulus due to the differential expansion of the grains.

2.3 Weathering Mechanisms

The weathering processes that occur in stone are attributed to physical, chemical and biological processes. A classification of mechanisms contributing to stone decay has been summarised by Tombach (1982) and is presented in Table 2.2. The five main generic classifications are:

a) External abrasion
b) Volume change of stone
c) Volume change of material in capillaries and interstices
d) Dissolution of stone or change in chemical form
e) Biological activity

Also presented in Table 2.2 are the atmospheric inputs that control the alteration processes. Rainfall and temperature can be seen to be the most frequent parameters controlling decay mechanisms. Gaseous pollutants and aerosols contribute to the alteration of the stone as a consequence of initiating chemical changes (see Section 2.4).

The crystallisation of salts on a stone surface is known as efflorescence and within the individual pores as cryptoflorescence. The salts are mainly the sulphate salts of potassium, sodium and calcium. Sources of soluble salts include; salts originally present in the material before incorporation into the building, salts derived from the decomposition of stone fabric and those from external sources, such as jointing materials, soil and the atmosphere. The growing salt crystal, formed as water evaporates from the stone surface, will exert pressure in the confined space of the pore.

Table 2.2 Classification of mechanisms relating to stone decay. (Tombach, 1982)

Mechanism	Rainfall	Fog	Humidity	Temperature	Solar Insolation	Wind	Gaseous Pollutants	Aerosol
External Abrasion								
Erosion by wind-borne particles						●		●
Erosion by rainfall	●							
Erosion by surface ice	●	●		●				
Volume change of stone								
Differential expansion of mineral grains				●			○	
Differential bulk expansion due to uneven heating				●	●			
Differential bulk expansion due to uneven moisture content	●	●	●	●	●	○	○	○
Differential expansion of differing materials at joints				●				
Volume change of material in capillaries and interstices								
Freezing of water	●	●		●				
Expansion of water when heated by the sun	●	●		●	●			
Trapping of water under pressure when surface freezes	●	●		●				
Swelling of water-imbibing minerals by osmotic pressure	●	●	●				○	○

Table 2.2 Classification of mechanisms relating to stone decay (continued).

Mechanism	Rainfall	Fog	Humidity	Temperature	Solar Insolation	Wind	Gaseous Pollutants	Aerosol
Hydration of effloresences, internal impurities and stone constituents	●		●				○	○
Crystallisation of salts			●	●	●	●	○	○
Oxidation of materials into more voluminous forms	●	●					○	
Dissolution of stone or change of chemical form								
Dissolution in rainwater	●			●			●	●
Dissolution by acids formed on stone by atmospheric gases or particles and water	●	●	●	●			●	●
Reaction of stone with SO_2 to form water soluble material	●	●		●			●	
Reaction of stone with acidic clay aerosol materials	●	●		●				●
Biological activity								
Chemical attack by chelating, nitrifying, sulphur reducing, or sulphur-oxidising material.			●	●			●	
Erosion by symbiotic assemblages and higher plants that penetrate stone or produce damaging excretions	○	○	●	●	●			

Note: Solid circles indicate principal atmospheric factors; open circles denote secondary factors

In addition, the salt can cause damage due to the increase in volume that occurs when the anhydrous salt becomes hydrated. For example, anhydrous sodium sulphate has a specific gravity of 2.66 g cm^{-3}, whereas a hydrated form of the salt, $Na_2SO_4.10H_2O$ has a specific gravity of 1.49 g cm^{-3}.

2.4 Deterioration in Polluted Atmospheres

Time-lapse photography and comparison of recession rates of similar stones such as tombstones located in urban and rural areas indicate that air pollution is responsible for deterioration. An example of time-lapse photography illustrating the deterioration of stone can be found in the British Museum where a set of photographs compare the West Frieze of the Parthenon, Athens, in 1938 with a plaster cast reproduction made by Lord Elgin in 1802. Although the monument dates from 447-432 B.C. the amount of damage from this time to 1802 compared to that between 1802 to 1938 is insignificant. The effect of the increasingly contaminated Athens environment since 1802 is further implicated in causing stone decay when the stones still present on the West front are compared to the those of the North Front, brought to the British Museum in 1802, by Lord Elgin. These stones, kept in a dry atmospheric environment, are preserved in a relatively good condition.

2.4.1 Structure of a Stone Surface Affected by Air Pollution

The form of deterioration that building materials suffer as a result of being exposed to a polluted atmosphere may be manifested as:

- recession of original stone surface
- chemical and physical change in the stone surface resulting in the formation of crustal material.
- a temporary reduction in the aesthetic quality of the stone due to accumulation of dust

2.4.1.1 Stone surface recession

The loss of material from a stone surface can lead to significant change in the appearance of the stone. Surface recession can be calculated by measuring the height

difference between the present surface and a marking device, such as a lead plug that records the original level of the stone (lead plugs are used to fill-in the aligning holes, required during the construction of a large building). Sharp *et al.* (1982) have calculated from the lead plugs at St. Paul's, which are 8-20mm above the present surface of the balustrade, that average recession rates range from 0.066 to 0.081 mm a^{-1}. This was assuming even deterioration rates throughout the 262 years the lead plugs were in position. An example of the erosion that has occurred to the Portland limestone stone surface at St. Paul's Cathedral is illustrated in Plate 2.1.

The location of stones on a building has been shown to be important in controlling the amount of deterioration that may occur. For example, Leysen *et al.* (1989) measured the leachable sulphate content of sixty samples collected from twenty two different wall sections at St. Rombout's Cathedral, Mechelen, Belgium. Each sample was collected in two portions; as a surface layer (Layer A) and as the loose material below it (Layer B). The samples that were collected from south-west facing walls were shown to accumulate most sulphate (Table 2.3) and hence these surfaces are likely to suffer a higher degree of deterioration. North facing walls, on average, contained lesser amounts of leachable sulphate. This may be due to an increased amount of incident rainfall coming from the northerly direction resulting in rapid removal of sulphur products. Trudgill *et al.* (1991) using a micro-erosion meter found that stone surfaces orientated to the south-west, at St. Paul's Cathedral, London, suffered the highest amount of recession.

Table 2.3 Leachable Content of Surface Layer A and underlying Layer B at St Rombout's Cathedral

Orientation	Leachable Sulphate Content (g 100 g^{-1} crushed stone)					
	Maximum		Minimum		Average	
	A	B	A	B	A	B
South	15.2	10.6	1.1	2.2	9.6	5.7
South-east	17.2	6.2	1.1	3.2	8.6	4.8
East	24.2	8.3	1.0	8.3	12.1	8.3
North-east	17.4	--	13.3	--	15.1	--
North	17.6	6.0	1.3	5.0	7.3	5.5
North-west	15.9	6.3	1.5	3.0	9.5	4.7
West	19.6	6.7	2.8	6.7	10.5	6.7
South-west	25.1	11.2	17.0	11.2	19.9	11.2

A represents the sulphate extracted from the surface layer
B represents the sulphate extracted from the sub surface layer (Source: Leysen *et al.*, 1989).

The recession rates of similar stones in polluted and non-polluted areas are presented in Table 2.4. The recession rates can be seen to be generally higher in the urban areas. Comparison of the results obtained from a study between 1981 and 1983 (Jaynes and Cook, 1987) with an earlier study (1955 to 1965) employing a similar methodology (Honeyborne and Price, 1977) suggests that the recession rates have decreased with time. For example, Jaynes and Cooke (1987) determined recession rates of 16 μm a^{-1} for Portland stone samples at an urban (central London) site and 10.3 μm a^{-1} at the three rural sites used in their study. The rates determined by Honeyborne and Price (1977) were higher at a Central London site (29 μm a^{-1}) and slightly lower at the comparable rural site at Garston (10.0 μm a^{-1}). The temporal decrease in recession rate at the urban site is attributed to reduction in ambient sulphur dioxide concentrations over this time period. Typical winter concentrations, expressed as annual mean values, at London and Garston were 275 and 41 μg m^{-3} respectively in 1960. Corresponding summer mean values were 132 and 13 μg m^{-3} respectively (BERG, 1989). By the 1980's there were disproportionate decreases in sulphur dioxide concentrations measured in central London. For example, the annual winter mean for 1983 was 77 μg m^{-3}, whereas, at Garston the concentrations of sulphur dioxide have remained more or less constant over the last thirty years.

Table 2.4 Spatial association between pollution levels and stone deterioration

Stone Type	Recession Rate/ Chemical change	Pollution Level in urban and rural areas	Author
Portland Limestone	2.6 × higher at urban location compared to rural. Measured as weight loss	SO_2 5 × higher at urban location compared to rural.	Honeyborne and Price (1977)
Portland Limestone Monk's Park Limestone	1.5 × higher at urban compared to rural Measured as weight loss 1.6 × higher at urban compared to rural Measured as weight loss		Jaynes and Cooke (1987)
Marble	Determined by measuring width difference of tombstone at top and bottom Rural 0.5 mm $(100\ a)^{-1}$ Urban 3.4 mm $(100\ a)^{-1}$	1.5 ppm SO_2 1956 0.2 ppm SO_2 1980 Peak levels have stayed constant due to inversions in Delaware Valley	Feddema and Meierding (1987)
Limestone	Sulphate content of 0.25 mm layer of limestone exposed for four years briquette: rural 2500 ppm suburban 11600 ppm urban 23000 ppm	SO_2 concentration 4 year range: rural 2.2-2.7 ppb suburban 2.7-3.7 ppb urban 8.6-13.7 ppb	McGee and Mossotti (1992)

2.4.1.2 Crustal material

The nature of this alteration will depend on the type of stone and its orientation with respect to the rest of the building. Camuffo *et al.* (1982) have classified the observed crustal into two groupings:

a) Black Crusts. These are situated in sheltered areas, which though not in direct contact with incident rain, do become moistened by water splashing and rebounding from other surfaces. The reaction products that may form on the surface are not removed.

b) White Crusts. These surfaces are situated in areas where rain can wash the deterioration products from the surface. The stone surface will appear white due to the presence of recrystallised calcite. This layer can range in thickness from several microns to several millimetres.

Plate 2.2 illustrates the presence of each type of crust on the stone work of Lincoln Cathedral. The black crust can be seen to be accumulating where the stone surface is protected by over-hanging masonry. Where the masonry is damaged, the water that passes over the surface can be seen to be producing a white crust.

Fassina (1976) has described two types of black crust morphology; the first having a very uniform thickness with a smooth, compact plume surface and the second having a rough and spongy appearance. A sample of this second type of black crusts, collected from St. Paul's Cathedral, London is illustrated in Plate 2.3.

The carbon, sulphate and chloride compositions of black crusts, determined by Fassina (1976), at two locations in Venice are presented in Table 2.5. The carbon composition (expressed as percentage ignition loss; % I.L.) was determined by loss on ignition at 800°C and the sulphate concentration was determined by nephelometric determination with barium chloride. The carbon will have arisen from fuel combustion. The presence of sulphate is due to the reaction of sulphur dioxide with the stone. The gypsum crystals within the black crusts were observed to have an acicular structure and a fibrous radial texture with the growth axis directed normal to the surface. Minor quantities of quartz

Table 2.5 Composition of black crusts in various locations in Venice (Fassina 1976)

Statue or Monument	Thickness of Crust	%I.L.	SO_4^{2-} (%)	Cl^- (%)
Papadopoli Palace Underneath guttering	1 mm	24.5	21.7	0.2
Rialto Bridge Underneath guttering	3 mm	24.9	16.4	0.2

and K and Na feldspars derived from soil dust were also found.

Fassina (1976) also examined the fly-ash particles contained within the black crusts by dissolving each collected sample in 10 M hydrochloric acid and separating them by gravimetric separation. The fly-ash was observed to be classified into two morphological groups:

a) Spherical shape with irregular rough surfaces, high porosity and irregular pore distribution. This type of particle could have originated from a coal burning furnace.

b) Spherical shape and a smooth surface even at high magnification. This type of particle would have originated from an oil burning furnace, in which the fuel has been converted into fine droplets before being introduced to the furnace.

An example of a flyash particle collected from St Paul's Cathedral, London, is illustrated in Plate 2.4. The porous, spherical appearance is indicative of an oil burning source. Due to the high abundance of sulphur, as measured by X-ray emission analysis, the white objects in the electron micrograph were identified as gypsum crystals. The role of fly-ash in the deterioration process will be discussed in Section 2.4.2.4.

2.4.2 Reported studies investigating the interaction between air pollutants and building materials

The determination of a reaction scheme to relate deterioration rates to levels of atmospheric pollution is difficult. This is due to the wide range of variables, such as time of wetness of the stone surface, concentration of gases and durability of the stone, which participate in the reaction system. Sulphur dioxide was first suspected by Angus Smith in 1872 to be causing an increase in the deterioration of limestone (Smith, 1872). Weathering products are expected to form on the stone due to a chemical reaction

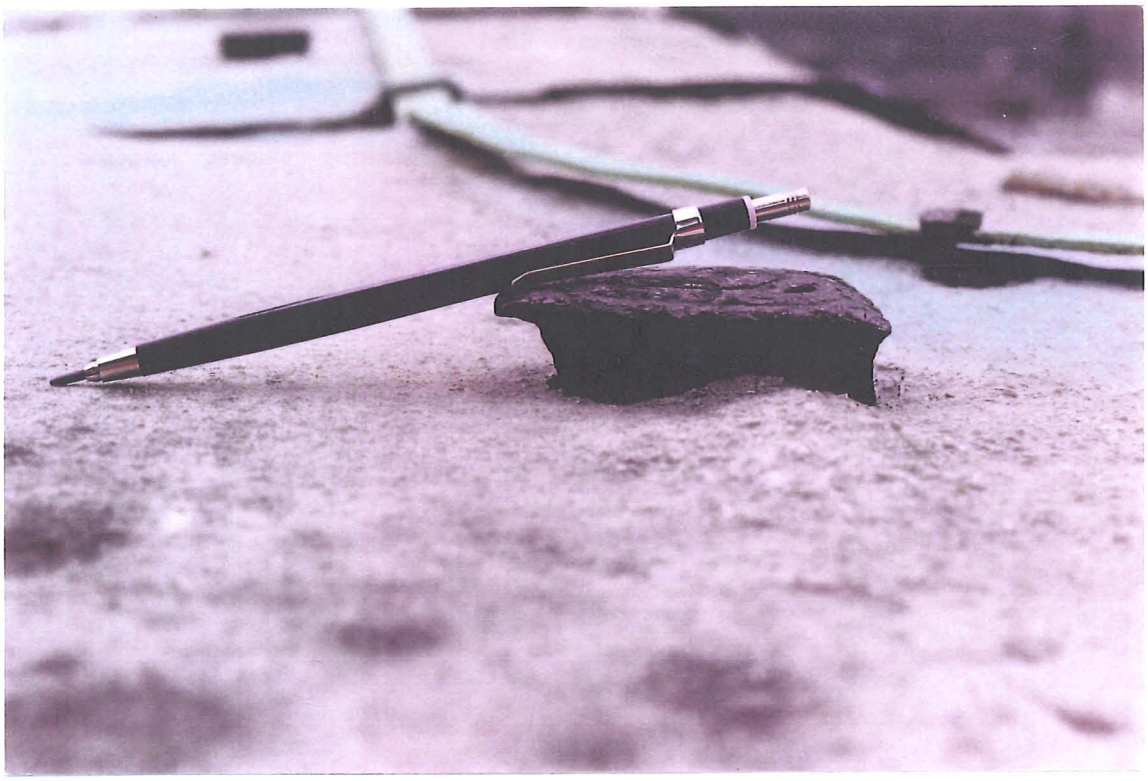

Plate 2.1 Photograph illustrating the surface recession at St. Paul's Cathedral, London

Plate 2.2 Photograph Showing Black and White Crusts at Lincoln Cathedral.

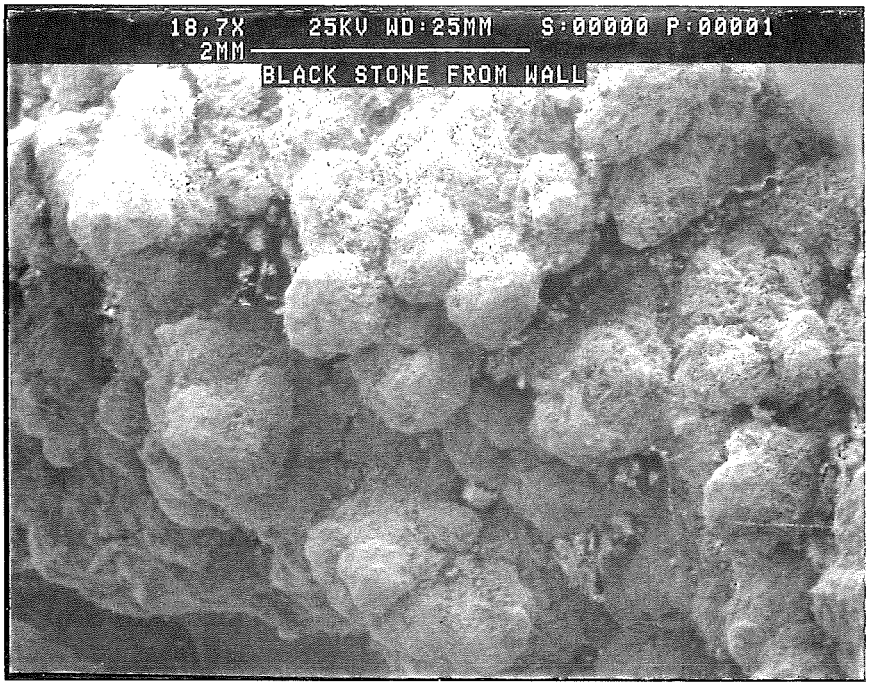

Plate 2.3 Electron micrograph showing the spongy appearance of black crust material collected from St. Paul's Cathedral, London.

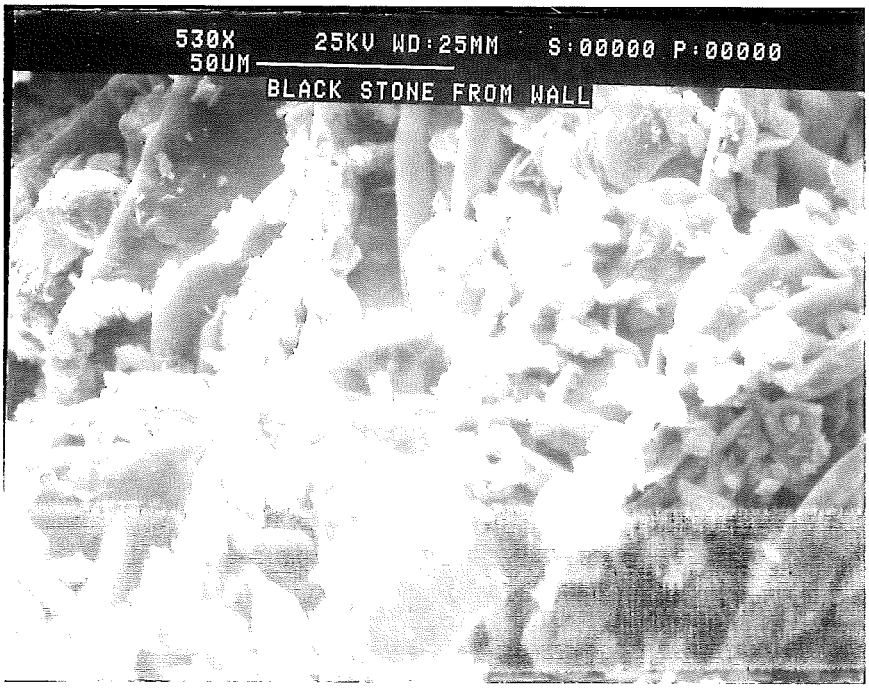

Plate 2.4 Flyash particle (upper centre of micrograph) collected from St. Paul's Cathedral, London.

between appropriate components of the building stone and certain constituents of the surrounding environment.

Gauri and Holdren (1981) suggested that sulphur compounds may react with calcium carbonate in one of two ways as illustrated by Equation 2.3 and either Equation 2.4 or Equation 2.5:

$$CaCO_3 + SO_4^{2-} + 2H^+ + H_2O \rightarrow CaSO_4.2H_2O + CO_2$$

. . . .Equation 2.3

$$CaCO_3 + SO_2 + \tfrac{1}{2}H_2O \rightarrow CaSO_3.\tfrac{1}{2}H_2O + CO_2$$

$$\downarrow \tfrac{1}{2}O_2 + 1\tfrac{1}{2}H_2O$$

$$CaSO_4.2H_2O$$

. . . .Equation 2.4

or

$$CaCO_3 + SO_2 + 2H_2O \rightarrow CaSO_3.2H_2O + CO_2$$

$$\downarrow \tfrac{1}{2}O_2$$

$$CaSO_4.2H_2O$$

. . . .Equation 2.5

Kozlowski *et al.* (1992) showed, under controlled laboratory conditions, that calcium sulphite hemihydrate is the intermediate species in the oxidation of calcium carbonate to gypsum (Equation 2.4).

A final stage in the deterioration will be dissolution of the gypsum that may have formed:

$$CaSO_4.2H_2O \rightarrow Ca^{2+} + SO_4^{2-} + 2H_2O$$

. . . .Equation 2.6

The experimental elucidation of a reaction mechanism will consider many more variables than those given in the reaction schemes shown above. This may involve

collection of water that has passed over a stone surface, analysis of air pollutants and measurement of the wetness time of stone. Studies conducted both *in situ* and under controlled laboratory conditions are discussed in the following sections.

2.4.2.1 *In situ* investigation

Investigation of rain water that has flowed over the surface of building stone will provide information regarding components preferentially removed from the stone matrix and reaction products that may have been formed. In addition, comparison between the composition of the runoff and rain water will allow an estimate of the annual material loss and the surface recession rate (Baedecker *et al.*, 1992).

Methods of collecting water that passes over stone surfaces include:

a) the construction of microcatchments (O'Brien *et al.*, 1992).

b) collecting the runoff directly from the surface of the historic building (Leysen *et al.*, 1987).

c) collecting from large stone tablets (Baedecker *et al.*, 1992).

The microcatchment approach involves placing a standardised stone sample (dimensions 25 cm × 25 cm) on a thermally insulated plinth, alongside a similarly configured ground glass control. Stone loss was determined by analysing the concentration of calcium and particulate matter in the collected runoff and hence estimating the stone loss rate (g m^{-2} $year^{-1}$). The microcatchments also employed an ion exchange resin to remove the Ca^{2+} ions from the bulk runoff. This had the advantage of reducing the volume of material required for analysis, since the cations were extracted from a relatively large volume of solvent and subsequently stripped from the ion exchange column in a laboratory using a small volume of eluent.

The amounts of calcium loss from experiments carried out in Copenhagen, Antwerp, Dublin and Manchester (for exposure times of three to four months) were: 1.8, 4.0, 5.3 and 11.6 g m^{-2} $year^{-1}$, respectively, indicating that the Manchester atmosphere is particularly abrasive to the stone tablets. However, O'Brien *et al.* (1992) have not presented environmental data such as precipitation volumes or gaseous pollutant

concentrations which are necessary in order to estimate a causal response.

Leysen *et al.* (1987) characterised the runoff from St. Rombout's Cathedral, Mechelen, by collecting four types of sample:

a) Runoff water.

A horizontal cylinder (diameter 12 cm) with a 3 cm slot was placed tightly against the cathedral wall in order to collect the runoff water. The collection surface was 50 cm (the length of the cylinder) and the cylinder drained the water into a collecting receptacle (illustrated in Plate 2.5).

b) Total deposition.

Collected by a funnel which was drained into a collecting cylinder.

c) Wet and dry deposition.

Measured using an automatic sampler designed to collect dust during dry only periods and wet deposition during wet only periods.

d) Dry loss.

Measured during dry periods, when the surface was washed regularly with demineralized water.

Analysis of the runoff samples showed enrichment of sulphate compared to rainwater, indicating again that gypsum is an important weathering product and deterioration is caused by sulphur-containing air pollutants. The presence of relatively low concentrations of chloride and nitrate in the runoff indicated that gypsum was the main product of deterioration.

Rainwater was postulated by Leysen *et al.* (1989) to be acting as an eroding agent rather than a corroding agent due to the fact that the pH of rainwater and total deposition was more alkaline at the St. Rombout's site compared to the pH of rain water and total deposition collected at a more rural site at St. Katelijine-Waver. This was attributed to a calcium carbonate "cloud" existing around the cathedral which reduced the acidity of the rainwater.

Analysis of the particles contained within the runoff samples showed that calcium was the most abundant species. A cluster analysis was also performed by Leysen *et al.*

Plate 2.5 An example of collection cylinder used to collected runoff at St. Rombout's Cathedral.

(1989) on the elemental concentrations to assess relationships between the elements leaving the stone surface. In some of the collected samples, Ca was found in association with Si, Fe, and Al. The Ca and Si association could be explained by conglomeration of $CaCO_3$ with soil dust or SiO_2 particles. The SiO_2 can be considered as a leaching product from that part of the stone which contained fine dentrital quartz grains. Calcium was also found in association with relatively minor groups such as Ba, P, S, Mn, Cu, Zn, and K, which have probably resulted from impaction of airborne particulate matter or from agglomerates of pollution particles with original stone material.

Calcium rich particles were also found in a "dry-loss" sample obtained by flushing the runoff collector with deionised water after a period of dryness. This fraction of stone loss was attributed to wind eroding the surface which had previously been weakened by the physical and mechanical stresses of crystallisation, hydration, and temperature cycles. However, no relationship could be established between the amount of eroded Ca-particles and the amount of dissolved sulphate.

Leysen *et al.* (1989) also measured the leachable sulphate, nitrate and chloride concentrations from stone surfaces, at two different heights above ground level, to ascertain the relative importance of each species in the deterioration process. Table 2.6 shows that sulphate is the prevalent leachable species in the stone. Although Leysen does not provide an explanation for the greater leachable amount of sulphate at the lower elevation (almost 50% more than that determined at the upper level), it may have been attributed to a sheltering effect that allowed the sulphate to accumulate at the lower level.

The leachable anion concentrations were also determined for one day (14/2/86) at the 40 m height site after a long period of dryness. The sulphate concentration was approximately two times that determined for the altitude comparison test, whereas the masses of nitrate and chloride were five and eight times greater, respectively. This would suggest either that the nitrate and chloride ions measured after the rain event were removed much more readily from the stone surface or more nitrate and chloride ions were dry deposited during the dry period. Laboratory experiments confirming the former hypothesis will be discussed in Section 2.4.2.2.

Table 2.6 Leachable concentration of sulphate, nitrate and chloride as a function of height (Adapted from Leysen, 1987)

	Composition (g 100 g^{-1})			
Altitude (m)	Number of Measurements	Cl^-	NO_3^-	SO_4^{2-}
		After Rainy Periods		
40	15	0.040	0.085	6.73
96	3	0.035	0.099	4.51
		After Dry Period		
40	8 (Outer Layer)	0.32	0.43	13.1
	3 (Underlying Layer)	0.23	0.18	13.4

An investigation into the role played by a polluted atmosphere in altering building materials has been provided by Baedecker *et al.* (1992) in a report of the results of a ten year monitoring programme conducted in the United States, as part of the U.S. National Acid Precipitation Assessment Programme. The NAPAP attempted to determine the influence of the following on the deterioration of stone tablets:

a) acidic gases (SO_2 and HNO_3)

b) wet deposition of H^+

c) natural effect of rainfall.

The study involved placement of two types of stone tablets; marble and limestone (dimensions 0.3 × 0.6 × 0.051 m) at five sites used as part of the NAPAP monitoring programme.

The contribution of SO_2 and HNO_3 to stone deterioration was assessed by measuring the sulphate and nitrate concentration in runoff which occurred after each rain event. The concentrations were corrected for the sulphate and nitrate concentrations measured in the runoff from a duplicate collection area (a roughened perspex sheet). The excess sulphate on the stone tablet was attributed to the formation of $CaSO_4$ by reaction of dry deposited SO_2 with $CaCO_3$. Nitric acid was assumed to react with calcium carbonate to form $Ca(NO_3)_2$.

The role of H^+, contained within precipitation, acting specifically on a carbonate stone surface was investigated by correcting for the amount of calcium displaced by the dry deposition of the acid gases and the effect of temperature on calcium solubility. This corrected calcium concentration was then plotted against the hydrogen ion concentration measured in the rainfall that was collected on a perspex surface. A typical scatter plot obtained by Baedecker *et al.* (1992) for the corrected calcium runoff concentrations from marble and the rainfall H^+ ion concentration measured at the New York site is presented in Figure 2.1. The two lines represent the stoichiometry of two reactions of $CaCO_3$ with H^+. The equations of these lines are represented as Equations 2.7 (least slope) and Equation 2.8 (greater slope).

$$CaCO_3 + 2H^+ \leftrightarrows Ca^{2+} + H_2O + CO_2 \quad \ldots \quad \text{Equation 2.7}$$

$$CaCO_3 + H^+ \leftrightarrows Ca^{2+} + HCO_3^- \quad \ldots \quad \text{Equation 2.8}$$

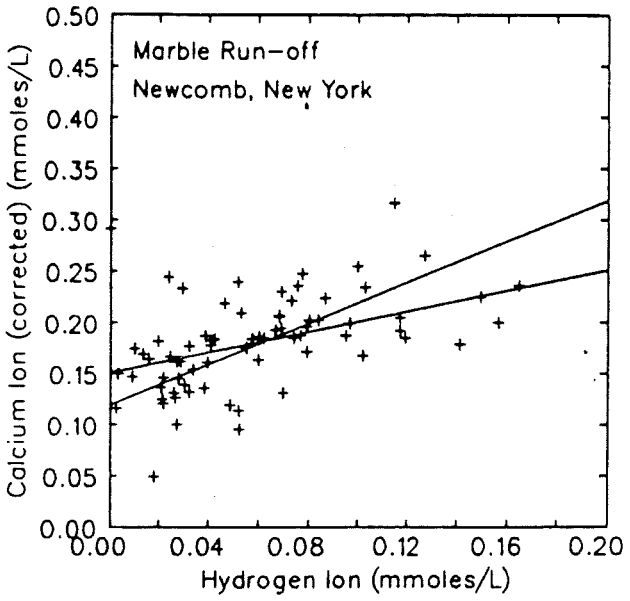

Figure 2.1 Plot of corrected calcium concentration against hydrogen ion concentration in incident rain (Baedecker *et al.*, 1992)

The molar ratios of Ca^{2+} to H^+ in each equation will be the same as described before for Equations 2.3 and 2.4, respectively, except that the concentration of $CaCO_3$ is presented with the concentration of H^+ only and not the sulphur species as in the

previous case.

The scatter in the data was attributed to hydrodynamic effects caused by variations in rain intensity. Although each line through the points on the graph appear to represent a line of best fit, only the reaction involving 1 mole of Ca^{2+} with 1 mole H^+ (Equation 2.8) was assumed by Baedecker *et al.* (1992) to occur in the atmosphere. Hence, the solubility of $CaCO_3$ in "clean rain" (determined as the line of greatest slope in Figure 2.1) was calculated as 0.12 mmoles l^{-1}.

The relative contributions of dry deposited gases, H^+ deposition and "clean rain" solubility to stone dissolution were determined by calculating the cumulative amounts of Ca^{2+}, SO_4^{-2}, NO_3^- removed and H^+ deposited by the cumulative rainfall volume over the ten year sampling programme. The proportion of dissolution attributed to sulphur dioxide dry deposition, for example, was calculated by dividing the cumulative sulphate concentration (mmoles l^{-1}) by the cumulative calcium concentration (millimole l^{-1}). The proportion of dissolution attributed to dry deposition of nitric acid was determined in a similar way, except two millimoles of NO_3^- were required to react with one millimole of Ca^{2+}. The dissolution attributed to the wet deposition of H^+ was predicted by assuming the 2:1 stoichiometry ($2H^+$: $1CaCO_3$) shown in Equation 2.7.

Altogether for the five NAPAP sampling sites discussed by Baedecker *et al.* (1992), thirty percent of the erosion of the tablets was attributed to the wet deposition of H^+ and the dry deposition of SO_2 and HNO_3 between rainfall events. The remaining 70% percent was assigned to dissolution by the natural acidity of rain water. The contribution of each species to the deterioration of marble and limestone tablets is further illustrated in Table 2.7 for two sampling sites; a rural site in New York State and an urban site, Washington D.C. Also presented are the measured SO_2, NO_2 and O_3 gaseous concentrations and the rain water acidity.

The higher concentration of sulphur dioxide measured at Washington D.C clearly produced a significant increase in weathering. This impact is greater for the limestone tablets compared to the marble tablets due to the greater porosity of the limestone resulting in a longer wetness time following rainfall or dew formation. The "clean rain"

Table 2.7 Percentage contributions of atmospheric inputs to stone dissolution. Also presented are mean atmospheric pollutant concentrations. (Adapted from Baedecker *et al.*, 1992).

	Newcombe, New York		Washington, D.C.	
	Marble (%)	Limestone (%)	Marble (%)	Limestone (%)
H^+	11.2	11.0	6.8	6.2
SO_2	3.7	10.3	18.5	22.3
HNO_3	0.8	1.1	1.8	2.7
"Clean rain" effect	84.3	77.6	72.9	68.8
SO_2 (ppb)	2 ± 3		12 ± 9	
NO_2 (ppb)	2 ± 2		28 ± 12	
O_3 (ppb)	30 ± 14		30 ± 20	
pH	4.3		4.1	

effect was the major deteriorating process at both sites .

The study of Baedecker *et al.* (1992) is significant in that it was one of the first to associate the origin of the nitrate in the runoff to atmospheric nitric acid and not to nitrogen dioxide as had been suggested by earlier studies (Jaynes and Cooke, 1987 and Gauri and Holdren, 1981).

An experiment to assess the relative contribution of sulphur dioxide, nitrogen oxides, sulphuric acid and nitric acid to the deterioration of building material in Greece was performed by Delopoulou and Sikiotis (1992). Two sampling trains consisting of different combinations of granulated marble and filter packs were run in parallel. The filter pack arrangements are shown schematically in Figure 2.2. One sampling train possessed a filter pack on either side of the granulated marble (System A) and the other possessed two filter packs following the granulated marble chamber (System B). The filter packs contained teflon, nylon and citric acid filters which removed total particulates, nitric acid gas and ammonia, respectively. Sampling was conducted for approximately one month periods during summer 1991 at the Acropolis, Athens.

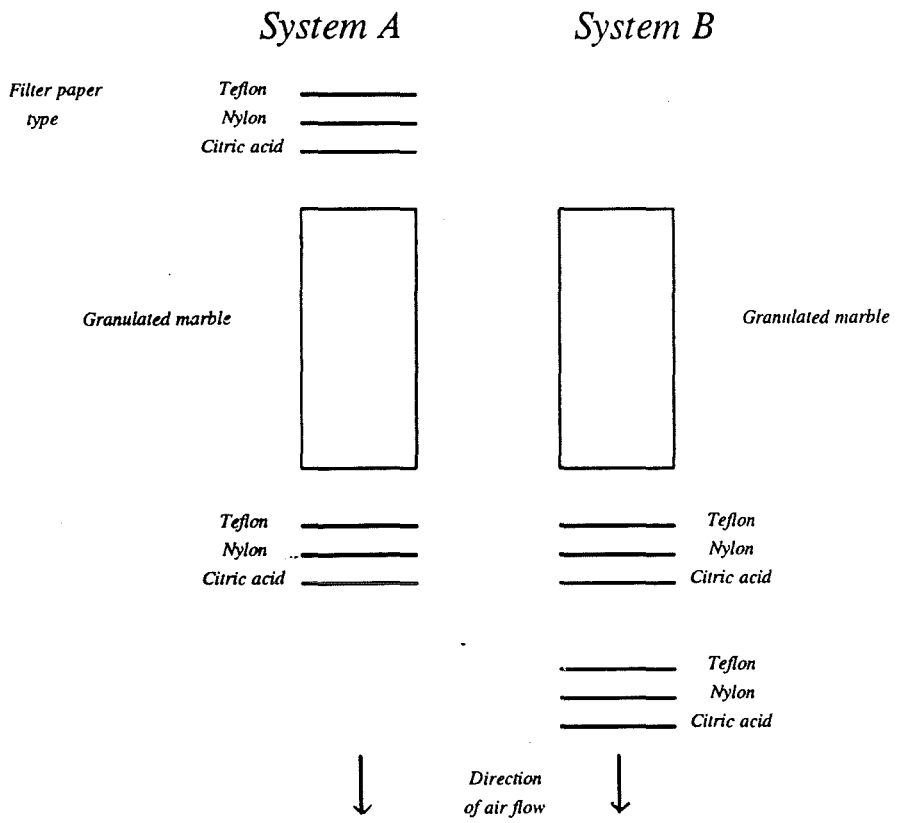

Figure 2.2 Schematic diagram showing the arrangement of granulated marble chamber and prefilters in the Delopoulou and Sikiotis (1992) study.

Analysis of the sulphate collected within both marble chambers showed that approximately ten times more sulphate was formed in the chamber not proceeded by a filter pack (System B). This observation, resulting from the reaction of calcium carbonate with sulphur in both the gaseous (SO_2) and acidic aerosol ($(NH_4)HSO_4^{2-}$) phases, would suggest that sulphate is being formed chiefly as a result of the reaction represented by Equation 2.3. Given the lower concentrations of the acidic aerosol in the Athens atmosphere, compared to the sulphur dioxide concentration, the former species can obviously be considered relatively more harmful to building stones in Athens.

Calcium nitrate formation was found to occur in the marble chamber for both systems, with three times more $Ca(NO_3)_2$ formed in System B due to the reaction of marble with HNO_3. The formation of $Ca(NO_3)_2$ in System A, even after passage through the filter pack, was attributed either to the:

a) reaction of marble with HNO_2 followed by the oxidation of the resulting

nitrite to calcium nitrate

or b) oxidation of adsorbed HNO_2 to HNO_3 which then reacts with the marble.

Although some HNO_2 is retained by the nylon filter, approximately 75 % was calculated to pass through the system at the flow rates used in the study. Nitrous acid is formed by photochemical reaction (the oxidation of NO will be discussed in Section 3.2.2.3). Delopoulou and Sikiotis (1992) suggest that high traffic density in Athens could produce HNO_2 concentrations approaching those of HNO_3; however they do not supply any atmospheric concentrations to back-up this claim.

A recommendation made by Delopoulou and Sikiotis to preserve the fabric of buildings is to prevent substances settling on the building that may catalyse the oxidation of sulphur dioxide to sulphate. One way of doing this, presumably, is to keep the surface of the building clean by using some type of dust removing device. Deloupolou and Sikiotis (1992) also recommended museums to install nylon air filters in their ventilation systems to remove nitric acid from the air entering the building.

2.4.2.2 Simulated dry and wet ambient exposure

Laboratory experiments, such as those performed by Johnson *et al.* (1990), Haneff *et al.* (1992) and Cheng (1987) attempt to recreate in controlled laboratory conditions the factors that may be causing stone deterioration.

The design criteria required to simulate atmospheric dry and wet deposition in controlled laboratory conditions have been described in detail by Johnson *et al.* (1990), with the results of these laboratory experiments presented by Haneff *et al.* (1992).

a) For the case of dry deposition

The dry deposition velocity, although acknowledged as the parameter connecting deposition flux and atmospheric concentration in the outdoor atmosphere, was not used to consider the deposition of the gaseous species in the laboratory chamber design. Instead, Johnson *et al.* (1990) considered the delivery of a pollutant to a stone surface in terms of a presentation rate, which assumed that the gas was totally removed by the

surface. The presentation rates for the laboratory experiment were calculated as follows:

- The 0.083 l s^{-1} of air delivered to the exposure chamber contained 10 ppmv of each test gas (SO_2, NO_2 and NO). This caused each stone tablet to receive 8.3×10^{-5} cm^3 of each gas per second (ten stones were considered in this example).
- Assuming that each 1 cm^2 of the 15 cm^2 stone tablet surface area (dimensions 5 × 3 × 0.5 cm) completely absorbed the 5.53×10^{-6} cm^3 of each gas delivered to the surface each second, multiplication by the appropriate gas density, 2.93×10^3 $\mu g\ cm^{-3}$ for the case of SO_2, gave a presentation rate of 16.2×10^{-3} $\mu g\ cm^{-2}\ s^{-1}$.

The presentation rates for SO_2, NO_2, and NO, determined for annual atmospheric mean concentrations of 60, 32 and 51 $\mu g\ m^{-3}$, respectively, can be seen in Table 2.8, to be approximately equal to the presentation rates calculated for the laboratory experiment. The atmospheric presentation rates were calculated assuming that the mean velocity of air passing over the ground surface was 2 m s^{-1}.

Table 2.8 Comparison of dry deposition presentation rates calculated for atmospheric and laboratory chamber study (Adapted from Johnson *et al.*, 1990).

		SO_2	NO_2	NO
Laboratory case	Presentation rate $\mu g\ cm^{-2}\ s^{-1}$	16.2×10^{-3}	8.0×10^{-3}	7.4×10^{-3}
Atmospheric case	Concentration ($\mu g\ m^{-3}$)	60	32	51
	Presentation rate $\mu g\ cm^{-2}\ s^{-1}$	12×10^{-3}	6.4×10^{-3}	10.2×10^{-3}

Note, the densities of SO_2, NO_2 and NO were 2.93, 1.45 and 1.34 g l^{-1}, these values can alternatively be expressed as $\times 10^3$ $\mu g\ cm^{-3}$.

The results of these dry deposition experiments were presented by Haneff *et al.* (1992). Altogether the stone samples were subjected to four different exposure regimes; dry stone plus test gas only, dry stone plus test gas in the presence of ozone (10 ppmv), wetted stone plus test gas only and wetted stone plus test gas in the presence of ozone (10 ppmv). The exposure period for each regime was thirty days. The wetting procedure involved dripping CO_2-equilibrated water over the stone surface at a rate of 2.5×10^{-6} ml $cm^{-2}\ s^{-1}$; this volume was chosen to imitate the annual rainfall rate falling in the Manchester area (800 mm).

In general, for each of the four stone types tested; Pentelic marble, Mansfield limestone, Massangis limestone and Portland limestone, an increase in stone tablet weight (mg) was observed when the dry stones were exposed to each gas (NO_2, NO and SO_2, without the presence of ozone). The magnitude of this increase in weight was at least doubled when the dry stones were exposed to each gas in the presence of ozone.

For the case of the wetted stones, all the stone types exposed to the NO_2 and NO gases lost weight. This effect appeared to be independent of the presence of ozone. Conversely, significant weight increase was obtained on exposure to SO_2. Again the effect was unaffected by the presence of ozone. The increase in weight for the wetted stones in the presence of SO_2 was approximately an order of magnitude greater than the case for dry stone without ozone, indicating the important role of moisture in the deterioration process.

Two methods, an equivalent calcium yield and a percentage conversion of each gas to their respective anions, were used to assess the interaction between each gas and the stone. The former method involved, for the case of the wetted stones, adding the masses of Ca^{2+} and anions present in the runoff to the mass of anions retained by the stone. For the dry stones, only the mass of anions retained by the stone was used to calculate an equivalent calcium yield. The latter method was calculated by measuring the concentration of anions on stone or runoff and dividing this by the anion concentration that would have resulted from complete oxidation of the incoming gases.

From the magnitude of the calcium equivalent yields and percentage conversions, Haneff *et al.* (1992) inferred the following:

- For dry stones, in the absence of ozone, the order of pollutant effect was $SO_2 > NO_2 \sim NO$. The increased SO_2 to sulphate reactions, much higher than the expected gaseous phase oxidation indicated the presence of catalysts on the stone (gas phase oxidations will be discussed in Section 3.2.2.2).
- For the dry stones, in the presence of ozone, the order of reactivity of the gases varied as follows: $SO_2 > NO_2 > NO$ for the less porous stones and $NO_2 > SO_2 \sim NO$ for the more porous stones (Portland stone and Mansfield sandstone). The reduction

in activity of the SO_2 was attributed to the masking of the active sites by precipitated gypsum. The increased activity of the nitrogen oxide gases, compared to activity without ozone, was attributed to the formation of nitric acid which consequently reacted with the calcite. Unlike the sulphate-calcite reaction, the nitric acid-calcite reaction is not limited by the formation of a precipitation product.

- For wet stones, in the absence of ozone, the calculated conversions ranged from 2-13% for SO_2 and 0.1-8% for NO_x. The higher conversions for the SO_2 were attributed by Haneff *et al.* (1992) to the gas having a greater solubility in water, compared to that of NO_2 and NO, which would allow more time for the gas, once dissolved, to form H^+. For example, the solubilities of SO_2 and NO are 228 $cm^3\ l^{-1}$ and 73.4 $cm^3\ l^{-1}$, respectively at 0°C, and 23.6 $cm^3\ l^{-1}$ and 5.8 $cm^3\ l^{-1}$, respectively at 60°C (Lide, 1990). Nitrogen dioxide solubility is not quoted by Lide (1990), presumably a consequence of the gas forming a reversible complex with N_2O_4 (Greenwood and Earnshaw, 1984) making measurement impossible.
- For wet stones in the presence of ozone, SO_2 was always the most reactive species. The reaction of the nitrogen oxides with each stone type actually decreased, compared to the dry stone regime. This was attributed to the oxidation of NO and NO_2 in the surface water being a rate controlling step. The oxidisation in the aqueous layer was assumed to occur via the production of the N_2O_5, which was lost before the oxidation to HNO_3 could be completed.

b) For the case of wet deposition

The wet deposition process was modelled using ambient concentrations for rain water measured in Manchester during 1986. The concentrations of SO_4^{2-}, NO_3^-, Cl^- were 8.64, 3.1 and 5.2 $\mu g\ ml^{-1}$, respectively, which when combined with the annual precipitation of 800 mm correspond to wet deposition fluxes of 21.9×10^{-6}, 7.8×10^{-6} and 13.1×10^{-6} $\mu g\ cm^{-2}\ s^{-1}$, respectively.

The samples in the test chamber were exposed to regular spraying using a solution with a concentration equivalent to a 10× increase in the measured rainfall concentration. The elevated concentration was used to produce an accelerated effect in deterioration. This artificial "acid rain" was made by dissolving the masses presented in Table 2.9 in 1 litre of water.

Table 2.9 Mass of salts and acids added to one litre of water to simulate a 10× acid rain solution

Compound added	Mass mg
H_2SO_4 (98% w/v, 1.84 s.g.)	31.85
$(NH_4)_2SO_4$	46.20
Na_2SO_4	31.95
HNO_3 (70% w/v,1.42 s.g.)	15.75
$NaNO_3$	21.25
NaCl	84.83

A second solution containing sulphate as the only anion in solution was also sprayed in an identical manner onto each stone. This solution was prepared by dissolving the same masses of H_2SO_4, $(NH_4)_2SO_4$, and Na_2SO_4 that were used to prepare the "acid rain" solution.

The test solutions were sprayed at a rate of 2.5×10^{-6} ml cm^{-2} s^{-1} for two hours followed by a two hour dry period. The results, expressed as weight loss per square metre are presented in Table 2.10.

Table 2.10 Weight loss from stone tablets exposed to wet precipitation

	Wet deposition (Weight loss $\times 10^{-3}$ kg per m^2 of stone)		
Sprayed solution	Artificial acid rain	Sulphate solution	De-mineralised water
Weight loss	80.9	56.6	11.5

Substantial dissolution of the limestone occurred due to both the action of the acidic sulphate and acid rain with the weight losses of the stone tablets being greater for the latter conditions. The difference in net weight loss, 24.3×10^{-3} kg m^{-2}, was attributed to the presence of other anions in the acid rain solution despite both solutions having a pH of 3.5.

In another laboratory study (Hutchinson *et al.*, 1992a) the relative roles of both SO_2 and HCl in the degradation of dry and moist stone surfaces were compared. The test cell

consisted of two chambers; a larger one (dimensions 35 × 35 × 10 cm) and a smaller one (dimensions 25 × 25 × 5 cm). Six small stone tablets were attached to each vertical side of the smaller chamber which in turn was placed within the larger chamber. The gases (concentrations of 25 ppb each) were introduced into the system using a dispersing manifold which was situated along the length of one side of the outer chamber. Three moisture regimes were applied to the stone tablets; two were exposed to 95% humidity, two had their surfaces dampened and two were wetted with enough deionised water to produce runoff. The sample run times were 25 days. The samples moistened by humidity had the largest amount of weight gain for the SO_2 study, followed by those dampened by water, with those which had water flowing over their surface showing least response. The weight gains were attributed to the formation of gypsum. No weight gain was observed for the stone samples exposed to hydrochloric acid. Conversely high concentrations of chloride were measured in the runoff samples. This was attributed to the high solubility of calcium chloride relative to calcium sulphate.

The reaction between the stone and hydrochloric acid was much more rapid than that with SO_2 as indicated by the observation that over 50% of the HCl introduced into the system was absorbed by the stone tablets opposite the gas inlet manifold compared to only 10% of the SO_2.

Cheng (1987) attempted to determine the relative importance of sulphur and nitrogen compounds in the stone deterioration process. Samples of U.S. and Italian marble were immersed separately in 30 and 100 μmol solutions of sulphuric and nitric acid. The 30 μmol solution was intended to simulate environmental concentrations of rainwater. The solutions of each acid were brought into contact with the marble in such a way as to imitate the splashing of rain. The solutions were replaced every four hours and the deterioration of each tablet was measured by weight loss. The loss of marble in 30 μmol sulphuric acid was almost 3× that from the 30 μmol nitric acid solution. For the 100 μmol solutions the sulphuric acid removed between 13 and 17 times more marble than the nitric acid solution.

2.4.2.3 Combined effect of SO_2 and NO_2 on limestone deterioration

The influence of NO_2 on the reaction between SO_2 and calcium carbonate was investigated in a laboratory experiment by Johannson *et al.* (1988). This study showed that the concentration of SO_2 leaving the reaction chamber decreased by 40% when NO_2 (3.1 ppm) was introduced into the reaction chamber. This was attributed to SO_2 being quickly adsorbed due to the NO_2 catalysing the oxidation of $CaSO_3.½H_2O$ to $CaSO_4.2H_2O$ (Equation 2.4). However, replication of this experiment in the ambient would be very problematic due to the difficulty in determining whether the adsorption of SO_2 was actually affected by NO_2. The role of NO_2 in altering limestones in the ambient atmosphere will be discussed in Section 2.4.3.

2.4.2.4 Investigation of the role played by flyash in the deterioration process

The extent to which the carbonaceous fly-ash component of black crusts will influence the decay process has been investigated in the laboratory by Hutchinson *et al.* (1992b). In this study, Portland and Monk's Park limestone samples were "seeded" with fly-ash particulate matter and transition metal oxide catalysts. Five types of fly-ash were selected and were sieved to obtain a size fraction <45 μm. The experiment was conducted using an industrial atmospheric test chamber into which sulphur dioxide was introduced. A summary of the results, presented in Table 2.11, shows that there was little difference in the amount of sulphate formed on the seeded and unseeded stone surfaces.

In fact, Hutchinson *et al.* (1992b) suggested that less sulphate was formed on the seeded samples due possibly to a surface blocking effect. When the metal oxides were tested in the absence of the stone samples an increase the amount of sulphate formed was observed. However, the mass of metal oxides used in the experiment was not considered typical of the masses found in atmospheric samples.

The higher accumulation of sulphate for Monks Park limestone samples was attributed to the higher porosity of the stone surface which provides a larger surface for reaction. The direct contribution of the sulphate contained within the fly-ash, typically 4.4 to 27

Table 2.11 Summary of results obtained when fly-ash and stone samples were exposed to sulphur dioxide

Experiment	Results	Comment
Glass slides each coated with fly-ash	Gypsum was formed in each sample	Gypsum was produced under varying humidities and temperatures
Monk's Park and Portland stones samples dusted with fly-ash.	* Sulphate accumulation 2.6 to 8.8 mg g^{-1} 1.9 to 6.0 mg g^{-1}	* Calculated deposition velocity: 3.3 to 7.5 mm s^{-1}
Unseeded stones	5.4 to 7.8 mg g^{-1}	3.3 to 5.3 mm s^{-1}
Metal catalysts:		* Calculated deposition velocity:
Fe_2O_3, MnO_2, CuO	4.5 to 7 mg g^{-1}	3.3 to 5.1 mm s^{-1}
Calcium carbonate only	4 to 6 mg g^{-1}	3.6 to 5.3 mm s^{-1}
Metal catalysts mixed with calcium carbonate:		
CuO and Fe_2O_3	5.5 to 14 mg g^{-1}	4.9 to 12.4 mm s^{-1}
MnO_2	18.5 to 24 mg g^{-1}	16.5 to 21.4 mm s^{-1}

* The sulphate accumulation is measured as milligrams of sulphate per gram of stone or metal ion catalyst

* The deposition velocity is determined by dividing the amount of accumulated sulphate by sulphur dioxide concentration in the chamber.

μg per application, was assessed to be insignificant when compared with the amount of sulphate formed on the stone (1.9 to 8.8 mg g^{-1} stone).

Hutchinson *et al.* (1992b) have compared their results to those obtained by Del Monte (1981) and Camuffo (1982) who found a correlation between the amount of particulate matter and black crust thickness and suggest that the observations found by the Italian authors could be attributed to high concentrations of SO_2 and fly-ash particles in Venice. In conclusion, Hutchinson *et al.* suggest that the role of fly-ash particulate matter has been exaggerated by Del Monte (1981) and is not essential for rapid sulphate formation on stone.

2.4.3 Determination of physical and empirical damage functions

A damage function attempts to assess and quantify the role of environmental variables and specifically air pollutants on the deterioration of a building material. Such functions have been developed by Lipfert (1989), Webb *et al.* (1992) and Butlin *et al.* (1992).

By performing a regression analysis on log transformed data, obtained from the Regional Air Pollution Study, RAPS (Mansfield, 1980), Lipfert (1989) showed the multiplicative effect of total rainfall deposition (cum prec.) and cumulative dry deposition of SO_2 (cum. SO_2 dep.) on weight loss (actually expressed by Lipfert as surface recession rate per year, $\mu m\ a^{-1}$) from exposed stone tablets. The relationship is represented by Equation 2.9:

$$Weight\ loss\ (\mu m\ a^{-1}) = 3.44(cum.\ SO_2\ dep.)^{0.12} + (cum.\ prec.)^{0.61}$$

. . . .Equation 2.9

The larger exponent for total rainfall deposition (0.61), compared to that for cumulative sulphur dioxide deposition (0.12), suggested the dominant role of rainfall on weight loss.

The importance of precipitation in assessing the damage function was reinforced when employing a linear regression (for annual RAPS data). An increase in the regression coefficient for rainfall (from 0.053 to 0.125) and a decrease for SO_2 (from 0.53 to 0.22) was obtained when two extra independent variables (total suspended particulates and temperature) were included. The relationships are expressed by Equations 2.10 and 2.11, respectively.

$$Loss\ (\mu m\ a^{-1}) = 0.71 + 0.53\ (SO_2\ dep.) + 0.053\ (annual\ prec.)$$

. . . .Equation 2.10

$$Loss\ (\mu m\ a^{-1}) = 4.72 + 0.22\ (SO_2\ dep.) + 0.125\ (annual\ prec.) - 0.49\ (temp.) - 0.021\ (TSP)$$

. . . .Equation 2.11

The negative value for the regression coefficient for TSP was attributed by Lipfert (1989) to the alkaline particles in the sampling area which neutralised a proportion of the acidity.

Lipfert (1989) subsequently converted the dependent variable (material loss per year) represented in Equation 2.9 into an equivalent variable; material loss per metre of precipitation, which reflects the role of rainfall in the deterioration process. Using such theoretical relationships as the dissolution in clean rain, attack by gaseous pollutants and the hydrogen ion concentration present in acid rain, Lipfert (1989) developed the following damage function,

$$\textit{Loss of material}\ (\mu m\ m^{-1}) = 18.8 + 0.016\ H^{+} + 0.18 \times \frac{(V_{ds} \times SO_2 + V_{dn} \times HNO_3)}{RI}$$

. . . .Equation 2.12

where:

the constant, 18.8, represents the solubility of calcite in equilibrium with 330 ppm CO_2,
V_{ds} is the dry deposition rate of sulphur dioxide, 0.8 cm s^{-1}
V_{dn} is the dry deposition rate of nitric acid, 3.0 cm s^{-1}
RI is the rainfall rate, mm h^{-1}
H^+, delivery rate of hydrogen ions, nanomoles cm^{-2} s^{-1}
SO_2, SO_2 concentration, μg m^{-3}
HNO_3, HNO_3 concentration, μg m^{-3}.

On the basis of this equation, the surface recession per metre of rain, assumed to fall in one year, is illustrated in Figure 2.3 for a range of pollutant concentrations. The constant amount of material lost from the stone surface per metre of rain, 18.8 μm, (referred to as the "clean rain" effect) was determined by considering the dissolution of calcite in aqueous solution (pH range 3 to 5). This mechanism can clearly be seen to be the main cause of surface recession, as previously described in this chapter by Baedecker *et al.* (1992).

The influence of SO_2 dry deposition, for a dry deposition velocity of 0.8 cm s^{-1}, will approach that of the clean rain effect for annual mean concentrations exceeding 120 μg m^{-3}.

Concentrations of nitric acid, greater than those commonly measured, 0.67 μg m^{-3} for a rural atmosphere in Eastern England (Harrison and Allen, 1990) and 15 to 30 μg m^{-3} for a polluted atmosphere in an urban environment (Spicer, 1977), would be required to approach the surface recession attributed to clean rain effect.

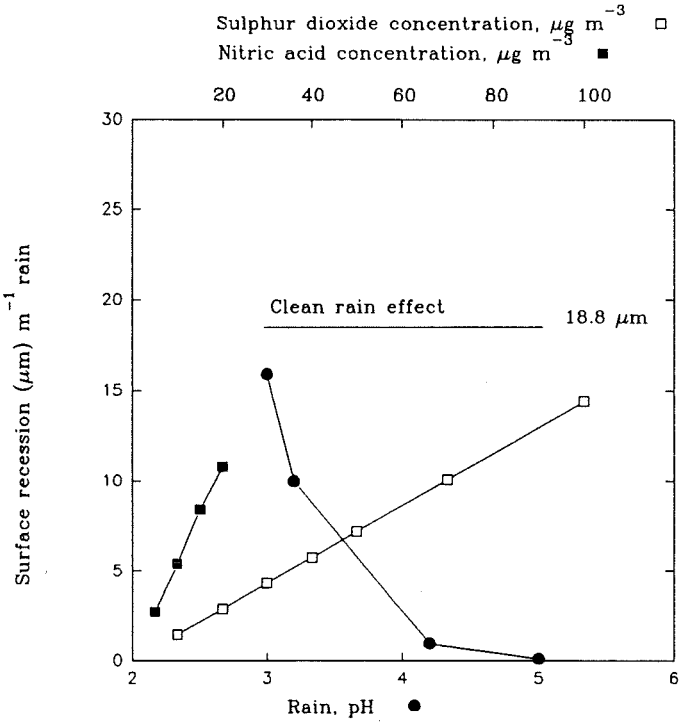

Figure 2.3 Theoretical recession rates from a calcite surface calculated using Equation 2.12.

The influence of the hydrogen ion concentration of the incident rainfall, calculated as the extra hydrogen ions in rain exceeding pH 5.6 ($[H^+] = 2.5 \times 10^{-6}$ mol l^{-1}), will approach the clean rain effect at a pH of approximately 2.8.

To a first approximation, the predicted recession rates, determined using Equation 2.12 and illustrated in Figure 2.3, are of a magnitude similar to the recession rates determined by Sharp *et al.* (1982) (range 31 μm to 117 μm a^{-1}) using the lead plug method described previously in Section 2.4.1.1.

Webb *et al.* (1992) derived a theoretical damage function from a chemical dissolution model. This model is similar to that derived by Lipfert (1989) in that there are three main components causing stone loss. Each of these processes are described mathematically to produce the overall model shown in Equation 2.13 which can be used to calculate stone loss:

$$\textit{stone loss (moles)} = A D V_d C_{SO_2} + \frac{K_H K_1 P_{CO_2}}{2[H^+]_r} \sum (A_i R - Evap) + \frac{[H^+]_i}{2} \sum A_i R$$

. . . .Equation 2.13

where: C_{SO_2} is the mean concentration (ppb) during exposure time D (days).
A is the surface area of the stone exposed, mm^2
V_d dry deposition velocity of SO_2, mm s^{-1}
K_H Henry's Law coefficient for CO_2, 0.045 mol l^{-1} atm^{-1}
K_1 rate constant for calculating the solubility of HCO_3^-, 3.8×10^{-7} mol l^{-1}
A_i is the rainfall interception area (mm^2)
P_{CO_2} is partial pressure for carbon dioxide (350 ppm)
R rainfall amount (mm)
$[H^+]_r$ is the volume-weighted mean hydrogen concentration of the runoff (μmol l^{-1})
$[H^+]_i$ is the volume-weighted mean hydrogen concentration of the rainfall (μmol l^{-1})
Evap is the volume of rainfall evaporated from the stone sample (ml).

Webb *et al.* (1992) adapted Equation 2.13 as follows, to calculate weight loss from small Portland limestone cubes (length 40 mm) placed at thirteen exposure sites located throughout Great Britain:

- the surface interception area, A_i, was approximated by an interception factor, $\acute{F}$ = 3.6.
- the fraction of water evaporated from the stone surface was found to range from 15 % to 35%.
- weight decrease was determined as grams lost per m^2 per day.

Equation 2.14 shows the connection between weight loss, sulphur dioxide concentration, incident rain pH and runoff pH.

$$\textit{Stone loss } (g\ m^{-2}\ day^{-1}) = 0.00037 v_d C_{SO_2} + \frac{5.6\times10^{-11}}{[H^+]_r} \frac{\Sigma(\acute{F}R - Evap)}{D} + 10[H^+]$$

. . . .Equation 2.14

The calculated weight loss was compared to measured weight loss from similar samples exposed in triplicate for 200 days. For all but one sample the variation between the stone loss calculated from the model and the mean rate measured for any exposure was less than the variation between the triplicate samples. This indicated the measured data was approximated by the model.

The contribution of sulphur dioxide dry deposition to stone dissolution was calculated, using Equation 2.14, to range from 5% at Clatteringshaws in south-west Scotland to 50% at York. For all considered samples the natural bicarbonate solubility term was dominant, contributing between 50 and >90% of the calculated stone loss. The neutralisation effect of the acidity in the rain contributed between 0.3 and 3.25% of the total calculated weight loss.

The role of nitrogen dioxide and total nitrogen oxides in the deterioration process was investigated by plotting the residual error between measured and calculated stone against the [NO_2] and [NO_x-total] values measured at each site. From the random distribution of residuals no dependence, and hence, NO_2 and/or NO_x-total, interaction was observed.

Substituting a range of hydrogen ion concentrations for runoff, $[H^+]_r$, and incident rain, $[H^+]_i$, as well as SO_2 concentrations, the influence of each deteriorating agent, on weight loss from Portland limestone cubes can be compared (Figure 2.4). In performing these calculations the following constituent parts of Equation 2.13 were kept constant: daily precipitation rate (3 mm), SO_2 dry deposition velocity (8 mm s^{-1}) and evaporation rate (20% of incident precipitation striking the surface).

In addition to increased weight loss at lower incident rain pH and higher SO_2 concentrations, as described previously by the Lipfert model (Equation 2.12), Figure 2.4 shows that decreases in the hydrogen ion concentration in surface runoff will infer that significant alteration of the stone surface has occurred.

An empirical model in which the weight loss from stone tablets was expressed in terms of measured environmental variables was determined by Butlin *et al.* (1992) using multi-regression analysis. The study, part of the National Material Exposure Programme conducted by the Building Research Establishment, involved the exposure of stone tablets that were suspended on freely rotating carousels to total deposition (wet and dry deposition) and dry deposition. Plate 2.6 shows an example of the sampling rig. Three types of stone were used in the study; Portland limestone, a shelly limestone; Monks Park, a fine grained limestone; White Mansfield limestone, a fine grained, dolomitic sandstone.

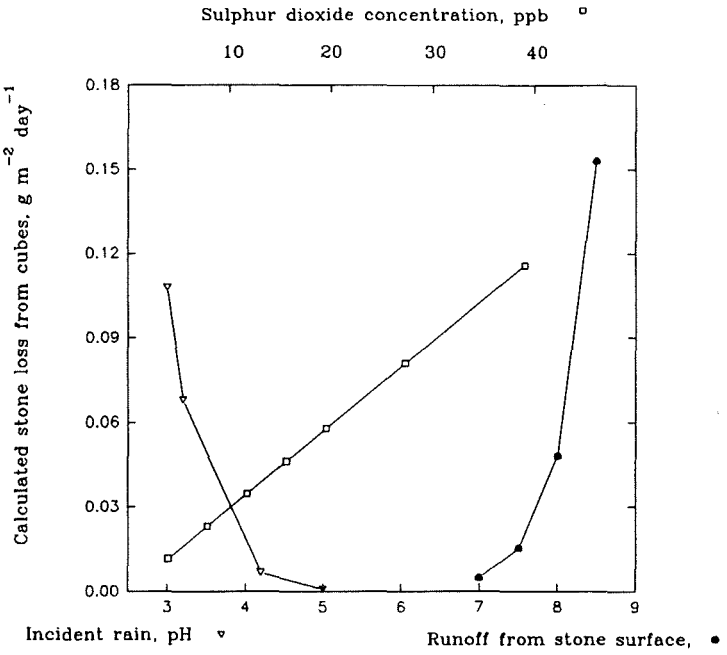

Figure 2.4 Calculated weight loss from Portland cubes as function of incident rain pH, SO_2 concentrations and runoff pH.

Selected samples on each carousel were replaced and analysed annually, while others were exposed in such a way that 2, 3 and 4 year exposures times were obtained. In this way single year changes in stone characteristics such as weight loss and ionic composition could be compared with changes over longer periods. The combined single year changes were generally greater than those produced from the continuous two year sampling period. This was attributed to a 'starting effect' in which there is a rapid weight loss due to the initial exposure of the tablets to rain.

For those samples on top of the sampling rig (unsheltered samples) Spearman's rank correlation analysis showed significant correlations between annual SO_2 concentration, rainfall volume, hydrogen ion loading ($\mu g\ H^+\ m^{-2}$) and weight change, suggesting the same three physical mechanisms explained above by Webb *et al.* (1992) were acting to cause deterioration.

The empirical model derived by Butlin *et al.* (1992) was obtained by regressing weight loss onto the annual average NO_2 and SO_2 concentrations, annual rainfall and mean hydrogen ion concentration. The equation for Portland limestone tablets for the year 1987-1988 is expressed by Equation 2.15:

Plate 2.6 Sampling rig used to support stone carousels at Bolsover Castle

$$Weight\ loss = 0.08 + 0.010\ SO_2 - 0.00012\ NO_2 + 0.00016\ Rain + 0.0026\ H^+$$

. . . .Equation 2.15

where SO_2 and NO_2 are expressed as $\mu g\ m^{-3}$,
Rain as mm,
H^+ as mg H^+ per m^2 of stone area.
$R^2 = 0.60$.

For the White Mansfield sandstone the equation for the same period was:

$$Weight\ loss = 0.37 + 0.017\ SO_2 - 0.009\ NO_2 + 0.0039\ Rain + 0.0026\ H^+$$

. . . .Equation 2.16

The higher coefficient of determination for the White Mansfield data set ($R^2 = 0.73$) compared to the Portland stone samples was due to the independent variables explaining more variation in weight loss.

Butlin *et al.* (1992) attribute the negative coefficient for NO_2 to the presence of unmeasured variables such as hydrocarbons or combustion material derived from road and automobile emissions which may reduce the reactive surface on a stone tablet. The NO_2 and rainfall terms can be seen to have an inverse relationship, with the magnitude of the NO_2 coefficient being less in the Portland sample compared to the White Mansfield sample, whereas the magnitude of the rain coefficient for the Portland sample is greater than the White Mansfield sample. This relationship was suggested to be caused by lower concentrations of NO_2 being found in higher rainfall areas.

Most of the sheltered tablets (96 of the 126) increased in weight. Significant correlations for all three stone types were found between weight change and atmospheric SO_2 and NO_2 concentrations. A negative correlation between weight change and rainfall was obtained indicating that driving rain was probably washing the tablets. There was no evidence of the 'starting effect' postulated for the exposed tablets.

2.5 Summary

Experimental evidence has been presented to show that air pollution causes increased levels of deterioration in limestone building materials. The structure of limestone

surfaces which have been exposed to air pollutants are described. Ugly black crusts, composed of gypsum and carbonaceous material, are a common manifestation of the reactions between air pollutants and the building surface. However, no quantification of the rate of growth of black crusts has been reported in the literature.

The reaction between the carbonate component of limestone and the following components of the atmosphere have been quantified for limestone tablets:

- natural acidity of the precipitation,
- acidic sulphur gas,
- additional acidity present in precipitation due to the washout of gases and acidic aerosols.

The quantification of each deteriorating agent was shown to be calculated by either:

- analyses of the components of collected runoff and coupling the calcium ions with other ions present in the solution (Baedecker *et al.*, 1992).
- theoretical derivation of the solubility of calcium carbonate in the presence of carbonic acid, sulphur dioxide and the additional acidity present in precipitation due to the washout of acid gases and acidic aerosols (Lipfert, 1989 and Webb *et al.*, 1992).

The method employed by Baedecker *et al.* (1992) measured the concentration of sulphate ions in runoff to determine the effect of dry sulphur dioxide deposition on stone loss. The dry deposition of HNO_3 was determined in similar way. The effect of the deposition of H^+ contained within the incident precipitation was determined similarly by equating two moles of H^+ ion with one mole of Ca^{2+} ion. The additional Ca^{2+} measured in runoff solutions was attributed to the natural acidity of the rain water.

The theoretical model presented by Lipfert (1989) (Equation 2.11) was found to approximate recession rates measured by Sharp *et al.* (1982), using a lead plug index. Similarly the model used by Webb *et al.* (1992) approximated the weight loss from stone cubes placed at Central Electricity Generating Board/Cathedral Advisory Board sampling sites.

Other experiments, such as those conducted by Leysen *et al.* (1989), have shown that

the pH of precipitation measured close to a limestone Cathedral is in fact alkaline due to the neutralisation action of a calcium carbonate cloud existing around the building. This provides an example of the difficulty in determining a definitive reaction scheme for the dissolution of stone in a polluted atmosphere.

Field and laboratory investigations have investigated various aspects of the deterioration process. For example, one important consideration was the important role of acidic sulphate aerosol on the deterioration process (Deloupolou and Sikiotis, 1992). This would have a serious consequence on the assessment of stone deterioration rates attributed to the dry deposition of sulphur as sulphur dioxide, since several authors in this review, attributed as much as 50% of stone loss in polluted atmospheres, to dry deposited SO_2. However, isolating the relative influence of dry deposited sulphuric acid and sulphur dioxide would be difficult.

In general, nitrogen dioxide was shown to be relatively unimportant in causing alteration to building stones exposed to the ambient atmosphere. However, field and laboratory studies have shown that NO_2 may play an ancillary role in altering building surfaces. For example, in a laboratory experiment performed by Haneff *et al.* (1992), nitrogen dioxide activity was found to increase in the presence of ozone. This was attributed to nitric acid formation (Section 2.4.2.2). Likewise, nitrous acid and nitric acid were both considered to play significant roles in the alteration of limestones exposed to the ambient atmosphere in Athens (Deloupolou and Sikiotis, 1992) (Section 2.4.2.1). In addition, nitrogen dioxide was shown to increase the uptake of SO_2 by limestones due to the catalysing role played by the former gas in oxidising $CaSO_3.½H_2O$ to $CaSO_4.2H_2O$ (Johannson *et al.*, 1988) (Section 2.4.2.3).

CHAPTER 3: SULPHUR AND NITROGEN IN THE ATMOSPHERIC ENVIRONMENT

3.1 Introduction

The oxides of carbon, sulphur and perhaps nitrogen will cause a degree of alteration to building stones. The levels of these oxides present in the urban atmosphere have increased steadily due to increased industrial activity. The rise in the concentration of carbon dioxide is suspected to be a major contributor to the increase in mean surface temperature at the earth's surface. Carbon dioxide dissolves in the water droplets to produce a dilute solution of carbonic acid that can react with calcareous stones. However, carbon dioxide is not normally regarded as an atmospheric pollutant due to the relatively high naturally occurring concentrations.

Anthropogenically produced sulphur dioxide is considered to be an important air pollutant. Concentrations in the urban environment have progressively decreased in the United Kingdom due to legislation introduced in the 1950's, which augmented the trend towards gas and electric domestic heating. Large amounts of sulphur dioxide continue to be released from power generating stations that consume oil or coal. This chapter will illustrate; the nature of sulphur dioxide sources, the transport processes through the atmosphere and eventual removal mechanisms. These aspects will also be discussed for nitrogen oxides although their exact role in stone deterioration, as was shown in Chapter 2, is much less well understood.

3.1.1 Global Sulphur Emissions

Most sulphur released naturally into the global atmosphere is in the form of organic or hydrogen sulphides which may be oxidised to sulphur oxides. Methods of estimating the natural emissions include calculating the difference between estimated total dry and wet depositions and anthropogenic emissions (Robinson and Robbins, 1968). Estimates of sulphur released globally into the atmosphere from natural and anthropogenic sources are shown in Table 3.1 to vary widely. For example, the amount of sulphur, as sulphur dioxide, released from anthropogenic sources (73×10^6 tonnes a^{-1}) was estimated by Fergusson (1982) to be twice that determined by natural sources (37×10^6 tonnes a^{-1}),

Table 3.1 Estimated natural and anthropogenic global sulphur emissions

	Source	Flux (10^6 tonnes S a^{-1})	Reference
Natural	Volcanic activity, (SO_2) Biological activity (H_2S)	37 92	Fergusson (1982)
Anthropogenic	Combustion (SO_2) Chemical industry (H_2S)	73 3	
Total		**205**	
Natural	Volcanic (H_2S and SO_2) Biogenic (from land) Biogenic (from sea)	10 33 35	Brimblecombe (1986)
Anthropogenic	N.D.	N.D.	
Total		**78***	
Natural	Volcanic (total S) Soil microbes (H_2S) Sea biota (H_2S) Sea spray aerosol (SO_4^{2-})	2 65 55 44	Bowen (1979)
Anthropogenic	Coal combustion Oil combustion	42 4	
Total		**210**	

N.D. Estimate not presented in Reference. * Total excludes anthropogenic input

whereas Bowen (1979), estimated that the amount of SO_2 released from anthropogenic combustion sources was more than twenty times the total sulphur released from volcanic sources.

Recent investigations have attempted to quantify the nature of the reduced sulphur compound sources. For example, Harrison *et al.* 1992 showed that the amount of dimethylsulphide released from the inter-tidal areas of the North Sea was relatively small (0.002×10^6 tonnes S a^{-1}) compared to the amount released from the total surface area of the North Sea (0.2×10^6 tonnes S a^{-1}).

On the basis of the amount of sulphur dioxide released per unit area of the earth's surface, the effect of sulphur dioxide, released from anthropogenic sources, is proportionally more damaging to building materials, compared to natural emissions. For example, Dignon (1992) estimated 90% of the total anthropogenic SO_2 is released from industrial areas in the northern hemisphere. The role of the reduced forms of sulphur (H_2S and $(CH_3)_2S$) in the building stone deterioration process has not been considered

by investigators to the same degree as the oxidised form. However, the reduced gases are unlikely to react on the stone surface to produce hydrogen ions, and therefore are expected to make an insignificant contribution to the overall stone deterioration process.

Anthropogenic sulphur dioxide emissions are calculated from a knowledge of some, or all, of the following:

- sulphur content (%) of the fuel combusted (sulphur content for a range of fuels is presented in Table 3.2)
- amount of fuel consumed (tonnes of fuel consumed per year)
- amount of material not retained by pollution control system (kg of dust per tonne of fuel burned)
- sulphur content in dust emitted (mg S kg^{-1} dust)
- type of furnace or boiler

For petroleum products, most of the sulphur will be released during combustion. The amount of sulphur retained following coal combustion depends on whether the coal is being burned by industrial or domestic burners. For example, the ash remaining after lignite coal has burned in industrial units will retain about 10% of the original sulphur content, whereas 25% will be retained in domestic consumption. Other industrial processes such as steel making, gas production and some lime kilns retain larger amounts of sulphur (Semb, 1978).

The historical increase in global sulphur dioxide emissions as a function of industrial activity is shown in Table 3.3. For the three main emission sources considered; coal, petroleum and non-ferrous ores, the increase is proportionally greatest for the petroleum source, reflecting the increase in demand from industries which require petroleum as a raw material. Such industries include the chemical, automobile and power generation industries.

3.1.2 Present U.K. sulphur anthropogenic emissions

The change in sulphur dioxide emissions, as a function of source, for the period 1970 to 1991 is presented in Table 3.4. The total emissions are reported within 10 to 15

Table 3.2 Sources and percentage of sulphur content in a range of fossil fuels.

Source	Fuel	End use	Percentage Sulphur by weight	Reference
Coal*	Coal**	Industrial and public utility	2.4	Cullis and Hirschler (1980)
		Domestic and small industry	2.5	Cullis and Hirschler (1980)
		Metallurgical industry	0.9	Cullis and Hirschler (1980)
Gas from North Sea	Natural Gas	Domestic	<0.01†	Cullis and Hirschler (1980)
Gas from Astrakhan (USSR)		Sulphuric acid production	25	Heaton (1986)
Crude oil‡	Petrol U.K.	Leaded	0.04	Cullis and Hirschler (1980)
	Petrol U.S.	Leaded Unleaded	0.10 0.15	Kirk-Ohmer (1982)
Crude oil	Diesel U.K.‡‡	City Buses	0.12	Cullis and Hirschler (1980)
		Lorries	0.24	Cullis and Hirschler (1980)
		Railway engines	0.32	Cullis and Hirschler (1980)
		Ships	0.45	Cullis and Hirschler (1980)
	Diesel U.S.	Small trucks	0.5	Kirk-Ohmer (1982)
Crude oil	Petroleum coke	Steel industry	2.25	Cullis and Hirschler (1980)

* The amount of sulphur in coal may range from 0.5 to 5% (Francis and Peters, 1980).
** Sulphur exists in coal in both an inorganic form (e.g. iron pyrites) and as an organic form (e.g. thiophene, 2,3 benzothiophene and dibenzothiophene) Hessely *et al.*, (1982)
† Mercaptans ($\approx$0.01%) are added to natural gas to act as odourising agents (Francis and Peters, 1980).
‡ The sulphur content for a selection of crude oils is as follows; Arabian light (2.99%), Iranian heavy (2.50%), Kuwait (4.11%) and Arabian heavy (4.19%) (Kirk-Ohmer, 1982).
‡‡ The sulphur content of diesel fuel in the U.K. is controlled by the requirements of EC Directive 87/219/EEC, which limits the sulphur content of fuel to 0.3% by weight. A recent amendment to this directive aims to reduce the sulphur content to 0.05%. (QUARG, 1993)

percent of the true values. The 1991 emission total can be seen to be about 56 per cent of that estimated for 1970. This decrease has been attributed to reductions in the amount of sulphur dioxide released by domestic emission sources (a percentage decrease of 75%) and other industrial sources (a percentage decrease of 75%). These percentages represent reductions of 0.39×10^6 and 1.71×10^6 tonnes a^{-1}, respectively.

Road transport is the only source category that has experienced an increase in the amount of sulphur dioxide emitted. The fifty percent increase observed is attributed to

Table 3.3 The historical increase in global anthropogenic sulphur dioxide emissions (10^6 tonnes SO_2 a^{-1})

Emission source	1880[a]	1910[a]	1930[a]	1950[a]	1960[a]	1965[a]	1980[b]
Coal	12.2	42.1	51.3	66.0	95.7	102.0	
Petroleum	0.1	0.7	3.1	8.3	19.9	28.5	
Non-ferrous ores	0.3	3.7	4.9	7.4	12.3	12.9	
Other			0.7	1.4	2.2	2.7	
Total	12.5	46.5	60.0	83.1	130.1	148.9	100-220

(Cullis and Hirschler, 1980)[a]
(Dignon, 1992)[b]

Table 3.4 Amount of sulphur dioxide released from various sources in 1970 and 1991 in the United Kingdom (Digest of Environmental Protection and Water Statistics, 1993).

	$SO_2 \times 10^6$ tonnes a^{-1}			
Source type	1970	% of total	1991	% of total
Domestic	0.52	8	0.13	4
Commercial/public service	0.26	4	0.08	2
Power stations	2.91	45	2.53	71
Refineries	0.21	3	0.12	3
Agriculture	0.04	1	0.008	0
Other industry	2.28	35	0.57	16
Railways	0.03	0	0.003	0
Road transport	0.04	1	0.06	2
Civil aircraft	0.001	0	0.002	0
Shipping	0.13	2	0.06	2
Total	6.42	100	3.57	100

the increased consumption of diesel fuel which has a higher sulphur content than petrol (Table 3.2).

The amount of sulphur dioxide emitted from electricity generating power stations has decreased by 13 percent (0.38×10^6 tonnes a^{-1}). However, the proportion of sulphur dioxide released from high flue stacks has increased compared to other sources. An EC Directive, 88/609, aims to reduce the emissions from this source. For example, by 1993 existing combustion installations with a capacity greater than 50 megawatts

(including power stations, refineries and a proportion of the "other industry" category) are required to reduce emissions by 20 percent compared to 1980 levels. By 1998 and 2003, reductions of 40 and 60 per cent, respectively, are required. The emissions from the large combustion stations in 1991 have reached the required level (a 23% reduction was obtained).

3.1.3 Global Nitrogen emissions

The global nitrogen cycle has been described by Söderlund and Roswell (1982), as existing in four subcycles, with minimum interchange occurring between each subcycle. These are:

a) NO_x and compounds related to NO/NO_2

b) ammonia/ammonium compounds

c) N_2/N_2O

d) organic nitrogen compounds

Total global emissions from subcycle a) have been estimated to range from 49 to 109 $\times 10^6$ tonnes a^{-1} by Söderlund and Roswell (1982). The individual source components are shown in Table 3.5. The Organisation for Economic Cooperation and Development (OECD) (1991) estimated the NO_x emissions for member countries in 1987 to be 36.2 $\times 10^6$ tonnes a^{-1} of which 17 $\times 10^6$ tonnes a^{-1} were attributed to motor vehicle emissions. Walsh (1990) estimated the 1980 global motor NO_x emissions to be 25.5 $\times 10^6$ tonnes a^{-1} and predicted a decrease to 19 $\times 10^6$ tonnes a^{-1} by 2000, due to improved control technology in the Western developed countries. However, a return to the 1980 levels could occur by 2015, as the developing world continues to industrialise.

3.1.4 Present U.K. nitrogen anthropogenic emissions

The estimation of nitrogen oxide emissions is less accurate than for sulphur dioxide emissions because the calculations are based on relatively few measurements and combustion conditions can vary widely. Consequently, estimated nitric oxide emissions are accurate to only 30% (Digest of Environmental Protection and Water Statistics, 1993). Almost all the oxidised nitrogen released from combustion processes is in the

Table 3.5 Estimates for global nitrogen oxide emissions (Söderlund and Roswell, 1982)

Source	Emission source 10^6 tonnes a^{-1}
Soils	3-33
Lightning strokes	10-40
Anthropogenic sources	19
Forest fires	17

form of nitric oxide, NO, which at ambient temperatures is oxidised to nitrogen dioxide. The nitrogen oxides emissions in the U.K. are presented in Table 3.6 as a function of source, for the period 1970 to 1991.

Table 3.6 Amount of nitrogen oxides released from various sources in 1970 and 1991 in the United Kingdom (Digest of Environmental Protection and Water Statistics, 1993)

	$NO_x \times 10^6$ tonnes a^{-1}			
Source type	1970	% of total	1991	% of total
Domestic	0.07	3	0.07	3
Commercial/public service	0.06	2	0.06	2
Power stations	0.84	37	0.72	26
Refineries	0.04	2	0.04	1
Agriculture	0.008	0	0.004	0
Other industry	0.45	20	0.22	8
Offshore oil and gas	0.003	0	0.05	2
Railways	0.05	2	0.03	1
Road transport	0.61	27	1.40	51
Civil aircraft	0.005	0	0.01	1
Shipping	0.16	7	0.13	5
Total	2.29	100	2.73	100

During the twenty one year period the power station and "other industry" sources decreased significantly, by 0.12×10^6 and 0.23×10^6 tonnes per year, respectively. The road transport source has increased by approximately 56% to become the major contributor to U.K. emission sources.

3.2 Reactions, transport and removal mechanisms

Following release into the atmosphere sulphur and nitrogen oxides may be deposited directly under wet or dry conditions or, following a series of oxidation reactions, form sulphate and nitrate compounds. These oxidised species are then removed by the same deposition processes as the precursor gases. The rate of sulphate or nitrate formation will depend mainly on the availability of oxidants and the relative humidity.

The two principal mechanisms by which gases and particulate matter are returned to the ground are:

a) Wet deposition

Wet deposition involves the incorporation of a pollutant into precipitation. It is calculated as a function of precipitation amount and concentration of a pollutant in the precipitation.

b) Dry deposition

Dry deposition is the removal and retention of a pollutant by a surface. This collecting surface can be vegetation, buildings or water. Removal mechanisms include sedimentation and diffusion processes. Dry deposition is measured by the deposition flux, which is the product of atmospheric concentration and deposition velocity.

3.2.1 Atmospheric reactions of sulphur and nitrogen oxides

Knowledge of the mechanisms by which sulphur and nitrogen oxides are oxidised in the atmosphere will facilitate understanding of how the pollutants will eventually be returned to the earths' surface. Sulphur and nitrogen oxides, if not removed by dry deposition or incorporated into cloud or water drops, may form sulphate and nitrate aerosol. Nitrogen oxides can, in addition, react to form significant amounts of gaseous nitrate. The three main mechanisms by which sulphur dioxide is oxidised include:

- direct oxidation in the gas phase,
- oxidation of dissolved SO_2 in water droplets,
- oxidation of adsorbed SO_2 on solid insoluble particles.

Oxidation of nitrogen dioxide and nitric oxide appear to occur chiefly in the homogeneous phase.

3.2.2 Homogeneous sulphur and nitrogen oxidations in the atmosphere

3.2.2.1 Background to photochemical processes

The homogeneous phase reactions are dependent on photochemical processes which occur in the atmosphere. These photochemical reactions provide the energy necessary to form reactive intermediates. The troposphere has an absence of radiation of less than 300 nm resulting from the absorption of shorter wavelengths in the stratosphere. Tropospheric ozone provides a central role in the atmospheric reactions due to the formation of the reactive hydroxyl radical, OH•, at radiation wavelengths less than 315 nm.

$$O_3 + h\nu \rightarrow O(^1D) + O_2 \quad \text{Equation 3.1}$$

$$O(^1D) + M \rightarrow O(^3P) + M \quad \text{Equation 3.2}$$

$$O(^1D) + H_2O \rightarrow 2OH\cdot \quad \text{Equation 3.3}$$

where M designates any other gaseous molecule that collides with the newly formed molecule removing excess energy released when the new bond has been formed.

Cox (1984) suggests that most (~70%) of the hydroxyl radical in a nonpolluted atmosphere will react with carbon monoxide and the remainder with methane. The hydroxyl radical can also oxidise sulphides to sulphur dioxide. The chemistry of OH• in polluted atmospheres is more complex. In polluted air containing high hydrocarbon levels, organoperoxy, RO_2•, species can be produced as part of photochemical smog formation.

3.2.2.2 Homogeneous oxidation of sulphur dioxide

The homogeneous oxidation of SO_2 by reactive intermediates generated photochemically may produce substantial amounts of atmospheric sulphate. The reaction can be represented as:

$$OH\cdot + SO_2 + M = HOSO_2\cdot + M \quad \text{Equation 3.4}$$

The rate constant, k, for this reaction was estimated by Calvert *et al.* (1978) to be

$1.1 \pm 0.3 \times 10^{-12}$ cm^3 mol^{-1} s^{-1}.

The importance of the reaction between SO_2 and OH· in a polluted atmosphere, compared to reaction between SO_2 and other radical species, was illustrated by Eggleton and Cox (1978). Table 3.7 presents radical concentrations, rate constants and oxidation rates per hour.

The portion of SO_2 oxidised by OH· will decrease with increasing latitude and time of year. For example, Altshuller (1979) estimated that the fraction of SO_2 oxidised by OH· will decrease from 81% at latitude 25°N to 74% at 65°N due to more hydroxyl radical being produced at the lower latitudes. Figure 3.1 illustrates the relative reaction rates for the homogeneous oxidation of SO_2 by OH·, HO_2· and CH_3O_2· and shows how the efficiency increases during the summer months.

Table 3.7 Calculated homogeneous oxidation rates for SO_2 in the presence of a range of potential oxidants (Adapted from Eggleton and Cox, 1978)

Oxidant	Atmospheric concentration molecules cm^{-3}	Rate constant cm^3 $molecule^{-1}$ s^{-1}	Oxidation rate for SO_2 % hr^{-1}
OH·	7.1×10^6	$0.5\text{-}1.0 \times 10^{-12}$	1.2-2.5
HO_2·	2.6×10^9	9×10^{-16}	0.84
CH_3O_2·	2.2×10^9	$\leq 10^{-15}$	≤ 0.8
Total RCO_2· excluding HO_2· and CH_3O_2·	5.1×10^9	$\leq 10^{-15}$	≤ 1.84
O_3	4.2×10^{12}	$\leq 10^{-23}$	3.5×10^{-8}
NO_3	1.4×10^8	$\leq 7 \times 10^{-22}$	1.0×10^{-6}
N_2O_5	7.6×10^{10}	$\leq 4 \times 10^{-23}$	1.4×10^{-8}

Key:
* The artificial atmosphere contained the following gases:
NO 20 ppb NO_2 20 ppb SO_2 100 ppb CO 1000 ppb CH_4 1500 ppb C_2H_5 100 ppb
Solar intensity simulated for 50°N

Eggleton and Cox (1978) have described the results of an isotopic labelling experiment, using ^{35}S, to show that the $HOSO_2$· free radical reacts further to form a sulphate bearing aerosol.

The first part of this sequence may be the reaction of $HOSO_2$· and oxygen:

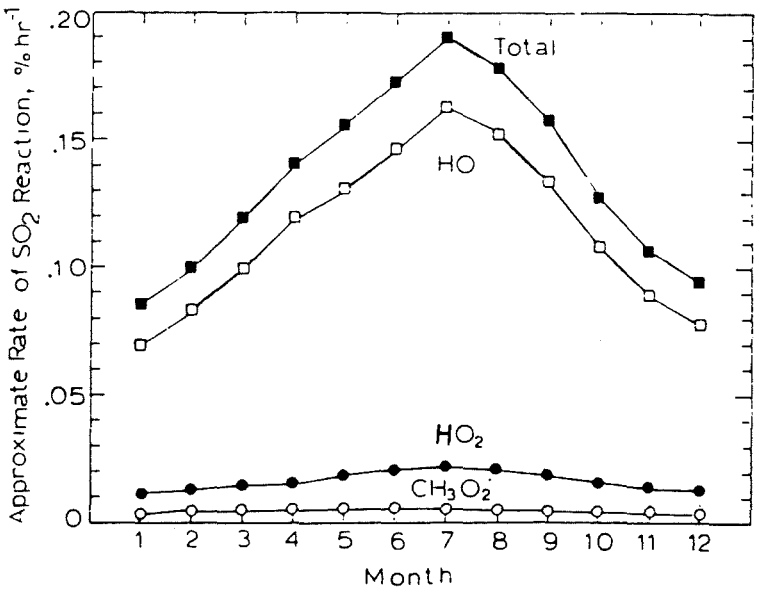

Figure 3.1 Theoretical monthly average of the rate of SO_2 oxidation in the presence of HO, HO_2 and CH_3O_2. (From Calvert *et al.*, 1978)

$$HOSO_2\cdot + O_2 \rightarrow HOSO_2OO\cdot \quad \text{Equation 3.5}$$

Subsequent reaction with NO, which may be present, produces another free radical; $HOSO_2O\cdot$:

$$HOSO_2OO\cdot + NO \rightarrow HOSO_2O\cdot + NO_2 \quad \text{Equation 3.6}$$

which can form sulphuric acid by abstracting a hydrogen atom from a hydrocarbon, aldehyde, or another H-containing species such as $HO_2\cdot$.

Other homogeneous reaction mechanisms, which are theoretically possible but not likely to occur in the troposphere, are oxidation by intermediates produced in thermal reactions and direct photo-oxidation of SO_2 (Eggleton and Cox, 1978). Experimental evidence that nitric oxide and low concentrations of olefinic hydrocarbons strongly influence the gas phase oxidation of sulphur dioxide was first provided by Cox and Penkett (1971).

Although the hydroxyl radical is the dominant photochemical oxidant, the degree of dominance will vary in a polluted atmosphere depending on the time of day. For example, the hydroxyl radical will dominate during the early morning hours but as the

peroxy radicals, $HO_2\cdot$ and $RO_2\cdot$, are formed the SO_2-OH reaction will only account for between 25 and 33 per cent of the overall homogeneous oxidation reaction rate for SO_2 (Altshuller, 1979).

3.2.2.3 Homogeneous oxidation of nitrogen oxides

As mentioned in Section 3.1.3 nitric oxide, NO, is the principal oxide of nitrogen released into the atmosphere as the result of combustion processes. The subsequent reaction pathways leading to oxidation and eventual removal are illustrated in Figure 3.2.

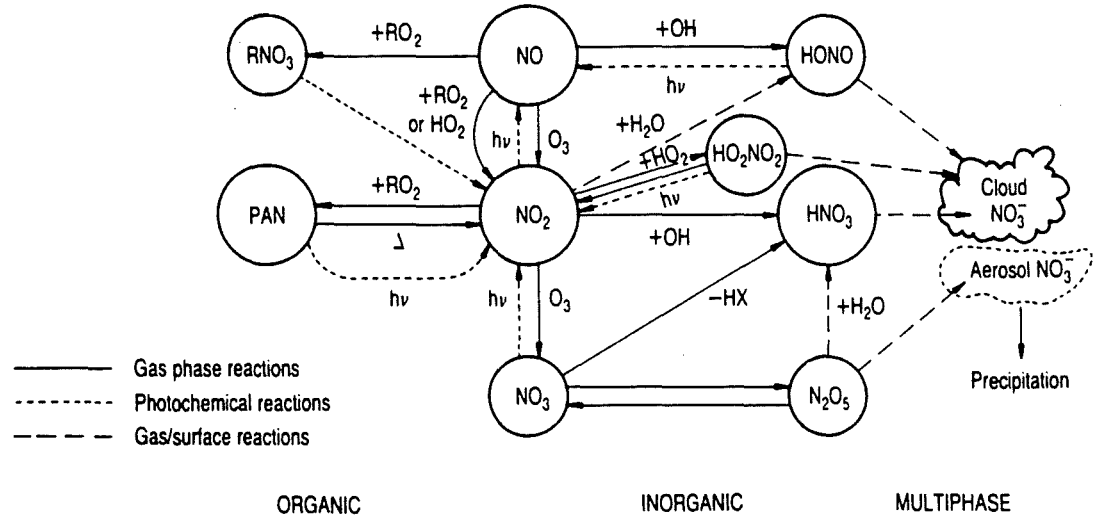

Figure 3.2 A summary of the interactions between the various atmospheric nitrogen species. (Photochemical Oxidants Review Group, 1990).

The oxidation of NO by ozone is considered the main oxidation route to NO_2. Brimblecombe (1986) has calculated production rates for NO_2 to be 3.8×10^{10} molecules cm^{-3} s^{-1}. This was assuming NO and O_3 concentrations to be 80 ppb and 40 ppb (1.1×10^{12} and 2.2×10^{12} molecules cm^{-3} respectively, assuming that 1 cm^3 of gas contains 2.7×10^{19} molecules) and a rate constant of 1.8×10^{-14} cm^3 $molecules^{-1}$ s^{-1}.

However, in the presence of light with a wavelength less than 310 nm, NO may be regenerated due to photodissociation. An equilibrium situation occurs, leading to the

establishment of a photostationary state, which can be described by the photochemical state number, φ, (Stedman and Jackson, 1975).

$$\varphi = \frac{J\,[NO_2]}{k\,[NO]\,[O_3]} \quad \text{. . . . . Equation 3.7}$$

where k = reaction rate constant

J = photodissociative constant.

At the photostationary state, φ is equal to 1.

With increasing solar intensity, J will increase leading to the production of NO and O_3. Continuous measurement of NO and O_3 concentrations for a given day in a polluted atmosphere shows that NO increases more rapidly than O_3 during the early part of the day. The NO level will have peaked about mid-morning, with the ozone concentration peaking a few hours later as the concentration of hydrocarbons, RH, and peroxy radicals $RO_2\cdot$, increases. The presence of the hydrocarbons and peroxy radicals provides a reaction pathway to oxidise NO without consumption of O_3 (Equation 3.8). The nitrogen dioxide produced can then be photolysed to produce oxygen atoms (Equation 3.9) which can react with molecular oxygen to produce ozone (Equation 3.10).

The reaction scheme can be summarised as:

$$RO_2\cdot + NO \rightarrow NO_2 + RO\cdot \quad \text{. . . . . Equation 3.8}$$

$$NO_2 + h\nu \rightarrow NO + O\cdot \quad \text{. . . . . Equation 3.9}$$

$$O\cdot + O_2 + M \rightarrow O_3 + M \quad \text{. . . . . Equation 3.10}$$

where M is an inert third body

The main gaseous phase source of HNO_3 is oxidation of NO_2 by the hydroxyl free radical:

$$NO_2 + OH\cdot + M \rightarrow HNO_3 + M \quad \text{. . . . . Equation 3.11}$$

The rate of formation for HNO_3 is relatively fast compared to the oxidation of SO_2 by OH·. A percentage conversion of 9.9% hr^{-1} (1.5 ppb hr^{-1}) has been calculated by Harrison (1990), on the basis of:-

a reaction constant of 1.1×10^{-11} cm^3 $molecules^{-1}$ s^{-1},

$[OH\cdot] = 2.5 \times 10^6$ molecules cm^{-3}, $[NO_2] = 4.05 \times 10^{11}$ molecules cm^{-3}.

Harrison and Allen (1990) determined mean 7 day averages for HNO_3 concentrations of 0.67 $\mu g\ m^{-3}$ (0.24 ppb) for a semi-rural area in south-east England between the months of August and November 1986. A peak day-time HNO_3 concentration of 8 ppb at this sampling site was reported by Harrison and Kitto (1992). This was attributed to the meteorological conditions during the summer of 1989 (stagnant air and high temperatures) which would have facilitated the production of photochemical oxidants.

Reported HNO_3 concentrations in clean air and mid-latitude regions range are in the range 0.15-0.18 ppb (Huebert and Lazrus, 1979). Calvert and McQuigg (1975) estimated, in model calculations, that HNO_3 could be formed at the rate of 12 ppb hr^{-1} under typical conditions associated with urban photochemical smog. Levine and Schwartz (1982) suggest that on a global basis most of the gaseous nitrate will exist as nitric acid with peroxyacetylnitrate making significant contributions in polluted atmospheres.

3.2.3 Heterogeneous sulphur and nitrogen oxidations in the atmosphere

The heterogenous oxidation of sulphur and nitrogen oxides requires an additional phase, such as water or a solid medium, to assist the oxidation process. Once incorporated into the water droplet, oxidising agents such as hydrogen peroxide or ozone will oxidise sulphur dioxide to sulphate, with or without the presence of metal catalysts. This section will describe the physical and chemical changes that occur as sulphur dioxide and nitrogen oxides are oxidised to sulphate and nitrate, respectively.

3.2.3.1 Incorporation of sulphur and nitrogen into water droplets

The amount of sulphur dioxide removed by water in the atmosphere, either by cloud water (liquid water or snow flakes) or by precipitation is a function of the initial pH of the rain, raindrop size, concentration of pollutant in the atmosphere and temperature. The uptake of SO_2 will be reversible when no oxidants are present in the water droplets which absorb the gas from the air (Hales, 1978). The rate at which falling droplets absorb gases is also controlled by diffusion of the gas from the atmosphere to the droplet surface and mixing inside the droplet. Beilke and Gravenhorst (1978) calculated,

using the appropriate equations for molecular diffusion and turbulent transfer, that sulphur dioxide would be incorporated into water and fog droplets within one minute (this absorption rate was determined for droplets with diameters less than 50 μm).

The uptake of sulphur dioxide by water droplets will also depend on the hydrogen ion concentration present in the drop, with low pH values inhibiting the uptake of gaseous SO_2. This observation can be explained by examining the behaviour of the three unoxidised forms of sulphur (IV) ($SO_2.H_2O$, HSO_3^- and SO_3^{2-}) in solution. For example, when pH is low (for values < 1), the sulphur, existing as S(IV), will occur as $SO_2.H_2O$. This will inhibit the uptake of SO_2 by a water droplet. For pH values ≥ 2 the sulphur will exist mainly as HSO_3^-. At pH values greater than 7, the sulphur will be present as SO_3^{2-}. At the higher pH values fresh SO_2 can be absorbed by the raindrop. The pH dependence of S(IV) is presented in Figure 3.3.

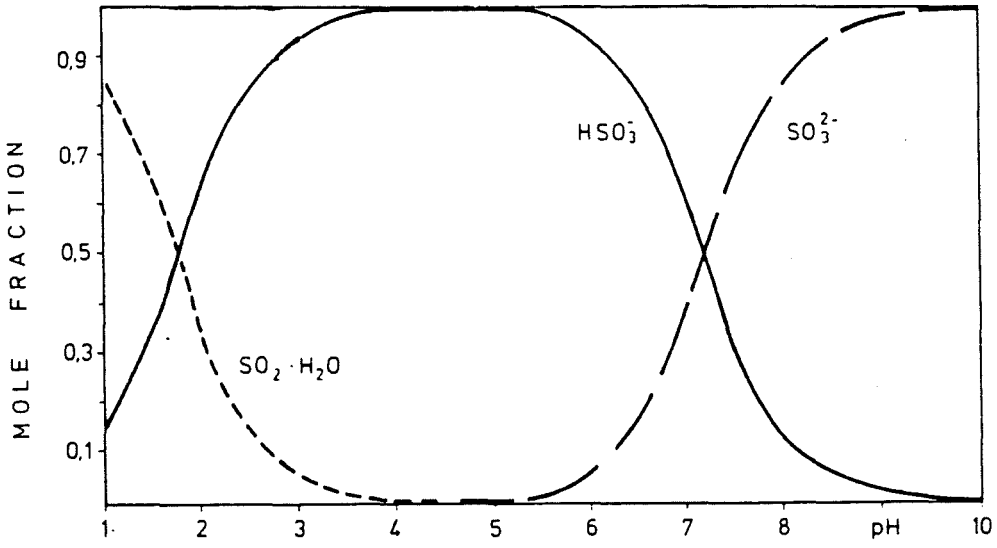

Figure 3.3 Mole fraction of sulphur (IV) species in equilibrium at 25°C as a function of aqueous solution pH (Beilke and Gravenhorst, 1978)

Theoretically, sulphur dioxide can be expected to reduce the pH of rain water droplets to 4.6. This is due to the higher solubility and associated dissociation constant of sulphur dioxide which releases more hydrogen ions than the corresponding atmospheric carbon dioxide. At this low pH the presence of hydrogen ions will inhibit further uptake of sulphur dioxide. The presence of ammonia will raise the pH and permit more sulphur dioxide to be incorporated into the raindrop. Under normal atmospheric conditions (pH 3-6) the most prominent form of S(IV) in water droplets will be HSO_3^-. However, an

oxidation mechanism proposed by Beilke and Gravenhorst (1978) suggested that SO_3^{2-} is the oxygen carrier in the oxidation and not the more abundant HSO_3^-.

Methods to measure the production rate of sulphate in both warm and ice crystal clouds were determined by Hegg and Hobbs (1981). The warm cloud water droplets were collected using an aerosol centrifuge, whereas the ice crystals were collected on a polythene coated aluminium rod exposed to the airstream from an aircraft. Altogether four methods (Hegg and Hobbs, 1981) have been described to measure the production of sulphate in the cloud;

a) observation of changes in cloud condensation spectra,

b) observation of changes in total particle volume due to cloud passage,

c) determination of particulate sulphate concentrations upwind and downwind of wave clouds and stationary low-lying stratus clouds

d) measurement of sulphate concentrations in cloud water collected at the leading and trailing edges of wave clouds.

Significant amounts of excess sulphate, that is, above ambient sulphate levels, were measured in those cloud samples collected from relatively long-lived low level stratiform clouds. The calculated oxidation rates were found to be much higher than homogeneous oxidation rates. In addition, the sulphate production in the cloud droplets was found to decrease with time, suggesting that the concentration of the oxidising agent (hydrogen peroxide) also decreased during the measurement period. Methods to determine the hydrogen peroxide concentration are presented in Section 3.2.3.2.

The scavenging efficiency of sulphate aerosol as a function of cloud location was discussed by Barrie (1985). Clouds found in tropical rain storms were expected to retain the solute within the actual cloud droplets as the cloud water was converted to precipitation, whereas clouds located in northern latitudes would release the sulphate back into the atmosphere when cloud water is transferred by evaporation into the ice phase (Bergeron process). Barrie suggests that in the absence of other processes this would mean that the pollutant concentration in warm clouds would be much higher than in frozen hydrometeors in the upper reaches of a well mixed cloud. However, the capture of supercooled cloud droplets on ice droplets by contact freezing or capture of

particles by ice crystals would have a compensatory effect.

Sulphate, existing as ammonium sulphate aerosol, will be incorporated quickly into the aqueous phase. This is due to the size, solubility and hygroscopic nature of the sulphate aerosols which act as condensation nuclei. Georgii (1971) determined that the particles exist in the size range, 0.02-0.5 μm. The condensing water vapour will enable the nuclei to grow into a cloud droplet having a radius in the size range, 5-20 μm (Garland 1978). Other physical processes to remove sulphate particles include diffusophoresis, Brownian motion and impaction by raindrops.

The uptake of NO_2 by water has been considered in detail by Lee and Schwartz (1981). From a series of laboratory experiments the reaction was found to proceed as follows:

$$2NO_2(g) + H_2O(l) \rightarrow 2H^+ + NO_3^- + NO_2^-$$

. . . .Equation 3.12

The second order rate constant, k_1, and Henry's Law constant, K_H, at 22°C, were determined to be $1.0 \pm 0.1 \times 10^8$ M^{-1} s^{-1} and $7.0 \pm 0.5 \times 10^{-3}$ M atm^{-1}, respectively. Lee and Schwartz (1981) consequently calculated a hypothetical residence time of approximately 1 year for NO_2 existing in clouds, without the presence of other oxidants. This would obviously suggest that the reaction NO_2 with cloud water is an inefficient removal mechanism compared to the gas phase reaction (Section 3.2.2.3 showed that the rate of removal of NO_2 by reaction with a concentration of hydroxyl radical of 2.5×10^6 molecules cm^3 was approximately 10% hr^{-1}).

Methods of quantifying removal of pollutants by atmospheric water will be discussed in Section 3.2.5.

3.2.3.2 Sulphur dioxide oxidation in the presence of hydrogen peroxide and ozone

The oxidants, hydrogen peroxide and ozone, required to oxidise sulphur dioxide, in either cloud or rain water, are formed in the gas phase. The formation of hydrogen peroxide in the gas phase involves reaction of hydroperoxy and hydrated hydroperoxy radicals (McElroy, 1986). The reactions can be represented by Equations 3.13 to 3.15.

$$HO_2\cdot + HO_2\cdot \rightarrow 2H_2O_2 \quad \text{. . . . . Equation 3.13}$$

$$HO_2\cdot + H_2O \rightleftharpoons H_2O.HO_2 \quad \text{Equation 3.14}$$

$$HO_2\cdot + H_2O.HO_2 \rightarrow 2H_2O_2 + H_2O \quad \text{Equation 3.15}$$

In polluted atmospheres there is strong competition for the HO_2 radicals by NO:

$$HO_2\cdot + NO \rightarrow NO_2 + OH\cdot \quad \text{Equation 3.16}$$

Hence, the relatively high concentrations of NO_x, hydrocarbons, and aldehydes associated with urban and industrial areas tend to favour O_3 production (a summary of possible reactions involving constituent parts of an urban atmosphere were presented by Equations 3.8 to 3.10), whereas the lower NO_x levels found in rural and the more remote troposphere, tend to favour H_2O_2 production.

Laboratory studies, such as those conducted by Penkett *et al.* (1979) to evaluate the oxidation rates of sulphur dioxide in the presence of oxygen, ozone and hydrogen peroxide, have shown that the oxidation of S(IV) in the aqueous phase occurs chiefly by reaction with hydrogen peroxide for the range of pH found in atmospheric aqueous solutions.

Penkett *et al.* (1979) determined the rate of sulphate formation in the presence of oxygen, ozone and hydrogen peroxide; initial reactant concentrations were 5 ppb SO_2, 50 ppb O_3 and 1 ppb H_2O_2. The oxidation rates can be seen to increase as pH increases (Figure 3.4). The rate of formation for sulphate (3.1×10^{-4} μg ml^{-1} min^{-1}), predicted at pH 5, in the presence of oxygen would take five days to reach a cloud water sulphate concentration of 2.2 μg ml^{-1}. At the same pH, oxidation by ozone would produce the same concentration in ten minutes (rate of formation 0.24 μg ml^{-1} min^{-1}). Oxidation by hydrogen peroxide, at pH 5, was calculated to reach this concentration within two minutes (rate of formation 1.1 μg ml^{-1} min^{-1}).

The greater reactivity of H_2O_2 towards SO_2 compared to ozone has also been demonstrated by Scire and Venkatram (1985), who showed less than 0.01% and 97% of the initial H_2O_2 and O_3 concentrations remained after twenty minutes of reaction time. Conversely, the oxidation of SO_2 by H_2O_2 in aqueous aerosols was shown by

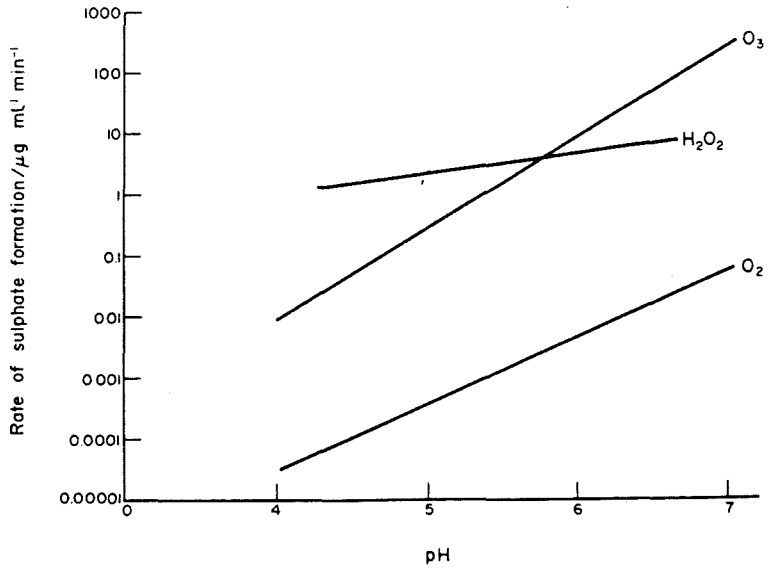

Figure 3.4 A comparison of the atmospheric oxidation rates of SO_2 by O_3, H_2O_2 and O_2 (Penkett *et al.*, 1979)

Saxena and Seigneur (1987) to be significant only at low temperatures, with the increased solubility of SO_2 and H_2O_2 more than compensating for the decrease in rate constant.

A laboratory study by Martin and Damschen (1981) investigated the oxidation of sulphur dioxide by hydrogen peroxide in the pH range 0 to 3 (a pH range suggested by the authors to the reflect the acidity of ammonium hydrogen sulphate aerosols present in the atmospheric environment). The rate of sulphate formation is shown by Equation 3.17:

$$\frac{d\,S(VI)}{dt} = \frac{8.3\times10^4\ [H_2O_2][SO_2.aq]}{0.1 + [H^+]} mole\ l^{-1}s^{-1} \quad \text{Equation 3.17}$$

The derivation of the constant value of 0.1 is presented by Martin and Damschen (1981).

This equation can alternatively be expressed in the form shown by Equation 3.18:

$$\frac{d(SO_4^{2-})}{dt} = 8.3 \times P_{H_2O_2} K_{H_2O_2} P_{SO_2} K_{SO_2} \; mole \; l^{-1} \; s^{-1} \; . \quad \text{Equation 3.18}$$

where: K_{SO_2} and $K_{H_2O_2}$ represent the Henry's Law constants: 1.23 mole^{-1} l^{-1} atm^{-1} and 7.1×10^4 mole l^{-1} atm^{-1} for SO_2 and H_2O_2 respectively.
$P_{H_2O_2}$ and P_{SO_2} represent the partial pressures of hydrogen peroxide and sulphur dioxide.

For a 1 ppb concentration of H_2O_2 in the gas phase, the rate of sulphate formation was calculated to be 1.8μg SO_4^{2-} ml^{-1} aerosol min^{-1}. In a typical cloud containing 0.3 ml m^{-3} liquid and a sulphur dioxide concentration of 14 μg m^{-3} (5 ppb) this would result in a 3% min^{-1} conversion of sulphur dioxide to sulphate.

Production of H_2O_2 within cloud water droplets was presumed by McElroy (1986) to occur by the disproportionation of OH· and HO_2· radicals. The HO_2· radicals in cloud water are derived mainly from gas phase scavenging. An important influence on the generation of H_2O_2 is the removal of the HO_2· radical by ozone. McElroy (1986) suggested caution in utilising some sulphur dioxide oxidation models in the aqueous phase since they assume an initial hydrogen peroxide concentration of 1ppb which is too high. Realistic oxidation rates, using hydrogen peroxide, were assumed to oxidise less than ten per cent of the total mass of sulphur dioxide.

Atmospheric gaseous and aqueous concentrations of hydrogen peroxide are presented in Table 3.8. The highest atmospheric concentrations of hydrogen peroxide are found in tropical areas of the world where high solar radiation and low anthropogenic emissions should allow the species to accumulate (Jacob *et al.*, 1990).

Kok (1980) calculated the aqueous phase concentration resulting from a cloud containing 1 ml of water m^{-3} and an atmospheric concentration for H_2O_2 of 2 ppb (3μg m^{-3}) to be 3000 ppbw. However, the measured aqueous phase concentration resulting from a similar cloud content and atmospheric concentration was almost 50% less at 1590 ppbw. Kok (1980) attributed this observation to possible reactions that may be occurring between H_2O_2 and sulphur dioxide or other acidic species. In addition, McElroy (1986) reports that hydrogen peroxide will be detected in rain water only when

Table 3.8 Hydrogen peroxide concentration measured at various locations.

Physical phase	Location and Date	$[H_2O_2]$	Method of measurement	Author
Gaseous	1.Bahia, Brazil Spring 1988 2. Dortmund, Germany Summer 1985, 1986	ppbv Range 0.2-2.87 1.16 Mean Range 0.01-0.54 0.07 Mean	Collection with cryogenic apparatus. Chemiluminescence using TCPO as reagent	Jacob *et al.* 1990
Gaseous	Whiteface Mountain New York State Summer 1986 Whitetop Mountain Virginia State Summer 1986	ppbv Mean 0.7 Number of observations 146 mean 0.8 Number of observation 171	Utilises a dual channel, fluorometric, enzyme-based system to discriminate H_2O_2 from organic peroxides	Meagher *et al.* (1990)
Gaseous	Eastern United States. Autumn 1984	ppbv Range 0.5 to 4.1 Highest in cloud tops above warm air masses.	Dual enzyme fluorimeter	Heikes *et al.* (1987)
Rainwater	1.Bahia, Brazil Spring 1988 2. Dortmund, Germany Summer 1985, 1986	ppbw Range 1860-3840 2450 Mean Range 100-2200 300 Mean	Chemiluminescence using TCPO as reagent	Jacob *et al.* 1990
Rainwater	California Collected during thunderstorm (Feb.'79) Collected following photochemical episode (Jul.'79)	ppbw 1090 1140	Chemiluminescence using luminol(5-amino2,3-dihydro-1,4phtalazonedione as reagent	Kok 1980

TCPO is *bis*-(2,4,6-trichlorophenyl)oxalate

* 1 hour average. Measurement in cloud free conditions

there is an absence of sulphate.

The oxidation of SO_2 by H_2O_2 was found by Fung *et al.* (1991) to be the most significant pathway during light precipitation events. In heavier precipitation events, O_3 was considered to be more important due to the rapid removal of H_2O_2. Ozone is much less soluble in water and due to a higher concentration in the atmosphere is less likely to be causing non-linear effects on the amount of H_2SO_4 produced.

The most reactive form of S(IV) with respect to H_2O_2 in solution has been suggested

by McArdle and Hoffmann (1983) and Kunen *et al.* (1983) to be HSO_3^-. This was attributed to the transition-state complex formed between HSO_3^- and H_2O_2 possessing a water leaving group which is eliminated much more readily than the hydroxide leaving group formed between the $SO_3^{2-}$and H_2O_2.

Hydrogen peroxide availability was shown by Meagher *et al.* (1990) in a field experiment to be a major contributor to the linearity of H_2SO_4 production. For example, at two rural sites in the United States, Whiteface Mountain, New York and Whitetop Mountain, Virginia, both SO_2 and H_2O_2 concentrations were measured. A linear relationship between SO_2 and amount of H_2SO_4 produced was found to exist where $[SO_2] < [H_2O_2]$. However in the plume of a power plant near the source, where $[SO_2] \geq [H_2O_2]$, the relationship was non-linear.

In their study, investigating the role of nitrogen oxides in the oxidation of SO_2, Martin *et al.* (1981) found that a nitrite/nitrous acid mixture oxidised the S(IV) species to S(VI). The stoichiometry of this reaction was found to be:

$$2H_2SO_3 + 2HNO_2 = 2H_2SO_4 + N_2O + H_2O$$

. . . .Equation 3.19

However, Martin *et al.* (1983) concluded that the formation of sulphate and nitrous oxide, N_2O, by this reaction mechanisms did not significantly contribute to ambient concentrations.

3.2.3.3 Sulphur dioxide oxidation in the presence of metals

Transition metal catalysts such as manganese and iron enable molecular oxygen to heterogeneously oxidise S(IV). Reported concentrations in precipitation are presented in Table 3.9 for manganese and iron. The concentrations of manganese can be seen to be an order of magnitude less than the iron concentrations.

Clarke and Radojevic (1987) attempted to relate the kinetics of S(IV) oxidation occurring in rainfall to simultaneously measured concentrations of iron and manganese. The concentrations of SO_3^{2-} determined were in the range from 0.27 to 4.92 $\mu g\ ml^{-1}$

with corresponding SO_3^{2-} to SO_4^{2-} molar ratios in the range 0.18 to 0.94 (mean 0.44), indicating a significant amount of the sulphur in precipitation was still in oxidation state (IV). The first order rate constant for the oxidation of S(IV) reaction was found to be strongly dependent on the iron concentration. However, no significant correlation was found between the rate constant and the manganese concentration.

Table 3.9 Manganese and iron concentrations measured in rainwater

Iron ppb	Manganese ppb	Conditions	Author
88[a]	3.8[a]	North Sea coastal site. July 1987 to July 1988	Balls (1989)
92[b]	2.8[b]	Rhode Island, USA. February 1985 to February 1988	Heaton *et al.* (1990)
340[a] 250[b]	31[a] 24[b]	Leeds; Three 3 month periods 1980 to 1981	Clarke and Radojevic (1987)

where [a] arithmetic mean
[b] rainfall weighted mean

Using a comprehensive model of cloud droplet chemistry, Graedel (1986) determined that at pH 4, 6-8% of the S(IV) oxidation was accounted for by Fe^{3+} catalytic action, 22-29% by Mn^{2+} catalysis, and the remainder mainly by reaction with H_2O_2. Another study, by Cocks and McElroy (1986) found the presence of Fe(III) to be as important as ozone in controlling the oxidation of sulphite to sulphate. Kraft and Van Eldik (1989) suggest that Fe^{3+} can either initiate the auto-oxidation of S(IV) by producing sulphite radicals via an electron transfer reaction or that it can act as a bridging species between the redox partners; S(IV)-oxide and oxygen.

The possibility of synergistic effects in the aqueous phase oxidation of sulphur dioxide due to the presence of more than one oxidant has been investigated in the laboratory by Ibusuki *et al.* (1990), Lagrange *et al.* (1993) and Grigić *et al.* (1992). From their laboratory studies, Ibusuki *et al.* (1990) postulated the H_2O_2-Fe^{2+} system to be the main contributor to sulphate formation at night, especially when the pH of the water droplets is high or can be maintained at a high value by the presence of alkaline species such as ammonia. Also the iron-hydrogen peroxide species were hypothesised to react to produce hydroxyl radicals via the initial formation of hydroperoxy radicals:

$$Fe^{3+} + H_2O_2 \rightarrow Fe^{2+} + H^+ + HO_2\cdot \quad \ldots . \text{ Equation 3.20}$$

$$HO_2\cdot + HSO_3^- \rightarrow HSO_4^- + OH\cdot \quad \ldots \ldots . \text{ Equation 3.21}$$

An alternative reaction mechanism involving the reaction of SO_2 and H_2O_2 with Fe^{2+} was proposed by Lagrange *et al.* (1993). Their mechanism involved two reactive intermediates, peroxysulphite and FeO^{2+}-sulphate complex, both of which were oxidised to sulphate:

$$HSO_3^- + H_2O_2 \rightleftharpoons \underset{(peroxysulphite)}{Intermediate\ 1} + H^+ \rightarrow Sulphate$$

. . . .Equation 3.22

$$Intermediate\ 1 + Fe^{2+} \rightleftharpoons \underset{(FeO^{2+}-\ sulphate\ complex)}{Intermediate\ 2} + H^+ \rightarrow Sulphate + Fe^{2+}$$

. . . .Equation 3.23

Grigić *et al.* (1992) investigated the synergistic effects of several transition metals (Mn(II), Pb(II) and Fe(III)) which catalysed the oxidation by molecular oxygen. For the pH conditions investigated, the rates of oxidation of S(IV) in the presence of both Mn(II) and Fe(III) were found to be much higher than the combined effect of the individual catalysts. The reaction scheme can be summarised as:

$$HSO_3^- + \tfrac{1}{2}O_2 \xrightarrow[Mn(II)\ \ Fe(III)]{} HSO_4^- \quad \ldots \ldots . \text{ Equation 3.24}$$

During night-time conditions the formation of sulphates on wetted urban aerosols was found by Middleton *et al.* (1980) to be an important pathway for the formation of sulphate from sulphur dioxide. The experimental procedure involved exposing particulate matter of varying size and composition of soot, iron and manganese to varying amounts of humidity, temperature and gaseous SO_2 concentration. Due to the high aerosol volume mixing ratio, particles in the size range 0.1 to 1.0 μm yielded the highest amounts of sulphate aerosol.

Using a detailed model of gas-phase chemistry, aerosol thermodynamics and aerosol chemistry, Saxena and Seigneur (1987) found the amount of sulphate formed during night-time conditions was approximately an order of magnitude less than day-time formation. This was attributed to low OH· concentrations. Approximately 82% of the

total sulphate formed in the aqueous aerosols during night-time was due to oxidation of SO_2 by O_2 (in the presence of Mn^{2+} and Fe^{3+}), with most of the remaining sulphate being formed due to oxidation of SO_2 by H_2O_2. In addition, Saxena and Seigneur (1987) found that increasing Mn^{2+} and Fe^{3+} concentrations in the aqueous aerosols by factors of 5 and 17, respectively, produced a 3-fold increase in the amount of sulphate formed.

3.2.3.4 Heterogenous oxidation of nitrogen oxides

The "heterogeneous" oxidation reactions for nitrogen oxides are indicated in Figure 3.2 by the long dashed lines. These reactions essentially involve the incorporation of those nitrogen oxide radicals, formed by homogeneous reaction in the gas phase, into cloud water. By analogy to the oxidation of sulphur dioxide in the liquid phase, these reactions are often described as heterogeneous oxidations. However, this term may be erroneous since, as mentioned before, the oxidised product is formed in the gas phase and is then removed by the cloud or rain droplets. This view is shared by Hegg *et al.* (1984) who state there are no known strictly aqueous phase oxidation reactions under atmospheric conditions that could produce significant amounts of nitrate ion within clouds. One reason for the low uptake of NO_2 by water droplets is the low solubility of the gas in water. For example, the Henry's Law constant $7.0 \pm 0.5 \times 10^{-3}$ mol l^{-1} atm^{-1} determined by Lee and Schwartz (1981) is approximately three orders of magnitude smaller than the corresponding Henry's Law constant for SO_2; 1.23 mol l^{-1} atm^{-1} presented by Brimblecombe (1986).

However, the presence of water has been shown by several authors (Heikes and Thompson, 1983, Damschen and Martin, 1983 and Jenkin *et al.*, 1988) to play a significant role in the production of the oxidised products of NO_2.

Heikes and Thompson (1983) describe three photochemical oxidations of NO_2, with the oxidised products all absorbed into water droplets to produce HNO_3. The first involves the formation of N_2O_4 via

$$2NO_2 + M \rightarrow N_2O_4 + M \quad \text{Equation 3.25}$$

followed by the diffusion of N_2O_4 to wet particles and its rapid reaction to produce

HNO_3 and HNO_2.

The second and third reactions are represented as:

$$NO_2 + O_3 \rightarrow NO_3\cdot + O_2 \quad \text{Equation 3.26}$$

$$NO_2 + NO_3\cdot + M \rightarrow N_2O_5 + M \quad \text{Equation 3.27}$$

The removal of $NO_3\cdot$ and N_2O_5 by water droplets will produce nitrate continuously and its relative importance is increased during night time when the main nitric acid formation mechanism is not working due to the absence of hydroxyl radicals (Equation 3.11).

In addition, Heikes and Thompson (1983) consider two aspects of the role of the atmospheric environment in controlling the oxidation of nitrogen oxides in clouds:

- the cool temperatures found at altitude in warm clouds (-10° to 10°C) increases the thermal solubility of the nitrogen oxide dimers, N_2O_4 and N_2O_5, with respect to the surface conditions of the droplets.
- due to the lower photolysis rates within clouds there will be a reduction in the importance of the gas phase production of HNO_3 (Equation 3.11) due to fewer $OH\cdot$ radicals being produced. However the longer lifetime of $NO_3\cdot$ in the clouds will produce a compensatory effect on HNO_3 production rates.

Damschen and Martin (1983) determined that the production of nitric acid via the oxidation of nitrous acid, HONO, by hydrogen peroxide may exceed the production of nitric acid by the homogeneous free radical mechanism which has decreased due to reductions in $OH\cdot$ concentrations during night-time conditions (the homogeneous oxidation of NO_2 was discussed in Section 3.2.2.3).

Conversely, Lee and Lind (1986) suggested that the aqueous phase oxidation of HONO by cloud water containing H_2O_2 was not an important sink for nitrogen removal. Both Lee and Lind (1986) and Damschen and Martin (1983) suggest that the reaction with ozone may be a more effective reaction mechanism.

The production of nitrous acid from NO_2 and water was investigated in the laboratory

by Jenkin *et al.* (1988). This study aimed to reproduce the conditions that lead to the formation of nitrous acid during night-time, when the concentration of OH· is low. However, when the results were extrapolated to account for observed nitrous acid concentrations an underprediction of approximately an order of magnitude was found. Jenkin *et al.* (1988) suggested that the higher HONO ambient concentrations originated from another formation process, namely production of HONO in automobile exhaust prior to emission, where high NO_x levels and water vapour concentrations may produce high nitrous acid concentrations.

Finally, investigations into the oxidation of NO_2 in the presence of metal catalysts are not as abundant as the SO_2-metal oxidation discussed in the previous section. However, one study, the oxidation of NO_2 in the presence of Fe^{2+}, by Lee and Schwartz (1981) was found to occur at a faster rate than the uncatalysed reaction, but was considered to make an insignificant contribution to NO_2 oxidation in the atmosphere.

3.2.3.5 Sulphur and nitrogen oxidations by solid catalysts in the atmosphere

The catalytic oxidation of sulphur dioxide in the presence of graphite and soot was investigated by Novakov *et al.* (1974). The experiment involved exposing finely divided graphite and soot, obtained from the burning of propane, to sulphur dioxide (300 ppm) under regulated concentrations of N_2, O_2 and water vapour. Sulphate formation was observed using electron spectroscopy for chemical analysis (ESCA). This technique identified sulphur species according to their binding energy (for example, SO_4^{2-} was identified at approximately 170 eV, while S^{2-} occurred at approximately 164 Ev). Although the sulphate formation was not directly measured under atmospheric conditions, Novakov *et al.* assumed the reaction to be occurring in the atmosphere due the observation that the concentrations of sulphate and soot followed the same diurnal pattern, even though the concentration of SO_2 present in the atmosphere was much smaller than the concentrations used in the laboratory.

Quantification of the oxidation of sulphur dioxide in the presence carbon was estimated by Santachiara *et al.* (1989). Quantities of graphite nuclei, generated by discharge from graphite electrodes, were exposed to a stream of humidified sulphur dioxide. The

amount of sulphate obtained from carbon-catalysed oxidation was determined as follows:

- The airstream containing the mixture of carbon nuclei and humidified SO_2 was impacted onto a plate coated with H_2O_2. The resulting sulphate concentrations were determined using ion chromatography. This sulphate will have originated from both oxidation of SO_2 by carbon and oxidation of sulphur in equilibrium with gaseous SO_2.
- The amount of S(IV) in the water droplets and in equilibrium with gaseous SO_2 was calculated by Santachiara *et al.* (1989) using Equation 3.28.

$$[S(IV)] = K_H\,[SO_2]_g + \frac{-[H_3O^+]_{ex} + ([H_3O^+]^2 + 4K_HK_1[SO_2]_g)^{1/2}}{2} \quad \text{. . . .Equation 3.28}$$

where K_H = Henry's Law Constant for SO_2, 5.4 mol l^{-1} atm^{-1}
$[H_3O^+]_{ex}$ is the concentration of hydrogen ions in solution not associated with dissolved SO_2
K_1 is the equilibrium constant, 2.7×10^{-2} mol l^{-1}
$[SO_2]$ = 25 ppm, 2.5×10^{-5} atm.

The method can be summarised as follows:

$$[SO_4^{2-}]_{\textit{attributed to oxidation by carbon only}} = \textit{total } [SO_4^{2-}] \textit{ measured} - [SO_4^{2-}] \textit{ in equilibrium with } SO_2$$

For a sulphur dioxide concentration of 25±2 ppmv the mean sulphate concentration produced after a contact time of 54 seconds was $0.56 \pm 0.1 \times 10^{-3}$ mole l^{-1} s^{-1}. The rate equation can be represented as

$$\frac{d[SO_4^{2-}]}{dt} = k\,[C]\,[S(IV)] \quad \text{. . . . . Equation 3.29}$$

where k, the reaction rate constant was calculated as 0.14 ± 0.03 mole l^{-1} s^{-1}.
[C] is the graphite concentration
[S(IV)] concentration of S(IV) in solution, determined using Equation 3.25

The heterogeneous reactions of both NO_2 and SO_2 on carbonaceous surfaces have been reported by De Santis and Allegrini (1992). Four types of carbonaceous subtances:

active carbon, graphitised carbon black, and flyash particles from two types of fuel burners (from a power plant and urban heating boiler) were tested. The carbon materials were coated on the inner surfaces of an annular denuder. Nitrous acid was observed to be formed in the presence of both NO_2 and SO_2 for all materials. The rate of formation of sulphate at 90% humidity in the presence of SO_2 only was greater than at a humidity of 60% for all materials except the active carbon, for which humidity did not appear to affect the amount of sulphate formed. Generally, more sulphate was formed on the active carbon. This was attributed to the higher surface area present. De Santis and Allegrini (1992) quote the specific surface areas for active carbon, graphitised carbon black and the flyash particles as 540, 11 and 10-100 $m^2\ g^{-1}$, respectively.

3.2.4 Wet deposition of sulphur and nitrogen

The amount of pollutant that is transferred to the earth's surface via wet deposition is expressed as the wet deposition flux. This is equal to the concentration of pollutant in rainwater multiplied by the precipitation rate. The episodic nature of wet deposition has been defined by Smith and Hunt (1978), in terms of "episodic days", to be those wettest days which, when summed, contribute 30% of the annual total wet deposition total. At an unspecified site in England in 1974, Smith and Hunt estimated that 30% of the annual wet deposition originated from only 5.3% of the wet days.

3.2.5 Washout and rainout

Washout describes the efficiency with which water removes a pollutant from a column of air below the cloud. The magnitude of the washout is described using the washout ratio, which can be expressed in two ways:

a) as a mass mixing ratio, W_m, (concentration expressed as kg kg^{-1} in precipitation divided by concentration expressed as kg kg^{-1} in air).

b) as a volume mixing ratio, W_v, (concentration expressed as kg m^{-3} in precipitation divided by concentration expressed as kg m^{-3} in air).

Barrie (1985) proposed that the mass ratio is more effective since this ratio will not change with altitude in a well-mixed layer of the atmosphere. The term "mixing ratio" employed by Barrie (1985) presumably accounts for the incorporation of the pollutant into precipitation within a well mixed boundary layer. The mass and volume mixing ratios are also described as scavenging ratios.

The mass and volume mixing ratios are related by the relationship:

$$W_v = \frac{\rho_w}{\rho_a} W_m \quad \text{. . . . . Equation 3.30}$$

where: ρ_a and ρ_w are the densities of air and water respectively. At 1 atmosphere pressure and 20°C the W_v/W_m ratio is 830.

Quoted washout values, defined as W_m and W_v are presented in Table 3.10. The highest washout ratios were observed for polluted atmospheres.

Table 3.10 Examples of washout ratios.

Type	Sulphate	Nitrate	Location Date	Author
Mass mixing, W_m	743[a]		Paris 1984-1985	Jaffrezo and Colin (1988)
	1050[b]	1800[b]	Chilton, UK. 1974	Garland (1978)
	1550[a] 831	2820[a] 832	Chalk River Montmorency Forest Both sites in Eastern Canada (1978-1981)	Barrie (1985)
	370[bx]	490[bx]	Marine locations (Pacific and Atlantic Oceans) 1982-1985	Savoie *et al.* (1987)
Volume mixing W_v	4.3×10^5	4.6×10^4	Precipitation network in Eastern Canada	Chan and Chung (1986)

[a] Geometric mean
[b] Arithmetic mean
[x] Only non-sea-salt sulphate considered

Rainout is used to describe the removal of sulphur and nitrogen oxides within the actual clouds. Hidy and Countess (1984) described the magnitude of the rainout in terms of the rainout efficiency, defined as

$$R_i = \frac{cL}{\rho C_A} \quad \ldots\ldots\ldots\ldots \quad \text{Equation 3.31}$$

where: c is the concentration in precipitation (cloud water) (mg l^{-1}).
C_A is the concentration of constituent in air at cloud level (μg m^{-3}) at STP.
L is the liquid water content (g m^{-3} of air) at STP.
ρ is the liquid water density (g cm^{-3}).

In calculating the rainout efficiency, Hidy and Countess (1984) approximated the cloud liquid water content from the precipitation rate using Scott's (1978) formula:

$$L\ (g\ m^{-3}) = 1.518 + 0.428 \ln (25.4\ V) \quad \ldots \quad \text{Equation 3.32}$$

where V is the rainfall intensity in inches per hour.

Hidy and Countess (1984) used several rainout efficiencies: R_1, R_2, R_3 , and R_4, each of which are described below, to show for data collected at nine non-urban sampling sites in the eastern United States, that a greater proportion of nitrate, compared to sulphate, originated from gaseous precursors. The rainout efficiencies were calculated, assuming constant ρ and L in each case, as follows:

R_1, c = cloud water sulphate, c_A = particulate sulphate ($R_1 = 0.83$)

R_2, c = cloud water sulphate, c_A = particulate sulphate + SO_2, as SO_4^{2-} ($R_2 = 0.11$)

R_3, c = cloud water nitrate, c_A = particulate nitrate ($R_3 = 10.2$)

R_4 c = cloud water nitrate, c_A = particulate nitrate + HNO_3, as NO_3^- ($R_4 = 0.13$)

The observed relatively greater decrease in magnitude of R_3 to R_4, compared to R_1 to R_2, was attributed to the relatively greater efficiency with which the gaseous nitrate compounds were absorbed by the cloud water.

Estimates of removal rates by rain or cloud water for sulphate aerosol and sulphur dioxide by a variety of different mechanisms were determined by Garland (1978). Table 3.11 shows the amount of sulphate removed by each mechanism. The sulphate removal rate due to the action of Brownian motion, impaction and interception can be seen to be inefficient removal mechanisms, requiring unrealistic lifetimes to reach the

Table 3.11 Estimated removal rates of sulphur by precipitation and cloud water (Garland, 1978)

	Conditions/ Mechanism	Expected concentration	Conditions
Sulphate removal	Brownian motion to cloud drops	Lifetime during rain 100 hr. Resulting concentration 0.2 mg l^{-1}	These estimates where calculated using a test cloud having 100 droplets of 10 μm radius per cm^3 and a precipitation rate 1 mm hr^{-1} falling as 1 mm raindrops in a moderately polluted atmosphere
	Brownian motion to rain drops	Lifetime during rain 10^4 hr. Resulting concentration 10^{-3} mg l^{-1}	
	Impaction and interception by raindrops	Lifetime during rain 400 hr. Resulting concentration 0.02 mg l^{-1}	
	Rainout of condensation nuclei	3-10 mg l^{-1}	Sulphate aerosol, composed of 80% particles with a diameter of 0.2μm atmosphere
SO_2 removal	Oxidation of SO_2 by cloud droplets*	3 mg l^{-1}	SO_2 concentration of 10 $\mu g\ m^{-3}$
	Uptake by falling raindrops*	1 mg l^{-1}	

* theoretically determined by consideration of the diffusion of SO_2 to the cloud droplet surface and solubility in water

concentrations calculated. Garland (1978) concluded that rainout of condensation nuclei was the main mechanism responsible for producing the sulphate concentrations of several mg l^{-1} found in field studies.

Using another scheme investigating sulphur dioxide uptake, Scire and Venkatram (1985) determined that 30-75% of the sulphate measured in precipitation originated from in-cloud oxidation of SO_2. This scheme incorporated the gaseous and aqueous phase distributions of SO_2, CO_2, NH_3, H_2O_2 and O_3,

By estimating washout ratios for sulphur and nitrogen and their respective concentrations in the aqueous and gaseous phases, Chan and Chung (1986) determined the relative contribution of the gases; SO_2 and HNO_3 and SO_4^{2-} and NO_3^- in particulate form to SO_4^{2-} and NO_3^- within collected precipitation. Removal of the SO_4^{2-} in the particulate phase was estimated to be ten times more efficient than SO_2. Nitric acid was estimated to be removed two times more efficiently than NO_3^-. The method used regression analysis and will be discussed in more detail in Section 6.4.2.

In summary, methods to quantify the amount of gaseous or particulate sulphur and nitrogen removed by water, either in cloud water or falling precipitation, range from the detailed consideration of the solubility of the gases in water, absorption processes and availability of oxidants to estimation using methods such as regression analysis.

3.2.6 Dry deposition of gases and aerosols

The dry deposition flux, F, for gases and particulates is proportional to the concentration, C_A, of the species immediately adjacent to the deposition surface. The proportionality constant can be expressed as the inverse of the resistance to deposition, commonly known as the deposition velocity, v_g, i.e.

$$F = r^{-1}C_A, \quad \text{where } r^{-1} = v_g \qquad \ldots\ldots\ldots \text{ Equation 3.33}$$

Flux can be expressed as μg m^{-2} s^{-1}, concentration as μg m^{-3} and deposition velocity as m s^{-1}.

The resistances to transfer are controlled by the nature of the surface and the regime that the surface imparts onto the air in the immediate vicinity. For example, air that circulates very close to the surface experiences viscous drag which will impede mixing and transport, and transfer is controlled by molecular diffusion (laminar layer resistance). At greater distances from the surface, advection or mixing by turbulent eddies produced by the movement of the wind over the surface will dominate. In addition, the gases or particles may have an affinity for the collecting surface in which case the surface resistance will be low.

The deposition velocity can be expressed as the inverse of the sum of the surface, r_s, aerodynamic, r_a, and laminar layer, r_b, resistances:

$$v_g = \frac{1}{r_s + r_a + r_b} \qquad \ldots\ldots\ldots \text{ Equation 3.34}$$

The surface resistance of a chemically complex system such as a soil system, vegetative canopy or building surface cannot be predicted readily and must be determined

experimentally. This is achieved by calculating the total resistance, r_t, determined by dividing the measured air concentration by the rate of accumulation on the surface and subtracting from this the aerodynamic, r_a, and laminar resistances, r_b. This relationship is summarised as:

$$r_s = r_t - (r_a + r_b) \quad \ldots\ldots\ldots \text{ Equation 3.35}$$

The aerodynamic resistance of gases and aerosols to transport through the atmosphere, and hence to deposition can be determined by considering the surface as a momentum sink. Reviews of methods to determine atmospheric resistances to gaseous pollutant transfer have been provided by Garland (1977), McRae and Russell (1984) and Nicholson (1988).

Methods to determine the deposition velocity include the concentration gradient method, and mass balance methods. An extensive tabulation of dry deposition velocities has been provided by McMahon and Denison (1979). A sample of measured deposition velocities for sulphur and nitrogen oxides in gaseous and particulate form are presented in Table 3.12. Generally the deposition velocities for each species increases in the order:
$NO < NO_3^-$(particulate) $\leq SO_4^{2-}$(particulate) $< NO_2 < PAN \leq SO_2 < HNO_3$.

The flux and profile deposition velocity measurement methods are synonymous, with different authors using either term to describe the method. The method measures deposition velocity by using approximations regarding the flux of momentum and heat transfer. Garland (1977) describes the necessary calculations. The eddy correlation method determines the deposition velocity by measuring fluctuations in concentrations and wind speed. The range of measured deposition velocities for sulphate, -0.53 to 0.51 and -0.33 to 0.55, determined by Nicholson and Davies (1987) and Allen *et al.*, (1991) respectively, were attributed to either experimental error or resuspension of particles.

The mass balance method determines deposition velocity by measuring the mass of substance collected on the surface and divides this by atmospheric concentration. This method has been used to determine the deposition velocity of radioactive isotopes onto buildings and the deposition of gases in controlled chamber studies. Nicholson (1988b) determined that the deposition for radioactive ^{134}Cs and ^{137}Cs isotopes, released from the Chernobyl accident to vertical surfaces, were in the range 4×10^{-3} to 5×10^{-4}

Table 3.12 Deposition velocities for sulphur and nitrogen species (Units are cm s^{-1}).

Species	Deposition velocity	Surface conditions	Measurement method	Reference
SO_2	0.1 night time 0.6 day time	Forest canopy	^{35}S tracer	Garland and Branson (1977)
		Grass	^{35}S tracer	Owers and Powell (1974)
	0.8			
	0.82-1.55	Grass	Profile	Nicholson and Davies (1988)
H_2SO_4	0.1	--	--	Irwin and Williams (1988)
Particulate	0.12-1.18	Grass	Eddy Correlation	Wesley *et al.* (1974)
	Mean 0.07 Range (-0.53 to 0.51)	Grass	Profile	Nicholson and Davies (1987)
SO_4^{2-}	Mean 0.1 ± 0.3 Range (-0.33 to 0.55)	Grass	Profile	Allen *et al.* (1991)
NO	0.1	Alfalfa	Flux	McRae and Russell (1984)
	0.1-0.2	Soil, cement	"	
NO_2	0.5-2.0	Alfalfa	Flux	McRae and Russell (1984)
	0.05-5.6	Soybean field	Eddy correlation	
	0.3-0.8	Soil, cement	"	
PAN	0.14-0.3	Grass, soil	Flux	McRae and Russell (1984)
	0.63	Alfalfa	"	
	0.800	"	"	
HNO_3	0.7-7.7	Cereal crops	Profile	Harrison *et al.* (1990)
	3.4	Grass	Profile	Erisman *et al.* (1989)
	0.25-2.19	Snow	Mass accumulation	Cadle *et al.* (1985)
Particulate NO_3^-	0.14	Grass	Profile	Erisman *et al.* (1989)

Key:-- information not provided

cm s^{-1} and 2×10^{-3} to 1×10^{-2} cm s^{-1} , respectively.

The deposition velocities determined in laboratory chamber studies (Hutchinson *et al.*, 1992, presented in Table 2.11) are approximately within the range determined by field measurements (Table 3.12).

The deposition velocities, as order of magnitude estimates, which will be used in Section 6.3.3 to calculate the fluxes for SO_2, SO_4^{2-}, NO_2 and NO_3^-, are 0.8, 0.1, 0.3 and 0.1 cm s^{-1} respectively.

3.2.7 Comparison of conversion rates

The homogeneneous and heterogeneous reactions that oxidise the sulphur and nitrogen compounds released from combustion sources have been described in this chapter. The removal mechanisms of both the gases before oxidation and the oxidised products have been discussed. This section will compare the removal rates for the various reaction and deposition pathways.

The half life and consequent distance travelled before chemical change or deposition for a range of atmospheric precursors and products have been determined by Irwin and Williams (1988). These are presented in Table 3.13.

Table 3.13 Estimated half lifes and total travel times for sulphur and nitrogen pollutants. (Removal rates are presented in parenthesis)

Process	Half life	Distance scale (km)
SO_2 dry deposition (0.5 cm s^{-1})	~1.3 days	~550
NO_2 dry deposition (0.25 cm s^{-1})	~2.5 days	~1000
NO + O_3 (O_3 = 8 × 10^{11} molecules cm^{-3})	~1 minute	~0.3
SO_2 oxidation (1 % hr^{-1})	~3 days	~1250
NO_2 + OH• (OH• = 0.8 × 10^6 cm^{-3})	~16 hours	~300
HNO_3 dry deposition (2.5 cm s^{-1})	~6 hours	~100
Aerosol, H_2SO_4 dry deposition (0.1 cm s^{-1})	~6 days	~2500
Scavenging of SO_2 in atmosphere	~7 hours	~125
Scavenging of HNO_3 by cloud	~3 seconds	~0.015
Scavenging of aerosols	~2 hours	~35

Illustrations of the competing removal mechanisms are given as follows:

- the reaction rate constant for the homogeneous oxidation of NO_2 to HNO_3 was shown in Section 3.2.2 to be an order of magnitude faster than the oxidation of SO_2 to H_2SO_4. Therefore, as the former reaction will proceed approximately ten times faster, higher HNO_3 concentrations will be expected, assuming equal concentrations of the precursor gases and hydroxyl radical.
- the rate of production of HNO_3 (9.9% $hour^{-1}$), determined in Section 3.2.2.3, can be shown to be approximately the same order of magnitude as the rate of removal by dry deposition. For example, an effective rate constant for the dry deposition of HNO_3 is

approximated by dividing the deposition velocity by mixing height, H:

$$Rate\ constant = \frac{v_g}{H} \quad \ldots\ldots\ldots \quad \text{Equation 3.36}$$

For a dry deposition velocity of 2.5 cm s^{-1} for HNO_3 and a typical mixing height of 800 m, the rate constant is calculated to be 3×10^{-5} s^{-1}, (Equation 3.36) equivalent to a percentage removal of approximately 11% per hour, assuming an initial HNO_3 concentration of 1 ppb (Harrison and Allen, 1990). However, actual calculation of the deposition of HNO_3, taking into account the various competing deposition mechanisms such as incorporation into water droplets, is more difficult.

For the case of the long range transport of nitric acid and sulphuric acid through the atmosphere, Rodhe *et al.* (1981) estimated that:

a) increases in emission rates for hydrocarbons will increase the production rates for both sulphuric and nitric acid.

b) if NO_x emissions increased at the same time as emissions of SO_2 and hydrocarbons remained the same, then more OH· would be used up in the production of HNO_3 resulting in a decrease in the rate of formation of H_2SO_4. Consequently more SO_2 would be dry deposited.

c) increased NO_x emission rates would have a reducing effect on H_2SO_4 formation due to an increase in the acidity of cloud water.

3.2.8 Relationship between measured concentrations of sulphur and nitrogen and emissions

Butler and Likens (1991) have investigated the relationship between sulphur and nitrogen emissions and the sulphate and nitrate content of precipitation by regressing annual SO_2 and NO_x emissions on precipitation sulphate and nitrate levels, respectively. The samples were collected at the five sites used as part of the Multistate Atmospheric Power Production Pollution Survey in the United States over a twelve year period.

Butler and Likens (1991) considered that the regression coefficient obtained (0.74 ± 0.15) when SO_2 emissions (expressed as deviation from long-term mean, 10^6 tonnes a^{-1})

were regressed onto SO_4^{2-} (expressed as deviation from long-term mean, μeq l^{-1}), represented the efficiency with which decreased SO_2 emissions (19% over the 12 years) could be translated into lower SO_4^{2-} concentrations.

Although nitrogen oxide emissions decreased by 17% from 1975 to 1987 no statistically significant relationship between NO_x emissions and NO_3^- concentrations in precipitation was determined. This was attributed to the high degree of variability in the annual NO_3^- precipitation concentration data. Also due to the faster rate of formation and consequent removal of HNO_3 the long range transport of NO_3^- is not as pronounced as SO_4^{2-}.

A similar study which investigated the SO_2, NO_x (emission) to SO_4^{2-}, NO_3^- (precipitation) relationship as a function of source area strength was performed by Hilst and Chapman (1991). Altogether four years of precipitation data from 110 monitoring sites through southern Ontario and continental United states were used. The results showed for areas of relatively low emissions of SO_2 and NO_x, that the associations between wet sulphate and anthropogenic SO_2 emissions and between wet NO_3^- and anthropogenic NO_x emissions within 560 km of each precipitation station were weak or non-existent. The remaining areas of the study, mainly the northeastern United States and southeastern Canada showed moderate to strong associations between SO_2 (emission) and SO_4^{2-} (precipitation) and NO_x (emission) and NO_3^- (precipitation) during the summer but weak to non-existent associations during the winter.

The effect of changes in the emissions of sulphur and nitrogen oxides released from combustion sources on the concentrations of ions in precipitation was investigated by Galloway and Likens (1981) in the Eastern United States (from 1964 to 1979). The NO_3^-/H^+ concentration ratio was found to have increased, whereas the SO_4^{2-}/H^+ ratio significantly decreased. The importance of nitrogen oxide emissions in controlling the acidity of the rainfall will probably increase in the future with increasing motor vehicle emissions of NO_x.

3.2.9 Summary

Over the last twenty one years in the United Kingdom total anthropogenic sulphur

dioxide emissions have decreased by 44%, whereas nitrogen oxide emissions have increased by 16% due largely to increases in the amount of NO_x released by road transport sources. The significance of this for limestone buildings is that the amount of deterioration attributed to sulphur dioxide will, obviously, decrease. An expected short-term increase in the amount of nitrogen oxides released into the atmosphere will have little direct effect on limestone (this increase should be arrested by the introduction of three-way catalytic converters). However, compounds formed from these gases, such as nitric acid, may have a more deleterious effect; being either directly adsorbed or incorporated into precipitation.

This chapter has outlined how sulphur and nitrogen oxides, formed by combustion processes, are further oxidised and removed from the atmosphere. For example, the role of the photochemically produced chemicals, such as the hydroxyl radical and hydrogen peroxide, in homogeneous and heterogeneous reactions have been discussed. The important role of metal ions, both individually and in association with other oxidants, in oxidising sulphur dioxide was also presented. However, the specific role that these oxidants may play in the alteration of building materials is difficult to quantify.

The relative importance of dry to wet deposition removal mechanisms will decrease with distance from the emission source for sulphur and nitrogen. In the case of sulphur this is due to the dry deposition route being faster than those processes which change the sulphur into the aqueous form. Conversely, close to an emission source sulphur is expected to exist in the same gaseous form as released from the combustion source. Nitrogen oxide will be converted quickly to nitrogen dioxide close to the combustion source, but depending on the photochemical conditions present the nitrogen dioxide may be reduced back to NO or further oxidised to HNO_3.

CHAPTER 4: SAMPLING AND ANALYTICAL METHODS

4.1 Introduction

The measurement of the composition and size range of airborne particulate matter currently impinging on three historic monuments in the United Kingdom has been carried out. The particulate matter was collected by two methods: high volume sampling using glass fibre filters and size selective collection using a cascade impactor. The high volume sampler provided a relatively large mass of atmospheric particulate matter which was subsequently analysed to determine the water soluble and trace metal concentrations. Data on gaseous pollutant concentrations during the different sampling periods was provided by the Building Research Establishment. Precipitation was collected using a wet-only sampler, designed to open only during rain events. The concentrations of both particulate and gaseous sulphur and nitrogen compounds were used to assess the routes (in terms of wet and dry processes) by which these two elements were delivered onto the stone surface at each of the sampling sites. Using all the available elemental concentration data, source receptor methods were used to investigate the origin and relative contribution of sources of atmospheric particulate matter.

4.2 Data Collection

4.2.1 Sampling Sites

The three sampling sites which are described in this thesis; Lincoln Cathedral, Wells Cathedral and Bolsover Castle (pictured in Plates 4.1a, 4.1b and 4.1c, respectively), are part of a wider study being conducted by the Building Research Establishment under their National Material Exposure Programme which was designed to assess the influence of atmospheric processes on historic buildings and selected building materials. The geographic location of the historic buildings, which are all situated in small towns away from major urban conurbations, are shown in Figure 4.1. The National Survey grid coordinates and population statistics for each sampling site are presented in Table 4.1. At each site, the high volume sampler was securely fixed in a strategic position either on the building surface or in a position in the immediate vicinity, as shown in Plates 4.2a, 4.2b and 4.2c.

Table 4.1 Location and population figures for towns where sampling took place.

Sampling site	Grid coordinates	Population in town*
Lincoln Cathedral	SQ471707	60,000
Bolsover Castle	ST551459	11,400
Wells Cathedral	SQ980717	10,000

Note: * the populations of each town are provisional estimates, determined during the 1991 Census.

At Lincoln Cathedral, the first of the three sites to be investigated, the high volume sampler was placed on the roof of the Exchequer Gate which is approximately fifty metres from the West Front of the Cathedral. The sampler, which was anchored with sand bags, was co-located with the wet-only rain sampler. The gaseous monitoring and meteorological data recording equipment were situated on the West Front.

At Bolsover, the high volume sampler was placed on the roof of the castle, close to the rest of the recording equipment. The scaffolding used to restrain the sampler was present due to major restoration work which was being carried throughout the sampling duration.

At Wells Cathedral, the sampler was placed on top of the north-west tower beside the other monitoring equipment. The sampler was restrained using a Dexion frame, which in turn was attached to the supporting structure on which the stone exposure samples were positioned.

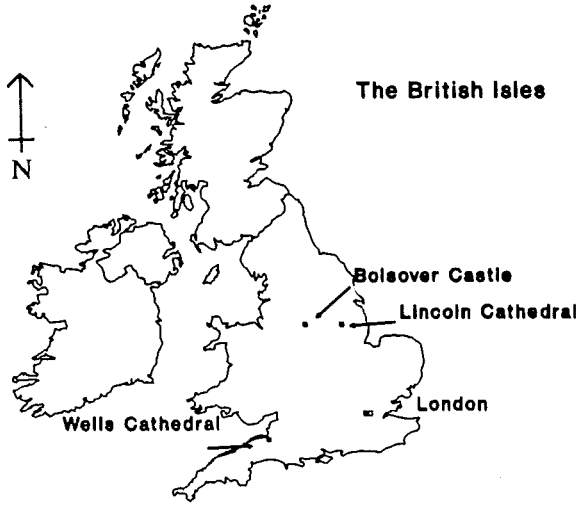

Figure 4.1 Location of Sampling Sites.

Plate 4.1 (a) View of Lincoln Cathedral.

Plate 4.1 (b) View of Bolsover Castle.

Plate 4.1 (c) View of West Front of Wells Cathedral.

Plate 4.2 (a) Positioning of the high volume sampler on the roof of the Exchequer Gate, Lincoln.

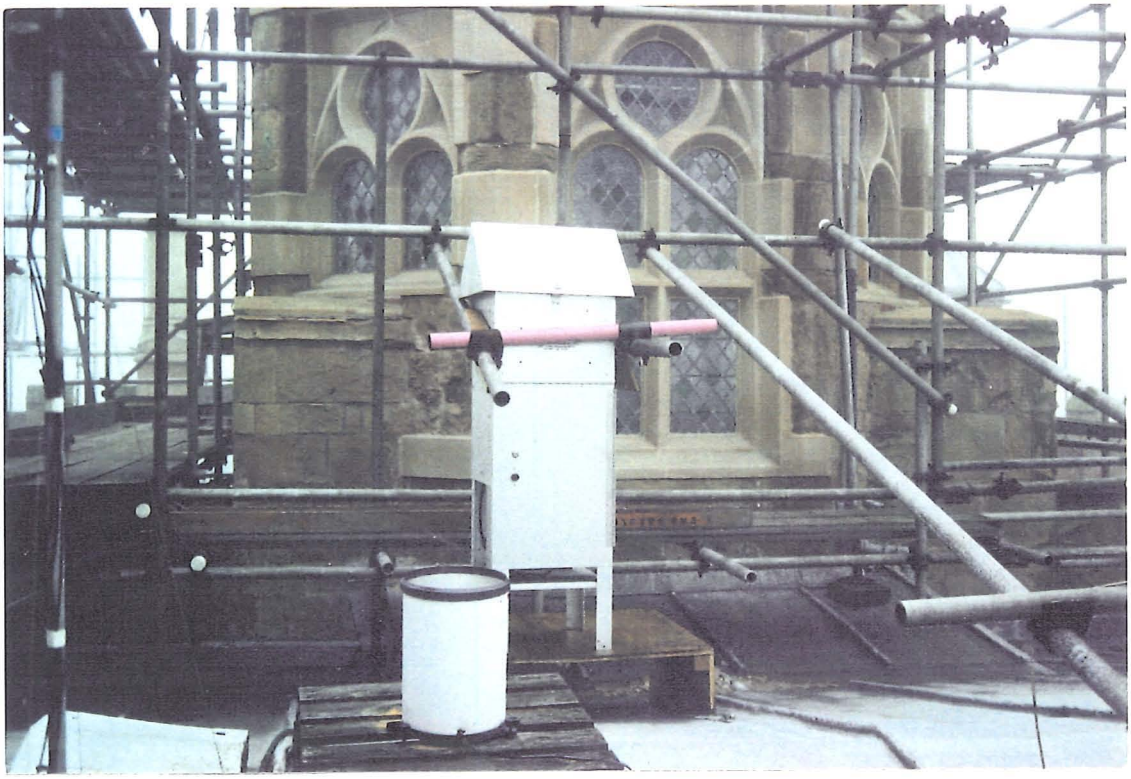

Plate 4.2 (b) Positioning of the high volume sampler on the roof of Bolsover Castle.

Plate 4.2 (c) Dexion frame restraining the high volume sampler on the north-west tower at Wells Cathedral.

4.2.2 Data collected at each site

In addition to the particulate matter collected in this study, gaseous pollutant concentrations and precipitation data were obtained using equipment provided by the Building Research Establishment. Details of the instrumentation used are presented in Table 4.2. The combined data contributes towards producing a more comprehensive picture of pollutant inputs as part of the National Material Exposure Programme.

Table 4.2 Parameters measured in the National Material Exposure Programme. (Adapted from Butlin *et al.*, 1992)

Variable	Method of measurement	Frequency of measurement
Relative humidity †	"Grant" relative humidity probe	Continuous (15 min. avg.)
Wind speed and direction †	Porton anemometer Potentiometer wind vane	Continuous (15 min. avg.)
Air temperature †	Thermo-couple thermometer	Continuous (15 min. avg.)
SO_2 †	a) SO_2 bubbler b) Monitor Labs 8850. Fluoresence analyser	a) Daily b) Continuous (15 min. avg.)
Rainfall pH †	pH meter suitable for rainwater	Weekly
NO_2 †	a) Diffusion tubes b) Monitor Labs 8840 Chemiluminescence analyser	a) Weekly urban; fortnightly elsewhere b) Continuous (15 min. avg.)
Rainfall intensity ‡	Tipping bucket rain gauge	Every 0.2 mm of rainfall
Wind-driven rainfall ‡	BRE wall gauge	Event
Wind-driven rainfall intensity ‡	Tipping bucket rain gauge	Every 0.2 mm of rainfall
Rainfall composition ‡	a) Ion chromatography b) Atomic absorption	Event
Time of wetness ‡	Electro-conductivity	Event

† Details of minimum meteorological and pollutant monitoring required for sites operated by BRE.
‡ Additional desirable meteorological and pollutant monitoring parameters which can ideally be placed on site.

4.2.3 Particulate matter collection

The atmospheric particulate matter was collected using one of two high volume samplers manufactured by Sierra Instruments (Models GMWL-2000 and GMWL-2000H). The former instrument required calibration using a calibrating orifice while the latter gave a direct volume reading by using a built-in pressure recorder. The flow for each instrument varied from 0.5 to 1.0 m^3 min^{-1}, the lower sampling rate was chosen for the later samples to alleviate wear on the electric brushes and commutator. The sampling time was twenty four hours. The particulate matter was collected on unwashed glass fibre filter papers (GMW810 or GF/A). Under optimum conditions the high volume samplers are designed to collect all particulates with an aerodynamic diameter less than 100 microns. The fibres within the glass fibre filter will remove particulates by five basic mechanisms (Hinds, 1982):

a) interception,
b) inertial impaction,
c) diffusion,
d) gravitional settling,
e) electrostatic attraction.

Percentage efficiencies for GF/A filters have been reported to be 99.9 % and 99.0 % by Harrison (1986) for particle diameters of 0.03 μm and 0.3 μm respectively. The filter papers used in this work have a total area 8" $\times$ 10" of which 7" $\times$ 9" is exposed to the throughput of air. The mass of particulate collected was determined by weighing the filter before and after sampling, the filter paper having been stored for twenty four hours at constant humidity before weighing. During transportation the filter papers were protected in sealed polythene bags. After sampling the filter papers were stored in a freezer at approximately -18°C.

4.2.4 Particle size range determination.

The size distribution of the particulate matter was determined using a cascade impactor (California Instruments, Model PC-1EH) sampling at a rate of 1.0 l min^{-1}. This instrument is designed to achieve size separation by impaction of the airborne

particulates onto one of ten impactor stages. Particle size calibration was performed using a scanning electron microscope (Stereoscan 240, Cambridge Instruments Inc.) in conjunction with energy disperive x-ray spectrometry (Link Systems AN 1085). The electron microscope was operated in the backscatter mode. The counting and sizing was performed using Digiscan computer software (model SR2-500-FDC-0784, Link Analytical Instruments). This is achieved by utilising a user specified range of grey levels, which correspond to the backscattered electron image strength that originated from the electron beam striking the elements in the specimen stage. This threshold level is set in such a way that the amount of background interference was set to a minimum.

The calibration was performed using an ambient atmospheric aerosol collected at Middlesex University, Bounds Green Road. Each stage is designed to collect fifty percent of impacting particles (d_{50}). The expected sizes of particles, according to manufacturers' information are compared in Table 4.3 to the determined particle diameters, obtained using the SEM and the Link particle sizing system, expressed as arithmetic mean. Although two different measures, d_{50} and arithmetic mean are compared, they are probably comparable to a first approximation since the particles have been segregated to produce a narrow size distribution.

Table 4.3 Expected and observed particle size ranges.

Stage	Manufacturers' d_{50} (μm)	Number of Particles Measured	Digiscan Determination Arithmetic mean (μm)	Standard Deviation (μm)
1	10	136	8.4	4.20
2	6	N.D.	N.D.	N.D.
3	4	N.D.	N.D.	N.D.
4	2.5	129	2.4	0.64
5	1.5	25	2.3	0.12
6	0.8	600	1.2	0.45
7	0.4	1922	0.4	0.25
8	0.2	518	0.25	0.05
9	0.1	2228	0.12	0.02
10	0.05	1952	0.057	0.01

N.D. not determined.

Size comparison was not performed on stages 2 and 3 as no particles were present in

these size ranges in the test aerosol. For the other particle sizes the results for each impactor stage were shown to be in good agreement with those determined by the manufacturer.

4.3 Laboratory analytical methods

4.3.1 Introduction

The analytical methods used to determine the concentration of major soluble ions and trace metals in the collected particulate matter include ion chromatography for anions; inductively coupled plasma - atomic emission spectroscopy and atomic absorption spectroscopy for trace metals; visible spectrometry for ammonium. Analar grade chemicals were always used for standard solutions and chemical reagents.

4.3.2 Sample preparation

The collected particulate samples were prepared for analysis using one of the methods outlined below according to selected analyte.

a) For the extraction of non-metal ions, a section (7" ×1") of filter was cut and placed into a 60 ml polythene sample bottle (BDH Laboratory Supplies, Catalogue Number 215/0407/21). Fifty millilitres of double distilled and deionised water (DDDW) was added to each bottle and shaken for 30 minutes, followed by 20 minutes of ultrasonification. The filtrate was removed from the filter paper residue by vacuum filtration.

b) The metal ions were extracted by acid digestion from a section of filter paper (7" ×4"). Concentrated HNO_3 was placed with the filter paper in a Teflon beaker (BDH Laboratory Supplies, Catalogue number 209/0755/02) and covered with a polyethylene lid (BDH Laboratory Supplies, Catalogue number 209/0760/02). The samples were then heated at 60°C on a sandbath for twelve hours with the polyethylene lid in place. The lid was then removed and the heating continued to dryness. The metal nitrate ions were then redissolved in 1% HNO_3 (~20 ml) with the solution being warmed to ensure that

all the ions had redissolved. The solution was then filtered using vacuum filtration with the residue being washed with two further 10 ml additions of 1% HNO_3. Next, the solution was transferred to a 50 ml volumetric flask and the solution made up to the mark with the required amount of 1% HNO_3. Finally, the sample was transferred to 60 ml sample bottles.

4.3.3 Anion determination

The concentrations of chloride, nitrate and sulphate were determined using ion chromatography. This method separates the ions by utilising differences in the attraction of each ion for active sites present on the surface of the polyvinyl resin. Chloride ion will be the first anion eluted from the column, followed by nitrate and sulphate. The retention times for the ions under the operating conditions were typically: 1.6, 3.3, 7.05 minutes, respectively.

The operating conditions were as follows:

a) eluent, consisting of an aqueous solution of Na_2CO_3 and $NaHCO_3$, at concentrations of 2.00 and 0.150 mM l^{-1}, respectively.

b) eluent flow rate 2 ml min^{-1}

c) regenerant flow rate 2-4 ml min^{-1}

d) regenerant concentration 25 $\times$ 10^{-3} N H_2SO_4

e) background conductivity $\sim$ 15.0 μS min^{-1}

f) the eluent and regenerant were prepared using DDDW.

g) sample injected via a 50 μl sample loop.

After passage through the separator column the background conductivity of the eluent is reduced by the addition of hydrogen ions and removal of the sodium ions using a suppressant device. The anions are monitored via their conductivity which is proportional to their concentration. Chloride is the most sensitive ion to electrical conductivity and for this reason the analytical standard contains chloride in half the concentration of the other two anions.

The ion chromatography instrument (Dionex model 2000i, Plate 4.3 (a)) used a AS4A separator column. The calibration standards used (10, 20 and 30 μg ml^{-1} for sulphate

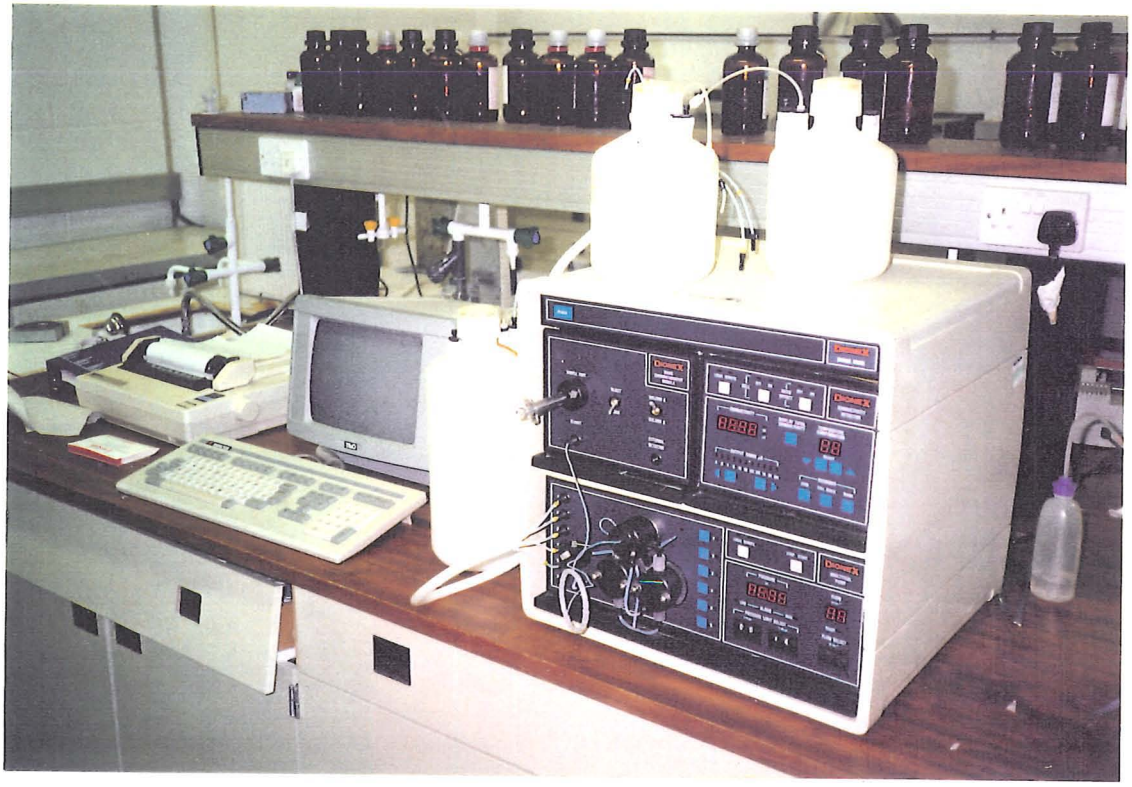

Plate 4.3 (a) Dionex 2000*i*. Ion chromatography apparatus used to determine concentration of anions.

and nitrate and 5, 10 , 15 μg ml^{-1} for chloride) were prepared by measuring 1, 2 and 3 ml, respectively, of a stock solution into a 100 ml volumetric flask and making up to the mark with DDDW. The required solution volumes were transferred using a micropipette (Eppendorf 4710). The stock solution concentration (1000 μg ml^{-1} of sulphate and nitrate and 500 μg ml^{-1} for chloride was prepared by weighing 1.479 g, 1.371 g and 0.842 g of the respective sodium salts into a 1 l volumetric flask and making up to the mark with DDDW. A typical chromatogram is presented in Figure 4.2.

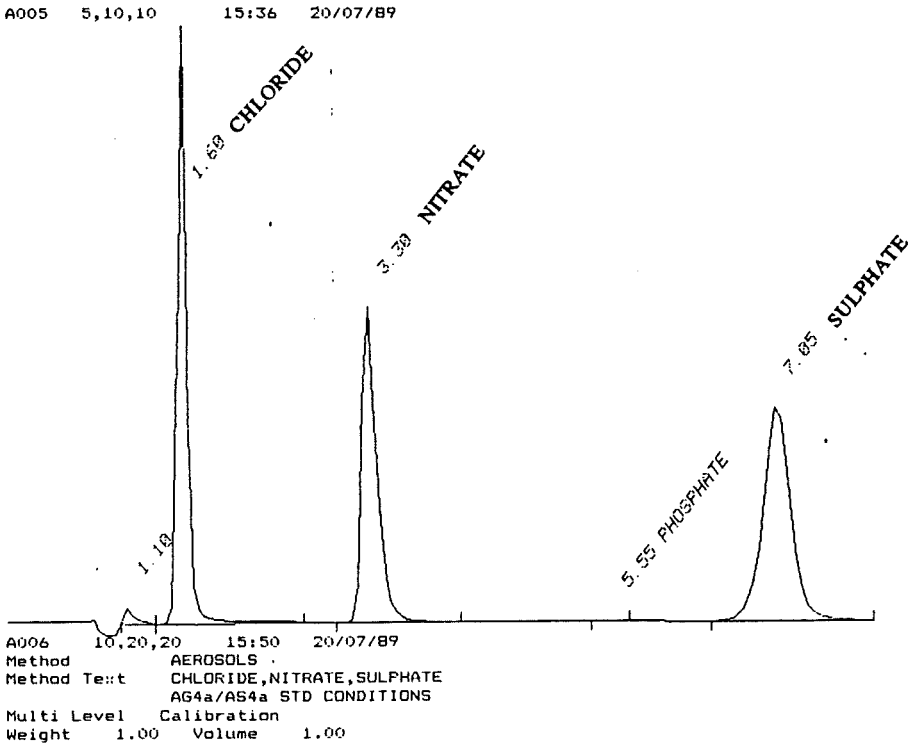

Figure 4.2 Typical ion chromatogram obtained for chloride, nitrate and sulphate (For 5, 10, 10 μg ml^{-1} concentrations, respectively).

The electronic signal corresponding to the conductivity produced by each of the eluting ions was processed by a TriVector integrator (Vinten Group plc). The integrator is programmed to receive the signals resulting from analysis of the standard solutions. The calibration curve is plotted automatically. The sample concentration is recorded directly after each sample run. Details of the method are presented in Table 4.4.

Table 4.4 Integrator parameters used in anion analysis.

	Parameter	Value
Data collection	Run time	10 minutes
	Peak width	5 seconds
	Input voltage	1000 mV
Peak detection	Start time	0.0 seconds
	End time	100 seconds
	Sensitivity	5
	Minimum baseline times	1 second
	Peak end slope	1

4.3.4 Non-metal cation determination

Ammonium ion concentration was determined using Nessler's method (Golterman *et al.*, 1978). Five hundred nanolitres of Nessler's reagent was micro-pipetted into a 10 ml volumetric flask which was made up to the mark with standard or sample. A stock solution containing 1000 μg ml^{-1} NH_4^+ was used to prepare the 1,2,3 and 5 μg ml^{-1} standards for calibration. The resulting yellow coloured complex was transferred to a 1 cm cell and the amount of visible light absorbed at 420 nm measured. The ammonium in solution is analysed as ammonia which is formed on contact with the Nessler's reagent. The ammonia then reacts with the reagent as follows:

$$2K_2[Hg]I_4 + 2NH_3 \rightarrow NH_2HgI_3 + 4KI + NH_4I \quad \text{Equation 4.1}$$

4.3.5 Metal determination

Inductively coupled plasma - atomic emission spectrometry, ICP-AES, (Perkin Elmer Model Plasma 40 Instrument; Plate 4.3 (b)) was used to determine the concentration of the metal ions; arsenic, selenium, chromium, antimony, zinc, cadmium, lead, nickel, iron, manganese, magnesium, copper, calcium, aluminium, potassium and sodium.

4.3.5.1 Inductively coupled plasma -theory

The inductively coupled plasma instrument provides the energy to convert the metal ions in solution into excited atoms or ions that emit a characteristic amount of ultra-violet and visible energy. The wavelength and intensity of this emitted radiation

determines the metal and its concentration in the original solution. The components of the plasma are formed at the top of three concentric quartz rings and within or above a copper coil. A radio frequency generator imparts to the copper coil an alternating current which oscillates at the frequency of the generator (40 MHz) which in turn generates electric and magnetic fields at the top of the coil.

When an electric spark is applied to the system, the purging argon atoms become stripped of their electrons which in turn enter the electric and magnetic fields and collide with more argon atoms causing more electrons to be stripped away from atoms. A chain reaction follows, resulting in the plasma consisting of argon atoms, electrons and argon ions. This plasma is the inductively coupled plasma which is continuously formed as the radio frequency is applied.

The different regions formed within the plasma are shown in Figure 4.3. The induction zone (IR) (typical temperature $\approx$ 10,000 K) is a doughnut shaped ring formed by the nebulising stream entering the plasma. In this region the inductive energy transfer from the copper coil to the plasma takes place.

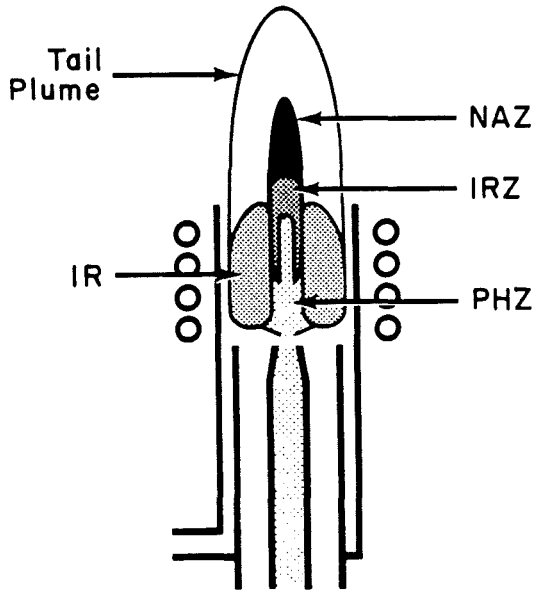

Figure 4.3 Zones of the ICP-AES: IR-Induction region. PHZ - Preheating zone, IRZ-Initial radiation zone, NAZ - Normal analytical zone (From Boss and Fredeen, 1989)

In the preheating zone (PHZ), the aerosol carrying the solvated ions is converted into

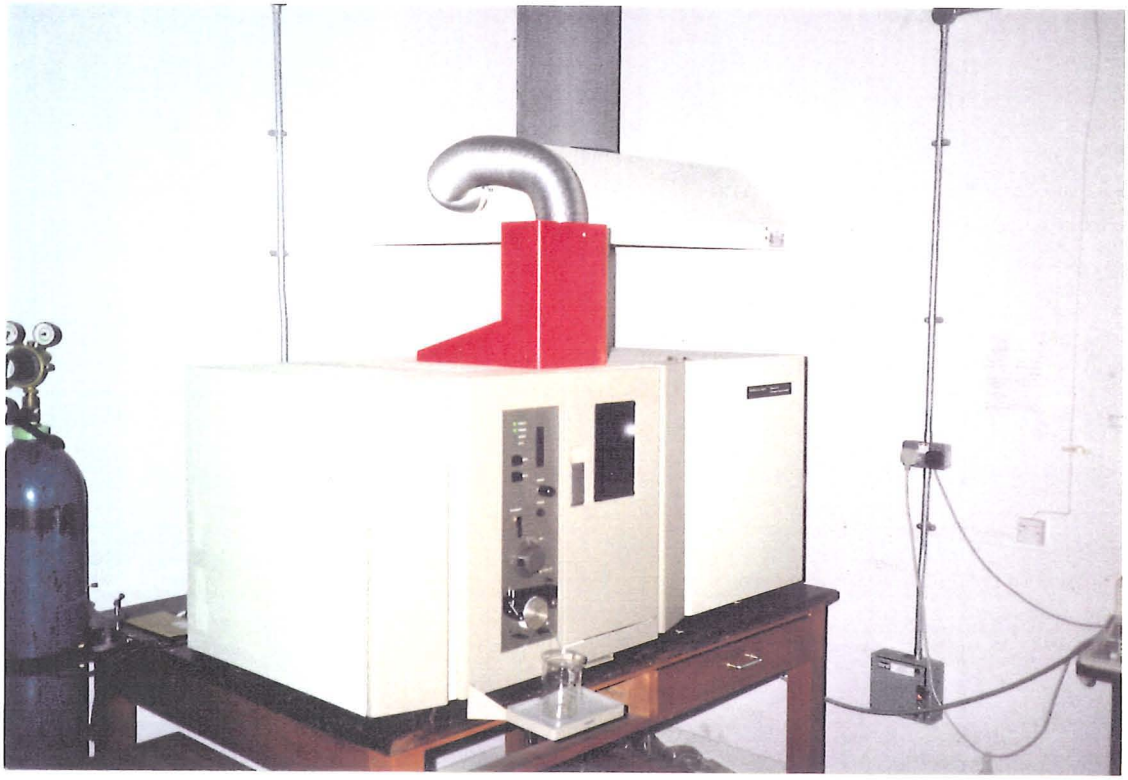

Plate 4.3 (b) Perkin-Elmer Plasma 40. Inductively coupled emission spectrometer used to determine the concentration of metals.

microscopic salt particles that are vaporised into molecules and consequently atomised into individual atoms. The aerosol will have been formed via a concentric pneumatic nebuliser system. In this type of nebuliser the solution is introduced through a capillary tube to a low-pressure region created by a gas flowing past the end of the capillary. The low pressure and high speed of the gas both act to break up the solution into an aerosol.

In the initial radiation zone (IRZ) (temperature 8000 K) and normal analytical zone (NAZ) (temperature in the range 6500 to 6800 K) the promotion of electrons from atoms or more often from ions to higher energy levels takes place.

The emitted radiation is focussed, using a convex lens, onto the entrance slit of the reflection diffraction grating which subsequently differentiates the incoming radiation produced by the different ions present in the sample solution. The Perkin-Elmer Plasma 40 instrument used in this study uses a monochromator which changes the diffraction angle by actually rotating the monochromator.

4.3.5.2 Analytical method and operating conditions

The ICP-AES instrument will measure the concentrations of a large number of elements in a relatively short period of time. However, to ensure that the concentrations determined are accurately represented the analytical methodology was prepared with care.
The analytical method described below was followed:

a) A 1 μg ml^{-1} solution of each metal was prepared by micro-pipetteing 100 μl of a 1000 μg ml^{-1} stock solution into a 100 ml polypropylene volumetric flask (BDH Laboratory Supplies, Catalogue Number 241/1574/02) and making up to the mark with 1% HNO_3. This solution was then analysed at the required wavelength and the emission intensity was recorded by the computer. This was repeated for each metal in turn.

In analysing the emission intensity for each element, background corrections were calculated automatically by means of an artificial intelligence algorithm. However, before the background corrections were calculated the wavelength calibration option on

the computer was employed to centralise the position of the cursor at the central point of the analyte peak. This helped to ensure that the instrument measured the exact wavelength of maximum emission.

The computer software then calculated the corrected analyte emission by subtracting the estimated background correction from the total emission at the wavelength of the analyte peak. A relatively large background correction was required to compensate a baseline that sloped significantly.

The instrument parameters utilised for each element are presented in Table 4.5. The largest magnitude for background correction can be seen to be occurring for sodium and potassium. The photomultiplier tube (PMT) voltage for each element was adjusted to ensure that the ratio of minimum emission peak area to maximum emission peak area was at least 10.

Table 4.5 The instrument parameters used in the ICP analysis

Element	Wavelength (nm)	Lower background correction (nm)	Upper background correction (nm)	PMT (v)	Element time (ms)	Spectral time (ms)	Read delay (s)
As	193.696	-0.057	0.070	750	500	32	20
Se	196.090	-0.057	0.072	600	100	32	20
Cr	205.552	-0.041	0.047	701	100	32	20
Sb	206.883	-0.043	0.041	701	500	32	20
Zn	213.856	-0.053	0.034	600	100	32	20
Cd	214.438	-0.083	0.028	701	1000	32	20
Pb	220.355	-0.044	0.032	701	100	32	20
Ni	221.656	-0.036	0.042	701	100	32	20
Fe	238.204	-0.052	0.039	600	100	32	20
Mn	257.610	-0.050	0.098	701	100	32	20
Mg	279.553	-0.044	0.044	400	100	32	20
Cu	324.754	-0.050	0.036	600	100	32	20
Ca	393.366	-0.077	0.148	400	100	32	20
Al	396.152	-0.040	0.118	701	500	32	20
Na	589.592	-0.202	0.155	600	100	32	20
K	768.490	-0.211	0.171	701	100	32	20

Most of the elements in the standard solution were measured at the default PMT voltage of 600 volts. The PMT voltages for calcium and magnesium were reduced to 400 volts. The element time (milliseconds) is the integration time required for each signal to be processed. The read delay time is the time allocated by the method to ensure that the instrument will be ready to measure the next element in the analytical sequence.

b) A multiple standard (1 μg ml^{-1} for each metal) was prepared by pipetting 2 ml of each metal ion (1000 μg ml^{-1} stock) into a 2 l polypropylene volumetric flask (BDH Laboratory Supplies, Catalogue Number 241/1570/03) and making up to the mark with 1% HNO_3. The analysis was repeated and the peak intensities observed on the computer screen. No significant difference for emission intensity between the single element peaks and the multiple element standard peaks such as overlapping emission peaks were observed. The background corrections for the elements in the multiple standard were also readjusted as necessary.

c) during each sampling run, periodic checks were performed on the reproducibility of the measured concentrations. This was achieved by analysing the multi-element standard as a sample and ensuring that the coefficient of variation (COV) obtained did not exceed 5%. If this COV was exceeded, action was taken to alleviate the problem.
Three common causes of increases in COV were:

- worn sample inlet tube. This was caused by the squeezing action of the rollers on the peristaltic pump. The problem was remedied by changing the sample tube.
- build up of water droplets in the spray chamber. This problem was solved by switching off the instrument and drying out the spray chamber.
- poor drainage through the waste drain. This problem was solved by passing Teepol down the waste drain tube to reduce the surface tension on the collected water droplets.

Each sample was analysed four times and only those elemental concentrations which produced a COV equal to or less than 5% were recorded for later statistical analysis. Metals, such as manganese, with high emission intensities were determined with high reproducibility and hence relatively low atmospheric concentrations for manganese could be determined. An example of the emission peak for manganese is presented in Figure 4.4. The ordinate axis of the plot has units of nm.

4.3.5.3 Detection limits

The method used to calculate the detection limits for the metal ion concentrations

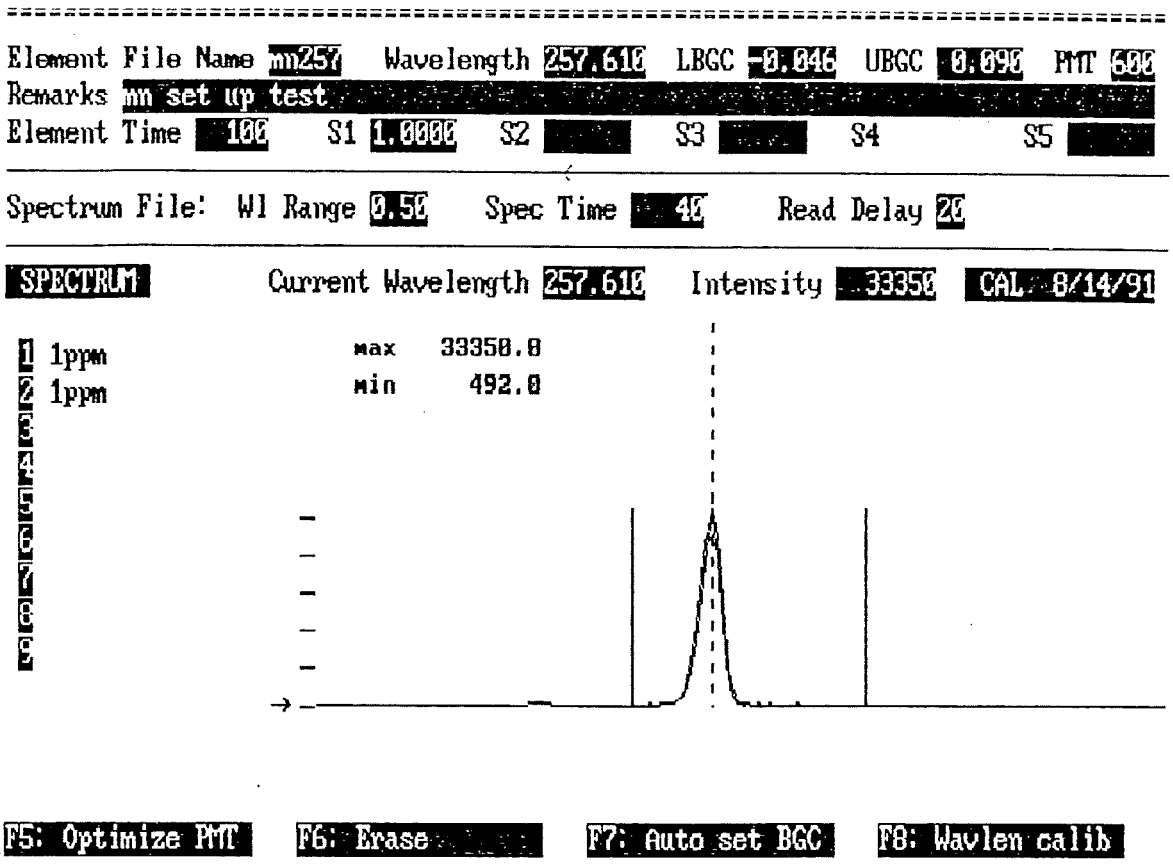

Figure 4.4 Emission peak determined for manganese (operating conditions were as follows: concentration 1 μg ml^{-1}, current wavelength 257.61 nm, PMT voltage 600 V).

involved calibrating the instrument using the multielement standard (1μg ml^{-1} for each element) and then analysing a 1% nitric acid solution as a sample (ten times in succession). The repeated analysis of this nitric acid solution, used to prepare the samples, assesses the stability of the response signal for each metal. The stability of the response will in turn provide an estimate of the detection limit, defined as three times the standard deviation obtained during analysis of the ten replicates. The statistical basis to this method is described by Millar and Millar (1984).

The most stable signal was obtained for magnesium and the least for potassium. The detection limits for the remaining elements are presented in Table 4.6.

4.3.5.4 Emission lines

The emission lines for different elements are selected by the instrument automatically

Table 4.6 Detection limits for metals determined by inductively coupled plasma emission spectrometry.

	As	Se	Cr	Sb	Zn	Cd	Pb	Ni	Fe	Mn	Mg	Cu	Ca	Al	K	Na
Value quoted from Perkin-Elmer manual ($\mu g\ l^{-1}$)	20	50	3	40	3	2	40	7	3	0.4	0.1	1	0.1	5	–	–
Determination 1 ($\mu g\ l^{-1}$)	39	74	14	30	4	7	75	9	4	1.5	0.3	6	0.6	10	104	37
Determination 2 ($\mu g\ l^{-1}$)	41	86	11	12	4	6	86	14	3	1.6	0.2	5	1.2	13	–	–
* Equivalent air concentration ($ng\ m^{-3}$)	12	25	4	7	1	2	25	4	8	0.5	0.05	1.5	0.4	4	33	12

– not determined.

* The equivalent air concentration has been determined to show the minimum mass concentration of a metal in air that must be present to register above the detection limit. This value was obtained by converting the concentration determined for the detection limit into an equivalent air mass concentration (units ng m^{-3}) assuming that the mass of ions was extracted on a 1"x7" filter and that the volume of air that passed through the whole filter was 1440 m^3, this is assuming that the sampler was sampling at 1.0 m^3 min^{-1} for twenty four hours.

rotating the diffraction grating. All the metals were determined in the one sample run, except for sodium and potassium which, were determined separately due to the relatively long time required for the diffraction grating to change from the *u.v.* region to 589.592 nm (for Na) and 766.490 nm (for K). The emission lines and typical emission intensities obtained in the study are presented in Table 4.7.

Table 4.7 Emission lines (nm) used and typical emission intensities obtained in this study for 1 $\mu g\ ml^{-1}$ multi-standard.

Metal	As	Se	Cr	Sb	Zn	Cd	Pb	Ni
Wavelength	193.759	196.090	205.552	206.833	213.856	214.438	220.353	221.656
Emission Intensity	3200	410	13280	2230	17700	35800	3180	14300
Metal	Fe	Mn	Mg	Cu	Ca	Al	Na	K
Wavelength	238.204	257.610	279.553	324.754	393.366	396.152	589.592	766.490
Emission Intensity	7600	113000	7100	18800	18800	10000	14000	2000

4.3.5.5 Determination of Blank Concentration

The metal concentration of two blank filter paper segments were determined during

each digestion run. The results expressed as mass of element per filter paper are presented in Table 4.8.

Table 4.8 Metal content of blank filter papers (ng cm^{-2}).

	As	Se	Cr	Sb	Zn	Cd	Pb	Ni	Fe	Mn	Mg	Cu	Ca	Al	K	Na
G810																
Mean	0.4	1.4	0.2	0.3	68	0.1	1.3	0.4	10	0.1	4.0	1.5	33.1	25.5	63.5	112.0
S.D.	0.2	0.6	0.1	0.2	34	0.1	0.6	0.3	26	0.1	2.0	0.7	15.2	13.8	31.0	59.4
GF/a																
Mean	0.3	1.0	0.2	0.3	144	0.1	0.7	0.3	1.3	0.1	7.7	0.6	52.0	85.4	93.0	424.8
S.D.	0.2	1.0	0.1	0.3	40	0.1	0.5	0.2	0.6	0.1	2.5	1.0	17.3	24.9	27.1	122.0
GF/a (Harrison 1986)	0.2	-	0.2	0.1	320	-	1.6	0.2	8	0.8	-	0.1	-	-	-	-

High filter blanks can seen to be occurring for zinc, magnesium, aluminium, potassium and sodium and calcium. However, the atmospheric concentration of zinc, typically of the order 50 ng m^{-3} (several actual values are presented in Table 7.2), would not produce sufficiently high mass loadings on the filter surface to be determined with confidence (50 ng m^{-3} corresponds to 210 ng cm^{-2}, assuming 1440 m^3 of air passed through a filter surface area of 338 cm^2). Consequently, due to the variations in ambient zinc concentration, a significant number of "negative" concentrations were obtained when the filter blank concentration was subtracted from the concentration determined for the filter paper extract. Hence zinc was not used further in the receptor modelling analysis.

The concentration of the other high blank metals, with the exception of aluminium, were used in the receptor modelling analysis as the ambient concentrations collected on the filter paper produced concentrations which were significantly greater than the blank concentrations. For example, ambient concentrations of sodium, typically 1 μg m^{-3}, would equate to a filter loading of 4142 ng cm^{-2}, an order of magnitude greater than the filter blank shown in Table 4.8.

4.3.5.6 Extraction efficiencies

To investigate the efficiency of metal extraction from the filter papers, the following tests were performed:

a) Determination of the optimum filter area. Two filter paper sizes (1"×7" and 4"×7")

were cut from 11 samples collected from Bolsover, between 3rd and 18th December 1990, and digested using 50 ml concentrated nitric acid. The ratio of extracted metal ion concentrations are shown in Table 4.9. The measured metal ion concentration will comprise that extracted from both the particulate matter and the filter paper. Ideally, the ratio should be 4 with the standard deviation about the mean being minimal. High standard deviations for Sb, Se, Zn and Al would indicate that these metals are being extracted in an uneven fashion from the filter. The low average ratio for Pb results from a low concentration in the 4" × 7" samples (mean concentrations 328 ± 106 and 311 ± 199 $\mu g\ l^{-1}$ were determined for the 1"×7" and 4"×7" filters respectively). The concentrations of Ni, Mn, Mg, and Cu were constantly reproducible between the two digestions.

Table 4.9 Ratios of metal ion concentration extracted from 4"×7" and 1"×7" filter segments

Element	Mean ± Standard Deviation	Element	Mean ± Standard Deviation
As	3.4 ± 1.7	Fe	2.1 ± 0.5
Se	3.7 ± 5.0	Mn	4.1 ± 0.5
Cr	2.3 ± 1.0	Mg	4.9 ± 0.8
Sb	2.3 ± 6.0	Cu	4.3 ± 0.2
Zn	5.5 ± 3.0	Ca	4.9 ± 1.4
Cd	2.2 ± 1.0	Al	7.1 ± 4.7
Pb	0.9 ± 0.4	K	4.2 ± 1.7
Ni	3.8 ± 1.0	Na	5.5 ± 1.8

b) The extraction efficiency for removing metals from the filter papers was investigated for different volumes of extracting acid and filter paper area. The volumes of concentrated HNO_3 acid were 10 and 50 ml and the filter paper areas 7"×1" and 7"×4". The extraction efficiency is determined as:

$$Efficiency = \frac{Mass\ determined\ for\ digestion\ 1}{Mass\ determined\ for\ digestion\ 1 + Mass\ determined\ for\ digestion\ 2}$$

. . . .Equation 4.2

where the mass of metal is determined as the product of extract concentration ($\mu g\ ml^{-1}$) and volume of acid used in the extraction (ml).

The volume of dilute nitric acid used to dissolve the metals in the residue was also varied from 25 to 50 ml. The results are presented in Table 4.10. Altogether ten filter

Table 4.10 Extraction efficiencies determined for a range of filter paper sizes and extracting acid volumes.

Samples Used Filter size	Volumes added to 1. Sample (c.HNO_3) 2. Extract (dil. HNO_3)	Zn (%)	Pb (%)	Mn (%)	Mg (%)	Ca (%)
Wells 7"×1" May 91	10 25	73 ± 4	38 ± 14	80 ± 5	79 ± 5	77 ± 4
Bolsover 7"×4" Jan. 91	50 50	71 ± 8	53 ± 16	72 ± 9	72 ± 10	74 ± 9
Bolsover 7"x4" Jun 91	50 25	89 ± 2	77 ± 6	90 ± 2	90 ± 2	90 ± 2
Wells 7"×4" Jul 91	50 25	90 ± 4	81 ± 6	91 ± 4	90 ± 4	90 ± 4
Lincoln 7"×4" Jan 91	50 25	91 ± 4	60 ± 15	93 ± 3	92 ± 3	92 ± 4

papers from a selection of acid digestions were tested for extraction efficiency. The most efficient extraction regimes appear to be obtained using the 7"×4" filter paper and 50 ml concentrated nitric acid which ensured that at least 90% of the metal ions were removed. However, the samples collected during January 1991 at Bolsover were extracted with less efficiency. The extraction efficiency of lead is poor, especially for those samples collected at Wells during May 1991.

c) The efficiency with which metals were extracted from the filter paper was checked by spiking 7"×4" blank filter papers with 1000 μg ml^{-1} solutions of the following metals: As, Se, Cr, Sb, Cd, Pb and Mn (100 μl of Analar grade standard solution was pipetted onto the filter paper). The filter paper was consequently subjected to the same digestion procedure outlined before (Section 4.3.2). The addition of 50 ml dilute nitric acid should result in a concentration of 2000 μg l^{-1} for each of the metals added (assuming the filter has a low blank for each metal).

The percentage recovery of five metal ions after acid digestion are shown in Table 4.11. The recoveries of spiked amounts of metal (added in a soluble form) from the filter paper may not be directly applicable to the removal of metals originating from atmospheric particulate matter but it is assumed that the acid digestion will solubilise

Table 4.11 Average percentage recoveries of metal ions from five digestions of spiked filter paper.

	As	Se	Cr	Sb	Cd	Pb	Mn
Mean concentration ± standard deviation $\mu g\ ml^{-1}$	1489 ± 54	1542 ±100	1521 ±63	654 ± 120	1477 ± 73	1399 ± 76	1769 ± 557
Percentage recovery	74	77	76	33	74	74	88

all particulate metals present (with the exception of aluminium, not tested in the 'spiking' experiment, which is securely bound within the alumino-silicate material). Altogether, five 4"×7" filter paper segments were 'spiked'. A particularly low recovery was obtained for antimony, which was attributed to volatilisation of the metal during sample digestion. The 'spiked' extraction efficiencies for As, Se, Cr, Cd, and Pb are consistent with each other (~75 %). These efficiencies are lower than expected, as the extraction efficiency determined by measuring the mass of metal remaining after the initial digestion was shown to be greater than 90% for the metals Zn, Mn, Mg, and Ca in Table 4.10 (with the exception of Bolsover January 1991). The reason for this is unclear as manganese is recoverable to almost the same extent in both cases.

d) Standard reference material. The standard reference material used in this study is the *National Bureau of Standards* Standard Reference Material 1648, Urban Particulate Material. The method involved placing one hundred micrograms of reference material into a Teflon beaker and digesting to dryness overnight using 50 ml concentrated nitric acid (in triplicate). The resulting material was reconstituted using 1% dilute nitric acid and filtered into a 50 ml volumetric flask. The determined and certified metal concentrations of the standard reference material are shown in Table 4.12. The agreement between the determined and certified concentration is poor for Se, Cr and Al. The poor aluminium and chromium determinations are likely to result from incomplete digestion of the particulate material. The poor result for Se probably results from the concentration being too close to the detection limit of the ICP technique (the aqueous concentration corresponding to 63 $\mu g\ g^{-1}$ is 126 $\mu g\ ml^{-1}$ which is only just above the determined detection limits of 74 and 86 $\mu g\ ml^{-1}$, Table 4.4). There is good agreement (100 ± 10 %) between the determined and certified metal concentrations for Zn, Cd, Pb and Cu. Lead is determined accurately in this procedure due to the

Table 4.12 Comparing determined metal concentration obtained from urban particulate matter (NBS 1648) with certified concentration.

	Certified Standard concentration $\mu g\ g^{-1}$	Determined Mean (n = 3) concentration ± standard deviation $\mu g\ g^{-1}$	Ratio of determined concentration to certified concentration (Percentage)
As	110 ± 10	97 ± 11	84.3
Se	27 ± 1	63 ± 8	233.3
Cr	403 ± 12	53 ± 8	13.2
Sb	(45)	-	-
Zn	4250 ± 0.002	4686 ± 189	110.0
Cd	75 ± 7	82 ± 4	109.0
Pb	6550 ± 0.008	6058 ± 354	92.4
Ni	82 ± 3	73 ± 5	89.0
Fe	39100 ± 0.10	28520 ± 1975	72.9
Mn	(860)	718 ± 54	83.4
Mg	8000	6014 ± 390	75.2
Cu	609 ± 27	600 ± 13	98.2
Ca	N.D.	48066 ± 1269	
Al	24,200 ± 0.11	876 ± 310	25.6

relatively high mass present in the certified standard.

4.3.5.7 Summary

The ICP-AES analytical system has been shown to be both rapid and accurate for most metals investigated in this study. The two main limiting factors in the method were high filter blank values and poor detection limit for several of the metals analysed. Washing of the filter paper may have reduced the blank content for the two metals; sodium and zinc, that were present in the highest abundance. Due to relatively high and low atmospheric concentrations for sodium and zinc, respectively, only the former metal is expected to be determined with certainity. An alternative filter paper media, such Teflon, with practically no inherent metal component could have been used but the cost of these filter papers is inhibitory. Other analytical techniques with lower detection limits for metals like lead are available but these were not used. The combination of systematic and random errors, to determine an overall error in the mass concentration for each element will be discussed in Appendix A.

CHAPTER 5: RECEPTOR MODELLING

Receptor modelling attempts to determine information about pollution sources by utilising the results obtained from a chemical analysis of particulate matter collected at a receptor site. In this study the receptor sites are the historic buildings where collection of the particulate matter was carried out.

There are three types of receptor model employed in this study;

a) regression of TSP mass concentration on elements or ions, selected due to their high loading on a determined principal component,

b) a designated statistical computer software package, FANTASIA,

c) regression on absolute principal component scores.

Before looking at these particular models, a brief history of receptor models will be given to illustrate how the models have evolved to analyse the data.

The early receptor modelling techniques attempted to measure at a sampling site the amount of collected particulate matter which originated from each contributing source. These models included chemical element balances and multiple linear regression analysis. The simplest chemical element balance method determined the contribution of a source to collected particulate matter by dividing the percentage of the element contained within the collected sample by the percentage of the most abundant element in the contributing source.

The multiple regression models used the measured elemental components within the collected particulate matter as the dependent variables and the elemental composition of source profiles as the independent variables. The aim of the regression analysis was to obtain regression coefficients, which when multiplied by the independent variables, would predict the amount of collected matter that originated from each contributing source.

The model was judged to have reproduced the data if positive regression coefficients were obtained and the standard deviation of the regression coefficient was small.

5.1.1 Early literature example of chemical element balance

One of the first chemical element balance models to be used was reported by Millar *et al.* (1972) who used the approach to determine the contribution of sources to the collected particulate matter in Pasadena, California. The authors assumed that four sources (sea salt, soil, automobile emissions and fuel oil fly ash) contributed to the collected samples. The elements used as tracers were sodium, aluminium, lead and vanadium, respectively. These were selected because, according to the authors, they were each the major component of one of the sources considered. However, given the variable nature of a source, the most abundant element or ion characteristic of a source found at one location may differ from the same source found at a different location. For example, in an experiment investigating the concentration of trace elements in flyash particles released from combustion of Virginian, Polish and German coal, Gay *et al.* (1989) found that the vanadium concentration released from the combustion process, decreased in the order: German coal (124 mg kg^{-1}) > Polish coal (118 mg kg^{-1}) > Virginian coal (41 mg kg^{-1}).

The source profile for sea salt was approximated to the gross composition of sea water. The soil dust source profile was determined by measuring the elemental composition of a soil sample. The percentage of the trace elements in emissions released from the two combustion sources (automobile and fuel oil), were determined by performing a chemical analysis on collected exhaust particulates.

The fractional contribution from each source, C_j, was determined by dividing the percentage of element (i) in the collected sample by the percentage composition of that element in the originating source (j).

$$C_j = \frac{\textit{Percentage of element } i \textit{ measured in collected sample}}{\textit{Percentage of element, } i \textit{ present as tracer in the source } j}$$

. . . .Equation 5.1

For example, the contribution from the soil source was calculated by dividing the amount of aluminium contained within the collected particulate matter sample (0.8%) by the amount of aluminium determined, on average, to be present in the soil samples

(8.2%).

$$C_{j=soil} = \frac{0.8\%}{8.2\%} = 0.098$$

. . . .Equation 5.2

On this basis, the contribution of the soil source was calculated to be 9.8%. The contributions for sea, auto and fuel sources were calculated as 2.5%, 8.2% and 0.24%, respectively.

Together these four sources accounted for approximately 20% of the collected mass. Other likely sources of mass, not used considered by Millar *et al.* (1972), are secondary particulate matter and crustal material containing calcium carbonate.

5.1.2 Illustrative example of chemical element balance

In order to clarify the receptor models described in this chapter a simplified data set is used to highlight the basis to each technique. This data set, consisting of the relative abundance of six elements in both the collected particulate matter and each of three contributing sources, is presented in Table 5.1. The most abundant element, and hence the one used in the element balance, is shown in the table by bold print.

Table 5.1 Hypothetical mass balance example

Metal	Abundance in collected particulate matter (%)	Abundance in Source **a** (%)	Abundance in Source **b** (%)	Abundance in Source **c** (%)	Percentage contribution
Mn	0.02	0.06	0.01	0.80	
Cu	0.04	0.10	0.04	**4.00**	1
K	1.00	0.12	**2.00**	2.00	50
Mg	0.50	1.00	0.05	0.70	
Na	3.00	**7.00**	0.20	0.80	43
Zn	0.01	0.05	0.20	0.10	

The source contributions were determined using Equation 5.1 above. On the basis of the most predominant elements, Source **b** is contributing the largest mass (50%) to the

collected sample, with Sources **a** and **c** contributing 43% and 1%, respectively. This example provides an illustration of a major disadvantage in the simple element balance technique, which is that one element, such as potassium in Source **c**, may be released from more than one source.

5.2 Multiple regression using emission profiles derived from the literature

The multiple regression method, using source profiles obtained from the literature as independent variables, and measured concentrations as dependent variables, was a logical step in the development of receptor models, since all elements in each source category would be used to calculate the percentage contribution from each source.

5.2.1 Literature example of multiple regression analysis

The multiple regression method using source profiles as independent variables and measured concentrations as dependent variables was first reported by Friedlander (1973) and developed further by Kowalczyk *et. al.* (1978). The 1978 study by Kowalczyk was conducted in Washington D.C. during 1974 with the mean elemental concentration of 10 collected samples used as the dependent variables. Although the literature source profiles employed in the study were reported for 27 elements, only eight elements (Al, Na, Fe, V, Zn, Pb, Mn and As) were measured in the collected samples. Six sources, each with a characteristic tracer element, were assumed to contribute mass to the collected aerosol.

The key parts to the Kowalczyk method are outlined in Stages 1 to 3 below.

Stage 1. Obtaining regression coefficients (matrix b). These are calculated by regressing the mass concentration of elements contained within the collected sample (matrix y, dependent variable) onto the abundance of elements contained within each source profile (matrix X, independent variables). Two methods to perform the necessary computations, manually and computer assisted, will be presented in Sections 5.2.2.2 and 5.2.2.3, respectively.

Stage 2. Predicting elemental composition at each receptor site. Each source profile was multiplied by the respective regression coefficient to give the elemental mass contribution from each source. Summing the elemental mass concentration of each element originating from the respective source profiles produced a "predicted" elemental concentration in the TSP.

Stage 3. Determine the contribution of each source to TSP collected at the receptor site. This was determined by dividing the predicted elemental mass concentration (ng m^{-3}) by the fraction of element contained within that source. For example, refuse combustion supplied about 120 ng m^{-3} of ambient zinc, and zinc made up 9% of the particles from that source, so that the contribution of refuse incineration to TSP was *120 ng m^{-3}/0.09 = 1.3 μg m^{-3}*.

The respective sizes of the matrices containing the independent variables (8 rows × 6 columns) and dependant variable (8 rows × 1 column) and the calculated regression coefficients (6 rows × 1 column) are illustrated schematically in Figure 5.1.

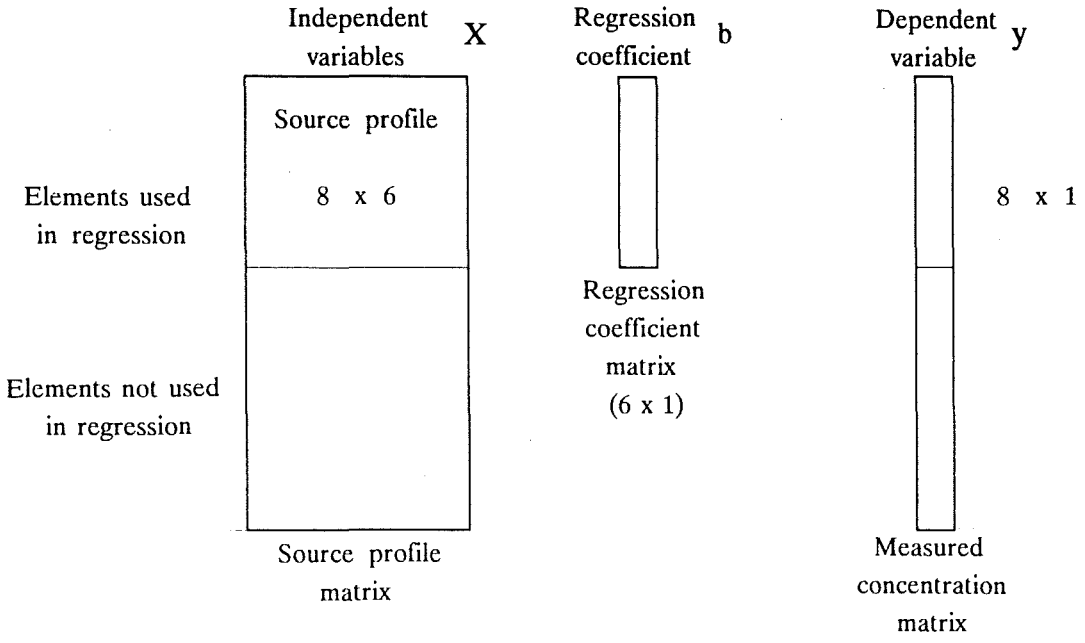

Figure 5.1 Schematic matrix representation showing relationship between source profiles, regression coefficients and measured concentrations.

In this way Kowalczyk accounted for 38.5 μg m^{-3} of the 69 μgm^{-3} T.S.P. measured.

This 55% represents the sources of primary aerosols, other sources (though not quantified) were attributed to secondary particulate matter and organic molecules that had condensed on the collected particulate matter.

5.2.2 Illustrative example of multiple regression analysis

5.2.2.1 Introduction

The following example, using the same data set as shown in Table 5.1 for the simple mass balance, will illustrate how source contributions are determined using the multiple regression method. Although the same numerical values are used in the method as presented previously in Table 5.1, the example assumes that the collected particulate matter will have a total mass concentration equal to 100 $\mu g\ m^{-3}$. The source profiles used in the calculation are expressed as percentage of element in source, as was the case for the simple mass balance method.

The multiple regression equation that will be determined is expressed as follows:

$$\textit{Predicted mass} = (0.417 \pm 0.01)(\textit{Source a}) + (0.473 \pm 0.04)(\textit{Source b}) - (0.003 \pm 0.02)(\textit{Source c}) \quad (\mu g\ m^{-3})$$

. . . .Equation 5.3

The following sections, using both manual computation and a computer software package, will show how these values are obtained.

5.2.2.2 Manual computation of regression coefficients

The theoretical derivation and manual computation of regression coefficients, for the case of no regression constant, is presented in this section. By omitting the regression constant, the model assumes that the sample collected at the receptor site will only receive material from the three considered sources, **a**, **b** and **c**. In addition, the manual computation of the regression coefficients is relatively more straight forward, compared to the inclusion of the regression constant.

Regression coefficients are obtained from a regression analysis so that the difference between the observed dependent variable and the predicted dependent variable is a

minimum, where the predicted dependent variable is the product of the independent variables and regression coefficients. Using statistical nomenclature similar to that employed by Neter *et al.* (1988), the subtraction of the predicted dependent variable from the original dependent variable can be expressed by Equation 5.4.

$$Q = \sum_{i-1}^{n} [y_i - \hat{y}_i]^2 \qquad \text{. . . .Equation 5.4}$$

Where: Q is the sum of the squared deviations; y_i, is the dependent variable; $\hat{y}_i$, (y_i *hat*) is the "predicted" dependent variable, which is equal to the product of independent variable, X_i, and regression coefficient, b_i. That is, $\hat{y}_i = X_i b_i$

The derivation of the regression coefficient is shown below for the case of one independent variable with no regression constant.

Stage 1 Substitute $X_i b_i$ for y_i *hat* in Equation 5.4.

$$Q = \sum_{i-1}^{n} [y_i - (X_i\ b_i)]^2 \qquad \text{. . . .Equation 5.5}$$

Stage 2 Expanding and differentiating with respect to b, produces an expression, that when rearranged yields the required equation to calculate the regression coefficients, b. The expansion and differentiation are presented in Equation 5.6 and Equation 5.7, respectively.

$$Q = \sum_{i-1}^{n} [y_i^2 - 2X_i b_i y_i + X_i^2 b_i^2]$$

. . . .Equation 5.6

Differentiating with respect to b

$$\frac{dQ}{db} = \sum_{i-1}^{n} [\ -2(X_i)y_i + 2\ (X_i^2 b_i\ )] = 0$$

. . . .Equation 5.7

since for min Q, $dQ/db = 0$.

The rearranged equation (Equation 5.8), can be described as the sum of the products of y_i and X_i, divided sum of the squares of X_i.

$$b = \frac{\Sigma X_i\, y_i}{\Sigma(X_i^2)} \qquad \text{. . . .Equation 5.8}$$

This expression can be alternatively expressed in matrix form as represented by Equation 5.9.

$$b = (X^T X)^{-1} X^T y \qquad \text{. . . .Equation 5.9}$$

Using the data presented in Table 5.1, and the necessary matrix operations, the regression coefficients are calculated as follows.

Where: b is the regression coefficient matrix
X is the matrix of independent variables, columns three to five in Table 5.1
X^T is the transpose of matrix X
$(X^TX)^{-1}$ is the inverse of the product of the matrices, X^T and X
y is the dependent variable matrix

Stage 1 Obtain X^TX. This is achieved by multiplying the number contained within each row by the corresponding number in each column. The products of this operation are added and placed into the matrix X^TX.

Matrix X^T

0.06	0.10	0.12	1.00	7.00	0.05
0.01	0.04	2.00	0.05	0.20	0.20
0.80	4.00	2.00	0.70	0.80	0.10

Matrix X

0.06	0.01	0.80
0.10	0.04	4.00
0.12	2.00	2.00
1.00	0.05	0.70
7.00	0.20	0.80
0.05	0.20	0.10

Matrix X^TX

50.031	1.705	6.993
1.705	4.084	4.383
6.993	4.383	21.780

Stage 2 Obtain the inverse of X^TX, that is, $(X^TX)^{-1}$. The inverse of the matrix X^TX will produce the identity matrix, I, when multiplied by X^TX. The necessary calculations to determine the inverse of a matrix are shown in Kaplan (1981).

Matrix $(X^TX)^{-1}$

0.0209	-0.0019	-0.0066
-0.0019	0.3125	-0.0623
-0.0063	-0.0623	0.0605

Stage 3 Obtain X^Ty. Again this is achieved by multiplying the number contained within each row by the corresponding number in each column. The products are added and placed into the matrix X^Ty.

Matrix X^T

0.06	0.10	0.12	1.00	7.00	0.05
0.01	0.04	2.00	0.05	0.20	0.20
0.80	4.00	2.00	0.70	0.80	0.10

Matrix y

0.02
0.04
1.00
0.50
3.00
0.01

Matrix X^Ty

21.176
2.606
4.612

Stage 4 Multiply $(X^TX)^{-1}$ by X^Ty. As before the numbers in each row are multiplied by the numbers in the corresponding column. The sum of each set of products will give the regression coefficients.

Matrix $(X^TX)^{-1}$

0.0209	-0.0019	-0.0066
-0.0019	0.3125	-0.0623
-0.0063	-0.0623	0.0605

Matrix X^Ty

21.176
2.606
4.612

The regression coefficients are determined as 0.417, 0.473 and -0.003.

The estimated standard deviations of the regression coefficients, indicated by $\pm$ in Equation 5.3, will provide a measure of the accuracy of the estimated standard deviation. For the case of "no regression constant", these are obtained by using the operation illustrated by Equation 5.10.

$$s^2(b_i) = \frac{MSE}{\Sigma(X_i)^2} \qquad \text{. . . .Equation 5.10}$$

Where: $s^2(b_i)$ is the estimated variance of the regression coefficient b_i
MSE is the error mean square, determined by dividing the error sum of squares, SSE, by the degrees of freedom. For the case of a multiple regression with three independent variables with no regression constant, the number of degrees of freedom (df) is equal to n-3. Where n, the number of cases in the example, is equal to 6, hence df = 3. $\Sigma(X_i)^2$ is the sum of each squared term in the independent variable.

The SSE values are determined by subtracting from each of the dependent variables, the "predicted" dependent variable obtained by multiplying each independent variable by the calculated regression coefficients. The multiplication of source profiles by each regression coefficient will be presented in Section 5.2.2.4. Subtracting each "predicted" mass from the measured mass, will produce the residuals, presented in Table 5.2.

Table 5.2 Residual values used to determine the error mean square in the worked multiple regression model.

Original dependent Variable *y*	Predicted dependent Variable	Residual	(Residual)^2
0.02	0.274	-0.007	0.00005
0.04	0.049	-0.008	0.00007
1.00	0.990	0.010	0.00010
0.50	0.439	0.061	0.00377
3.00	3.011	-0.011	0.00001
0.01	0.115	-0.105	0.01110
			Σ(0.0150)=SSE

The error mean square is consequently obtained by dividing SSE by the degrees of freedom (3). When the MSE (0.005) is divided by each squared independent variable (50.03, 4.08, 21.78, for Variables **a**, **b** and **c**, respectively), the estimated variance for each regression coefficient is obtained.

Finally, the standard deviation, *s*, of each regression coefficient is determined as the square root of the variances: 0.01, 0.04 and 0.02, for Sources **a**, **b** and **c**, respectively.

5.2.2.3 Obtaining regression coefficients using LOTUS 123

The computer package chosen to perform the multiple regression was LOTUS 123. This was because both data entry and computation were relatively straight forward. The dependent variable (column two) was regressed onto the independent variables (columns three to five in Table 5.1). By setting the regression constant to zero, only the selected source profiles were used to calculate the predicted mass concentration. The standard deviations of the regression coefficients can also be calculated using LOTUS 123. The resulting regression equation obtained (Equation 5.3) is, of course, identical to that determined by the manual computation method (Section 5.2.2.2).

5.2.2.4 Multiplication of source profiles by regression coefficients

The calculated regression coefficients are then multiplied by each source profile to give mass of material originating from each source. The mass contributions from each source are presented in Table 5.3 (columns three to five). The sum of each element from Source **a**, **b** and **c** will give a "predicted" mass concentration for that element at the receptor.

5.2.2.5 Amount of collected particulate originating from each source

According to Kowalczyk *et al.* (1978), the amount of collected matter originating from each source is calculated in a similar way as performed for the simple element balance. That is, the contribution of each source is calculated by dividing the predicted elemental mass concentration from a source (Table 5.3) by the abundance of each element in each

Table 5.3 Elemental contribution from each source.

Metal	Collected mass $\mu g\ m^{-3}$	Source **a** $\mu g\ m^{-3}$	Source **b** $\mu g\ m^{-3}$	Source **c** $\mu g\ m^{-3}$	Predicted mass $\mu g\ m^{-3}$	Ratio Collected/Predicted concentration
Mn	0.02	0.03	0.005	-0.002	0.03	0.67
Cu	0.04	0.04	0.02	**-0.012**	0.05	0.80
K	1.00	0.05	**0.95**	-0.006	0.99	1.00
Mg	0.50	0.42	0.02	-0.002	0.44	1.14
Na	3.00	**2.94**	0.10	-0.002	3.02	1.00
Zn	0.01	0.02	0.10	-0.0001	0.12	0.08
	$\Sigma = 4.57$				$\Sigma = 4.65$	

source (Table 5.1). The contributions from Sources **a**, **b**, and **c** were calculated as 2.92 $\mu g\ m^{-3}/0.07$, 0.95 $\mu g\ m^{-3}/0.02$ and -0.012 $\mu g\ m^{-3}/0.04$, respectively. Hence, the contributions of mass from the contributing sources was determined as 42 $\mu g\ m^{-3}$, 48 $\mu g\ m^{-3}$ and -0.3 $\mu g\ m^{-3}$ for Sources **a**, **b**, and **c**, respectively, which together account for 89.7 $\mu g\ m^{-3}$ of the total mass collected.

However a serious descrepancy in this example is apparent, since although the sum of the predicted mass (4.65 $\mu g\ m^{-3}$) is relatively close to the measured mass (4.57 $\mu g\ m^{-3}$) the calculated contribution from each source is under estimated (only 89.7% of the total 100 $\mu g\ m^{-3}$ was accounted for). However, as this example was contrived to illustrate the mathematical operation behind the multiple regression chemical-element balance approach, this discrepancy may not be considered important. Nevertheless, the selection of suitable source profiles as independent variables and their subsequent use in a regression analysis may not necessarily provide statistically significant regression coefficients.

The significance of a regression coefficient can be determined by calculating the t statistic, (the regression coefficient divided by the estimated standard deviation of the regression coefficient, indicated by the symbol "$\pm$" in Equation 5.3). The calculated t statistic is then compared to the critical t-statistic, a t value obtained for a given level of significance and appropiate degrees of freedom. For the worked example, at the 0.05 level of significance and three degrees of freedom, the critical value is 2.35. The t

statistic values for Sources **a**, **b** and **c** were calculated to be 41.7, 11.8 and -0.15, respectively. As only Sources **a** and **b** are greater than the critical value, this would suggest that only these two sources are related to the observed dependent variable. Hence the inclusion of a third source, although considered important may not be statistically significant.

5.3 Regression of total suspended particulate mass concentrations on selected variables

The introduction of principal component analysis (PCA) to the receptor modelling technique by Kleinman *et.al.* (1980) allowed information regarding the nature of a source to be obtained directly from the measured elemental concentrations. An obvious advantage of this method is that literature profiles were not required.

Principal components are linear combinations of variables, determined in such a way that the variance contained within the original variables is redistributed. The linear combinations can be expressed by Equation 5.11.

$$PC = e^{t}X \qquad \text{. . . .Equation 5.11}$$

where: PC is matrix of principal components, e^{t} is the transpose matrix of eigenvectors, X is the matrix of original variables.

Each principal component has an associated eigenvalue that represents the variance of the principal component. The illustrated example showing the calculation of eigenvalues and eigenvectors, presented in Section 5.5.1, shows that the first eigenvalue describes the largest amount of variance, with the remaining eigenvalues describing progressively lower amounts of variance.

The principal component analysis in receptor modelling is generally performed on the matrix of correlation coefficients, where each correlation coefficient represents the association between measured components of the collected sample. The PCA will provide:

- the number of independent variables to be used in the regression analysis, determined as the number of principal components with eigenvalues greater than

one. This in turn will equal the number of contributing sources.

- identification of the independent variables which are used subsequently in the regression analysis. These are determined as the element or ion with the highest loading on a factor. The calculation of factor loadings will be presented in Section 5.5.2.

5.3.1 Literature example showing the regression of TSP mass concentrations on selected elements or ions

The example provided by Kleinman *et al.* (1980) illustrated the method by regressing the TSP mass concentrations onto the concentrations of five variables: Pb, Mn, Cu, V and SO_4^{2-}. The five variables were selected as those variables which had high loadings on the five principal components with eigenvalues greater than 1.0, with each factor loading indicating the association between the original variable and the principal components. The chosen variables were each assumed to be characteristic of a particular source. The resulting regression equation was represented by Equation 5.12:

$$TSP = 12.0\,(Pb) + 54\,(Cu) + 103.0\,(V) + 1.7(SO_4^{2-}) + 420\,(Mn) + 26.8$$

. . . .Equation 5.12

The TSP and the constituent components were measured in units of $\mu g\ m^{-3}$ and $ng\ m^{-3}$, respectively. The residual 26.8 $\mu g\ m^{-3}$ accounts for the mass not explained by the model, and was attributed by Kleinman to sea-salt sulphate. The source contributions were determined as:

$$Source\ Contribution = \frac{Regression\ Coefficient \times Mean\ Concentration\ of\ Element\ or\ Ion\ in\ TSP\ (ng\ m^{-3})}{Mean\ TSP\ Mass\ Concentration\ (\mu g\ m^{-3})}$$

. . . .Equation 5.13

The calculation of source contribution was illustrated for the case of manganese (a soil tracer), where the regression coefficient multiplied by the arithmetic mean concentration value (28 $ng\ m^{-3}$) gave a calculated contribution of 11.7 $\mu g\ m^{-3}$. When this concentration was divided by the arithmetic mean TSP mass concentration, 80 $\mu g\ m^{-3}$, the resulting percentage contribution was determined as 14.6%. The remainder of the determined source contributions are shown and compared to those of Pio *et al.* (1990) in Table 5.4.

Table 5.4 Percentage source contributions determined by regression of TSP values on selected elements

Source	Kleinman (1980)	Pio *et al.* (1990)
Automobiles	22.8 (Pb)	18.0 (Organic Carbon).
Fuel Burning	10.3 (V)	Not investigated
Soil	14.6 (Mn)	37.0 (Al)
Sulphates oxidised from SO_2	20.5 (SO_4^{2-})	18 (SO_4^{2-})
Incineration	3.2 (Cu)	Not investigated
Sea Salt	Not investigated	8 (Na)
Industrial Source 1	Not investigated	1.4 (Ni)
Industrial Source 2	Not investigated	0.3 (Cr)
(%) Mass Not Explained by Model.	33	7

The tracer element is shown in brackets.

The contribution of sulphate to the collected samples is similar for both studies. The contribution from automobiles was also similar even though different tracers, Pb and organic carbon, were used. Pio *et al.* (1990) determined that their soil source contributed twice as much as that determined by Kleinman. This may be attributed to the difference in geographical location; the Kleinman (1980) study was conducted in New York City, whereas the Pio *et al.* (1990) study was conducted in a small town in north west Portugal. In addition, both studies only partially accounted for collected TSP, with the Pio *et al.* (1990) study more successful (93%) than the Kleinman (1980) study (77%).

5.3.2 Illustrative example showing the regression of TSP mass concentrations on selected elements

The same numerical values presented in Table 5.1 are also used to highlight the basis to this method. However a crucial difference to the previous use of this data set is that

the dependent variable represents TSP values, in $\mu g\ m^{-3}$, for 6 collected samples and the independent variables are the concentration of three elements, or ions, that are constituent parts of each collected sample. The variables are redefined in Table 5.5.

Table 5.5 Redefined independent variables and dependent variable used to illustrate the regression of TSP values on selected elements or ions

Sample	TSP ($\mu g\ m^{-3}$)	Element or ion **a** ($\mu g\ m^{-3}$)	Element or ion **b** ($\mu g\ m^{-3}$)	Element or ion **c** ($\mu g\ m^{-3}$)
1	2	0.06	0.01	0.80
2	4	0.10	0.04	4.00
3	100	0.12	2.00	2.00
4	50	1.00	0.05	0.70
5	300	7.00	0.20	0.80
6	1	0.05	0.20	0.10
Mean	76	1.38	0.42	1.40

An unfortunate consequence in the continued use of this data set is the wide range in TSP values (1 to 300 $\mu g\ m^{-3}$). This fluctuation is considered unlikely to occur in the ambient atmosphere.

The PCA performed on the correlation matrix between Variables **a**, **b** and **c**, produces eigenvalues and factor loadings (Table 5.6) that will aid the identification of the independent variables which should produce the "best" regression equation (the derivation of eigenvalues and factor loadings will be presented in Sections 5.5.1 and 5.5.2, respectively).

Table 5.6 Factor loadings and eigenvalues (λ) determined for each principal component

Variable	PC1	PC2	PC3
a	0.710	0.324	-0.618
b	-0.609	0.797	-0.015
c	-0.707	-0.352	-0.610
λ	1.37	0.86	0.76

As shown in Section 5.3.1, the number of contributing sources are determined by the

number of principal components with eigenvalues greater than 1.0. As only PC1 has an eigenvalue greater than 1.0, only one source (for which Variable **a** is the characteristic tracer) is estimated to contribute to the collected particulate matter.

The ability of Variable **a** to act as a suitable tracer is also suggested by regression analysis. That is, examination of the regression output obtained when the TSP mass concentration is separately regressed onto each variable (Table 5.7), shows that the estimated standard deviation of the regression coefficient is smallest for Variable **a** (6 $\mu g\ m^{-3}$), indicating that the regression coefficient for Variable **a** is the most statistically significant compared to those of Variables **b** and **c**. In addition, the coefficient of determination, R^2, when Variable **a** is the independent variable is also large (0.91), indicating that this independent variable has significantly accounted for the variance in the TSP variable. The R^2 values for Variables **b** (0.16) and **c** (0.11) are much lower, suggesting that each does not play a role in accounting for the variance in TSP.

Table 5.7 Regression coefficients, estimated standard deviation of regression coefficient and coefficient of determination resulting from the regression of TSP onto Variables **a**, **b** and **c**

	Variable **a**	Variable **b**	Variable **c**
Regression coefficient (RC)	43.3	64.4	22.7
Estimated standard deviation of RC	6.0	64.7	29.0
R^2	0.91	0.16	0.11
Source contribution (%)	79	35	42

By examining the source contributions determined using Equation 5.13, Source **a** does produce the highest source contribution (79%). Whereas, Variables **b** and **c** contribute less than half of the TSP mass concentration. The suitability of the method to select an independent variable, on the basis of a high loading on a principal component, appears to be successful.

In common with the literature derived source profiles, the regression of TSP values onto elemental concentrations will produce error in the regression coefficients if there is dependency (collinearity) between the independent variables (methods to overcome this are described in Section 5.6).

5.4 Additional combinations of statistical techniques used in receptor models.

In addition to the combination of multiple regression with PCA analysis, other statistical techniques have been combined to provide information regarding the nature of the contributing sources. A selection of the statistical techniques is presented in Table 5.8.

Table 5.8 Examples of statistical techniques used in receptor modelling

Statistical techniques	Inferred information	Author
Factor analysis * Cluster analysis	Identification of contributing sources	Hopke *et al.* (1976)
† Factor analysis ** Multiple regression (TTFA)	Mass contribution from each source and elemental components of each source	Alpert and Hopke (1980)
† Factor analysis ** Multiple regression (FANTASIA)	Mass contribution from each source and elemental components of each source	Hopke *et al.* (1983)
PCA ** Multiple regression (RAPCS)	Mass contribution from each source and elemental components of each source	Thurston and Spengler (1985)
Factor analysis ** Multiple regression (RAFS)	Mass contribution from each source and elemental components of each source	Okamoto *et al.* (1990)

Key: * Overall the method required relatively little interaction between the techniques.
** Overall the method requires a high degree of interaction between the techniques.
† The method has been described by each author as involving factor analysis, but, on inspection of the statistical background presented in each reference the method would more correctly be described as PCA. However, the methods are interchangeable.
RAPCS, regression on absolute principal component scores.
RAFS, regression on absolute factor scores.

Factor analysis is a technique similar to principal components, in that, both are concerned with approximating either a covariance or correlation matrix, (Johnson and Wichern, 1988). In addition, as the factor analyses described in the sections below all used principal component analysis as an initial stage to estimate the number of factors required to reproduce the correlation matrix, the two methods can, for the purposes of

source apportionment be considered similar.

5.4.1 Factor analysis and cluster analysis

Hopke *et al.* (1976) applied both factor analysis and cluster analysis to ninety samples, each analysed for eighteen elemental components, collected throughout the Boston metropolitan area. The factor analysis, a technique related to PCA in that distinct sources of variation are identified, suggested that six sources/factors contributed to the measured TSP. The form of cluster analysis used was hierarchial aggregative cluster analysis which defined each variable as a dimension in hyperspace. The distance between points, representative of the elemental concentrations within each dimension, was used to organise the samples into groups which, when presented in a dendogram, showed the similarity between samples. The cluster analysis was used to assist in the interpretation of factor scores which resulted from the factor analysis (a method to derive factor scores is presented in Figure 5.5). One sub-cluster, ***J***, contained samples which showed high factor scores for both Factor 4 (identified as an incineration source) and Factor 6 (automotive exhaust). However, this result did not provide quantitative information regarding the nature of the sources, but confirmed that the samples were originally collected from a busy road close to the international airport and near an incinerator plant.

5.4.2 Using principal component analysis and multiple regression to determine mass contributions and source profiles

The calculation of source contributions by the method outlined in Section 5.3 produced a relatively generalised result, since only one set of contributions were calculated for all samples. Further information, using additional aspects of PCA can be used to determine:

- contribution of mass, from each source, to individual TSP mass concentration
- elemental profile of contributing sources (these profiles differ to those described previously in Section 5.2, as they are generated from the receptor model and not by measuring source composition at point of release into the atmosphere).

Two procedures were used in this study to calculate both the mass contributions and elemental compositions of each source from the measured elemental concentrations. The first generated the source profiles initially and calculated the mass contribution at a later stage. This method was demonstrated previously by Alpert and Hopke (1980), Alpert and Hopke (1981) and Alpert and Hopke (1983). A designated software package for receptor modelling (FANTASIA, Factor Analysis to Apportion Sources in Aerosols, 1989 version) is used to perform the necessary calculations (the basis of this method is presented in Section 5.4.2.2.).

The second procedure calculated the mass contribution from each source as a first step using the assumption that the mass contribution was equivalent to absolute principal component scores (derivation of APCS will be presented in Section 5.4.2.4.). The elemental compositions of each source were developed at a later stage. This method was first developed by Thurston and Spengler (1985) and Keiding *et al.* (1986). A variant on the model was provided by Okamoto *et al.* (1990), who calculated absolute factor scores. The calculation of absolute principal component scores, for a simplified data set, will be presented in Section 5.5.3.

5.4.2.1 Previous use of Fantasia

Early versions of this program have been applied to aerosols collected in Boston (Alpert and Hopke 1980) and in St. Louis, U.S.A. (Alpert and Hopke 1981).

The Boston study determined the percentage mass contribution of six sources (soil, oil, refuse, marine, automobile and road dust) to the collected particulate matter. The profiles were determined by applying TTFA to 57 urban and 33 sub-urban aerosol samples. However as sulphur and carbon were not included in the analysis, only a partial identification of the sources could be achieved.

The St. Louis study investigated the effect of different sampling strategies on source profiles. The collected samples included both coarse and fine samples collected using a dichotomous sampler. The first sampling programme collected samples over a long period (2 months) at a single site, whereas the second programme collected from ten

sites over a shorter period of time (one week). For the single site, 99 fine and 101 coarse fraction particulate samples were obtained over the two month period using 12 hour collection periods. For the multiple sample site study, ten sampling sites operated continuously over a one week period. This sampling programme collected 139 fine and 132 coarse particulate samples. The percentage contribution of the calculated sources to the fine and coarse fractions for both sampling regimes are shown in Figure 5.2.

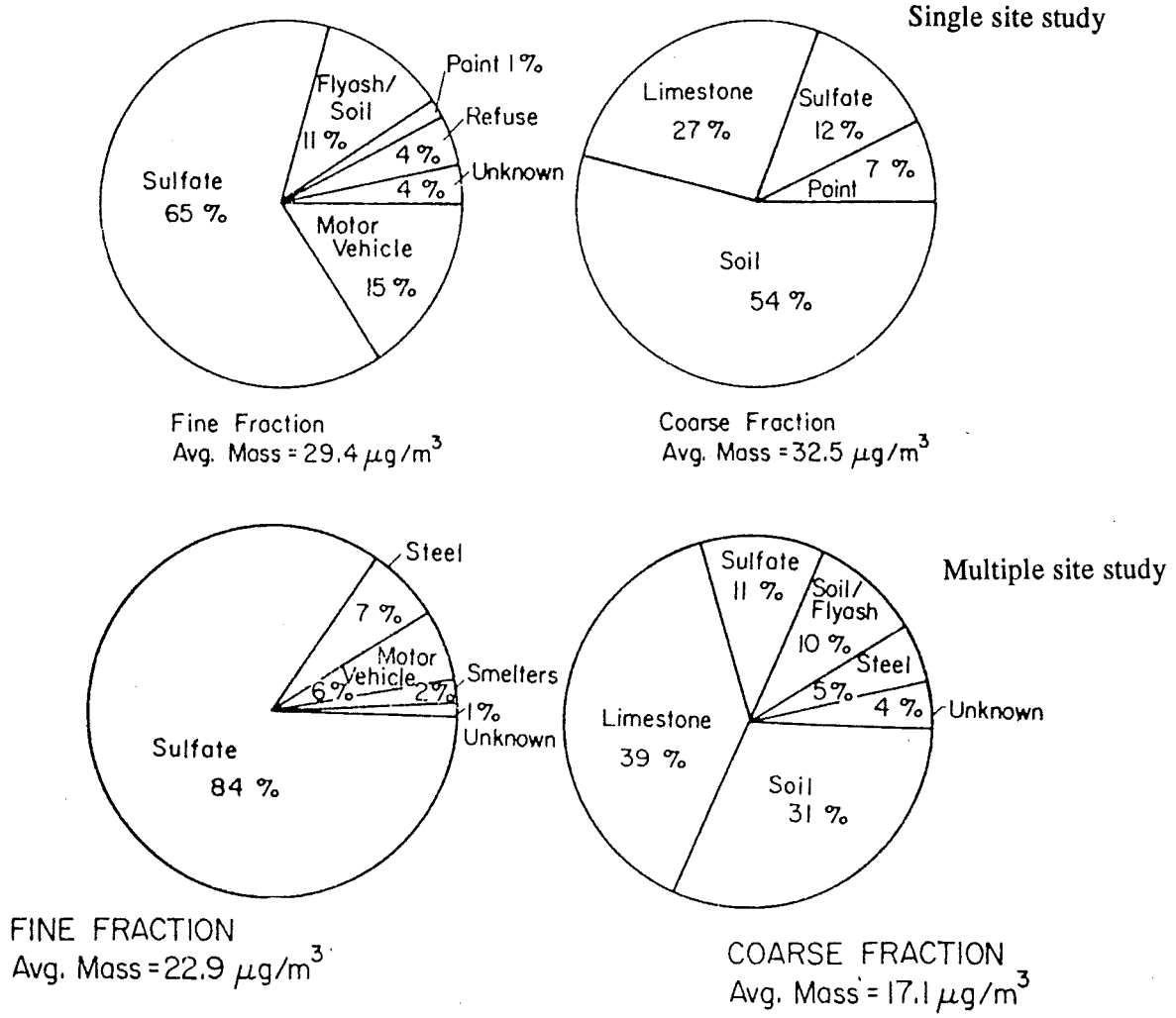

Figure 5.2 Percentage contribution to collected fine and coarse fractions for two sampling regimes (Alpert and Hopke, 1981)

Differences in the nature of the sources contributing to the mass collected at each site in the multi-site study resulted in this sampling regime giving a poorer resolution of the contributing sources for the fine particulate fraction. For example, only 4 sources (secondary particulate sulphate, steel, motor vehicles and smelters) were resolved for the fine fraction of the nine site study, whereas 5 sources were observed to be contributing to the collected fine particulate mass in the single site study (Figure 5.2).

Conversely, the multi-site study was found to give better resolution of sources for the coarse fraction with 5 sources resolved compared to the 4 sources resolved for the single site study.

5.4.2.2 Background to the Fantasia program

The key stages in the FANTASIA program (1989 version) are discussed below. A program flow diagram and annotated flow chart, illustrated in Figures 5.3 and 5.4 respectively, are used to assist the explanation.

a) The initial stage assesses the number of sources contributing to the collected particulate matter by calculating a factor loading matrix (Stage 1, Figure 5.4). The eigenanalysis in FANTASIA is performed on the correlation matrix which shows the associations between samples (known as Q mode analysis), as opposed to the correlation between elements (known as R mode analysis). The Q mode analysis was chosen since differences in concentration between specific elements or ions measured for each sample within the data set is relatively small compared to the concentration range of all elements or ions measured within a sample. This can be illustrated by using the concentration values of sulphate and manganese determined in this study: mean sulphate and manganese concentrations value were determined to be approximately the same order, indicated by the fact that most concentration values (67%) are present around the mean values (sulphate and manganese mean and standard deviations concentration values were determined as 9.5 ± 7.0 $\mu g\ m^{-3}$ and 22 ± 13 $ng\ m^{-3}$, respectively). Whereas, the manganese and sulphate mean concentration values typically differ by more than two orders of magnitude (for example, at Lincoln sulphate concentrations values were 9.5 $\mu g\ m^{-3}$ and manganese concentrations were 22 $ng\ m^{-3}$).

In addition, the FANTASIA is unique in utilising the Q mode analysis since most commercial statistical software packages appear to perform the eigenanalysis on the R mode correlation matrix.

According to the statistical nomenclature of Hopke (1984) the factor loading matrix, A_Q, is defined by the combination of the matrices according to:

$$A_Q = XV^{-1}Q_Q \quad \ldots\ldots\ldots\ldots \text{Equation 5.14}$$

where: X = data matrix
V^{-1} = represents a diagonal matrix with elements:
$v_{ij} = \delta_{ij}[\Sigma_i x_{ij}^2]^{1/2}$
where δ_{ij} = Kronecker Delta.
and x_{ij} represents the *ith* elemental concentration measured for the *jth* sample
Q_Q = matrix of eigenvectors associated with the eigenvalues

b) The factor loading matrix is then converted into unscaled source profiles by using the target transformation option (Stage 2, Figure 5.4). This involves realigning A_Q with a matrix of test vectors. This matrix of test vectors will initially be:

$$\begin{bmatrix} 1 & 0 & 0 \\ 0 & 1 & 0 \\ 0 & 0 & 1 \end{bmatrix}_n$$

where **n** equals the number of elements measured in the study.

The program performs this task by regressing individually each **(1 0 0)**n column onto the factor loading matrix (the basis to regression analysis was discussed in Section 5.2.2.2.). Next, the resulting regression coefficients multiply each term in the factor loading matrix to obtain a predicted test vector. This process is repeated until the difference between the predicted and initial test vector is negligible. Using the terminology of Hopke (1989), the regression coefficient matrix is described as matrix $\mathbb{R}$ and the factor loading matrix, A_Q, which has undergone the transformation is described as the matrix of unscaled source profiles, *B*.

c) Following the target transformation stage, source profiles are selected by performing a cluster analysis (Stage 3, Figure 5.4). Those profiles located relatively well apart on the dendogram will be selected for further use (examples of dendrograms produced from the cluster analysis will be presented in Chapter 7, Figure 7.8). The profiles are saved in the LOADMX file in FANTASIA.

d) The elemental concentrations are then regressed onto the selected profiles determined for each sample to give the mass contribution from each source (Stage 4, Figure 5.4).

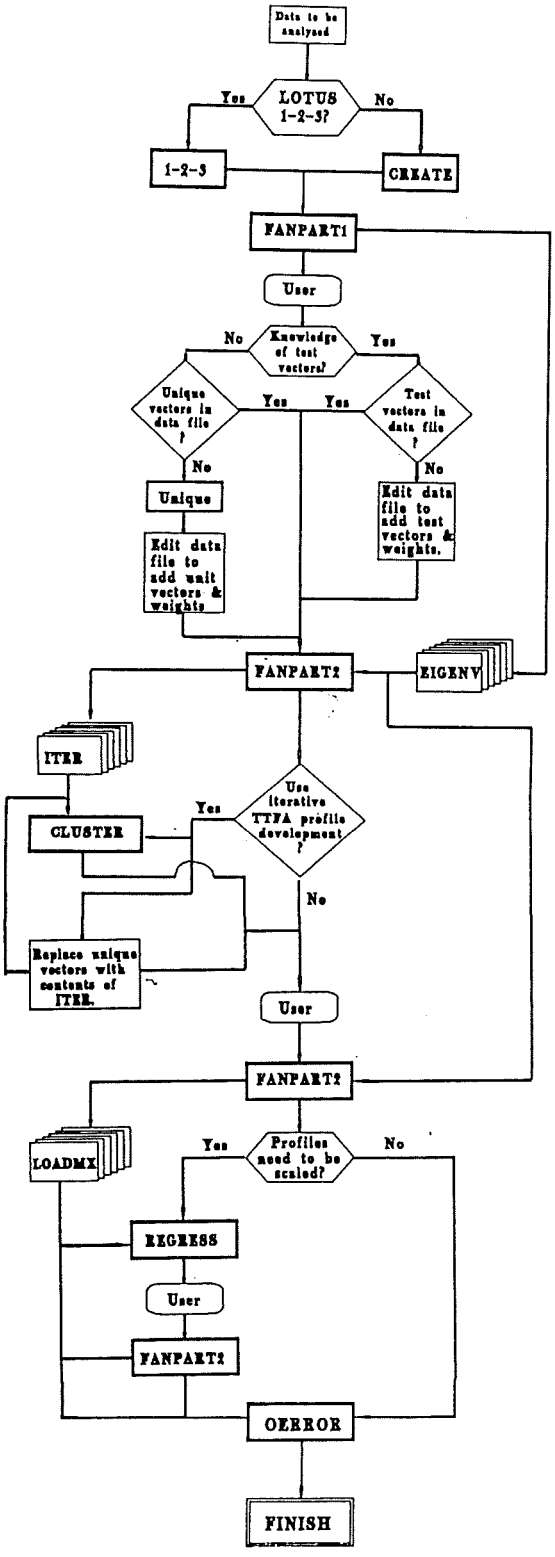

Figure 5.3 Program flow diagram for FANTASIA (Hopke 1989).

Flow chart to illustrate the key stages in the FANTASIA receptor model.

Stage 1

FANPART 1

Comment

Factor analysis is performed on the data. The data reproduction summary is examined to see if the factors reasonably reproduce the correlation matrix.

Stage 2

FANPART 2

A range of possible source profiles are developed using a rotation matrix which is produced iteratively from the factor loading matrix. This is the target transformation stage of the FANTASIA method. The rotation matrix will be of the form:

$$\mathbb{R} = \frac{A_Q^t W v}{A_Q^t W A_Q} \quad \ldots\ldots \text{Equation 5.15}$$

where: v = matrix of test vectors
A_Q = factor loading matrix
W = weighting factor. Equal to the inverse of the variance obtained in the analytical determination of each element

Stage 3

Cluster analysis

CLUSTER

A cluster analysis aids in the selection of possible source profiles.

Stage 4

FANPART 2 (Again)

The measured concentrations, u, for each sample are regressed onto possible profiles (independent variables). The inverse of the variance for the measured concentrations are again used as weightings. The resulting regression coefficient, m, when multiplied by the independent variables contained within B, will provide an estimate of the amount of each element contributing to the collected particulate matter.

$$m = \frac{B^t W u}{B^t W B} \quad \ldots\ldots \text{Equation 5.16}$$

By ensuring that a minimum number of negative source contributions are obtained, the appropriate set of profiles will be selected.

Figure 5.4 Flow chart to illustrate the important stages in the FANTASIA program
(continued over)

	Comment
Stage 5 Scale up source contributions, performed with REGRESS	The particulate matter mass concentrations are then regressed onto a matrix of regression coefficients, m, obtained from the regression analysis illustrated by Equation 5.16. The regression coefficients obtained from this regression analysis are consequently used as scaling factors to determine the contribution of mass from each source to the total collected mass.
Stage 6 Mass source contributions are plotted and examined in relation to other variables	The mass contributions can be plotted and compared with other measured variables to provide further insight into the nature of the sources.
Stage 7 Source profiles	The source profile is expressed as a percentage of the mean measured mass for each element or ion at the receptor site.

Figure 5.4 Flow chart to illustrate the important stages in the FANTASIA program.

The regression is weighted, using the diagonal matrix W, which contains the inverse of the variance obtained in measuring the concentration of each element. The regression is summarised in matrix form by Equation 5.16.

$$m = \frac{B^t W u}{B^t W B} \quad \text{Equation 5.16}$$

where: m = regression coefficient
B = unscaled matrix
W = weighting matrix
u = measured concentrations for sample
B^t = transpose unscaled matrix

A trial and error method is used to select source profiles so that the number of negative regression coefficients that are produced in the regression analysis are kept to a minimum.

e) The regression coefficients, m, one for each source, are then grouped into a matrix. The total suspended particulate mass concentrations determined for all samples are regressed onto this matrix (Stage 5, Figure 5.4). The mass contribution (in terms of μg m^{-3}) from each source is then obtained by scaling the matrix of regression coefficients, m, by the regression coefficients obtained when the matrix m is regressed onto TSP.

f) Finally the same scaling factors calculated in e) are used to scale the source profiles, B (Stage 7, Figure 5.4).

5.4.2.3 Previous use of the regression on absolute principal components scores method

Thurston and Spengler (1985) developed their regression on absolute principal component scores method using 332 daily samples of atmospheric particulate matter in both fine and coarse fractions collected over a two year period. Each sample was measured for 30 elements. The elements with high factor loadings, and which were therefore indicative of a pollution source are shown in Table 5.9.

The Keiding *et al.* (1986) study performed the factor analysis on 322 collected total suspended particulate samples which were each analysed for 15 elements. Six contributing sources (soil, fuel oil, marine, traffic, straw burning and long-range

Table 5.9 Source tracers and source contributions calculated in the Thurston and Spengler (1985) study.

		Soil	Motor vehicle	Refuse burning	Coal aerosol	Residual oil	Salt
Source tracers	Fine	Si,Fe,Ca	Br,Pb	--	Se,S	Ni,V	Cl
	Coarse	Al,Si,K,Ca, Ti,Mn,Fe	Br,Pb	Cu,Zn	S	Ni,V	Cl
Source Contribution ($\mu g\ m^{-3}$ ± S.E. of mean)	Fine	1.9±0.1	2.5±0.2	--	6.9±0.4	2.1±0.2	†
	Coarse	4.9±0.4	0.6±0.01	0.5±0.03	--	0.2±0.08	0.04±0.08

-- Not identified by the PCA analysis as a particle source for the fraction
† Not statistically significant contributor (at p = 0.05) to regression

transport sources) were calculated to be contributing to the collected mass.

Okamoto *et al.* (1990) apportioned the sources of collected aerosol in Tokyo using absolute factor scores instead of the absolute principal component scores devised by Thurston and Spengler (1985). Altogether 40 samples were collected in the study with each sample being analysed for 30 elements by neutron activation analysis. Cadmium, Pb, S and Si were measured by X-ray fluorescence. The concentration of SO_4^{2-}, NO_3^-, Cl^-, NH_4^+ and total carbon were also determined. However due to the high number of measured components relative to collected samples, the number of components was reduced to 19 to avoid the Heyward case (a situation that gives rise to large error when the number of variables approaches or exceeds the number of collected samples).

Five factors were found to represent the data as, in common with all previous applications of PCA and factor analysis, sources were identified by elements which possessed high factor loadings on the individual factors. For example, the first source (high loadings for As, Br, Sb, Zn, Pb and C) was attributed to refuse burning, with confirmatory evidence being provided by examining the correlation with the gaseous pollutants. In addition, this factor was shown to correlate significantly with CO (r = 0.412) and NMHC (0.524) but the correlation with NO was low (r = 0.295), at the significance level of 0.05, indicative of the incomplete burning of wastes.

The second factor with high loadings for Al, Ca, Fe, Sc, Si and weaker loadings for NO_3^- and carbon was considered to be derived from a mixture of soil and automobile emissions. That automobile exhaust was contributing to this source was reinforced by the relatively high correlation with NO (r = 0.507).

The third source had high loadings for NH_4^+, NO_3^-, SO_4^{2-} and V indicating that a proportion of the secondary particulate matter had originated from oil combustion. This source had the highest association with the measured gaseous pollutants. For example, the correlation coefficients between the gaseous pollutants SO_2, NO_2, CO, NMHC, CH_4, THC and the third component were 0.573, 0.611, 0.581, 0.512, 0.706 and 0.576, respectively. This was probably due to the stable meteorological conditions that allowed these gaseous pollutants to accumulate. This is reinforced by this factor having a correlation coefficient of -0.549 with measured wind speed. The fourth factor possessed high loadings for Na and Cl and was attributed to sea salt. The fifth factor with high loadings for Cr, Fe, Mn and Zn, was proposed to originate from steel mills and metal works.

5.4.2.4 Background to regression on absolute components scores method

This method, first shown by Thurston and Spengler (1985), determined the mass contributions from each source by unstandardising the principal component (PC) scores, which were assumed to represent the mass contribution from each source to the measured TSP mass concentration. The standardised source contribution *(G)* can be represented as:

$$G = \frac{f-\bar{f}}{f_s} \quad \text{Equation 5.17}$$

Where: f = contribution from a source on a particular sampling day
$\bar{f}$ = mean source contribution
f_s = standard deviation of the source contribution

An annotated flow chart (Figure 5.5), similar to that used to describe FANTASIA, is used to assist the explanation.

The procedure performs a PCA analysis on a data set which contains, in addition to all the variables analysed, an extra sample with zero concentration for each variable (Figure 5.5, Stage 1). The principal component score corresponding to the zero concentration case will provide an estimate of $\bar{f}/f$. Principal component scores can be determined by a method presented by Harman (1976). The basis to this calculation is depicted in Figure 5.5 (Stage 2) and illustrated by means of an example in Section 5.5.3.

By subtracting $\bar{f}/f$ from each principal component score (G) absolute principal component scores (APCS) are obtained (Stage 4). The observed TSP mass concentration determined for each sample are then regressed onto APCS's (Stage 5). According to Thurston and Spengler, the resulting regression coefficients are equivalent to the standard deviation, f_s, of each source contribution. Hence, when f_s is multiplied by the absolute PC scores, the mass contribution from each source to the collected TSP mass concentration will be obtained. The source profiles are subsequently determined by regressing each measured constituent onto the absolute PC scores (Stage 8).

Another method of achieving the unstandardisation was given by Keiding *et al.* (1986). This approach first estimates the standard deviation of the source contributions, followed by estimation of the mean source contribution. Keiding (1988) compared the calculated mass contribution determined by the Thurston and Spengler (1985) and Keiding *et al.* (1986) methods. The differences are illustrated in Figure 5.6. Diagram **A** shows how the determined normalised source contribution (principal score) will vary with each observation. The points on the graph can be seen to vary about the zero line producing a mean concentration of zero. This is due to the standardised nature of the principal scores which would also have a standard deviation of 1. Diagram **B** (the Keiding, 1986 approach) shows the effect of multiplying the principal source by the standard deviation. The mean of the scores can still be seen to be zero. Diagram **C** (the Thurston and Spengler, 1985 approach) shows the effect of subtracting the zero concentration case. The mean source contribution is no longer zero but the standard deviation still remains 1. Diagram **D**, the final result for both methods, shows the contribution of mass, from the particular source to the collected particulate matter. In performing regression on absolute principal component technique the number of

Flow Chart to illustrate the regression on absolute principal component scores method.

Comment

Stage 1.

PCA.
i variables
k cases
j factors

Perform PCA on all the variables measured. This will include an extra sample with zero concentrations. The eigenanalysis reduces the dimensionality from *i* (number of variables) to *j* (number of sources). *k* is the number of collected samples.

$$Z_{ik} = \sum_{j=1}^{p} A_{ij} G_{jk} \quad \text{Equation 5.18}$$

where: Z_{ik} = standardised variables.
A_{ij} = loading matrix.
G_{jk} = matrix of component scores.

Stage 2

Obtain PC scores

The PC scores are obtained using

$$G_{ij} = \sum_{j=1}^{p} B_{ji} Z_{ik} \quad \text{Equation 5.19}$$

where: B_{ji} = score coefficients.
Determined as $B_{ji} = A_{ji}/\lambda_j$. Where λ_j are the eigenvalues.
Z_{ik} standardised variables.

Stage 3

Unstandardise the *G* values using the regression on APCS method

Principal component scores are equivalent to standardised source contributions.

$$G = \frac{f - \bar{f}}{f_s} \quad \text{Equation 5.17}$$

The method involves finding values for the mean, f, and standard deviation, f_s of the source contribution.

Stage 4

Subtract the PC score corresponding to a zero mean concentration

The mean value is determined first by using a zero concentration case. This is subtracted from each of the standardised scores. Essentially $f/\bar{f}$ will be subtracted from each PC score to give f/f_s. Where f/f_s is the absolute principal component score.

Figure 5.5 Flow chart to illustrate the regression on absolute principal component scores method (continued over).

	Comment
Stage 5 Regress particulate matter collected on APCS	The resulting regression coefficient, being equivalent to the standard deviation, f_s, can therefore be multiplied by each APCS to give the unstandardised source contribution, f.
Stage 6 Plot determined source contributions	The elements or ions with the highest loading for a particular PC act as tracers to identify the nature of the source
Stage 7 Examine source contributions in relation to meteorological parameters	By examining the meteorological conditions, better interpretation of the source characteristics can be made.
Stage 8 Source profile determination.	The source profiles are derived by regressing the absolute PC scores onto each of the collected masses and multiplying the regression coefficients by each of the corresponding scores. The mean contribution of that element or ion is then expressed as a percentage of the collected mean concentration.

Figure 5.5 Flow chart to illustrate the regression on absolute principal component scores method.

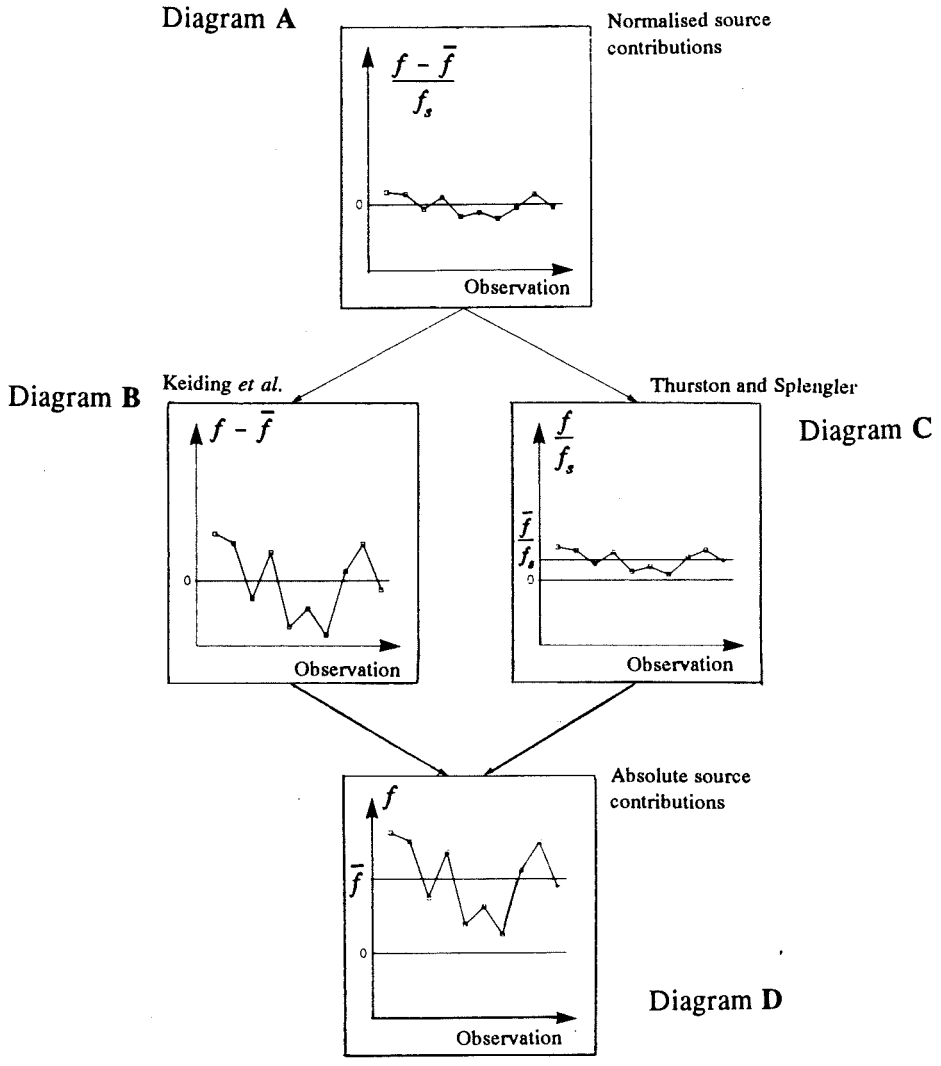

Figure 5.6 Comparison of procedures for modelling for source contributions (Keiding, 1988).

negative source contributions must be kept minimal, since a negative value will have no physical meaning.

5.5 Calculation of principal components

This section will describe the theoretical background to PCA and illustrate how the method is used in receptor modelling to apportion sources of mass to collected particulate matter. The numerical values contained within Table 5.1 (for abundances of **a**, **b**, and **c** in each source) are used to demonstrate the method. These values are re-presented in Table 5.10 (a) along with their standardised equivalent values (Table 5.10

(b)). These standardised variables were determined by subtracting from each original variable the calculated mean value for the original variable, and in turn, dividing each by the standard deviation. Table 5.10 (b) also shows that the standard deviation and mean values possessed by each variable are equal to one and zero, respectively.

Table 5.10 Original variables, standardised variables and their respective mean and standard deviations.

a) Original variables

Case	Variable A	Variable B	Variable C
1	0.06	0.01	0.80
2	0.10	0.04	4.00
3	0.12	2.00	2.00
4	1.00	0.05	0.70
5	7.00	0.20	0.80
6	0.05	0.20	0.10
Mean	1.39	0.42	1.40
Standard Deviation	2.53	0.71	1.29

b) Standardised variables

Case	Variable A	Variable B	Variable C
1	-0.52	-0.57	-0.46
2	-0.51	-0.53	2.01
3	-0.50	2.22	0.46
4	-0.15	-0.51	-0.54
5	2.21	-0.30	-0.46
6	-0.53	-0.30	-1.00
Mean	0.00	0.00	0.00
Standard Deviation	1.00	1.00	1.00

For the purpose of this explanation, the standard deviation can be assumed to be equivalent to the variance possessed by each standardised variable. The sum of the number of variables in the data set will equal the total variance possessed by the data. A correlation matrix will display this information along the principal axis (Table 5.11 (a)).

5.5.1 Eigenanalysis of the correlation matrix

When a eigenanalysis is performed on this matrix a readjustment of the variance along the principal axis will occur. This is illustrated in Table 5.11 (b),. The basis to the eigenanalysis is the characteristic equation, represented in matrix form as:

$$|\mathbf{R} - \lambda\mathbf{I}| = \mathbf{0}$$

. . . .Equation 5.20

Table 5.11 Correlation matrix (R mode) showing associations between variables presented in Table 5.1 and its diagonalised form

(a)

	A	B	C
A	1	-0.163	-0.238
B	-0.163	1	0.160
C	-0.238	0.160	1

(b)

	PC1	PC2	PC3
PC1	1.37	0.00	0.00
PC2	0.00	0.86	0.00
PC3	0.00	0.00	0.76

where: R is the correlation matrix
λ is the matrix of eigenvalues
I is the identity matrix, a matrix of 1's in the principal diagonal and zero's in every other position.

Substituting the correlation matrix shown in Table 5.11(a) into Equation 5.20 gives the following matrix

$$\begin{vmatrix} 1-\lambda & -0.16 & 0.24 \\ -0.16 & 1-\lambda & 0.16 \\ 0.24 & 0.16 & 1-\lambda \end{vmatrix} = 0$$

Expansion of this matrix will give Equation 5.21

$$-\lambda^3 + 3\lambda^2 - 2.8912\lambda + 0.8769 = 0$$

. . . .Equation 5.21

As shown in Table 5.11(b) the eigenvalues that solve this equation are 1.37, 0.86 and 0.76.

Associated with the eigenvalues are eigenvectors which define the principal components in space. The association is described by Equation 5.22:

$$\mathbf{R}\,\mathbf{x} = \lambda\,\mathbf{x}$$

. . . .Equation 5.22

The eigenvectors are determined by placing the eigenvalues obtained using Equation 5.14 and solving the resulting simultaneous equations. The eigenvectors determined for the eigenanalysis of the correlation matrix presented in Table 5.11 are shown in Table 5.12. These were determined using the statistical software package MINITAB.

Table 5.12 Eigenvectors determined as result of the eigenanalysis on the correlation matrix shown in Table 5.11 (a)

	PC1	PC2	PC3
A	0.61	0.35	-0.71
B	-0.52	0.86	-0.02
C	-0.60	-0.38	-0.70

5.5.2 Calculation of factor loadings

The next stage in the PCA analysis is the calculation of the factor loadings. The factor loadings, determined as the product of the eigenvector and $\lambda^{½}$, relate the variables to the calculated principal components. The factor loadings for the first principal component, calculated as a result of the eigenanalysis on the correlation matrix presented in Table 5.11(a), were shown earlier in Section 5.3.2 (Table 5.6). The factor loading for PC1, Variable A, for example, was calculated as $0.61 \times (1.37)^{½}$. As the highest loading is on Variable A, this would suggest that Variable A is most closely associated with Principal Component 1.

In addition, the sum of the squared value for each factor loading will, in turn, equal the eigenvalue for the principal component. As the number of principal components to be used in this method is chosen on the basis of those with eigenvalues greater than 1, only one principal component is used.

5.5.3 Calculation of absolute principal component scores

The data presented in Table 5.1 is also used to illustrate the derivation of absolute principal component scores, equivalent to the actual mass contribution from each source. As discussed in Section 5.4.2.4, the first stage in the procedure is to perform the principal component analysis using an extra sample with zero concentration values for each variable measured. This extra sample will result in a correlation matrix different to that presented in Table 5.11 (b) and will consequently produce different eigenvalues ($\lambda_1 = 1.32$, $\lambda_2 = 0.905$ $\lambda_3 = 0.772$) and factor loadings ($a_1 = -0.554$, a_2

= 0.670 and a_3 = 0.726). The principal component score was determined by the formula shown by Equation 5.19. The Software Package for Social Scientists, Advanced Statistics V2.0 (SPSS) was used to calculate the component scores. The scores were saved as a listing file and transferred to LOTUS 123, via WordPerfect 5.1, where the rest of the method was completed.

The principal component score corresponding to the zero value is subtracted from each of the principal scores (Stage 4, Figure 5.5 and Diagram **C**, Figure 5.6) to give the absolute PC score. The regression analysis is then performed, using the sum of the variables as the dependent variable and the absolute factor score as the independent variable, to determine the regression coefficient (equivalent to the standard deviation of the source contribution (Stage 5, Figure 5.5)). The outputs at the various stages are presented in Table 5.13. The unstandardised PC scores are interpreted as the contribution of the three variables; A, B and C from the hypothetical source to the sum of the three variables. Figure 5.7 shows that the unstandardised principal component scores approximate the sum of the three variables. This diagram provides the same information as that presented in Figure 5.6, Diagram **D**, for the contribution of sources to collected particulate matter.

Table 5.13 Regression on absolute component scores for worked example

Variables			PC score	Absolute PC score	Unstandardised score *	Sum of variables A+B+C
A	B	C				
0.06	0.01	0.80	-0.22	0.31	0.42	0.87
0.10	0.04	4.00	1.04	1.58	2.15	4.14
0.12	2.00	2.00	1.67	2.22	3.01	4.12
1.00	0.05	0.07	-0.38	0.15	0.02	1.75
7.00	0.20	0.80	-1.21	-0.67	-0.91	8.00
0.05	0.20	0.01	-0.36	0.17	0.24	0.35
0	0	0	-0.54			

* determined by multiplying the absolute principal component score by the regression coefficient (1.36) obtained when the absolute PC scores are regressed onto the sum of the variables A, B and C.

In geometric terms, the factor loading is equivalent to the angle between the vector

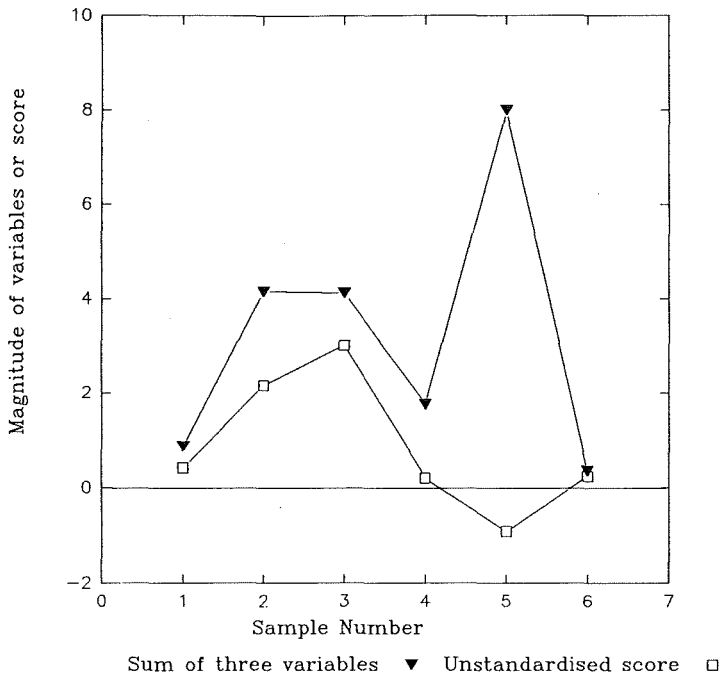

Figure 5.7 Comparison of the sum of the three variables, A, B and C to the unstandardised principal component score

representing the original variable and the vector representing each principal component. The geometric interpretation to principal component analysis has been presented in standard texts (Harman, 1976 and Johnson and Winchern, 1988)

5.6 Summary

Receptor models attempt to apportion the sources of material that are being collected at a receptor site. The success of a receptor model will depend on whether the models can be shown to have physical significance. A summary of the chief characteristics of each receptor model discussed in this chapter is provided below:

The simple mass balance method required only the percentage composition of the most abundant element in the source and the amount of the element actually determined in the collected sample to determine the contribution of each source to the collected particulate matter.

The multiple regression of the constituent components of particulate matter onto element

source profiles, provided in addition to the contribution of each source to the collected particulate matter, the contribution of each element from each source. The statistical basis to the model can be used as an aid in the selection of relevant profiles. For example, sources can be chosen or rejected on the basis of the amount of collinearity existing between the source profiles used as independent variables. A method to assess the amount of collinearity present in a matrix of supposedly independent variables involves the calculation of condition indices. These are obtained as a result of a singular value decomposition performed on the source profile matrix (where the singular value decomposition is equivalent to an eigen analysis on a non square matrix). This method was first described by Lawson and Hanson (1974) and has been applied to air pollution source apportionment studies by Hopke (1989). Investigation of the error associated with the regression coefficients has been described in detail by Henry (1992).

A disadvantage with the simple and regression on elemental profile methods is that each assumes that the number of contributing sources must be determined by the investigator. The introduction of principal component analysis and factor analysis allows the receptor model to estimate the number of contributing sources. Three different models, using various statistical methods, have been described in this chapter and are summarised below:-

a) regression of particulate matter mass concentration onto constituent elements, selected using principal component analysis. The resulting regression coefficients when multiplied by the concentration of the component element yielded the percentage contribution from each source.

b) calculation of source profiles from the factor loading matrix obtained initially in a principal component analysis. This particular method is performed using a designated computer software package FANTASIA, which also utilises several other statistical techniques such as multiple regression and cluster analysis. The number of contributing sources, for this and the factor analysis methods, is determined as the number of factors which possess an eigenvalue greater than 1.0. The mass contribution of each source is calculated at a late stage in the method.

c) determination of absolute principal component or factor scores. This method determines the mass contribution of each source to the collected particulate matter at an early stage in the method. The method unstandardises the calculated factor scores that were obtained as a result of the factor analysis. A disadvantage of the method is the occurrence of negative mass contributions which have no physical significance. A method of overcoming the occurrence of negative source contributions by using certain constraints has been described by Henry (1987). Percentage source profiles are determined as the last stage in the model when the mass contribution of each element from each source is divided by the total mass contribution from each source.

CHAPTER 6: DEPOSITION OF SULPHUR AND NITROGEN ONTO HISTORIC MONUMENTS

In Chapter 2 those atmospheric pollutants which literature studies suggest have played the greatest role in altering historic limestone buildings were identified. Chapter 3 showed that the amounts of sulphur dioxide, the largest single cause of stone deterioration, released into the atmosphere in the United Kingdom, has decreased significantly over the last twenty years. This chapter describes the nature of those atmospheric pollutants, originating from combustion processes, and collected in close proximity to historic building. Interaction between sulphur and nitrogen in the particulate, gaseous and aqueous phases will also be examined. In addition, the deposition of sulphur and nitrogen as particulate matter is compared to deposition in the gaseous and precipitation phases to determine the relative role of each phase in delivering pollutants onto the building surface.

6.1 Characterisation of atmospheric aerosol

The composition of ambient particulate matter can be complex reflecting the diversity of contributing sources. As the sampling sites in this study were located on top of, or in close vicinity to, large buildings, turbulent flow patterns may occur causing a reduction in the sampling efficiency of the sampler. For example, Hinds (1982) cited a collection efficiency for a high volume sampler of 50% for 30 μm particles at a wind speed of 8 km hr^{-1}. The efficiency would be greater at low wind speeds and lower at high wind speeds (Hollander, 1990). Despite the possible alterations to the collected atmospheric particulate matter and variation in particulate matter collection efficiency, the high volume sampler is a standard sampling method (Harrison and Perry, 1986).

6.1.1 Size segregation of atmospheric particulate matter

The size distribution of atmospheric particulate matter is generally expected to be bi-modal with the finer components attributed to gas to particulate reactions plus anthropogenic particulate emissions and the coarser fraction attributed to the abrasive action of wind on the earth's surface (Hinds, 1982). Two methods of assessing the size distribution of atmospheric particulate matter; a dichotomous sampler and a cascade impactor, were employed in this study.

6.1.1.1 Dichotomous sampler

The dichotomous sampler used in this study (Beckmann) is designed to separate particulate matter into fine (< 2.5 μm) and coarse (> 2.5 μm) particle size ranges. Teflon filters were used to collect the particulate matter. The effectiveness of the dichotomous sampler as a collector of particulate matter was investigated by comparing the mass of the particulate matter collected using this method with that collected using a high volume sampler.

Samples were collected, on the roof of the Exchequer Gate at Lincoln Cathedral, during May 1990. Altogether 9 twenty four hour samples were collected from 17th May until 25th May. However, only five of those samples coincided with collection by the high volume sampler over this collection period (high volume sampling was conducted from Monday until Friday). The mass concentrations collected within the fine and coarse fractions are presented in Figure 6.1 which shows, in the majority of collected samples, that the particulate matter mass concentration determined by the high volume sampler exceeded the sum of the fine and coarse mass concentrations collected by the dichotomous sampler. For only one of the collected samples (17/5/90) did the sum of the fine and coarse fractions virtually equal the mass concentration determined by the high volume sampler.

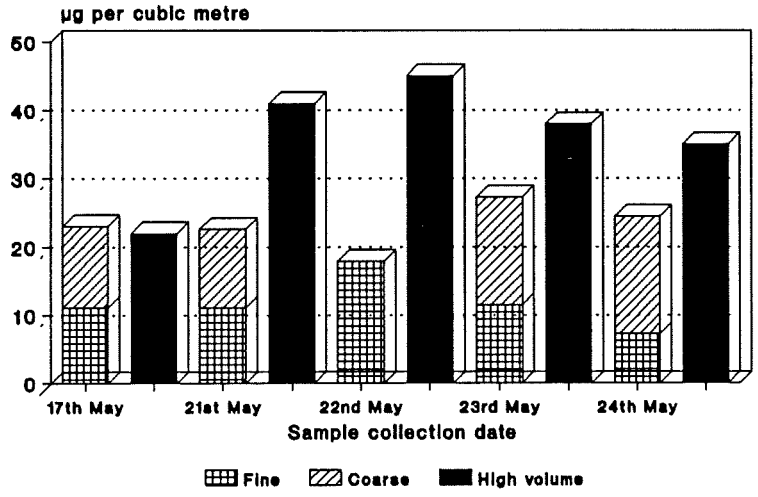

Figure 6.1 Comparison of particulate mass concentrations determined by dichotomous and high volume samplers

The low correlation (correlation coefficient = -0.34) between the particulate matter mass concentrations determined using each respective sampler may be explained by:

- Artifact sulphate and nitrate formation on the glass fibre filter. This artifact would have resulted from reaction of SO_2 and HNO_3 with alkaline sites present on the glass fibres. The artifact formation of sulphate and nitrate on glass fibre filters was shown by Coutant (1977) to be particularly significant on those filter papers which when immersed in water produced a pH greater than 8.5 (See Appendix B).
- Loss of collected particles from the surface of the Teflon filter during shipment back to the laboratory. This loss may be accentuated by the relatively small masses collected on the Teflon filters. For example, typically 250 μg was collected on the filter (diameter 4 cm), whereas 250 mg of particulate matter was typically collected on the glass fibre filter (dimensions 20 $\times$ 30 cm). As particulates present on a Teflon filter are not bound as tightly as those particulates bound to the fibrils of a glass fibre, this loss may be expected.

Given the uncertainty in the masses collected and the requirement that two subsequent sets of extractions were to be performed, one involving double distilled deionised water and the other an acid digestion (see Section 4.3.2), with the necessary requirement that the filter was to be cut into two parts, the dichotomous sampler was not further used in the analysis. Expected problems in preparing the filter sample for further analysis, would include both metal contamination and loss of collected matter due to the cutting action of the knife.

6.1.1.2 Cascade impactor

Atmospheric particulate samples were also collected using a cascade impactor (California Instruments, Model PC-1EH; calibration of this instrument was discussed in Section 4.2.4) at Lincoln Cathedral on 28th February 1991. The mass concentrations determined for each particle size range are shown in Table 6.1. The amount of particulate mass in each size range is illustrated in Figure 6.2, which shows a unimodal distribution centred on 0.3 μm.

The particle size distribution centred on 0.3 μm occurred in the "accumulation mode"

Table 6.1 Mass concentrations of particulate matter determined as a function of particle size.

Stage	d_{50} (μm)	* Particle size range (μm)	$\Delta \log_e$ particle size- range limits, d_p	Mass Concentration ($\mu g\ m^{-3}$)	$\frac{\Delta \text{ mass}}{\Delta \log_e d_p}$
1	10	12 - 8	0.41	--	--
2	6	8 - 5	0.47	--	--
3	4	5 - 3.25	0.43	--	--
4	2.5	3.25 - 2	0.49	--	--
5	1.5	2 - 1.15	0.55	--	--
6	0.8	1.15 - 0.6	0.65	--	--
7	0.4	0.6 - 0.3	0.69	10.6	15.3
8	0.2	0.3 - 0.15	0.69	13.6	19.6
9	0.1	0.15 - 0.75	0.69	5.1	7.35
10	0.05	0.075 - 0.025	1.10	1.4	1.27

* The size ranges for each d_{50} were estimated in such a way that d_{50} approximated the midpoint.
-- indicates no particle collection, hence no mass concentrations were determined for these size ranges.

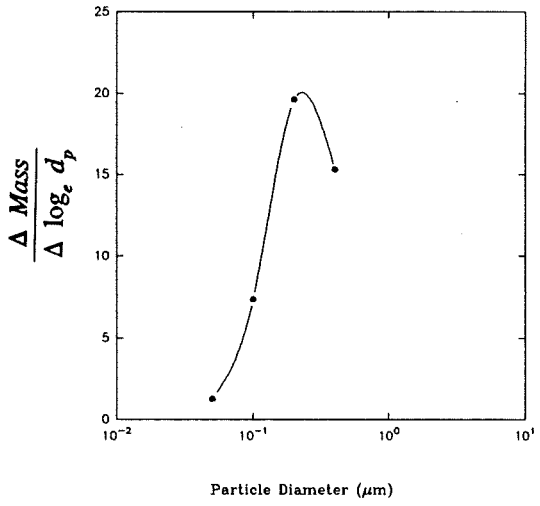

Figure 6.2 Mass distribution of atmospheric particulate matter determined at Lincoln (28/2/91).

of the ambient aerosol. Other categories of this size classification for the ambient aerosol, described by Hinds (1982), include "nucleation mode" and coarse particles. According to Hinds (1982) the "accumulation mode" particles will have reached this size due to coagulation of smaller particles released from combustion processes or formed as a result of gas to particle reactions.

Although a high volume atmospheric particulate mass concentration was not determined on 28/2/91, the arithmetic monthly mean concentration for February, 75.5 $\mu g\ m^{-3}$, was

more than twice the total mass determined by the cascade impactor (30.7 $\mu g\ m^{-3}$). Given the uncertainty in comparing a monthly average concentration determined using the high volume sampler with a single determination determined using the cascade impactor, further discussion regarding the efficiency of the cascade sampler is difficult. A more rigorous assessment of the cascade impactor, dichotomous sampler and high volume sampler as particulate matter samplers, could be more properly obtained by operating each instrument simultaneously over an extended time period.

6.1.2 Ionic composition of collected atmospheric particulate matter

This section will discuss both the overall electronic balance of collected particulate matter and the concentrations of four major ions used in determining the electronic balance (NH_4^+, Cl^-, SO_4^{2-} and NO_3^-). Samples were collected between September 1989 and August 1991.

6.1.2.1 Ion balance

The ion balance of the collected aerosol, calculated as nanoequivalents per cubic metre (neq. m^{-3}) for each collected sample, is presented in Table 6.2. The extent of the balance, expressed as the ratio of Σ(cations) to Σ(anions), is an indicator of the ability of the filter paper to remove, from the air that passes through the filter, a representative sample of atmospheric particulate matter. That is, a ratio of Σ(cations) to Σ(anions) measured on the filter paper should equal 1.0, the same ratio that exists between ionic species in atmospheric particulate matter.

The arithmetic mean ratio of Σ(cations) to Σ(anions) obtained in this study was 1.19, with a standard deviation of 0.46. The geometric mean was 1.11. Further insight into the nature of the ion balance was investigated by subtracting from the obtained ratio the theoretically expected ratio (1.0) for each sample, in order that deviations from zero could be observed. The resulting variation in the ion balance ratio is depicted in Figure 6.3.

The ion balance for eight samples (Samples 46-50, 63, 91 and 115) have the

Table 6.2 Ion balance determined for collected particulate matter (ionic concentrations are expressed as neq. m^{-3})

Sample Date	Sample Number	Mg^{2+}	Ca^{2+}	K^+	Na^+	NH_4^+	Σ Cations	Cl^-	NO_3^-	SO_4^{2-}	Σ Anions	Ratio Σ(Cation) to Σ(Anion)
Lincoln												
5-9-89	1	38	90	13	19	129	289	118	69	2	189	1.53
6-9-89	2	26	64	11	27	128	257	41	96	81	218	1.18
7-9-89	3	27	70	23	36	327	484	48	155	143	346	1.40
8-9-89	4	36	17	6	50	37	146	83	25	42	150	0.98
9-9-89	5	52	20	2	64	41	179	155	15	45	215	0.83
10-9-89	6	38	18	N.D.	39	106	201	90	45	100	235	0.85
1-5-90	7	10	48	N.D.	28	216	301	11	105	267	383	0.79
2-5-90	8	13	51	3	31	203	300	17	258	117	392	0.77
3-5-90	9	23	122	7	39	338	530	N.D.	329	333	662	0.80
4-5-90	10	26	110	7	32	479	654	48	389	713	1149	0.57
8-5-90	11	19	54	5	38	118	234	45	82	96	223	1.05
9-5-90	12	28	61	39	131	262	521	28	147	254	429	1.21
10-5-90	13	14	29	14	64	243	365	37	95	200	332	1.10
14-5-90	14	14	30	4	36	372	456	20	208	494	722	0.63
15-5-90	15	19	19	N.D.	33	70	141	70	48	77	196	0.72
16-5-90	16	21	45	1	36	124	227	96	63	119	277	0.82
17-5-90	17	22	29	3	56	61	171	20	23	96	138	1.24
21-5-90	18	13	20	2	38	67	140	8	44	94	146	0.96
22-5-90	19	14	34	4	34	183	270	23	84	167	273	0.99
23-5-90	20	19	41	2	32	75	169	39	60	87	187	0.91
24-5-90	21	28	47	20	99	36	230	31	29	54	114	2.02
28-1-91	22	25	54	22	71	868	1040	143	312	440	894	1.16
29-1-91	23	10	27	22	63	242	365	82	82	181	344	1.06
30-1-91	24	21	63	27	89	1075	1275	245	284	442	971	1.31
31-1-91	25	19	54	44	93	779	989	83	297	334	715	1.38
4-2-91	26	25	27	20	82	878	1031	217	356	434	1007	1.02
5-2-91	27	34	59	20	92	158	363	221	48	121	390	0.93
6-2-91	28	24	36	24	67	159	309	85	43	214	342	0.90
11-2-91	29	20	37	16	49	572	694	219	147	309	674	1.03
18-2-91	30	28	53	17	62	459	619	204	196	195	595	1.04
19-2-91	31	32	69	30	86	768	985	167	408	221	796	1.24
20-2-91	32	5	2	4	13	351	375	43	148	141	332	1.13
21-2-91	33	28	36	2	100	217	384	124	78	116	318	1.21
25-2-91	34	44	60	11	100	634	850	81	299	229	609	1.40
26-2-91	35	17	33	4	100	543	696	57	208	236	501	1.39
14-3-91	36	31	102	18	27	438	615	219	121	219	559	1.10
18-3-91	37	29	124	18	43	98	313	134	38	131	302	1.03
19-3-91	38	58	84	19	76	131	368	319	34	125	478	0.77
20-3-91	39	22	77	39	93	46	277	43	23	93	160	1.73
22-3-91	40	28	72	17	40	161	317	132	64	139	335	0.95
Bolsover												
6-11-90	41	29	66	37	123	389	644	200	99	127	427	1.51
7-11-90	42	52	59	14	59	217	401	188	56	103	346	1.16
8-11-90	43	21	37	12	57	386	514	112	176	156	443	1.16
9-11-90	44	44	83	6	51	140	325	76	102	100	278	1.17
12-11-90	45	11	21	6	32	270	340	195	94	204	493	0.69
13-11-90	46	22	26	8	50	654	759	129	59	100	288	2.64
14-11-90	47	54	211	30	137	529	962	178	21	186	384	2.50

Sample Date	Sample Number	Mg^{2+}	Ca^{2+}	K^{+}	Na^{+}	NH_4^{+}	Σ Cations	Cl^{-}	NO_3^{-}	SO_4^{2-}	Σ Anions	Ratio Σ(Cation) to Σ(Anion)
15-11-90	48	37	58	7	66	601	768	174	37	111	322	2.38
16-11-90	49	7	5	4	51	78	144	16	5	45	65	2.20
19-11-90	50	29	79	43	105	153	408	97	30	105	232	1.75
20-11-90	51	19	36	16	49	283	403	87	60	149	296	1.36
21-11-90	52	42	72	21	57	592	783	360	130	271	761	1.03
22-11-90	53	34	69	33	83	548	767	360	89	194	643	1.19
23-11-90	54	N.D.	N.D.	4	N.D.	118	122	115	43	115	273	0.45
26-11-90	55	30	29	23	81	127	290	179	33	93	304	0.95
27-11-90	56	29	24	5	35	352	444	272	68	140	479	0.93
3-12-90	57	35	33	12	55	234	369	140	26	242	408	0.91
4-12-90	58	37	79	21	48	174	359	136	38	110	284	1.26
5-12-90	59	57	106	40	105	481	789	332	122	161	615	1.28
6-12-90	60	17	42	16	34	460	569	196	176	167	539	1.06
7-12-90	61	31	51	43	109	204	438	116	84	92	292	1.50
11-12-90	62	39	37	22	76	157	331	99	16	193	309	1.07
12-12-90	63	57	76	50	143	270	596	168	12	54	234	2.54
13-14-90	64	58	42	19	80	337	536	323	58	189	569	0.94
14-12-90	65	96	114	66	199	581	1056	452	125	291	868	1.22
17-12-90	66	43	53	27	55	705	883	346	144	198	688	1.28
18-12-90	67	24	35	25	52	776	912	233	182	326	741	1.23
15-1-91	68	35	76	9	50	335	506	251	74	140	466	1.09
16-1-91	69	41	68	9	50	458	625	341	72	159	571	1.09
17-1-91	70	28	102	11	50	795	986	327	159	208	695	1.42
21-1-91	71	33	38	11	50	330	463	276	44	139	459	1.01
22-1-91	72	37	61	10	50	302	460	225	62	130	418	1.10
23-1-91	73	16	38	6	50	749	860	299	217	375	891	0.96
24-1-91	74	9	17	13	50	668	757	144	201	312	657	1.15
28-1-91	75	20	34	7	50	1144	1255	273	225	337	835	1.50
29-1-91	76	12	26	17	50	689	794	127	124	314	564	1.41
30-1-91	77	23	33	10	50	1031	1148	225	179	338	742	1.55
4-2-91	78	10	35	15	50	398	508	115	56	321	492	1.03
5-2-91	79	10	30	17	50	1198	1306	125	298	492	916	1.43
6-2-91	80	10	30	2	50	579	670	163	150	208	521	1.29
25-2-91	81	4	22	N.D.	50	869	945	274	258	363	895	1.06
13-6-91	82	28	68	35	82	76	289	86	19	67	173	1.67
14-6-91	83	15	28	9	17	167	236	64	33	141	239	0.99
18-6-91	84	8	34	15	12	77	146	42	21	85	148	0.99
19-6-91	85	23	87	66	85	41	301	36	25	109	169	1.78
20-6-91	86	29	44	15	9	63	159	37	107	171	316	0.50
24-6-91	87	8	24	20	25	129	206	44	61	91	197	1.05
25-6-91	88	11	27	14	16	59	127	34	20	63	117	1.09
26-6-91	89	10	23	12	11	69	126	60	25	56	142	0.89
27-6-91	90	21	46	36	74	204	381	88	56	57	200	1.90
2-7-91	91	24	51	31	52	732	890	41	147	206	394	2.26
Wells												
13-5-91	92	24	61	46	102	129	361	71	82	147	301	1.20
14-5-91	93	24	95	49	108	74	350	56	79	62	197	1.78
15-5-91	94	30	69	27	69	51	246	96	37	82	215	1.14
16-5-91	95	20	65	42	95	38	260	39	33	61	133	1.95
20-5-91	96	12	52	34	69	120	287	14	55	193	262	1.09
21-5-91	97	12	67	41	78	156	353	26	51	210	287	1.23
22-5-91	98	25	113	39	82	79	338	23	94	88	204	1.66
24-5-91	99	23	132	36	69	106	366	17	109	112	238	1.53
28-5-91	100	24	97	37	87	88	333	73	61	150	284	1.17

Sample Date	Sample Number	Mg^{2+}	Ca^{2+}	K^{+}	Na^{+}	NH_4^{+}	Σ Cations	Cl^{-}	NO_3^{-}	SO_4^{2-}	Σ Anions	Ratio Σ(Cation) to Σ(Anion)
29-5-91	101	24	130	45	113	135	448	47	84	240	371	1.21
30-5-91	102	19	78	56	125	479	757	0	81	602	682	1.11
3-6-91	103	21	80	38	88	60	287	61	47	100	207	1.38
4-6-91	104	18	86	40	83	42	269	30	50	74	155	1.74
5-6-91	105	15	40	31	74	49	208	46	42	89	177	1.18
12-6-91	106	51	56	34	117	3	261	254	21	67	342	0.76
13-6-91	107	55	54	25	103	28	266	260	13	89	361	0.74
17-6-91	108	21	70	23	41	28	183	52	30	66	148	1.24
18-6-91	109	27	35	21	50	34	167	88	21	72	181	0.93
19-6-91	110	14	99	20	28	54	215	47	81	65	193	1.12
20-6-91	111	15	105	16	10	88	233	17	98	90	205	1.14
24-6-91	112	7	32	27	45	21	131	12	29	27	68	1.94
25-6-91	113	14	32	28	58	1	134	43	13	76	132	1.01
26-6-91	114	25	57	40	92	3	217	65	13	83	161	1.35
27-6-91	115	11	49	32	54	3	149	14	7	30	51	2.92
9-7-91	116	22	27	17	27	37	129	81	37	52	170	0.76
10-7-91	117	10	88	20	10	43	170	N.D.	53	145	196	0.87
16-7-91	118	21	60	7	2	33	123	77	17	41	135	0.91
17-7-91	119	N.D.	N.D.	4	22	13	39	9	15	19	44	0.89
18-7-91	120	13	7	11	12	11	53	73	7	25	105	0.51
22-7-91	121	4	19	16	6	545	590	N.D.	153	235	369	1.60
23-7-91	122	12	9	11	4	55	91	49	36	64	149	0.61
24-7-91	123	10	N.D.	9	N.D.	51	66	67	24	59	151	0.44
25-7-91	124	14	30	24	37	217	321	24	71	170	266	1.21
30-7-91	125	9	29	19	15	41	113	73	39	47	159	0.71
31-7-91	126	16	21	11	15	75	139	4	61	86	151	0.92
1-8-91	127	5	18	5	N.D.	57	63	N.D.	39	85	124	0.51
2-8-91	128	N.D.	-8	10	N.D.	50	40	8	20	71	99	0.40
3-8-91	129	4	1	8	N.D.	33	36	24	30	37	90	0.40

N.D. Not detected

Σ(cations) exceeding Σ(anions) by at least 100%. The most likely reason for the sum of the cations exceeding the sum of the anions is that two different extractions (Section 4.3.2) were performed to remove the ions from the glass fibre filter media. Since the nitric acid extraction is more severe than the DDDW extraction, those ions more strongly held within other composite fractions of the particulate matter, such as the organic component, will dissolve and hence are analysed. The fact that Sample 115 exhibits a high Σ(cation) to Σ(anion) ratio, with Na^{+} and Ca^{2+} concentrations being particularly high, would infer that contamination has arisen due to rough handling of the glass fibre filter (the sodium ions may have arisen from perspiration released from a sweating hand and the calcium ions from the surface of the building).

Most of the samples collected at Wells (Samples 92 to 129) have Σ(anions) exceeding Σ(cations). A possible reason for the Σ(cations) values being low is that relatively low

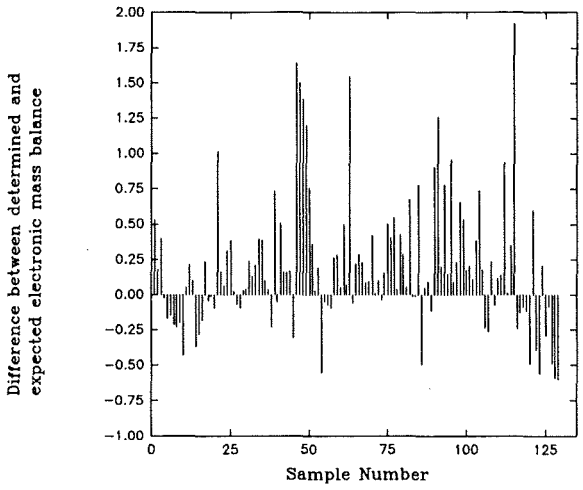

Figure 6.3 Variation in ion balance expressed by subtracting the expected ratio (1.0) from the determined ratio

filter loadings occurred which did not register sufficiently above the metal content of the filter paper (the metal content of the filter paper was presented previously in Table 4.8).

Compared to previously reported ion balances (Table 6.3) the ion balance determined in this study most closely resembles that determined by Harrison and McCartney, (1980). This study was similar in that the hydrogen ion concentration was not measured.

The ion balance reported by Cheng (1991) is exceptional, since low concentrations of both cations and anions would be not be expected to produce filter loadings sufficiently greater than the filter blank. This effect was compensated for by using a sampling period of one week, during which time approximately 4,000 m^3 of air was sampled. A possible reason for the obtained ratio of 1.0 was the large number of weekly samples that were collected (282) resulting in an averaging out of possible deviations.

The washing technique employed by Harrison and Pio (1985) had two main objectives; removal of metals and neutralisation of alkaline sites. The former objective involved soaking each filter overnight in distilled water, removing the water by suction and drying in an oven. The latter objective involved soaking and agitating (using ultrasonics) in a 1 N HCl solution. The filters were then rinsed to remove the acid and

Table 6.3 Reported ion balances

Σ(cations) neq. m^{-3}	Σ(anions) neq. m^{-3}	Ratio $\frac{\Sigma cat.}{\Sigma an.}$	Comment	Reference
26.6	26.6	1.00	Samples collected in the Canadian Arctic (Alert), using Whatman 41 filters. 282 samples collected from 7/80 to 6/86.	Cheng *et al.* (1991)
171.2	154.0	1.11	Samples collected in NW England, using Whatman 41 or HAWP filters. Daily samples collected during July 1977. Hydrogen ion concentration not determined.	Harrison and McCartney (1980)
338	355	0.95	Samples collected in NW England, using QAO quartz, washed quartz or Teflon filters. Seventeen samples collected, throughout 1979 to 1981	Harrison and Pio (1981)

The elements used in the ion balance, with the exception of Harrison and McCartney (1980), are H^+, NH_4^+, Na^+, Ca^{2+}, Mg^{2+}, K^+, SO_4^{2-}, NO_3^- and Cl^-.

finally dried in an oven. The less than unity ratio obtained by Harrison and Pio (1985) may have resulted from neutralisaton of the alkaline sites by H^+. The neutralisation product, H_2O, would than have been removed during the drying stage, increasing the relative proportion of the chloride ion.

6.1.2.2 Concentrations of sulphate, nitrate, chloride and ammonium ions in collected particulate matter

The particulate matter concentrations and concentrations of four water soluble ions are presented in Table 6.4. The results are expressed as monthly arithmetic and geometric means. As the number of samples used to calculate the monthly mean ranged from 5 to 16, the representativeness of each monthly concentration will vary. The arithmetic and geometric mean concentrations measured for atmospheric particulate matter at all sites were 60.7 and 51.4 $\mu g\ m^{-3}$ respectively.

Three of the four soluble ions (SO_4^{2-}, NO_3^-, NH_4^+) presented in Table 6.4, will coexist with H^+ within the atmospheric particulate matter as part of the following compounds: $(NH_4)_2SO_4$, $NH_4NO_3(NH_4)_3H(SO_4)_2$, and $(NH_4)HSO_4$ (Weiswheiler and Schwarz, 1990). The latter two compounds may produce the following effects in the atmospheric environment:

Table 6.4 Monthly arithmetic and geometric means of soluble ion concentrations collected at all sites

	T.S.P.		SO_4^{2-}		NO_3^-		Cl^-		NH_4^+	
	$\bar{x}$ s	Geom. mean	$\bar{x}$ s	Geom. mean	$\bar{x}$ s	Geom. mean	$\bar{x}$ s	Geom. mean	$\bar{x}$ s	Geom. mean
All Sites n = 125	60.7 37.0	51.4 1.9	8.1 6.0	6.57 2.1	6.1 5.3	4.2 2.6	4.1 3.6	2.4 2.7	4.9 4.8	2.7 3.3
Lincoln										
9/89 n=6	51.6 21.9	46.4	3.3 2.2	1.3	4.2 2.9	3.2	3.2 1.4	2.8	2.3 1.7	1.8
5/90 n=15	59.3 28.0	53.6	10.3 8.5	7.6	8.1 6.8	5.8	1.1 0.8	0.7	3.4 2.3	2.7
1/91 n=4	74.9 34.4	62.1	16.7 5.1	15.9	15.1 5.8	13.3	4.9 2.3	4.4	13.3 5.5	11.7
2/91 n=10	75.5 31.1	69.0	10.6 4.3	9.9	11.9 7.5	9.4	5.0 2.4	4.3	8.5 4.3	7.3
3/91 n=5	49.7 24.3	42.6	6.8 2.0	7.1	3.5 2.2	2.9	6.0 3.3	5.0	3.1 2.5	2.4
Bolsover										
11/90 n=16	66.6 28.8	61.7	6.6 2.6	6.1	4.3 2.6	3.3	6.1 3.3	5.0	6.1 3.4	5.1
12/90 n=11	92.3 47.5	80.3	8.8 3.7	7.9	5.5 3.8	3.9	8.2 3.9	7.3	7.2 3.7	6.2
1/91 n=10	109.0 20.9	107.0	11.8 4.5	10.9	8.4 4.1	7.3	8.8 2.4	8.4	11.7 5.0	10.5
2/91 n=4	101.4 35.7	96.1	16.6 4.8	15.9	11.8 5.8	9.9	6.0 2.2	5.7	13.7 5.5	12.6
6/91 n=9	35.9 18.3	32.4	5.0 2.4	4.5	3.2 2.6	2.4	1.9 0.7	1.8	2.9 3.5	1.9
Wells										
5/91 n=11	40.7 10.7	39.1	7.6 6.5	6.1	4.0 1.4	3.8	1.5 0.9	1.0	2.1 2.0	1.6
6/91 n=13	37.1 8.7	36.0	3.2 1.0	3.0	2.0 1.8	1.4	3.0 3.1	1.8	0.5 0.5	0.2
7/91 n=11	27.9 14.3	23.7	3.9 2.0	3.1	2.4 2.2	2.0	1.2 1.2	0.4	1.6 2.4	0.9

Levels are expressed in $\mu g\ m^{-3}$

Standard deviations, s , are given below the arithmetic means value, $\bar{x}$, for each set of monthly data whereas geometric deviations are listed for the combined data set only.

- contribute extra hydrogen ions to rainfall, which, as was shown in Section 2.4.3.1, will cause increased deterioration of limestone building materials.
- contribute to the fine fraction of the atmospheric aerosol causing significant reductions in visibility (Stevens *et al*, 1984).
- act, in association with H^+, as respiratory irritants (Koutrakis *et al.*, 1988b, Keeler *et al.*, 1990, Waldman *et al.*, 1991).

The percentage contribution of combined SO_4^{2-}, NO_3^-, Cl^- and NH_4^+ to collected particulate matter is illustrated in Figure 6.4.

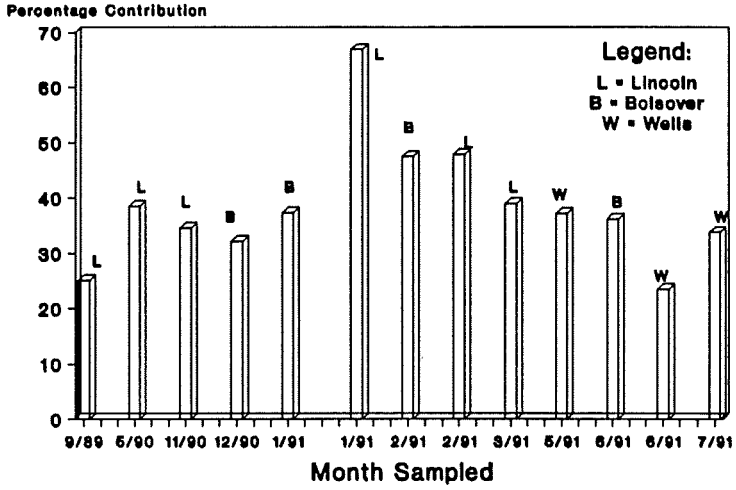

Figure 6.4 Percentage contribution of $\Sigma(SO_4^{2-}, NO_3^-, Cl^-$ and $NH_4^+)$ to total collected particulate matter.

The largest contribution of the four ions to TSP occurred during the winter months, January 1991 (66%), February 1991 (48%) for samples collected at Lincoln and February 1991 (47%) at Bolsover. The lowest percentage contribution of the four ions to TSP occurred during the summer, June 1991 (24%) at Wells and September 1989 (26%) at Lincoln.

The importance of the four ions in contributing mass to the observed particulate mass concentration is also highlighted by Table 6.5, which shows the contributions determined by several other workers. The high contribution (44%) determined by Pio (1991) is most similar to the values determined during February 1991 at Lincoln (48%) and at Bolsover (49%).

The mean contribution (36%) determined by Willison *et al.* (1985) for samples (n=330) collected at Leeds over an eighteen month period is similar to that determined in this study (38%), in which 125 samples were collected. This would indicate the importance of collecting a large number of samples to provide estimates on the "typical" contribution of the ions; SO_4^{2-}, NO_3^-, Cl^- and NH_4^+ to collected particulate mass.

The ammonium concentrations determined by Lee *et al.* (1974) are relatively small,with the concentrations of greatest magnitude obtained for samples collected in London

Table 6.5 Measured total suspended particulate matter and four major soluble ion components, $\mu g\ m^{-3}$. (Standard deviations are in parenthesis)

TSP	SO_4^{2-}	NO_3^-	Cl^-	NH_4^+	$\Sigma(SO_4^{2-}+NO_3^-+Cl^-+NH_4^+)$	Percentage of TSP	Comment	Site	Reference
47	11.4	1.3	*	0.5	13.2	28.1†	n=75 1/1/70 to 15/4/70	Kinder	Lee *et al.* (1974)
52	12.6	2.2	*	0.5	15.3	29.4†	n=45 16/4/79 to 1/6/70		
119	26.1	2.1	*	1.8	30.0	25.2†	n=51 1/1/70 to 15/4/70	London	
151	32.3	5.4	*	2.0	39.7	26.3†	n=36 16/4/70 to 1/6/70		
*	6.0 (3.5)	2.3 (2.4)	*	2.5 (1.5)	10.8		Arithmetic mean (s.d)	N.W England	Harrison and McCartney (1980)
*	4.9 (2.1)	1.3 (3.1)	1.1 (1.8)	2.1 (2.0)	9.4		geometric mean (s.d) May to Sep 1977		
46.8 (23.7)	8.3 (4.4)	6.1 (5.3)	2.7 (1.4)	4.3 (2.9)	21.3 (11.5)	44.9 (11.5)	Arithmetic mean (s.d) n=8 Mar.to Apr. 1980	N.W. England	Pio (1981)
Fine 26.3	6.6	1.2	0.8	2.8	11.4	43.3	Samples collected 6/82 to 12/83		Willison *et al* (1985)
Coarse 15.3	1.0	0.9	1.2	0.2	3.3	21.6	using a dichotomous	Leeds	
Total 41.6	7.6	2.1	2.0	3.0	14.7	35.5	sampler. n=330		

* Value not presented by Author

† Percentage calculated without Cl^- concentrations

($\bar{x} = 2.0\ \mu g\ m^{-3}$). Similarly low ammonium concentrations were determined for samples collected at Wells in this study. The low ammonium concentrations determined during the summer reflect the lower sulphate concentrations found during the corresponding summer months.

6.2 Gaseous-particulate matter relationship.

The amounts of sulphur and nitrogen compounds existing in particulate form will depend on the amounts of precursor gases and availability of oxidants, respectively (homogenous and heterogeneous oxidation mechanisms were discussed in Sections 3.2.2 and 3.2.3). In this section the measured concentrations of sulphur and nitrogen in particulate and gaseous form are compared and any interdependent relationships established.

6.2.1 Gaseous pollutant concentrations

The concentrations of sulphur dioxide and nitrogen dioxide were supplied by the Building Research Establishment. Sulphur dioxide levels were determined by collecting the gas, via oxidation to sulphate in a 1% aqueous solution of hydrogen peroxide, and subsequent concentration measurement using ion chromatography (see Section 4.3.3). The sampling period was twenty four hours.

The nitrogen dioxide levels were determined using diffusion tubes. These tubes, containing a wire mesh coated with triethanolamine, were exposed for a sampling period of one week. The atmospheric concentrations were determined by dividing the mass of NO_2^- that had diffused to the wire mesh by the volume of air that carried the NO_2 to the wire mesh over the sampling period. The mass of NO_2^- collected was obtained by measuring the light absorbed (at 550 nm) by the azo-complex, formed when the NO_2^- ion reacts with N-1-naphthyl ethylene diamine. The volume of air that carried the NO_2 to the wire mesh was calculated, using Fick's First Law of diffusion, as 12 litre $week^{-1}$. The determination of atmospheric nitrogen dioxide using diffusion tubes has been discussed by Palmes *et al.* (1976). The monthly measured concentrations for both pollutants are summarised in Table 6.6.

Table 6.6 Monthly arithmetic mean gaseous concentrations determined for all sites.

		Lincoln Cathedral					Bolsover Castle				Wells Cathedral	
	Month	9/89	5/90	1/91	2/91	3/91	11/90	12/90	1/91	2/91	6/91	7/91
SO_2	Range	0.4-90.0	0.7-36.1	5.1-169.3	0.5-50.1	0.7-92.9	9.7-96.3	5.5-111.3	12.9-117.6	7.5-133.2	0.2-11.1	0.6-10.8
	$\bar{x}$	16.2	11.9	34.0	24.0	17.5	30.7	41.1	52.8	56.0	2.0	5.1
NO_2	Range	30.5-41.4	14.7-22.0	29.0-35.7	27.1-65.0	17.7-37.2	36.7-51.7	12.0-56.4	64.2-61.1	20.7-53.0	12.0-15.0	10.6-17.2
	$\bar{x}$	36.1	19.3	31.3	42.4	31.3	44.0	24.8	41.4	42.6	12.7	13.2

Notes:
Concentrations are expressed as $\mu g\ m^{-3}$.
The ranges and monthly mean concentrations for the NO_2 concentrations were determined using weekly samples.

The highest monthly mean SO_2 and NO_2 concentrations are observed to be occurring during the winter months. For example, monthly arithmetic SO_2 means of 52.8 and 56.0 $\mu g\ m^{-3}$ were observed at Bolsover during January 1991 and February 1991, respectively. Conversely the lowest SO_2 concentrations were recorded at Wells during June and July 1991; 2.0 and 5.1 $\mu g\ m^{-3}$, respectively.

Monthly mean concentrations for NO_2 exceeding 40 $\mu g\ m^{-3}$ were recorded at Bolsover during November 1990, December 1990, February 1991 and at Lincoln during January 1991. The lowest concentrations were determined at Wells during June and July 1991; 12.7 and 13.2 $\mu g\ m^{-3}$, respectively. In addition, as the monthly mean concentrations were calculated from weekly samples, the range of observed concentrations can be seen in Table 6.6 to be less than the range in SO_2 concentrations (SO_2 samples were collected daily).

The monthly mean concentrations for Lincoln shown in Table 6.6 are lower than the annual mean sulphur dioxide concentrations reported by Eggleston *et al.* (1992) for Lincoln during recent years (35 $\mu g\ m^{-3}$). This concentration value measured at Lincoln Cathedral has decreased from a peak of approximately 135 $\mu g\ m^{-3}$ in the early 1960s. The current concentration is similar to the U.K. rural concentration which has remained at 30 to 50 $\mu g\ m^{-3}$ for the last forty years. This would indicate that the contribution of sulphur emission sources within the city of Lincoln to the measured concentrations is negligible.

Dispersion models used to calculate ground level concentrations at Lincoln resulting from emissions originating from the three Trentside power stations situated to the west and north-west of the city suggested that only 3 $\mu g\ m^{-3}$ (8%) of the measured 35 $\mu g\ m^{-3}$ was derived from these sources. Hackman *et al.* (1992) determined that 42% of the annual average SO_2 concentration at Lincoln originates from other British power stations. Summed together these two values would suggest that 50% of the annual average of sulphur dioxide measured at Lincoln originates from power stations.

6.2.2 Sulphate in particulate matter

In addition to the monthly arithmetic and geometric mean concentrations presented in Table 6.4, other characteristics of the particulate sulphate concentration such as frequency distribution and individually observed concentrations will be discussed in this section.

6.2.2.1 Sulphate frequency distributions

Sorting the daily sulphate concentrations into successive 2 $\mu g\ m^{-3}$ range groups will allow the most frequent concentrations to be readily observed from the frequency diagrams presented in Figure 6.5. Concentrations ranging from 4.01 to 6.00 $\mu g\ m^{-3}$ are most abundant at Lincoln and Bolsover, whereas concentrations 2.01 to 4.00 $\mu g\ m^{-3}$ are most frequent at Wells. Concentrations of sulphate exceeding 28 $\mu g\ m^{-3}$ can be seen to be occurring only at Lincoln and Wells.

6.2.2.2 Monthly sulphate concentrations

The mean monthly sulphate concentrations in the collected particulate matter were shown in Table 6.4 to be highest during the winter months; January 1991 at Lincoln (16.7 $\mu g\ m^{-3}$) and February 1991 at Bolsover (16.6 $\mu g\ m^{-3}$). The lowest mean value was obtained for June 1991 at Wells (3.2 $\mu g\ m^{-3}$). However, the two highest daily sulphate concentrations were obtained during summer months; 4 May 1990 (34.2 $\mu g\ m^{-3}$) at Lincoln and 30 May 1991 (28.9 $\mu g\ m^{-3}$) at Wells. The meteorological conditions for 4 May 1990 were such that an anti-cyclone over the North Sea was producing very high

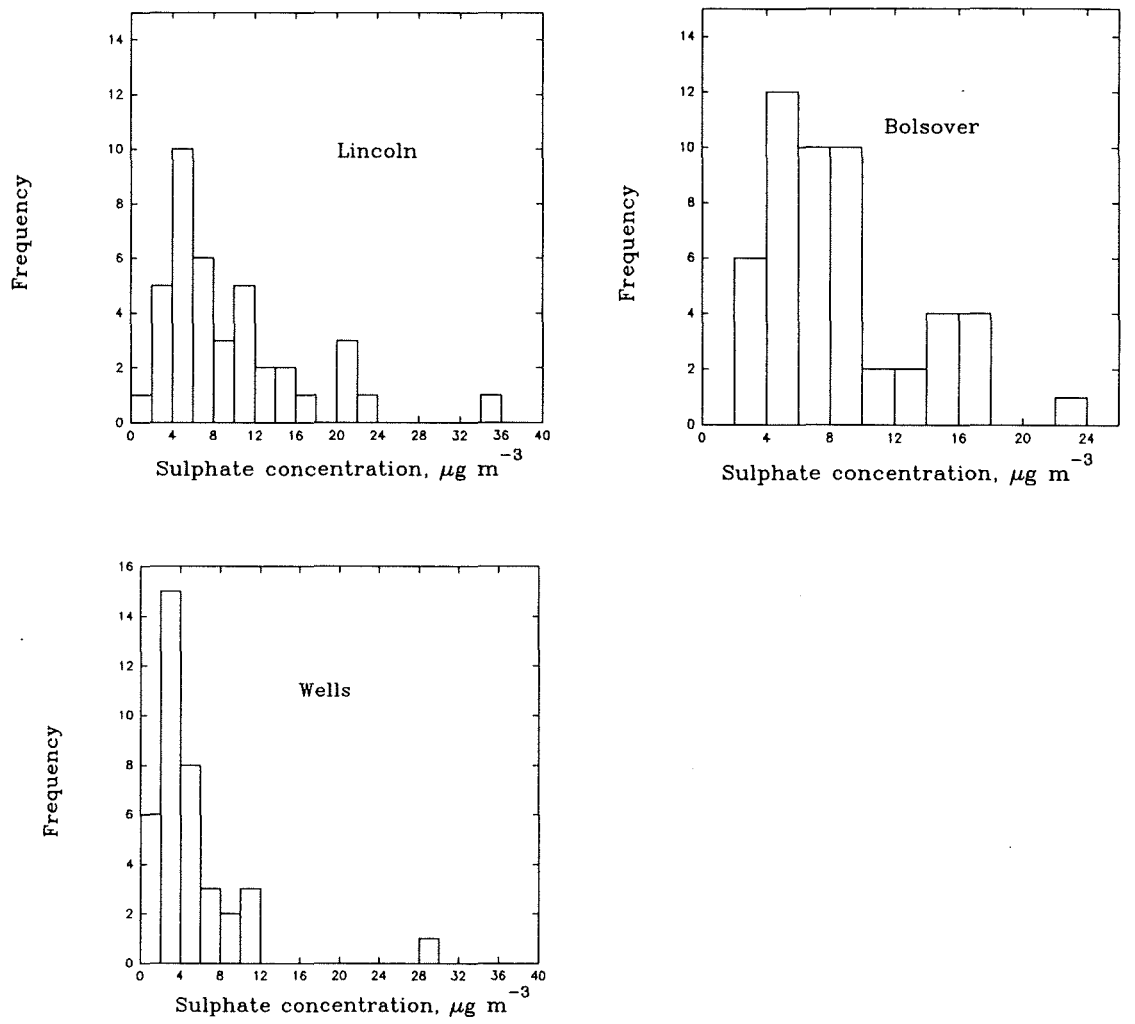

Figure 6.5 Frequency distributions for sulphate concentrations.

temperatures (the highest May temperatures since 1875) all over the country (Weather, 1991). The second highest sulphate concentration was recorded at Wells on 30 May 1991, when a mixture of dry and stable conditions allowed the accumulation of atmospheric sulphate.

The highest daily sulphate concentrations for winter values occurred at Bolsover on 25 February 1991. This could be due to the abundant sunshine (7.9 hours was the highest value monitored in the country on that day) as recorded at the local Meteorological Office station (Finningley). Such meteorological conditions may have provided the necessary photochemical oxidants for the oxidation of sulphur dioxide to take place.

However, the photochemical oxidation mechanism is probably a less prevalent oxidation

mechanism during the winter time. For example, from an extensive study involving the simultaneous collection of seven hundred samples collected at five sites in the U.K. and measurement of relative humidity, between 1976 and 1979, McInnes (1981) showed that high sulphate concentrations existed in the winter when the relative humidity was high (temperature low) and during the summer when the relative humidity was low (temperature high). The high sulphate conditions during the winter were attributed to oxidations in the liquid phase (Section 3.2.3.2), whereas those during the summer were assumed to occur in the gaseous phase (Section 3.2.2.2).

The seasonal nature of elevated sulphate concentrations has also been noted by Altshuller (1980). By choosing a sulphate concentration of greater than or equal to 15 $\mu g\ m^{-3}$ as a classification for "high" sulphate concentration, 40 out of a total of 332 daily samples collected at 11 sites throughout the eastern United States between 1965 and 1977, were found to exceed this level. Those samples collected during the second quarter (April to June) and third quarter (July to September) of each year represented 28 and 53%, respectively of the exceedences. Conversely, the first and fourth quarter, with meteorological conditions less conducive to the production of photochemical oxidants, produced only 9% and 10%, respectively, of the high concentrations.

Meteorological conditions will therefore play a critical role controlling the ambient sulphate concentrations and will affect the selection of a "typical" sulphate concentration. For example, the winter mean (12.3 $\mu g\ m^{-3}$) concentration determined by Nicholson (1987) was less than the summer mean (17.9 $\mu g\ m^{-3}$). This study involved the collection of aerosol samples (n=78) in a rural location in Norfolk from 7 June 1979 to 6 June 1980. This observation is contrary to the findings in this study, in which winter monthly mean values are greater than summer monthly mean values.

6.2.3 Sulphur concentrations in the particulate and gaseous phases

The concentrations of sulphur contained within the gaseous phase (as sulphur dioxide) and the atmospheric particulate matter for samples collected at all sites are compared in this section.

6.2.3.1 Relationship between sulphur dioxide and sulphate concentrations

An investigation was performed to assess whether the $S\text{-}SO_2$ and $S\text{-}SO_4^{2-}$ concentrations at each site were related. The data was analysed in two parts; winter samples and summer samples. The winter season was defined as being from 1 October to 31 March and the summer season from 1 April to 30 September. At Lincoln both winter and summer data were collected. At Bolsover only winter data was collected, whereas, at Wells only summer data was collected. The associations between $S\text{-}SO_4^{2-}$ and $S\text{-}SO_2$ at the different sites can be observed in Figure 6.6. Higher concentrations of sulphur, as $S\text{-}SO_2$ and $S\text{-}SO_4^{2-}$, are observed for the winter data at both Lincoln and Bolsover, compared to the sulphur concentrations measured in each phase during the summer months at Lincoln and Wells.

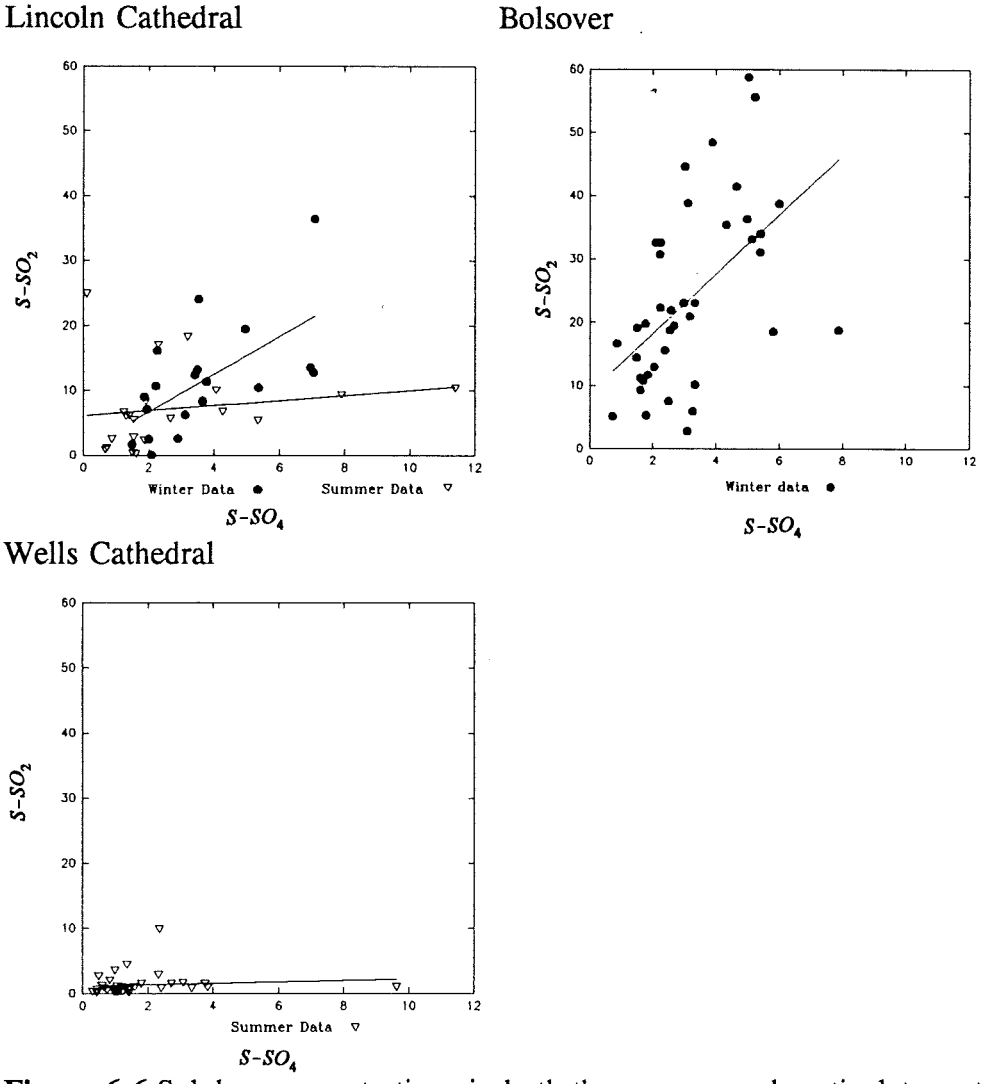

Figure 6.6 Sulphur concentrations in both the gaseous and particulate matter forms as determined at Lincoln, Bolsover and Wells. All concentrations are $\mu g\ m^{-3}$.

By using a regression analysis, in which the $S\text{-}SO_2$ concentration was the dependent variable and the $S\text{-}SO_4^{2-}$ concentration the independent variable, the association between sulphur in the gaseous and particulate phases was further investigated. A statistically significant relationship was found to occur if the t-ratio obtained was more than the critical t-ratio (the calculation of t-ratios was presented previously in Section 5.2.2.5).

The calculated t-ratios and critical t-ratios are presented in Table 6.7. The winter data collected at both Lincoln and Bolsover had t-ratios exceeding their respective critical t-ratio, which would suggest that a statistically significant relationship existed between sulphur dioxide and sulphate. The t-ratios calculated for the summer data at Lincoln and Wells had t-ratios less than the critical value, suggesting no significant relationship exists between the sulphur dioxide and sulphate. However, although a significant relationship is observed between the winter sulphur dioxide and sulphate concentration values, an inference regarding the amount of sulphur dioxide actually oxidised to sulphate cannot be made.

Table 6.7 Regression coefficients and constants obtained when $[S\text{-}SO_2]$ is regressed against $[S\text{-}SO_4^{2-}]$ for data collected during winter and summer seasons.

Sampling Site and Season	Regression coefficient *A*	Estimated standard deviation of *A*	Regression constant *B*	Degrees of freedom*	t-ratio	Critical t-ratio†	R^2
Lincoln							
Winter	2.92	0.90	0.84	17	3.24	1.74	0.38
Summer	0.38	0.53	6.10	19	0.76	1.73	0.03
Bolsover							
Winter	4.69	1.11	8.86	39	3.97	1.68	0.29
Wells							
Summer	0.11	0.18	1.11	36	0.61	1.68	0.01
Tanner and Leaderer (1982)							
Winter	12.8‡		10.8‡				0.64
Summer	0.025‡		20.2‡				0.06

Note: * the degrees of freedom were calculated by subtracting 2 from the number of samples in data set
† The hypothesis was tested at the 0.05 level of significance
‡ The t-ratio and level of significance were not presented by Tanner and Leaderer (1982)

Also presented in Table 6.7 is the coefficient of determination, R^2. The high R^2 values for the winter data, compared to the summer R^2 values, suggests further that sulphur dioxide and sulphate associate together during the winter time. Similar results were

obtained by Tanner and Leaderer (1982) when they regressed the observed SO_2 concentrations onto the SO_4^{2-} concentrations collected at an urban site in New York. The higher R^2 value obtained for the winter compared to the summer value, was attributed by Tanner and Leaderer (1982) to result from sources local to the sampling site emitting sulphur as both sulphate aerosol and as sulphur dioxide.

Unfortunately, as the NO_2 concentrations were determined on a weekly basis, a similar analysis could not be performed for nitrogen. However, measurement of a linear association between NO_2 and NO_3^- is more difficult, compared to the SO_2 to SO_4^{2-} reaction, due to competing reaction pathways for NO_2, as illustrated in Figure 3.2 and described in Section 3.2.7.

6.2.3.2 Evidence for increased oxidation of sulphur dioxide to sulphate during summer months

A plot of S-SO_2 concentrations against S-SO_4^{2-} concentrations normalised by S-SO_2 concentrations, allows the extent of oxidation of SO_2 to SO_4^{2-} to be inferred (Figure 6.7). For example, a lower ratio of S-SO_4^{2-}/S-SO_2 would indicate that most sulphur is still present in valence state (IV), a situation observed for the winter data, whereas a higher ratio would indicate that most of the sulphur has been oxidised to valence state (VI), a situation observed for the summer data. The arithmetic mean and geometric mean S-SO_4^{2-}/S-SO_2 ratios are 0.26 and 0.19 respectively for the winter data and 2.04 and 1.02 respectively for the summer data. The winter data is comparable to that found by Nicholson (1990) who determined a geometric mean ratio of 0.17 for 5 urban sites in Norwich during a monitoring period of nine months in 1979/80.

6.3 Deposition Fluxes

This section assesses the relative magnitude of sulphur and nitrogen compounds being delivered to building surfaces by dry deposition (either as particulate matter or gaseous forms) or by wet deposition. The amount of material reaching the surface by dry deposition will be calculated as the product of deposition velocity and atmospheric concentration. Wet deposition is calculated as the product of sulphur and nitrogen

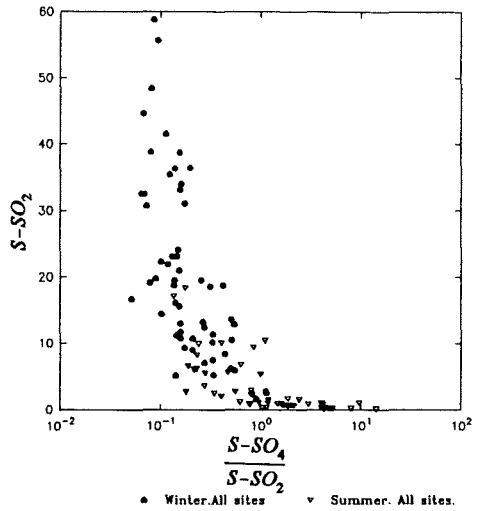

Figure 6.7 Comparison of the ratio of $S\text{-}SO_4^{2-}/S\text{-}SO_2$ to $S\text{-}SO_2$ concentrations.

compound concentrations contained within the precipitation (expressed as a volume weighted mean, VWM) and the volume of precipitation collected at the receptor site.

6.3.1 Dry gaseous and dry particulate deposition

The various processes controlling deposition velocity have been discussed in Chapter 3 and the ranges of experimentally derived deposition velocities for each species are presented in Table 3.12. The deposition velocity values used to determine deposition fluxes are given in Table 6.8.

Table 6.8 Deposition velocities for SO_2, SO_4^{2-}, NO_2 and NO_3^- used to calculate dry deposition fluxes

Species	SO_2	SO_4^{2-}	NO_2	NO_3^-
v_g (cm s^{-1})	0.8	0.1	0.3	0.1

The SO_2, SO_4^{2-} and NO_3^- concentrations were determined daily, and the NO_2 concentrations determined weekly. The role of SO_2 in the deterioration process has been discussed in Sections 2.4.2 and 2.4.3.

The NO_2 flux will not necessarily provide estimation of an important corrosive input. That is, the role of NO_2 in causing an alteration to stone surfaces was shown in Chapter

2 to be relatively minimal. Evidence was provided using the results of both laboratory and field experiments. Laboratory experiments, such as those carried out by Haneff *et al.* (1992) (see Section 2.4.2.2.), have shown that dry stone tablets exposed to NO_2 increased in weight, whereas wet stones exposed to NO_2 slightly lost weight. The former observation was attributed to nitrate formation on the stone surface, whereas insufficient reaction time for NO_2 to form nitrate in the continually changing water layer suggested that NO_2 did not contribute to stone alterations for the case of wet stones. Extrapolation of these findings to an ambient situation, with the inevitable moisture variation of exposed surfaces, would suggest that NO_2 deposited to a dry surfaces, will be oxidised to nitrate, and removed during wet events, without causing significant damage to the stone surface. Field experiments involving the simultaneous measurement of stone loss and atmospheric NO_2 concentrations, such as those performed by Webb *et al.* (1992) (see Section 2.4.3.), showed no dependence of stone loss on NO_2.

The most reactive gaseous nitrogen compound towards limestone is nitric acid. Unfortunately nitric acid atmospheric concentrations were not available in this study. However given the lower atmospheric concentrations for HNO_3 compared to SO_2, this gas will not contribute significantly to stone loss in the ambient atmosphere. Estimated surface recession rates for a range of HNO_3 concentrations were presented in Figure 2.3.

Finally, the role of particulate sulphate and nitrate in altering building materials is considered by Lipfert (1989) to be insignificant. Verification of this assertion is difficult however, since from the other available literature, sulphate is known to participate in the deterioration process by forming gypsum with calcium ions (see Equation 2.3). But the actual amount of sulphate delivered by this mechanism will be shown in Section 6.3.3 to be relatively small. Likewise the amount particulate nitrate delivered is also small, and as was shown in Section 2.4.2.2. any nitrate present will be quickly removed by water passing over the stone surface.

6.3.2 Wet deposition

Ionic concentrations (sulphate and nitrate) in the precipitation, expressed as volume

weighted mean values (VWM), and precipitation depth (mm) are presented in Table 6.9. The monthly VWM is defined as the sum of the product of precipitation volume (ml) and ionic concentration ($\mu g\ ml^{-1}$) for each collected rainfall sample divided by the total precipitation volume (ml) for that month.

Table 6.9 Monthly precipitation depth (mm) and volume weighted mean concentrations for SO_4^{2-} and NO_3^- at Lincoln, Bolsover and Wells.

			Lincoln Cathedral					Bolsover Castle				Wells Cathedral	
		Month	9/1989	5/1990	1/1991	2/1991	3/1991	11/1990	12/1990	1/1991	2/1991	6/1991	7/1991
Meteorological Data		Precipitation (mm)	3	16	20	13	5	24	19	15	21	99	57
Wet Precipitation Data	SO_4^{2-}	[VWM] ($\mu g\ ml^{-1}$)	3.7	3.1	2.5	4.2	2.6	6.1	11.0	13.5	14.4	5.0	5.7
	NO_3^-	[VWM] ($\mu g\ ml^{-1}$)	1.7	1.3	0.3	1.3	0.5	1.9	7.0	4.6	4.7	4.2	9.7

6.3.2.1 Sulphate and nitrate concentrations

The volume weighted mean concentrations for sulphate were lowest at the Lincoln site with concentrations ranging, for the five months studied, from 2.6 to 4.2 $\mu g\ ml^{-1}$. The two highest VWM concentrations were determined for Bolsover in January 1991 (13.5 $\mu g\ ml^{-1}$) and February 1991 (14.4 $\mu g\ ml^{-1}$). The VWM concentrations at Wells were intermediate in magnitude between the Lincoln and Bolsover concentrations.

The sulphate concentrations determined at Bolsover, during November 1990, January 1991 and February 1991, are approximately twice those estimated by Szepesi and Fekete (1987) for a local-urban scale average concentration. These high VWM concentrations would have resulted from the high monthly sulphur dioxide and particulate sulphate concentrations which may have contributed to the sulphate in precipitation. An estimation of the relative contribution of sulphur dioxide and particulate sulphate to precipitation sulphate is presented in Section 6.4.2. The precipitation sulphate concentrations for the remaining months in this study are approximately equal to those reported for other urban and sub-urban sampling locations (Table 6.10).

The highest nitrate concentrations were found for samples collected at Wells (July

Table 6.10 Selected concentrations of sulphate and nitrate in precipitation for a range of sample locations

	Concentration ($\mu g\ ml^{-1}$)	Sampling details	Reference
Sulphate	6.00* 5.01* 0.48*	Local-urban scale average (Budapest, Hungary) Regional scale average (rural central Europe) Continental avarage (rural Europe)	Szepesi and Fekete (1987)
	0.74†‡	Miami, Florida 4 year average	Savoie *et al.* (1987)
	3.66‡ 3.69‡	Urban site, lakefront Chicago. Suburban site, 35 km SW of urban site, near large residential areas	Sisterson and Shannon (1990)
	3.62†‡ 5.47†‡	Lyme Park, Cheshire Manchester city centre	Lee and Longhurst (1992)
Nitrate	0.51‡	Miami, Florida 4 year average	Savoie *et al.* (1987)
	0.80‡	Norwegian Arctic, Bjørnøya 1978 to 1984. Clean site	Joranger and Semb (1987)
	1.51‡ 1.39‡	Urban site, lakefront Chicago. Suburban site, 35 km SW of urban site, near large residential areas	Sisterson and Shannon (1990)
	1.02‡ 2.20‡	Lyme Park, Cheshire Manchester city centre	Lee and Longhurst (1992)

* Concentrations are presented as background concentrations. These concentrations were determined for an areal averages measured over the representative territory.
† as non marine sulphate
‡ Volume weighted concentration

1991). The lowest concentrations were determined at Lincoln (January 1991). The high precipitation nitrate concentration observed at Wells during July 1991 does not mirror the concentrations of particulate and gaseous nitrate, (presented in Tables 6.4 and 6.6, respectively) as was observed for the case of high sulphate concentrations measured at Bolsover during February 1991. A possible reason for this may be that the nitrate concentration measured during this month was greatly influenced by precipitation nitrate concentration collected on 18 July 1991 (35.6 $\mu g\ ml^{-1}$). Reasons for this high concentration are uncertain, since the weather pattern observed on the synoptic weather chart for this day shows that a low pressure air mass travelled west from the Atlantic, which presumably was carrying relatively "clean" air (Weather, 1991).

The nitrate concentrations determined at Bolsover and Wells, with the exception of November 1990 at Bolsover, are approximately a factor of two higher than the highest concentration presented in Table 6.10. Whereas the concentrations determined at Lincoln are comparable to those determined by Sisterson and Shannon (1990) and Lee and Longhurst (1992) for both urban and sub urban sampling sites.

6.3.2.2 Precipitation amounts

The measured monthly depth precipitation ranged from 3 mm at Lincoln in September 1989 to 99 mm at Wells in June 1991 (Table 6.9). Caution must be observed when interpreting these precipitation values as they cannot be considered to be typical. For example, the monthly average precipitation values recorded at the two nearest Meteorological Office stations are compared in Table 6.11 to the values determined at the specific sites in this study. The precipitation amounts determined in this study, can be seen to be lower than the amounts determined at each meteorological station (except for Lincoln during May 1990). The lower values could be due to sheltering effects of nearby structures impeding the entry of rain into the rain collector. An additional consideration in comparing monthly precipitation amounts is that the collected precipitation may have resulted from single localised precipitation events. The lack of a definite trend in precipitation levels between sites can be seen by comparing data presented in Table 6.11. In November 1990, Watnall (Station 1) recorded 25 mm and Finningley (Station 2) 47 mm, whereas September 1989 showed similar precipitation amounts of 22 mm and 21 mm at each station, respectively.

6.3.3 Comparison of the magnitudes of wet and dry deposition in this study

The wet and dry deposition rates (expressed as mg m^{-2} $month^{-1}$) for sulphur and nitrogen to the three historic buildings are presented in Table 6.12 and illustrated in Fig 6.8. The monthly arithmetic mean concentrations and volume weighted means are also listed in Table 6.12. The wet fluxes for both sulphate and nitrate were determined by calculating the deposition for each precipitation event and grouping these into monthly totals.

The daily gaseous SO_2 concentrations were each multiplied by the appropriate

Table 6.11 Comparison of total rainfall data determined during this study with that recorded by the Meteorological Office (nearest two Meteorological Office sites only).

Site	Sampling Month	This study (mm)	Nearest Station (1)	Nearest Station (2)	Mean of two nearest Metorological. stations * (mm)
Lincoln	September 1989	3	22	21	22
	May 1990	16	11	15	13
	January 1991	20			
	February 1991	13	42	45	44
	March 1991	5	27	43	35
Bolsover	November 1990	24	25	47	36
	December 1990	19	78	87	83
	January 1991	15			
	February 1991	21	42	45	44
	June 1991	N.D.	46	53	50
Wells	May 1991	N.D.	8	5	6
	June 1991	99	90	134	112
	July 1991	57	74	82	78

* The two nearest meteorological stations for Lincoln and Bolsover are at Watnall (Station 1) and Finningley (Station 2) and for Wells at Rhoose (Cardiff Airport) (Station 1) and R.A.F. Lyneham, Wiltshire (Station 2).

deposition velocity and summed to produce the monthly dry deposition flux. The fluxes for gaseous nitrogen were derived from nitrogen dioxide concentrations measured as weekly averages. As mentioned before, other nitrogen containing gases such as HNO_3 and NO were not considered in this study.

The particulate sulphur and nitrogen flux values were derived from the concentrations of sulphate and nitrate measured in the collected airborne particulate matter. However, as the number of samples collected each month ranged from 5 to 16, calculation of the monthly flux required scaling by an appropriate factor. For example, the measured flux for a ten day sampling period required multiplication by three to approximate a thirty day sampling period.

The deposition of sulphur and nitrogen in dry form (gaseous $S\text{-}SO_2$ and $N\text{-}NO_2$) can be seen to exceed the wet deposition ($S\text{-}SO_4^{2-}$ and $N\text{-}NO_3^-$) at Bolsover by an order of

magnitude, with this situation being reversed at Wells during June and July 1991.

The dry deposition of particulate sulphate was approximately two orders of magnitude less than the main deposition pathway which was dry deposition of gaseous S-SO_2 at Bolsover and Lincoln and wet deposition of S-SO_4^{2-} at Wells.The dry deposition of sulphur in particulate form can be seen to equal the wet deposition of sulphur at Lincoln, whereas the dry deposition of particulate nitrate exceeded wet deposition by at least a factor of two (with the exception of May 1990).

These results for sulphur are in accordance with those of Girardet and Furlan (1989) who measured the uptake of sulphur, in aerosol and gas form, by stone tablets placed at forty sites throughout Switzerland. The uptake via the aerosol was shown to represent only between 2 to 5% of the total uptake. At less polluted sites the contribution of the aerosol ranged from 5 to 20%. In all cases the amount of sulphur deposited in the aerosol form was similar.

Lipfert (1989) suggests that the dry deposition of SO_2 to a stone surface will have a dependence on precipitation since the rainwater will wash away gypsum deposits.This will allow fresh SO_2 to be taken up. This was originally demonstrated by Braun and Wilson (1970) who showed that the rate of uptake by a freshly exposed Eton limestone surface was the same as by a weathered surface that had been continually washed by rainfall.

Also presented in Table 6.12 are the washout ratios obtained from monthly precipitation and aerosol concentrations. Washout ratios will be discussed further in Section 6.4.

6.3.4 Comparison with other deposition studies

The deposition of sulphur and nitrogen, in both dry and wet forms, at different locations, will be compared to the deposition fluxes determined by other authors in this section. Deposition of pollutants can be calculated by either:

a) Measurement of the pollutant near ground level, which for the case of the dry

Table 6.12 Wet and dry deposition fluxes for sulphur and nitrogen compounds.

			Lincoln Cathedral					Bolsover Castle				Wells Cathedral	
		Month	9/89	5/90	1/91	2/91	3/91	11/1990	12/1990	1/1991	2/1991	6/1991	7/1991
Meteorological Data	Species	Precipitation (m)	0.0026	0.016	0.020	0.013	0.0047	0.024	0.019	0.0145	0.021	0.099	0.057
Wet Precipitation Data	Sulphate	[VWM] ($\mu g\ ml^{-1}$)	3.69	3.11	2.5	4.22	2.58	6.1	11.0	13.5	14.4	5.0	5.7
	Nitrate	[VWM] ($\mu g\ ml^{-1}$)	1.73	1.33	0.3	1.25	0.52	1.9	7.0	4.6	4.7	4.2	9.7
Atmospheric Concentrations Expressed as Arithmetic Mean	SO_2	($\mu g\ m^{-3}$)	16.2	11.9	34.0	24.0	17.5	30.7	41.1	52.8	56.0	2.0	3.1
	SO_4^{2-}	($\mu g\ m^{-3}$)	3.3	10.1	16.8	10.6	6.8	6.6	8.8	11.8	16.6	13.2	3.9
	NO_2	($\mu g\ m^{-3}$)	36.1	19.3	31.3	42.4	31.3	44.0	24.8	41.4	42.6	12.7	13.2
	NO_3^-	($\mu g\ m^{-3}$)	4.2	8.1	15.1	12.0	3.5	4.3	5.5	8.4	11.8	4.0	2.0
Wet Flux	$S\text{-}SO_4^{2-}$	($mg\ m^{-2}\ mth^{-1}$)	3.2	16.6	16.6	18.2	4.5	48	69	66	101	166	108
Dry Flux	$S\text{-}SO_2$	($mg\ m^{-2}\ mth^{-1}$)	168	123	353	250	187	320	427	550	582	28	33
Dry Flux	$S\text{-}SO_4^{2-}$	($mg\ m^{-2}\ mth^{-1}$)	2.9	8.8	23.2	6.6	5.9	5.7	7.6	10.2	14.4	3.0	3.6
Wet Flux	$N\text{-}NO_3^-$	($mg\ m^{-2}\ mth^{-1}$)	1.0	4.7	1.3	3.5	0.5	11	30	15	22	95	127
Dry Flux	$N\text{-}NO_2$	($mg\ m^{-2}\ mth^{-1}$)	87	47	54	103	76	106	60	100	103	31	32
Dry Flux	$N\text{-}NO_3^-$	($mg\ m^{-2}\ mth^{-1}$)	2.9	4.5	8.9	7.1	2.0	3.7	4.8	7.3	10.2	3.5	1.7
Wash-out ratio for SO_4^{2-}			1342	370	204	478	455	1110	1500	1370	1050	460	1760
Wash-out ratio for NO_3^-			494	197	68	125	178	540	1530	660	470	1260	5920

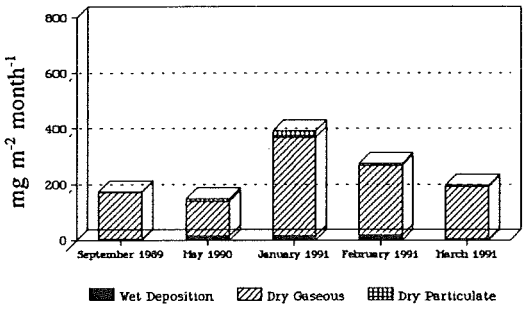

a) Sulphur – Lincoln

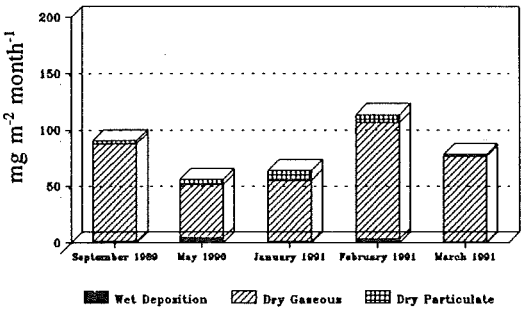

b) Nitrogen – Lincoln

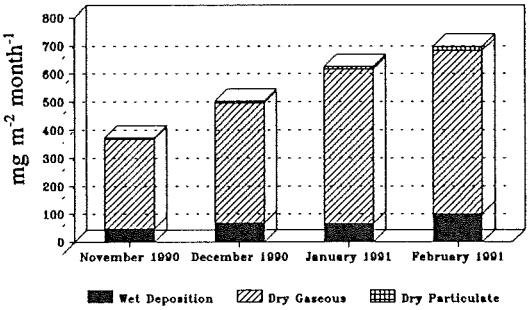

c) Sulphur – Bolsover

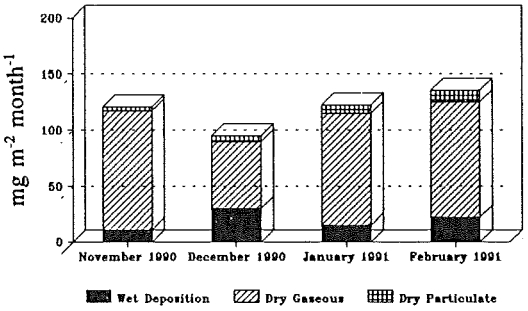

d) Nitrogen – Bolsover

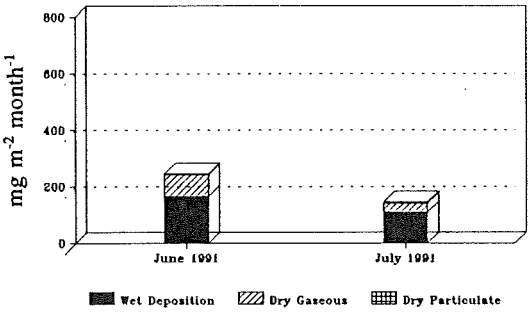

e) Sulphur – Wells

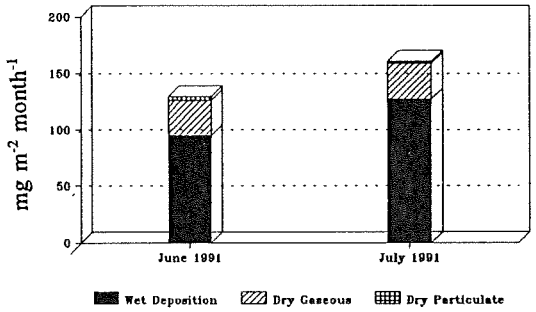

f) Nitrogen – Wells

Figure 6.8 Magnitude of sulphur and nitrogen deposition at each sampling site

pollutants, is multiplied by the appropriate deposition velocity. For the case of pollutants in the wet form, the pollutant concentration is multiplied by the rainfall amount. These measures were used to determine pollutant deposition in this study.

or

b) Theoretically. An atmospheric concentration is initially estimated by calculating the amount of material released from various sources and the volume occupied by the material in the troposphere. This concentration will then be scaled by the appropriate removal factors; dry deposition velocity for a gas (Garland and Branson, 1976) to produce the dry deposition flux; and washout ratio and expected rain intensity to produce the wet deposition flux (Barrie, 1981).

or

c) Direct measurement. Mass of material accumulated on the surface is divided by the concentration of pollutant above the surface. Examples of this method were presented in Table 2.11 for deposition of SO_2 to stone surfaces under laboratory conditions. Section 3.2.6. presented deposition velocities for radioactive isotopes.

6.3.4.1 Deposition of sulphur

The wet and dry deposition fluxes for sulphur are compared in Table 6.13. The deposition fluxes determined by other authors were calculated on an annual basis. For the purposes of comparison, the monthly deposition fluxes determined at each sampling site in this study are scaled up accordingly and represented as g m^{-2} a^{-1}. The wet deposition fluxes were found to be lowest at Lincoln and were similar to the wet flux determined by Fisher (1982) over Ireland. The wet flux for Bolsover, with the exception of February 1991, was about half that determined by Fisher (1978) for the mean wet deposition throughout Europe. The greatest amount of wet deposition occurred at Wells during the summer months, reflecting the high precipitation volume that occurred during this period (Table 6.9). The dry deposition at Lincoln was approximately of the same magnitude as determined by Fisher (1978) for the mean dry deposition throughout Europe.

Table 6.13 Comparison of wet and dry deposition values for sulphur.

Model Type	Deposition Flux as determined by Author		Deposition flux, presented as g m^{-2} a^{-1}		Wet/Dry Deposition ratio	Authors
	Wet Deposition	Dry deposition	Wet deposition	Dry deposition		
WD = VWM × Rainfall amount DD = [S-SO_2] × v_g The Netherlands.	280 mol ha^{-1} a^{-1}	700 mol ha^{-1} a^{-1}	2.6	6.7	0.4	Erisman *et al.* (1986)
WD = VWM × Rainfall amount DD = [S-SO_2] × v_g Eastern North America	20 kg ha^{-1} a^{-1}	Range 1.5 kg ha^{-1} a^{-1} to 12 kg ha^{-1} a^{-1}	2	1.5 to 12	1.3 to 0.2	Summers *et al.* (1986)
Statistical model incorporating emissions, wind speed and direction, dispersion category and rainfall. Europe	2 g m^{-2} yr^{-1}	3 g m^{-2} yr^{-1}	2	3	0.7	Fisher (1978)
Statistical model incorporating emissions, wind speed and direction, dispersion category and rainfall. Ireland	0.6 g m^{-2} a^{-1}	0.6 g m^{-2} a^{-1}	0.6	0.6	1	Fisher (1982)
This study: equivalent annual deposition*	Wet deposition	Dry deposition**	Wet deposition	Dry deposition**	Wet/Dry Deposition ratio	
Lincoln	g m^{-2} a^{-1}	g m^{-2} a^{-1}	g m^{-2} a^{-1}	g m^{-2} a^{-1}		
September 1989	0.04	2.1	0.04	2.1	0.02	
May 1990	0.2	1.5	0.2	1.5	0.13	
January 1991	0.2	4.5	0.2	4.5	0.04	
February 1991	0.2	3.1	0.2	3.1	0.06	
March 1991	0.05	2.3	0.05	2.3	0.02	
Bolsover						
November 1990	0.6	3.9	0.6	3.9	0.15	
December 1990	0.8	5.2	0.8	5.2	0.15	
January 1991	0.8	6.7	0.8	6.7	0.12	
February 1991	1.2	7.2	1.2	7.2	0.17	
Wells						
June 1991	2.0	0.4	2.0	0.4	5.0	
July 1991	1.3	0.4	1.3	0.4	3.3	

* The equivalent annual deposition was calculated by multiplying the monthly deposition values determined in this study by a factor of 12.

** The dry deposition was calculated as the sum of dry gases and dry particulate forms.

The wet to dry deposition ratios were lowest (0.02) during September 1989 and March

1991 at Lincoln. The ratios determined for each of the four months at Bolsover were similar (range 0.12 to 0.17). The highest ratios were obtained at Wells (5.0 and 3.3 for June and July, respectively). This high wet to dry ratio for sulphur provides further verification that a significant amount of sulphur is present in the oxidised form as was indicated in Figure 6.7. Since, as was shown by Smith (1985) the wet to dry deposition ratio for sulphur will increase significantly when the pollutant has travelled several hundered kilometres from the point of release into the atmosphere. This is expected as sulphur dioxide is oxidised to sulphate. Mechanisms by which sulphate is incorporated into water droplets were presented in Section 3.2.3.1.

The spatial distribution of dry and wet deposition of sulphur and nitrogen in the United Kingdom has been determined by Review Group on Acid Rain (RGAR). This study divided the surface area of the country into 20 × 20 km squares and calculated the dry and wet deposition accordingly. The wet (determined for 1981-1985) and dry (determined for 1983) deposition fluxes are shown in Figure 6.9. In general, areas of wet deposition are greatest in north-west Scotland, Cumbria and in the Pennines, around Sheffield. High dry deposition fluxes coincided with urban and industrial areas.

The wet deposition fluxes determined for Lincoln in the RGAR study, 1.00 to 1.25 g S m^{-2} a^{-1}, are higher than those determined at Lincoln in this study (range 0.1 to 0.7 g S m^{-2} a^{-1}). At Bolsover the RGAR wet flux, >1.25 g S m^{-2} a^{-1}, approximates to those determined in this study (range 0.8 to 2.2, mean 1.35 g S m^{-2} a^{-1}). Unfortunately for comparative purposes, the wet deposition flux at Wells cannot be compared to the incomplete RGAR database.

Both the dry deposition fluxes for Lincoln (range 1.6 to 3.7, mean 2.5 g S m^{-2} a^{-1}) and Bolsover (range 2.5 to 6.9 g S m^{-2} a^{-1}, mean 4.1 g S m^{-2} a^{-1}), are similar to the dry deposition fluxes, 2 to 4 g S m^{-2} a^{-1}, reported by RGAR. Likewise the dry deposition flux at Wells, (RGAR 0.5 to 1.0 g S m^{-2} a^{-1}), is similar to the values of 0.5 and 1.0 g m^{-2} a^{-1} determined for June and July 1991, respectively.

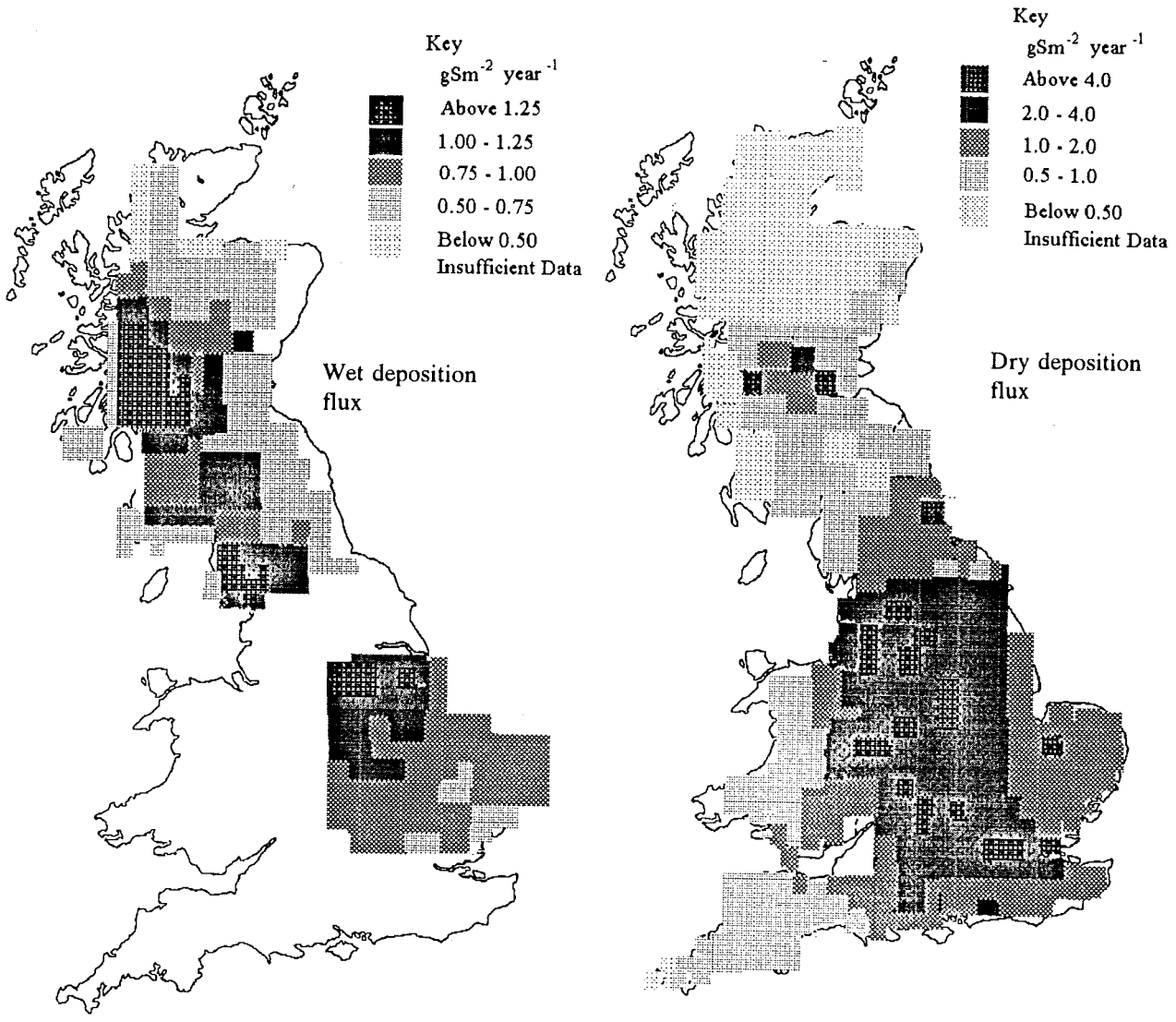

Figure 6.9 Wet and dry deposition fluxes in the United Kingdom (After RGAR, 1987)

6.3.4.2 Deposition of nitrogen

The wet and dry deposition fluxes measured for nitrogen at each sampling site are compared in Table 6.14. The deposition rates (in terms of g m^{-2} s^{-1}) determined by other workers are also presented. However as different nitrogen containing gases are used to determine the dry deposition fluxes a direct comparison between the gaseous deposition flux will be incomplete.

The lowest wet nitrogen deposition rates occurred at Lincoln in September 1989 and March 1991. These values are an order of magnitude less than wet depositions

Table 6.14 Comparison of wet and dry deposition values for nitrogen

Model Type	Deposition Flux as determined by Author		Deposition flux, presented as g m^{-2} a^{-1}		Wet/dry deposition ratio	Authors
	Wet Deposition	Dry deposition	Wet deposition	Dry deposition		
Data obtained from air quality and precipitation data. The Netherlands 1986.	NO_3^- [a] 330 mol ha^{-1} a^{-1}	NO_y [b] 1240 mol ha^{-1} a^{-1}	0.46	1.74	0.26	Erisman *et al.* (1989)
WD = $[N\text{-}NO_3^-]$ × rainfall amount 4 year survey (1982-1985) Mid-West, New York and New England	$[N\text{-}NO_3^-]$ 3.4 kg ha^{-1} a^{-1}		0.34			Zemba *et al.* (1988)
Dry deposition over North Sea DD $\Sigma([N\text{-}NO_3^-] + [N\text{-}HNO_3])$ Surface area: 5.3 × 10^5 km^2		89.5 × 10^7 kg a^{-1}		0.17		Ottley and Harrison (1992)
South-East Europe Surface area: 1.25 × 10^{12} m^2	0.7 Tg N a^{-1}	0.08-0.3 Tg N a^{-1} [c] 0.04-0.2 Tg N a^{-1} [d]	0.59	0.064-0.24 0.032-0.16	9.2-2.5 18.4-3.7	Katsoulis and Whelpdale (1986)
This study: equivalent annual deposition [e]	Wet deposition	Dry deposition [f]	Wet deposition	Dry deposition [f]	Wet/Dry Deposition ratio	
Lincoln	g m^{-2} a^{-1}	g m^{-2} a^{-1}	g m^{-2} a^{-1}	g m^{-2} a^{-1}		
September 1989	0.05	1.07	0.05	1.07	0.05	
May 1990	0.26	0.62	0.26	0.62	0.42	
January 1991	0.20	0.75	0.20	0.75	0.27	
February 1991	0.19	1.32	0.19	1.32	0.14	
March 1991	0.03	0.94	0.03	0.94	0.03	
Bolsover						
November 1990	0.13	1.32	0.13	1.32	0.10	
December 1990	0.36	0.78	0.36	0.78	0.46	
January 1991	0.18	1.29	0.18	1.29	0.14	
February 1991	0.86	1.36	0.86	1.36	0.63	
Wells						
June 1991	1.14	0.41	1.14	0.41	2.8	
July 1991	1.52	0.40	1.52	0.40	3.8	

[a] N as NO_3^-

[b] Where NO_y is composed of NO_x, HNO_3 and NO_3^- with fluxes of 840, 340 and 60 mol ha^{-1} a^{-1}, respectively.

[c] N as nitrogen oxides

[d] N as nitric acid and nitrate

[e] The equivalent annual deposition was calculated by multiplying the monthly deposition values determined in this study by a factor of 12.

[f] The dry deposition was calculated as the sum of dry gases and dry particulate forms.

determined by the other authors as shown in Table 6.14 (this illustrates a weakness in this method of comparing monthly depositions directly with annual depositions since the episodic nature of wet deposition is directly dependent on precipitation events).

The wet deposition rates of nitrogen at Lincoln and Bolsover are generally lower than the other depositions quoted in Table 6.14, with the exception of February 1991 at Bolsover. The large amounts of nitrogen deposited by wet processes during June and July at Wells were an order of magnitude higher than the other values quoted in the table.

As this study considered only two forms of total nitrogen dry deposition (nitrogen dioxide and particulate nitrate), a significant proportion of the nitrogen dry depositing will be not be taken into account. For example, HNO_3 was estimated by Erisman *et al.* (1989), to contribute 27% of the total nitrogen oxides (NO_2, NO_3^-, HNO_3 and NO) dry depositing in the Netherlands between 1980 and 1986.

The dry deposition rates of nitrogen at each site increases in the order: Wells (mean 0.41 $\pm$ 0.05 g N m^{-2} a^{-1}) < Lincoln (mean 0.94 $\pm$ 0.24 g N m^{-2} a^{-1}) < Bolsover (mean 1.18 $\pm$ 0.27 g N m^{-2} a^{-1}), and their magnitudes lie between the two dry deposition values quoted for the Netherlands (Erisman *et al.*, 1989) and the North Sea (Ottley and Harrison, 1992), which are stated to be representative of industrial and relatively "clean" marine areas, respectively.

The wet to dry nitrogen deposition ratios were basically similar to the sulphur ratios; the lowest ratios were obtained during the September 1989 and March 1991 at Lincoln, whereas the highest ratios were determined at Wells.

6.3.4.3 Occult deposition

Other deposition mechanisms, not investigated in this study, involve the deposition of pollutants via cloud or fog water (commonly referred to as occult deposition). Lindberg and Lovett (1992) estimated cloud water to contribute approximately 50% of total

sulphate deposited to a site (elevation 1740 m) at the Great Smoky National Park, USA. However at the other eleven sites, all at lower elevation (elevation range 65 to 725 m) investigated by Lindberg and Lovett (1992), cloud water deposition made an insignificant contribution to sulphate deposition.

Occult deposition is calculated as the product of the weighted mean ion concentration in the cloud water and the total annual hydrologic flux of cloud water, determined by a variety of methods, including direct measurement of cloud water drip and approximation methods.

6.4 Washout ratios

The washout ratios presented in Table 6.12 were determined using the VWM for the monthly precipitation event and the average aerosol concentration determined for that month. The wash-out ratio, W_m, was determined on a mass basis, where

$$W_m = \frac{[SO_4]_p \times \rho(air)}{[SO_4]_a \times \rho(precipitation)} \quad \text{....Equation 6.3}$$

Where: ρ (density of air) = 1260 g m^{-3}
ρ (density of precipitation) = 1 g ml^{-1}
$[SO_4^{2-}]_p$ = concentration of sulphate in precipitation (units μg ml^{-1}).
$[SO_4^{2-}]_a$ = concentration of sulphate in aerosol (units μg m^{-3}).

The washout ratio for sulphates, with the exception of December 1990 at Bolsover, June 1991 and July 1991 at Wells, are all at least twice the washout ratio for nitrate. Comparing the VWM concentrations and particulate matter concentrations for both ions in Table 6.12 shows that the higher washout ratio for sulphate is governed by higher sulphate concentrations in the precipitation, since the concentrations of both ions in the particulate matter are within the same order of magnitude. This would suggest either the sulphate in particulate matter is selectively removed by the precipitation (an unlikely occurrence) or there was an extra source of sulphate, expected to be sulphur dioxide. However as the washout ratios in Table 6.12 were determined using monthly mean and VWM concentrations, not necessarily collected on the same day, the determined washout ratios may only approximate the true washout ratio.

In order to investigate the "coupling" between rain and associated aerosol at the sites under investigation, washout ratios were determined on those twenty nine days when particulate matter was collected and precipitation events occurred (Table 6.15). There was only one day (5/2/91) on which aerosol collection and precipitation was collected simultaneously at two sampling sites (Lincoln and Bolsover). The washout ratio for sulphate at Lincoln (3321) is almost three times that determined at Bolsover (1090), while the washout ratio for nitrate is almost an order of magnitude greater (3333 vs. 474). By examining the sulphate concentrations in the aqueous and particulate phases the controlling variable on this sampling day may be tentatively proposed to be the high particulate concentration at Bolsover, since the aqueous concentrations (14.88 $\mu g\ ml^{-1}$ at Lincoln and 20.42 $\mu g\ ml^{-1}$ at Bolsover) are closer in magnitude than the particulate concentrations (5.82 $\mu g\ m^{-3}$ and and 23.61 $\mu g\ m^{-3}$ at Bolsover).

The role of SO_2 in contributing to the sulphate in precipitation will be investigated by a regression method, originally devised by Chan and Chung (1986). This method is described in Section 6.4.2.

6.4.1 Washout ratio as a function of precipitation amount

When the log transformed washout ratio for sulphate is plotted against log transformed daily precipitation amount (Figure 6.10) the washout ratio can be seen to decrease with increasing precipitation amount. This is due to the dilution effect of larger volumes of water which effectively reduce the concentration of sulphate in rainfall.

The linear least squares regression equation through the plotted points in Figure 6.10, is represented by:

$$\log_{10}(\textit{Washout ratio for sulphate}) = -0.20 \log_{10}(\textit{rainfall, mm}) + 3.4 \quad \text{. . . .Equation 6.4}$$

The regression coefficient obtained, -0.20, is compared to other values in Table 6.16, which all show, with the exception of the nitrate washout ratio determined in this study, the inverse dependence of washout ratio on precipitation amount. Also presented in Table 6.16 are the coefficient of determination, R^2, which provides an indication of the

Table 6.15 Washout ratios for nitrate and sulphate, expressed on a mass basis, determined for those days in which precipitation and particulate matter were collected simultaneously.

	Sampling date	$W_{SO_4^{2-}}$	$W_{NO_3^-}$	Preciptation amount (mm)
Lincoln	10/5/90	1862	2012	2.4
	14/5/90	345	408	5.7
	15/5/90	1553	2310	4.7
	5/2/91	3221	3333	8.1
	19/2/91	1260	103	2.2
	20/3/91	916	176	0.9
	22/3/91	1720	202	0.7
Bolsover	9/11/90	4555	1351	0.4
	12/11/90	407	206	5.5
	13/11/90	1128	406	1.9
	16/11/90	4100	8778	2.8
	19/11/90	2752	1448	1.3
	20/11/90	3098	1448	0.3
	16/1/91	2806	810	5.7
	29/1/91	6513	7388	0.08
	5/2/91	1090	474	7.4
Wells	12/6/91	2380	976	0.4
	13/6/91	1360	1244	1.4
	17/6/91	3271	2200	1.5
	18/6/91	5624	11916	8.9
	24/6/91	4688	4102	7.6
	25/6/91	1377	6690	17.2
	26/6/91	882	4666	15.2
	17/7/91	4213	9785	12.5
	18/7/91	18060	102600	1.4
	23/7/91	3682	3640	4.4
	24/7/91	2530	9828	8.7
	25/7/91	7248	17182	0.3
	30/7/91	1680	3111	5.2

Notes:
Weekly precipitation data has been used to determine the washout ratios for aerosols collected on 16/1, 29/1 and 5/2/91 at Bolsover and for 5/2/91 and 19/2/91 at Lincoln.

scatter of the data points about the regression line. The lowest value shown in Table 6.16 was obtained in this study for nitrate (0.03) and suggests that the washout ratio for nitrate was not dependent on precipitation amount.

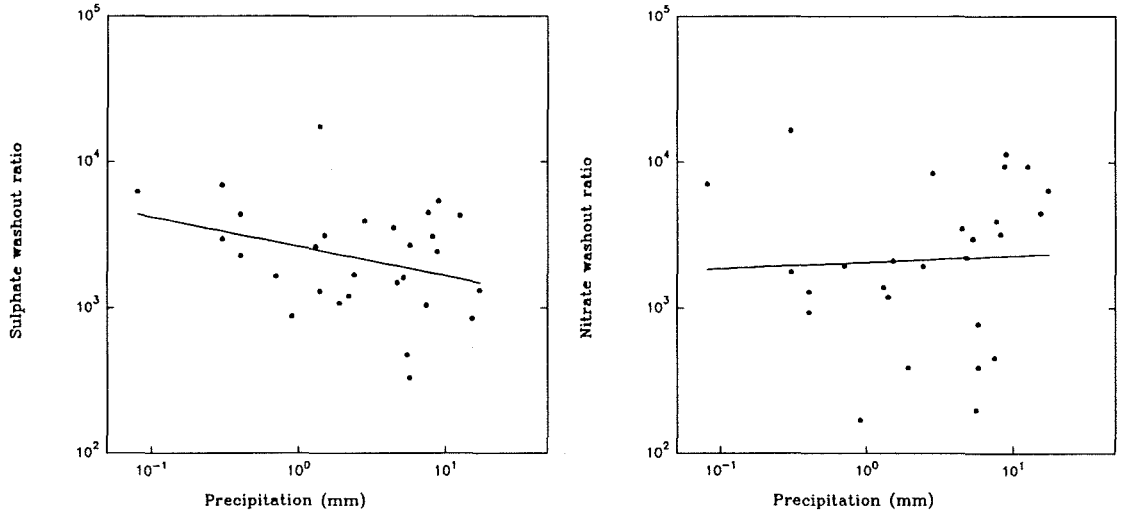

Figure 6.10. Sulphate and nitrate washout ratio as a function of precipitation amount for those sampling days in which precipitation and particulate matter were collected together.

Table 6.16 Washout ratio as a function of precipitation amount

Species	Regression coefficient	Regression constant	R^2	Conditions	Reference
Sulphate	-0.20	2510	0.32	Precipitation collected on or close to historic buildings	This study
	-0.34 -0.27	5011 1450	0.25 0.11	Algoma, Eastern Canada, relatively high SO_2 present‡ relatively little SO_2 present	Barrie (1985)
	-0.26 -0.51	1260 2900	0.35 0.55	Sampling conducted in: Miami, Florida American Samoa, Pacific Ocean*	Savoie *et al.* (1987)
	-0.26	NP	NP	Theoretical derivation†	Scott (1978)
Nitrate	0.04	3160	0.03	Precipitation collected on or close to historic buildings	This study
	-0.31	NP	0.20	Algoma, Eastern Canada.	Barrie (1985)

‡ Relatively high SO_2 is defined by Barrie (1985) as those days in which SO_2 contributed >70% of total atmospheric sulphur. Relatively little SO_2 is defined by Barrie (1985) as those days in which SO_2 contributed <40% of total atmospheric sulphur.

* As non-salt sulphate

† The regression coefficient, relating washout ratio to precipitaion amount, was calculated by relating rain rate to scavenging parameters such as size and solubility of the aerosol.

NP value not presented in reference.

6.4.2 Contribution of aerosol SO_4^{2-} and SO_2 to sulphur in precipitation

The contribution of sulphur contained within both the aerosol and gaseous phases to the sulphur contained within precipitation has been calculated by a method originally devised by Chan and Chung (1986). The method uses the 29 rainfall events for which gaseous and particulate measurements were simultaneously collected at all sites and hence will produce a regional scale approximation for the origin of sulphur in precipitation.

The concentrations of sulphur in each phase are presented in Table 6.17. As described by Chan and Chung (1986) the washout ratios are calculated on a volume basis, where the concentrations of ions in precipitation are expressed as μg per m^3 of water and aerosol and gas concentrations are expressed as μg per m^3 of air.

All the sulphur in precipitation, $[S\text{-}SO_4^{2-}]_p$, is assumed to originate from sulphur in both the aerosol phase, $[S\text{-}SO_4^{2-}]_{p'}$, and in the gaseous phase, $[S\text{-}SO_2]_{p''}$. This relationship is shown by Equation 6.5

$$[S\text{-}SO_4^{2-}]_p = [S\text{-}SO_4^{2-}]_{p'} + [S\text{-}SO_2]_{p''} \quad \text{....Equation 6.5}$$

The terms on the right hand side of Equation 6.5 can alternatively be represented as $W_{SO_4^{2-}}\ [S\text{-}SO_4^{2-}]_a$ and $W_{SO_2}[S\text{-}SO_2]_g$, respectively, where these terms originated from cross multiplication of the volume washout ratio, described previously in Section 3.2.5.

Hence Equation 6.5 can be re-expressed as

$$[S\text{-}SO_4^{2-}]_p = W_{SO_4^{2-}}\ [S\text{-}SO_4^{2-}]_a + W_{SO_2}[S\text{-}SO_2]_g \quad \text{. . . .Equation 6.6}$$

The washout ratios in Equation 6.6 are estimated as regression coefficients, obtained when the sulphur in precipitation is regressed onto the sulphur concentrations in the aerosol and gaseous phases. This regression analysis was performed using the LOTUS 123 statistical package, with the sulphur in precipitation the dependent variable and sulphur in the aerosol and gaseous phases the independent variables. The regression

Table 6.17 Aerosol sulphur, gaseous sulphur and precipitation sulphur concentrations used to determine the contribution of gaseous sulphur and aerosol sulphur to sulphur in precipitation

	Sample date	Precipitation $[S\text{-}SO_4^{2-}]$ * $\times 10^6$ $\mu g\ m^{-3}$	Aerosol $[S\text{-}SO_4^{2-}]$ $\mu g\ m^{-3}$	Gas $[S\text{-}SO_2]$ $\mu g\ m^{-3}$
Lincoln	10/5/90	5	3.2	18.3
	14/5/90	2.2	7.9	9.3
	15/5/90	1.5	1.2	6.6
	5/2/91	4.7	1.9	7.1
	19/2/91	2.7	3.5	24.1
	20/3/91	1.6	1.5	1.7
	22/3/91	3.7	2.2	10.7
Bolsover	9/11/90	5.8	1.6	9.3
	12/11/90	1.1	3.3	5.9
	13/11/90	1.2	1.6	11.2
	16/11/90	2.3	0.7	5.1
	19/11/90	3.7	1.7	10.8
	20/11/90	5.9	2.4	15.6
	16/1/91	5.7	2.5	18.8
	29/1/91	27	5	58.8
	5/2/91	6.8	7.9	18.8
Wells	12/6/91	2	1.1	0.3
	13/6/91	1.5	1.4	0.1
	17/6/91	2.7	1.1	1.1
	18/6/91	5.1	1.1	0.7
	24/6/91	2	0.4	0.1
	25/6/91	1.3	1.1	0.3
	26/6/91	0.9	1.2	0.9
	17/7/91	1.1	0.3	0.3
	18/7/91	5.7	0.4	0.4
	23/7/91	2.0	1	0.6
	24/7/91	1.9	0.9	0.6
	25/7/91	15.7	2.7	1.5
	30/7/91	1.0	2.7	1.5
	Arithmetic mean	4.3	2.1	8.3
	Geometric mean	2.9	1.5	2.6

Notes: * The $S\text{-}SO_4^{2-}$ concentration in precipitation used in calculating the washout ratios for SO_4^{2-} and SO_2, via the Chan and Chung (1986) method, is expressed as μg per m^3 of water.

analysis was performed using the "no constant" option in LOTUS 123, so that no regression constant was produced (the basis to the regression technique was discussed in Section 5.2.2). The regression equation obtained is represented by Equation 6.7.

$$[S\text{-}SO_4^{2-}]_p = 2.8\times10^5\ [S\text{-}SO_4^{2-}]_a + 3.4\times10^5\ [S\text{-}SO_2]_g \quad \text{Equation 6.7}$$

Hence the volume washout ratios for SO_4^{2-} and SO_2 are calculated to be approximately equal (2.8×10^5 and 3.4×10^5). This is in contrast to the results obtained by Chan and Chung (1986) for which the washout ratio for SO_4^{2-} (4.3×10^5) was ten times that determined for SO_2 (4.6×10^4). A possible reason for the relatively higher washout ratio for SO_4^{2-} compared to SO_2 in the Chan and Chung study may have been the fact that the sampling sites were situated in relatively rural areas in Canada, where the concentration of SO_2 was relatively small.

Following the Chan and Chung (1986) method, the $W_{SO_4^{-2}}$ and W_{SO_2} coefficients are divided by the washout ratios W_1 and W_2, respectively. W_1 and W_2 are described by Equations 6.8 and 6.9, respectively.

$$W_1 = \frac{\textit{arithmetic mean [sulphur] in precipitation}}{\textit{arithmetic mean [sulphur] in aerosol}} \quad \text{....Equation 6.8}$$

$$W_2 = \frac{\textit{arithmetic mean [sulphur] in precipitation}}{\textit{arithmetic mean [sulphur] in gas}} \quad \text{....Equation 6.9}$$

W_1 represents the washout of aerosol sulphur, neglecting scavenging of aerosol sulphur
W_2 represents washout of gaseous sulphur, neglecting scavenging of gaseous sulphur.

The arithmetic mean concentrations for sulphur in the precipitation, aerosol and gaseous phases used to calculate W_1 and W_2 are 4.26×10^6 $\mu g\ m^{-3}$, 2.1 $\mu g\ m^{-3}$ and 8.3 $\mu g\ m^{-3}$. W_1 and W_2 were calculated as 2.0×10^6 and 5.2×10^5, respectively.

According to Chan and Chung (1986) the sum of $W_{SO_4^{-2}} / W_1$ and W_{SO_2} / W_2 is expected to be unity. However, the value calculated in this study was 0.8, which lies outside the range (0.6 to 0.7) determined by Chan and Chung (1986). When $W_{SO_4^{-2}} / W_1$ and W_{SO_2} / W_2 are each normalised by their sum the contribution of sulphur from aerosol and gaseous phases are determined to be 18% and 82%, respectively. This result may be expected, since the correlation coefficient, presented in Table 6.18, between the sulphur

Table 6.18 Correlation coefficients between sulphur concentrations in the precipitation, aerosol and gaseous phases.

	Sulphur in precipitation	Sulphur in aerosol	Sulphur in gaseous phase
Sulphur in precipitation	1	0.38	0.74
Sulphur in aerosol	0.38	1	0.57
Sulphur in gaseous phase	0.74	0.57	1

The critical values for the correlation coefficients, below which an association between two variables is attributed to chance, are 0.36 and 0.46 at the 5% and 1% significance levels, respectively, for 28 degrees of freedom.

concentrations in the precipitation and gaseous phases would suggest that the concentration of sulphur in precipitation and sulphur in the gaseous phase are closely associated. Conversely no association between the sulphur in precipitation and aerosol was observed at the 1% significance level.

An obvious criticism in using arithmetic mean concentrations in calculating both W_1 and W_2 is that each ratio will be influenced by high concentration values, due to the log-normal nature of atmospheric concentrations. However, when the method is repeated using the geometric mean concentrations, shown in Table 6.17, SO_2 is still found to contribute most sulphur to the sulphur in precipitation (67%).

6.5 Summary

The amount of sulphur and nitrogen dry deposited at each sampling site increased in the order: Wells < Lincoln < Bolsover, whereas the amount of wet deposited sulphur and nitrogen increased in the order: Lincoln < Bolsover < Wells. The vast majority of sulphur and nitrogen dry deposited was in the gaseous form, with atmospheric particulate matter contributing an insignificant amount of each element.

Analysis of the particulate matter showed that a significant proportion of the particulate matter depositing onto building surfaces consisted of sulphate, nitrate and ammonium ions.

The acidic nature of dry deposited particulate matter, such H_2SO_4 and $(NH_4)HSO_4$ was not assessed in this study. This could be a significant omission, since field experiments such as those carried out by Delopoulou and Sikiotis (1992) (Section 2.4.3.1) suggest that the most reactive form of sulphur is H_2SO_4. Similarly, nitric acid gas may have been the most pertinent nitrogen containing gas requiring measurement,instead of the NO_2 used in this study.

In comparing the amounts of particulate and gaseous sulphur in the atmosphere during the summer months, a significant proportion existed as particulate sulphate. This would have resulted from the photochemical reactions, which oxidise the sulphur dioxide to sulphate. On the other hand, during the winter months sulphur dioxide is the principal form of sulphur in the atmosphere. In general, the monthly mean sulphate concentrations are highest during the winter, although individual concentrations were highest during the summer.

The washout ratios for sulphur were shown to decrease with increases in the volume of rain delivered to the surface, indicative of the cleansing function of precipitation. Finally, approximately eighty percent of the sulphur contained within precipitation was estimated to originate from the sulphur dioxide present in the atmosphere with the remainder originating from particulate sulphate.

CHAPTER 7: RECEPTOR MODELS

The receptor models used in this study utilise the trace element and major ion concentrations of the collected particulate matter as inputs to estimate the contribution of material from resolved pollution sources. The theoretical background to the receptor models was provided in Chapter 5. The frequency distributions and mean concentrations of both trace elements and major ions measured in the collected particulate matter are presented in Section 7.1. The concentrations of several major ions (sulphate, nitrate, chloride and ammonium) were discussed previously in Section 6.1.2.2. Section 7.2 compares the measured trace metal concentrations with concentrations determined by other workers. The three receptor models used to apportion the sources of collected particulate material are presented and contrasted in Section 7.3.

7.1 Components of particulate matter

The concentration of trace elements and major ions contained within particulate matter were measured to provide the necessary data required as input to the receptor modelling technique. However, some trace elements (Se, Sb, Zn, Al, and Ni) were not used further in the technique. Reasons for the unsuitability of these elements were presented in Chapter 4, these include low detection limit (Section 4.3.5.3), high filter paper blank (Section 4.3.5.5) or reluctance to dissolve in the concentrated nitric acid (low percentage recovery from certified standard reference material, Table 4.12).

The frequency distributions of metals obtained at each site are illustrated in Figures 7.1, 7.2 and 7.3 for Lincoln, Bolsover and Wells, respectively. The frequency distribution was obtained by sorting the data into groups. These groups contained the number of measured concentrations which fell between the boundaries defining the group. For example, the concentration of major ions (SO_4^{-2}, NO_3^-, Cl^- and NH_4^+) at each site were arranged into groups covering 2 $\mu g\ m^{-3}$ ranges. Magnesium and Cu were arranged into 50 ng m^{-3} range groups at all sites. At Bolsover, 250 ng m^{-3} range groups were used for the iron concentrations due to the large range of concentrations present (50 ng m^{-3} were used for iron at the other two sites). Range groups of 250 $\mu g\ m^{-3}$ were used for Ca, K and Na at each site. Manganese concentrations were divided into 5 ng m^{-3} range groups

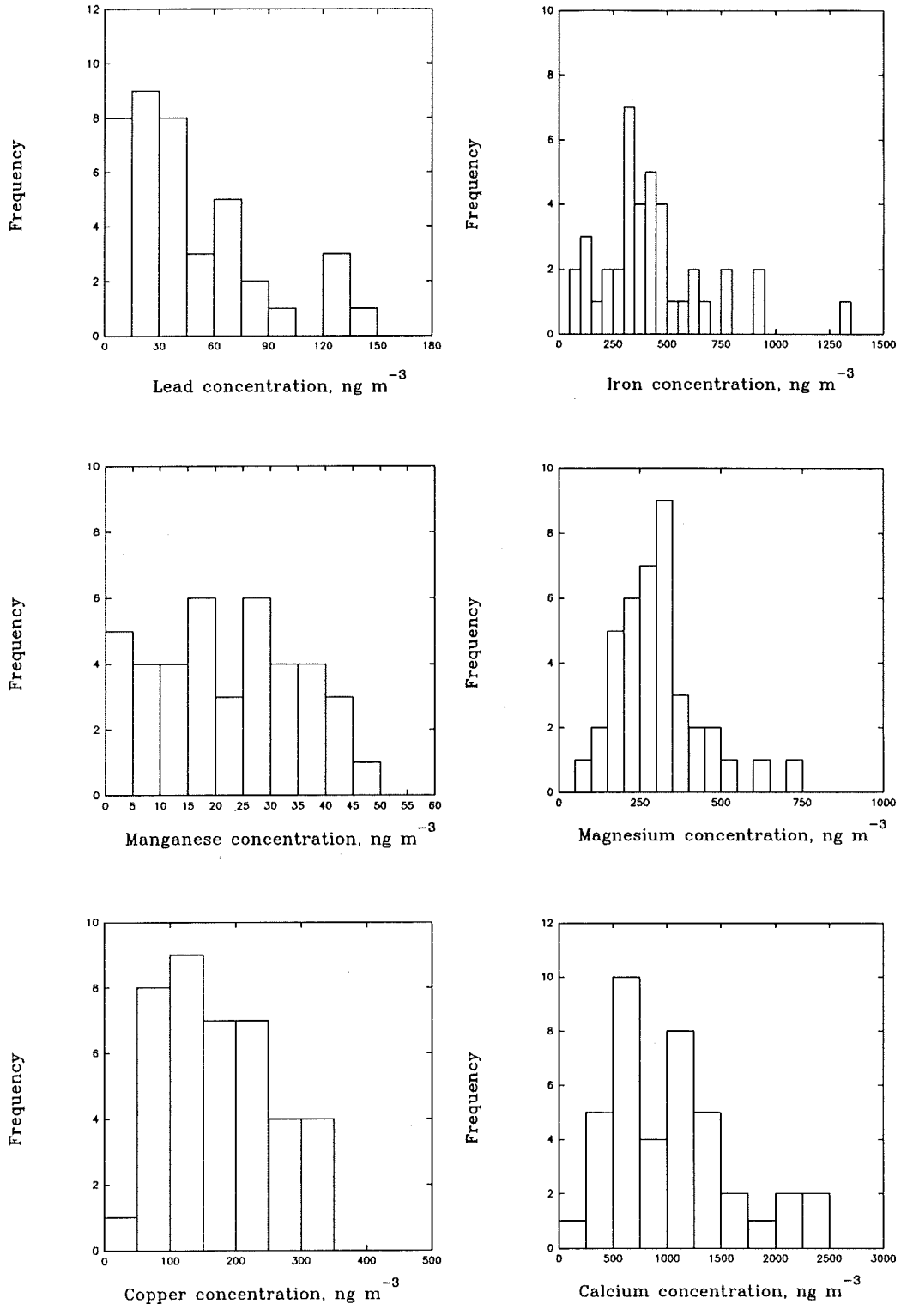

Figure 7.1 Frequency distributions of trace metals and major ions collected at Lincoln (continued over)

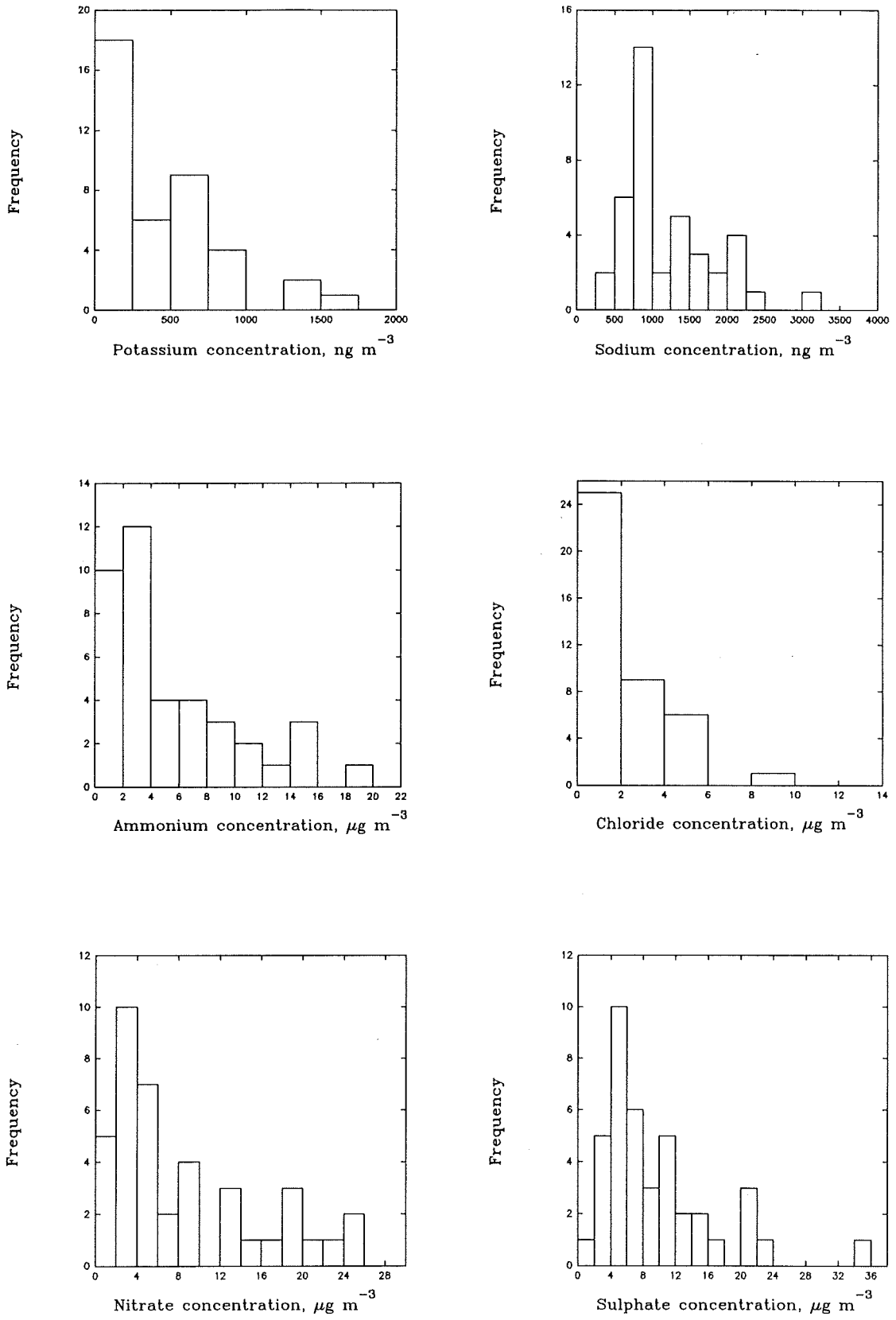

Figure 7.1 Frequency distributions of trace metals and major ions collected at Lincoln (continued over)

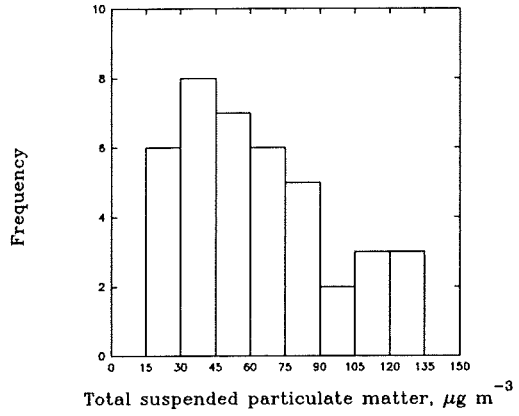

Figure 7.1 Frequency distributions of trace metals and major ions collected at Lincoln

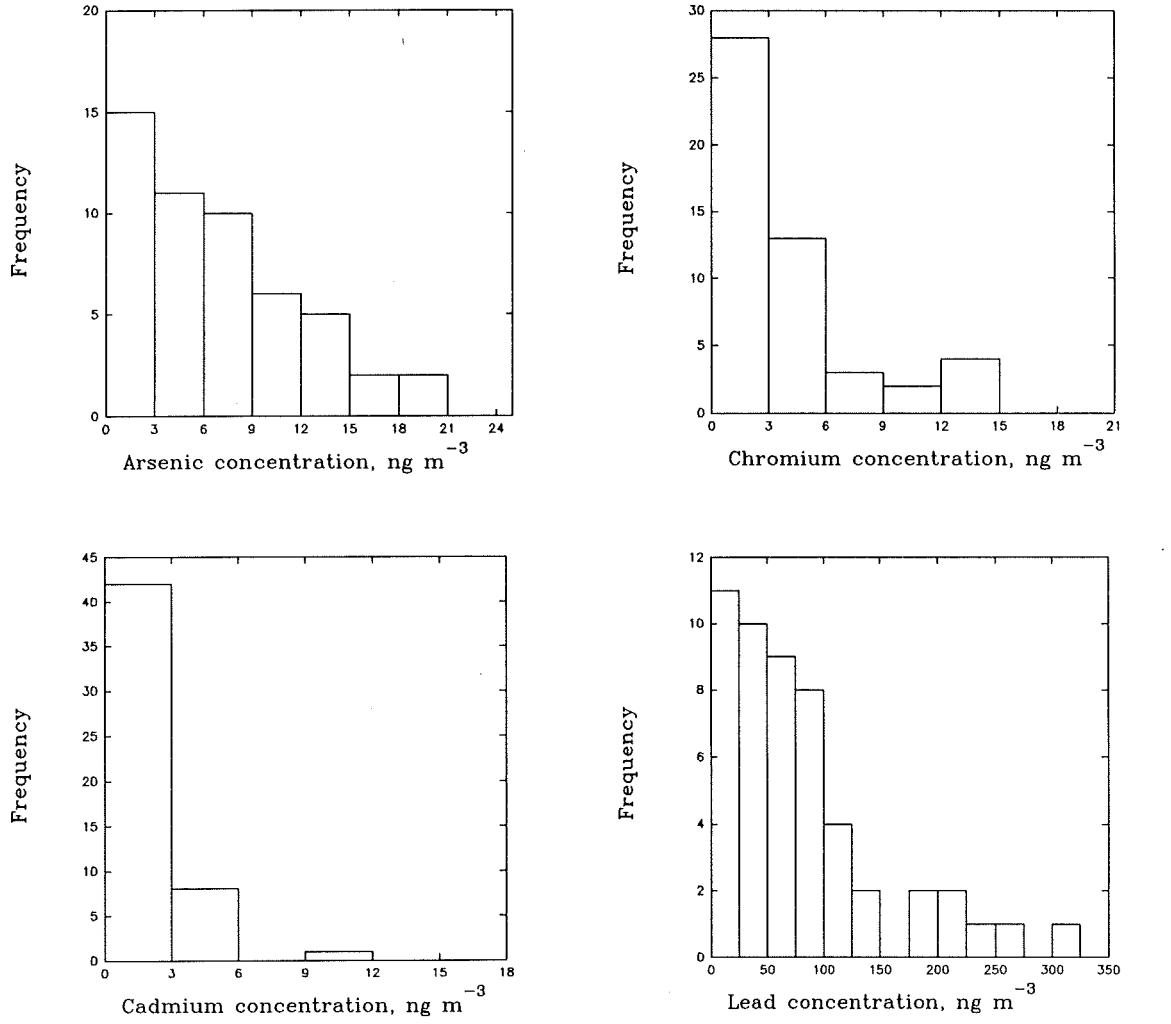

Figure 7.2 Frequency distributions of trace metals and major ions collected at Bolsover (continued over)

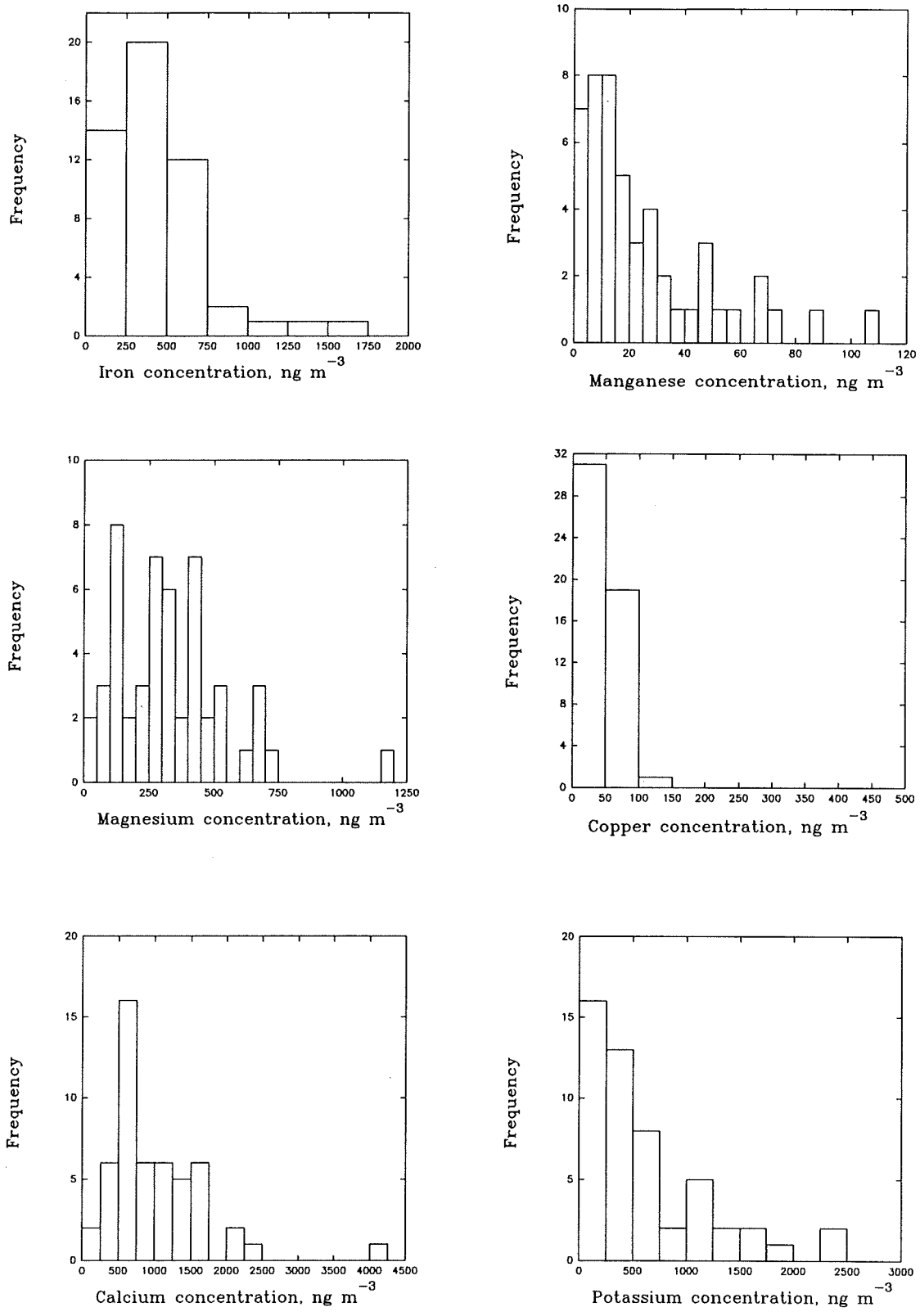

Figure 7.2 Frequency distributions of trace metals and major ions collected at Bolsover (continued over)

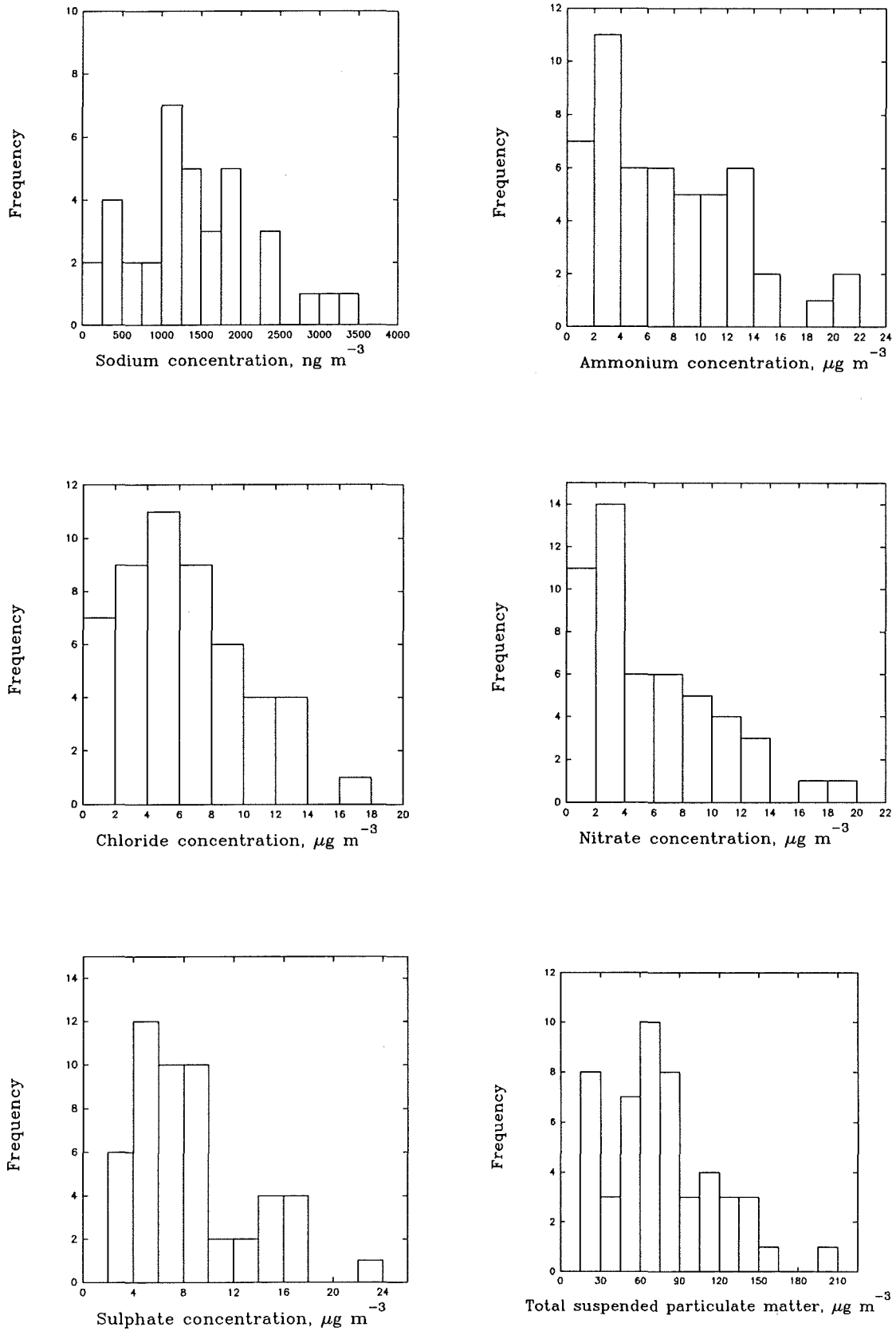

Figure 7.2 Frequency distributions of trace metals and major ions collected at Bolsover

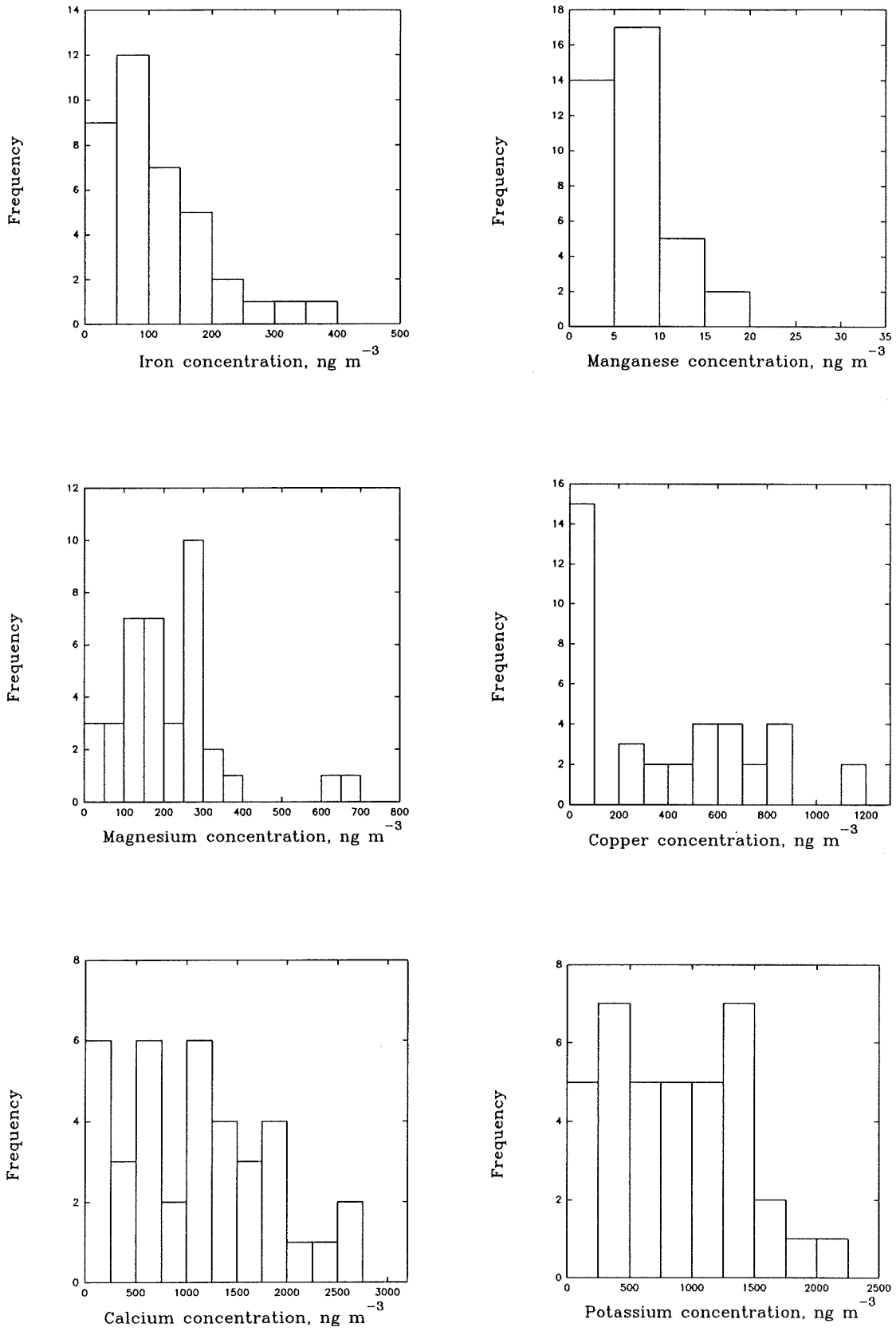

Figure 7.3 Frequency distributions of trace metals and major ions collected at Wells (continued over)

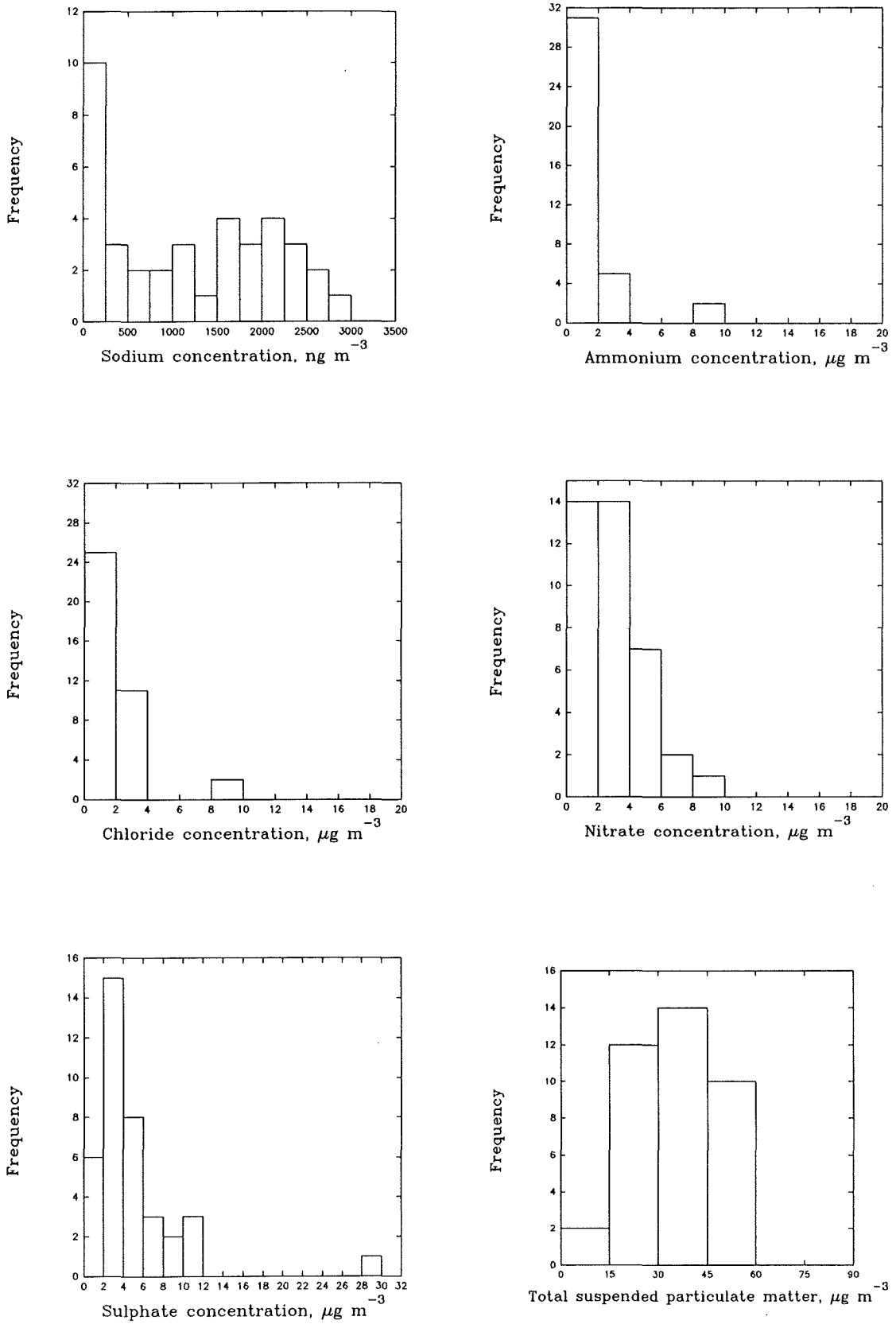

Figure 7.3 Frequency distributions of trace metals and major ions at Wells

at each site. Total suspended particulate matter was divided into 15 μg m^{-3} range groups. Arsenic, Cr and Cd were measured in sufficient concentration above the filter blank only at Bolsover and these were divided into 3 ng m^{-3} range groups. Lead concentrations were divided into 15 and 25 ng m^{-3} range groups at Lincoln and Bolsover, respectively. Lead was not found in sufficient concentrations at Wells to be used further in the statistical analysis.

The observed frequency distributions represented by Figures 7.1 to 7.3, show that most of the measured concentrations at each site appear to approximate a log-normal distribution, which is to be expected for air pollutant concentrations (Hinds, 1982). The geometric mean is used to determine the concentration which represents the central location of a log-normal distribution (in a similar manner to which the arithmetic mean is used to provide the central location for a normal distribution). The geometric mean values, $\bar{x}_g$, were calculated by multiplying together the sample concentrations (N) obtained for each variable and consequently obtaining the inverse power of the number of samples measured (n). This is outlined by Equation 7.1. The calculation was performed using Lotus 123.

$$\bar{x}_g = (N_1 \times N_2 \times N_3 \times N_n)^{1/n} \qquad \ldots \text{Equation 7.1}$$

The arithmetic and geometric means determined at each site are also shown in Table 7.1. As expected for those distributions which appear to be log-normal, the geometric mean concentration is less than the arithmetic mean concentration. For example at Lincoln, the geometric mean and arithmetic mean TSP concentrations are 55.1 μg m^{-3} and 62.6 μg m^{-3}, respectively. For metals commonly measured at each site, manganese is measured in the lowest abundance. Sodium is measured in the highest abundance at Lincoln and Bolsover, with calcium measured in the highest abundance at Wells.

From the chloride frequency distributions, most of the chloride concentrations at Lincoln (63%) and Wells (66%) can be seen to exist in the 0-2 μg m^{-3} range.
Likewise, at Wells, most of the ammonium concentration values (79%) also exist in this concentration range.

Table 7.1 Arithmetic mean, geometric mean and modal concentrations determined at each site. (Expressed as ng m^{-3})

Sampling site	Mean	As	Cr	Cd	Pb	Fe	Mn	Mg	Cu	Ca	K	Na	NH_4^+	Cl^-	NO_3^-	SO_4^{2-}	T.S.P.
Lincoln n = 40	Modal range				2.1-4.0	250.1-300	--	300.1-350	150.1-200	500.1-750	0-250	750.1-1000	2.01-4.00	0-2	2.01-4.00	4.01-6.00	30.1-45.0
	Arithmetic mean s.d.				47 36	431 250	22 13	303 131	170 79	1040 570	370 440	1240 620	5.4 4.8	3.4 2.7	8.6 7.0	9.4 6.9	62.6 30.0
	Geometric mean				29	360	18	270	160	860	180	1100	3.7	2.1	5.9	6.2	55.1
Bolsover n = 51	Modal range	0-3	0-3	0-3	0-25	250.1-300	--	100.1-150	0-50	500.1-750	0-250	1000.1-1250	2.01-4.00	4.01-6.0	2.01-4.0	4.01-6.0	60.1-75.0
	Arithmetic mean s.d.	7 5	15 52	4 5	80 70	430 320	29 24	340 210	43 30	1010 670	610 580	1480 950	7.4 5.3	6.2 3.8	5.8 4.3	8.6 4.8	77.2 40.7
	Geometric mean	5	3	1	58	340	22	280	31	870	400	1220	5.4	5.0	4.1	7.4	66.4
Wells n = 38	Modal range					50.1-100	5.1-10	250.1-300	0-50	**	**	0-250	0-2	0-2	0-4	2.1-4.0	30.1-45.0
	Arithmetic mean s.d.					110 80	7 4	210 140	410 350	1080 740	870 530	1150 980	1.5 2.0	1.8 2.0	3.0 2.0	5.1 4.7	35.0 13.0
	Geometric mean					87	6	110	220	890	580	770	0.78	1.39	2.34	3.92	31.8

s.d. = standard deviation

** = indicates at least two modal peak concentrations

7.1.1 Lincoln

As mentioned above, the determined concentrations for the constituent parts of the particulate matter collected at Lincoln, with the exception of the manganese frequency distribution, can be seen to follow a log-normal distribution (Figure 7.1). The manganese concentrations appear to be evenly distributed throughout the concentration range 0 to 40 ng m^{-3}. This would suggest a continuous source of manganese is contributing to the collected particulate matter.

The two highest individual nitrate concentrations (both exceeding 24 $\mu g\ m^{-3}$) were found in samples collected at Lincoln on 4/5/90 and 19/2/91. The meteorological condition for the former sample was discussed in Section 6.2.2.1 with reference to a correspondingly high sulphate concentration (34.2 $\mu g\ m^{-3}$). The latter sample was collected during a cold period for which a relatively high sulphate concentration (10.6 $\mu g\ m^{-3}$) was also determined. These individual concentrations are probably responsible for producing the relatively high nitrate geometric mean concentration of 5.9 $\mu g\ m^{-3}$, compared to the other two sites (4.1 $\mu g\ m^{-3}$ and 2.3 $\mu g\ m^{-3}$ for Bolsover and Wells, respectively).

7.1.2 Bolsover

Bolsover is similar to Lincoln in that most concentrations also follow a log normal distribution. The determined copper concentrations are much lower than concentrations determined at the other two sites. This could result from using a different high volume sampler at Bolsover, which generated less copper from the copper commutator coil. Bolsover also collected the highest geometric means for the following components of the collected particulate matter: Mg, Na, NH_4^+, Cl^-, and SO_4^{2-}.

7.1.3 Wells

At Wells the concentration ranges for copper, calcium, potassium and sodium appear to be evenly distributed. As mentioned above, the concentrations of ammonium and chloride appear to show similar frequency distribution patterns indicating a probable

association between the two ions.

The copper frequency distribution at Wells appears to be composed of two distinct components, one in which 15 concentrations exist in the concentration range 0 to 50 ng m^{-3}, and the second in which the remainder of the concentration values are fairly distributed from 200 to 1200 ng m^{-3}. This may have resulted from two high volume samplers used in succession to collect particulate matter. The first, used previously at Lincoln produced the evenly spread concentration distribution, whereas the second used at Bolsover produced the narrow distribution range.

Compared to the other sites, the lowest geometric mean concentrations for most constituents of the collected particulate matter, Fe, Mn, Mg, Na, NH_4^+, Cl^-, NO_3^-, SO_4^{2-} were measured at Wells. One single high sulphate concentration of 28.9 μg m^{-3} which was collected on 30/5/91 has already been discussed in Section 6.2.2.1. The highest potassium concentrations were determined at Wells. The calcium concentrations were more or less equivalent at each site.

7.2 Comparison with reported trace metal concentrations

Reported literature values for the concentrations of metals contained within atmospheric particulate matter collected from urban, rural, marine and remote sampling sites are shown in Table 7.2. However, comparing mean atmospheric concentration values, determined using varying numbers of samples, will result in a comparison between data sets that are not strictly comparable. This lack of comparability is accentuated in this section since the geometric mean value was chosen as the most suitable mean to represent the log-normal distributions and most previous studies report concentrations using the arithmetic mean. Despite these failings, the comparisons will probably be satisfactory to within an order of magnitude.

7.2.1 Cadmium

Sufficient cadmium was collected only at Bolsover to accurately determine the mass concentration (geometric mean 1 ng m^{-3}). This concentration was similar to the

Table 7.2 Trace metal concentrations determined in atmospheric particulate matter (previous workers). (Units are ng m^{-3}, standard deviations are in parenthesis)

Cr	Cd	Pb	Fe	Mn	Mg	Cu	Ca	K	Na	Zn	Ni	Al	Comment	Method of Analysis	Sampling Site/s	Reference
	1.1 (1.0)	34 (71)	216 (203)	10 (11)	247 (162)		329 (218)	234 (129)		41 (37)	2.7 (2.9)		Arithmetic mean for 302 samples Collected from March 1987 to March 1988	Atomic Absorption	Rural Hemsby, Norfolk	Yaaqub *et al.* (1991)
			536 261	17 20						55 39			Episodic event, defined as those days when $[SO_4^{2-}]$ exceeded 10 $\mu g\ m^{-3}$ Non-episodic event, $[SO_4^{2-}] < 10 \mu g\ m^{-3}$	INAA	Rural Whiteface Mt. New York	Parekh and Husain (1981)
	2.8 (2.2)	96 (100)	300 (370)	14.9 (19)		14.7 (10)			2000 (1400)	67.4 (90)		140 (150)	Geometric mean. Samples collected each year ranged from 49 to 70. Collected between January 1980 and August 1985	Atomic absorption	Marine West-Hinder light ship North Sea	Baeyens and Dedeur-waerder (1991)
16	<2.4	414	800	18		22				94	8.6		Annual mean determined from 8 monthly mean concentrations 1983/84	Atomic absorption	Urban Victoria London	Carroll and Innes (1988)
		110 (50)	330 (190)	9.6 (7.0)		7.5 (4.4)	300 (190)	170 (92)		41 (20)	6.1 (2.1)		At least 8000 individual particles collected for sixteen 12 hour samples. Samples were collected July 1986.	Automated probe micro-analysis	Urban Antwerp	Van Borm *et al.* (1989)
4.3 0.7	1.3 0.7	1450* 120 –	1687 657	25 24		28 21				139 66	9 10		Sampling conducted 1991 as part of Multi-Element Survey, Warren Spring Laboratory	Atomic absorption	Urban Bridge Place, London Vicar Lane, Leeds	DEPWS (1993)
1.03 (0.82)		1.9 (0.3)	284 (174)	4.8 (3.0)	100 (60)	0.5 (0.25)	109 (63)	128 (28)	100 (62)	2.5 (0.7)	0.37 (0.24)		Twenty three samples. Sampling period ranged from 8 to 24 days. Collected from July 1977 to August 1977	XRF and INAA	Remote Chacaltaya Bolivia	Adams *et al.* (1980)

* Atmospheric concentration determined in 1985 at a monitoring site (Cromwell Road) operated by WSL

– Concentration not presented in reference.

arithmetic mean determined by Yaaqub *et al.* (1991) and less than half the concentrations determined at a marine sampling site (Baeyens and Dedeurwaerder, 1991) and at an urban site (Carroll and Innes, 1988)

7.2.2 Lead

The highest lead concentrations (1450 ng m^{-3}) in Table 7.2 were determined for a site in London (Digest of Environmental Protection and Water Statistics, 1993). This study was conducted in 1985, when lead concentrations in petrol were 0.4 g l^{-1} and estimated lead emissions from vehicular sources in the United Kingdom were 6.5×10^3 tonnes a^{-1}. The most recent (1991) datum for lead concentrations at this site is 360 ng m^{-3}. This decline in atmospheric lead concentrations, like that at sampling sites throughout the UK, is due to the decrease in lead concentration in petrol (from 0.4 g l^{-1} to 0.15 g l^{-1}) and the increase in the proportional of the motor vehicle fleet using unleaded petrol (from less than 0.1% in 1985 to 41.1% in 1991). This combined effect of decreased lead concentrations and increase in the use of unleaded petrol consumed resulted in approximately 2.0×10^3 tonnes of lead being released into the atmosphere in 1991 (DEPWS, 1993).

The geometric mean lead concentrations for those samples collected at Lincoln and Bolsover were 29 ng m^{-3} and 58 ng m^{-3}, respectively, which are both lower than the samples in the marine environment, collected from 1980 to 1985, by Baeyens and Dedeurwaerder (1991).

7.2.3 Iron

The concentration of iron at Lincoln and Bolsover (360 and 330 ng m^{-3}, respectively) were less than four times the concentrations determined at the Warren Spring Laboratory (WSL) sites in London and almost half the concentration values determined at Leeds (DEPWS, 1993). Comparison with the earlier multi-element composition work, reported by Carroll and Innes (1988), shows that the iron concentrations have doubled at the London sampling site. The atmospheric concentration of iron at Wells (87 ng m^{-3}) is lower than any of those reported in Table 7.2.

7.2.4 Manganese

The geometric mean concentrations of manganese at Lincoln and Bolsover (18 and 22 ng m^{-3}) were similar to those reported by Carroll and Innes (1988) and DEPWS (1993) for a site in London (18 ng m^{-3} and 25 ng m^{-3}, respectively); by Parekh and Husain (1981) for an urban site (17 ng m^{-3}) and for a rural site (20 ng m^{-3}) in the United States. The concentration at Wells (6 ng m^{-3}) is lower than previously quoted values (Table 7.2), with the exception of the samples collected at a remote site by Adams *et al.* (1980).

7.2.5 Magnesium

The geometric mean concentrations for magnesium at Lincoln and Bolsover (270 and 280 ng m^{-3}, respectively) were similar to those determined by Yaaqub *et al.* (1991) for a rural site in Norfolk. As in common with the iron and manganese concentrations, the magnesium concentration at Wells was less than twice those reported at Lincoln and Bolsover (110 ng m^{-3}). In addition, the magnesium concentration at Wells was similar to those determined at a remote site in Bolivia by Adams *et al.* (1980).

7.2.6 Calcium

As mentioned before, the concentrations of calcium were similar (range 860 to 890 ng m^{-3}) at the three sites in this study. These concentrations were almost three times greater than the highest concentration reported in Table 7.2. This could reflect the presence of a calcium carbonate "cloud" which has been observed by Leysen (1989) to exist in close vicinity to a limestone building surface. Section 2.4.2.1 showed that the calcium carbonate cloud may neutralise the acidity of precipitation collected on a building surface.

7.2.7 Potassium

The geometric mean concentrations for samples collected at Wells (580 ng m^{-3}) and Bolsover (400 ng m^{-3}) were both higher than those concentrations quoted in Table 7.2.

Only the geometric concentrations determined at Lincoln (180 ng m^{-3}) approached those measured by previous researchers.

7.2.8 Sodium

The highest geometric mean sodium concentrations, presented in Table 7.2, are for particulate matter collected on a light ship in the North Sea. This would obviously reflect the proximity of the sea source to the particulate sampler. The concentrations of sodium at Lincoln (1.1 $\mu g\ m^{-3}$) and Bolsover (1.2 $\mu g\ m^{-3}$) were approximately half this concentration. The sodium concentrations measured at each site are significantly greater than that determined for a remote site in Bolivia (0.10 $\mu g\ m^{-3}$) by Adams *et al.* 1980, suggesting that each mean concentration at each site received at least 1.0 $\mu g\ m^{-3}$ from a sea source

7.3 Statistical receptor models used in this study

The receptor models used in this study all attempt to apportion the contribution of sources to the collected particulate material. As shown in Chapter 5, principal component analysis and multiple regression analysis are each fundamental constituents of the models.

The receptor models used to obtain information about the contributing sources are:

- principal component analysis/multiple regression (PCA/MR). An illustrative example, using a hypothetical data set, was presented in Section 5.3.2.
- regression on absolute principal component scores. The statistical background and an illustrative example, using the same hypothetical data set as used for the PCA/MR example, were presented in Sections 5.4.2.4. and 5.5.3., respectively.
- target transformation factor analysis (TTFA). The TTFA is performed using the FANTASIA program. The basis to the computer software was presented in Section 5.4.2.2.

7.3.1 Correlations between trace elements and major ions

The correlation coefficients determined between the measured components of atmospheric particulate matter collected at Lincoln, Bolsover and Wells, are shown in Tables 7.3, 7.4 and 7.5, respectively. Inspection of each correlation matrix represents an initial step in performing a principal component analysis based receptor model. At this stage, the number of contributing sources may be tentatively proposed from groups of elements or ions that are associated together. This association between variables is highlighted in Tables 7.3 to 7.5 by shaded cells for those coefficients which were considered significant at the 0.001 probability level. For example, the high correlation coefficients values (> 0.7) among the measured concentrations for ammonium, nitrate and sulphate and total suspended particulate matter for samples collected at Lincoln (Table 7.3) indicate the presence of secondarily formed particulate matter. Likewise calcium, iron and manganese form a grouping of correlation coefficients, which although of smaller value than the secondarily formed particulate matter grouping, does suggest the presence of crustal material. Other groupings of variables include: TSP, NO_3^-, Mn and Fe; NH_4^+, TSP and Pb; and K and Na. However identification of unique sources from which these latter groupings have originated is difficult, as such groupings are intuitively unexpected to occur in possible contributing sources.

The correlation coefficient matrix for data collected at Bolsover (Table 7.4) showed that seven variables (As, Cr, Cd, Fe, Cu, Cl^- and TSP) associated together to form a major grouping. Reasons for this association are uncertain. A second grouping of variables with high correlation coefficients are NH_4^+, NO_3^-, SO_4^{2-}, Cl^- and TSP. As discussed previously, these variables are important constituent components of secondarily formed particulate matter. A third grouping of variables appears to exist in the middle portion of the table. Correlated variables include Na, Mg, Cl^-. This association of variables would suggest the presence of sea-salt aerosol in the collected particulate matter.

The correlation coefficient matrix for data collected at Wells (Table 7.5) showed a Mn, K, Fe, Na and Ca grouping suggestive of crustal or soil sources. The ions characteristic of secondary particulate matter are again grouped together. However unlike the previous correlation matrices at Lincoln and Bolsover, the ammonium concentration is

Table 7.3 Correlation matrix showing associations between trace metals and major ions measured at Lincoln.

	Pb	Fe	Mn	Mg	Cu	Ca	K	Na	NH_4^+	Cl^-	NO_3^-	SO_4^{2-}	TSP
Pb	1												
Fe	0.24	1											
Mn	0.48**	0.66**	1										
Mg	0.09	0.02	0.11	1									
Cu	0.07	-0.08	0.14	-0.07	1								
Ca	0.20	0.62**	0.59**	0.31	0.08	1							
K	0.22	0.08	0.38*	0.14	0.15	0.34	1						
Na	-0.16	-0.07	0.06	0.16	0.13	0.05	0.74**	1					
NH_4^+	0.62**	0.24	0.46*	-0.09	0.20	0.11	0.41*	0.17	1				
Cl^-	0.50*	-0.11	0.23	0.56**	0.23	0.19	0.31	0.27	0.39*	1			
NO_3^-	0.46*	0.49**	0.50**	-0.11	-0.03	0.23	0.24	0.05	0.84**	0.09	1		
SO_4^{2-}	0.29	0.44*	0.35	-0.22	0.02	0.23	0.21	0.13	0.72**	0.10	0.76**	1	
TSP	0.51**	0.59**	0.57**	0.08	0.05	0.39*	0.17	-0.03	0.77**	0.24	0.88**	0.73**	1

Significance level:

* One-tailed probability of less than 0.01

** One-tailed probability of less than 0.001

n = 40

not correlated significantly with TSP. In addition, the association of chloride with ammonium, as suggested by the frequency distribution diagrams (Figure 7.3) does not appear to occur since an insignificant correlation coefficient (-0.3) was obtained.

However using groups of elements or ions with high correlation coefficients to assess the nature of possible TSP sources is obviously subjective since assumed knowledge regarding possible sources will influence the choice of variables used to form a group. Extra information regarding the nature of sources will result from an eigenanalysis, which will ascertain which variables are "loaded" onto a particular principal component. This grouping of variables is less subjective than mere grouping correlation coefficients and will further aid the identification of possible contributing sources. The use of eigenanalysis and multiple regression analysis was shown in Chapter 5 to provide extra information regarding the nature of the sources contributing to the collected particulate

Table 7.4 Correlation matrix showing associations between trace metals and major ions measured at Bolsover.

	As	Cr	Cd	Pb	Fe	Mn	Mg	Cu	Ca	K	Na	NH_4^+	Cl^-	NO_3^-	SO_4^{2-}	T.S.P.
As	1															
Cr	0.63**	1														
Cd	0.59**	0.59**	1													
Pb	0.42*	0.59**	0.65**	1												
Fe	0.73**	0.83**	0.79**	0.71**	1											
Mn	0.64**	0.85**	0.69**	0.61**	0.89**	1										
Mg	0.43*	0.28	0.39*	0.25	0.41*	0.45*	1									
Cu	0.62**	0.66**	0.81**	0.57**	0.76**	0.75**	0.53**	1								
Ca	0.46*	0.19	0.28	0.10	0.29	0.21	0.66**	0.26	1							
K	0.14	0.05	0.10	0.09	0.06	0.16	0.51**	0.10	0.56**	1						
Na	0.35	0.19	0.38*	-0.15	0.26	0.27	0.77**	0.49**	0.69**	0.79**	1					
NH_4^+	0.51**	0.30	0.48*	0.26	0.55**	0.47*	0.39*	0.51**	0.28	0.19	0.29	1				
Cl^-	0.65**	0.61**	0.65**	0.45*	0.74**	0.76**	0.68**	0.75**	0.32	0.26	0.48*	0.64**	1			
NO_3^-	0.32	0.10	0.47*	0.46	0.37	0.34	0.16	0.29	0.03	0.06	0.03	0.65**	0.45*	1		
SO_4^{2-}	0.69**	0.35	0.45*	0.35	0.63**	0.57**	0.40*	0.43*	0.21	0.11	0.19	0.66**	0.61**	0.61**	1	
T.S.P.	0.66**	0.53**	0.63**	0.48*	0.72**	0.75**	0.62**	0.63**	0.25	0.28	0.40*	0.67**	0.86**	0.64**	0.81**	1

Significance level:
* One-tailed probability of less than 0.01
** One-tailed probability of less than 0.001
n = 51

Table 7.5 Correlation matrix showing associations between trace metals and major ions measured at Wells.

	Fe	Mn	Mg	Cu	Ca	K	Na	NH_4^+	Cl^-	NO_3^-	SO_4^{2-}	TSP
Fe	1											
Mn	0.87**	1										
Mg	0.29	0.14	1									
Cu	0.33	0.21	0.34	1								
Ca	0.75**	0.64**	0.43	0.53**	1							
K	0.61**	0.36	0.44*	0.58**	0.66**	1						
Na	0.54**	0.26	0.70**	0.60**	0.62**	0.93**	1					
NH_4^+	0.27*	0.32	-0.14	-0.06	0.08	0.24	0.13	1				
Cl^-	-0.11	-0.20	0.88**	0.10	0.02	0.08	0.38*	-0.30	1			
NO_3^-	0.58**	0.63**	-0.07	0.11	0.50**	0.29	0.15	0.71**	-0.35	1		
SO_4^{2-}	0.35	0.23	-0.04	0.15	0.28	0.50**	0.40*	0.82**	-0.21	0.49**	1	
TSP	0.52**	0.52**	0.36	0.43	0.62*	0.47*	0.48*	0.42*	0.10	0.57**	0.53**	1

Significance level:
* One-tailed probability of less than 0.01
** One-tailed probability of less than 0.001
n = 38

matter. These methods have been applied to the composition of particulate matter collected at each sampling site and the results are described in the following sections.

7.3.2 Principal component analysis/multiple regression (PCA/MR)

The PCA/MR method to apportion the contribution of sources to a receptor was described previously in Section 5.3. This method selects the tracer variables via a principal component analysis. The selected variables are then used as independent variables in a multiple regression analysis, with the TSP mass concentration used as the dependent variable. Both the principal component and multiple regression analysis were performed using SPSS-PC+.

The PCA of a correlation matrix, (the PCA of a 3 × 3 correlation matrix was presented in Section 5.5.1), shows that the variance contained within a data set can be alternatively expressed by eigenvalues. In addition, the amount of variance explained by each component can be calculated using Equation 7.2:

$$\textit{Variance attributed to component } x = \frac{\textit{Eigenvalue, } \lambda \textit{ , for component } x}{\textit{Number of variables subjected to eigenanalysis}}$$

. . . .Equation 7.2

The amount of variance attributed to three eigenvalues is determined by summing each eigenvalue and dividing by the number of variables in the data set. For example at Lincoln, the three components presented at the bottom of the first three columns in Table 7.6, have eigenvalues 5.05, 1.90 and 1.61, which together sum to 8.55. Dividing this value by the total variance contained with the standardised data set (12), showed that the three eigenvalues accounted for 71% of the total variance. The three components determined for the data at Bolsover and Wells, accounted for 76% and 85%, of the total sample variance, respectively. These high percentage values would suggest that three components do adequately model the data at each site.

7.3.2.1 Rotated principal component loadings

The PC loadings presented in Table 7.6 were rotated using the varimax option within the SPSS-PC+ software. The varimax rotation, which minimises the number of variables with high loadings on a particular factor, was performed in order to make interpretation easier.

The variables with the highest loadings on each principal component and hence those chosen for the regression analysis are presented below:

Lincoln	Variable (loading)	**Bolsover**	Variable (loading)	**Wells**	Variable (loading)
PC1	NH_4^+ (0.91)	PC1	Fe (0.90)	PC1	Mn (0.92)
PC2	Ca (0.88)	PC2	SO_4^{2-} (0.93)	PC2	Mg (0.88)
PC3	Cl^- (0.88)	PC3	Na (0.93)	PC3	SO_4^{2-} (0.92)

7.3.2.2 Regression of TSP mass concentrations on selected variables

The backward elimination method of regression analysis was chosen as the multiple regression method (Draper and Smith, 1981). This method, operates by performing the multiple regression analysis using all the selected variables and consequently rejecting those variables determined to have insignificant regression coefficients (see Section

Table 7.6 Rotated PC loadings determined at each sampling site

Lincoln					Bolsover					Wells				
	PC 1	PC 2	PC 3	Comm-unality		PC 1	PC 2	PC 3	Comm-unality		PC 1	PC 2	PC 3	Comm-unality
Pb	0.54	0.19	0.19	0.50	As	0.67	0.25	0.29	0.59	Fe	0.86	0.25	0.20	0.85
Fe	0.38	0.81	-0.18	0.85	Cr	0.79	-0.13	0.04	0.64	Mn	0.92	0.01	0.13	0.87
Mn	0.43	0.70	0.21	0.72	Cd	0.80	0.05	0.13	0.67	Mg	0.14	0.88	-0.09	0.81
Mg	-0.29	0.43	0.69	0.73	Pb	0.83	0.13	-0.11	0.71	Cu	0.37	0.56	0.05	0.46
Cu	0.12	0.001	0.42	0.19	Fe	0.90	0.21	0.15	0.88	Ca	0.79	0.45	0.12	0.84
Ca	0.08	0.88	0.16	0.81	Mn	0.84	0.08	0.25	0.78	K	0.40	0.68	0.47	0.84
Na	0.14	-0.03	0.59	0.37	Mg	0.41	-0.00	0.80	0.79	Na	0.28	0.86	0.33	0.93
NH_4^+	0.91	0.01	0.35	0.95	Cu	0.70	0.23	0.14	0.57	NH_4^+	0.17	-0.19	0.90	0.87
Cl^-	0.11	0.08	0.88	0.80	Ca	0.27	-0.02	0.77	0.67	Cl^-	-0.25	0.76	-0.30	0.74
NO_3^-	0.91	0.25	0.02	0.89	K	-0.11	-0.09	0.87	0.78	NO_3^-	0.68	-0.17	0.54	0.78
SO_4^{2-}	0.85	0.17	-0.01	0.75	Na	0.11	0.06	0.93	0.88	SO_4^{2-}	0.14	0.13	0.92	0.89
TSP	0.81	0.44	0.16	0.86	NH_4^+	0.15	0.92	-0.00	0.88	TSP	0.56	0.36	0.41	0.61
					Cl^-	0.67	0.49	0.30	0.78					
λ =	5.04	1.90	1.61		NO_3^-	0.03	0.92	-0.15	0.86	λ =	6.20	2.69	1.31	
% var	42.0	15.8	13.4		SO_4^{2-}	0.05	0.93	-0.04	0.87	% var	51.7	22.4	10.9	
					TSP	0.49	0.77	0.19	0.88					
					λ =	6.88	3.21	2.14						
					% var	43.0	20.0	13.4						

Key % var = the variance in data set explained by factor coefficients.

5.2.2.5). The use of the backward elimination method in receptor modelling was presented previously by Ito *et al.* (1987) who used the method to perform the regression analysis in the Airborne Toxic Element and Organic Subtances project, carried out in New Jersey.

The initial regression for Lincoln produced a negative regression coefficient for the Cl^- variable. As this would result in a negative mass contribution with no physical significance the regression was repeated using another variable characteristic of the

source. The choice of variable was the Mg variable with a PC loading of 0.69, the second highest loading for component 3. But the backward elimination regression method rejected this variable as insignificant. However, since rejection of this variable would result in a decrease in the resolution of the number of contributing sources, from three to two sources, the variable was kept in the equation. This final regression equation determined for the Lincoln data is represented by Equation 7.3.

$$TSP = 0.0047 \pm 0.0006\ NH_4^+ + 0.015 \pm 0.005\ Ca + 0.013 \pm 0.022\ Mg + 16.9$$

. . . .Equation 7.3

Likewise when the TSP mass concentration values are regressed onto the selected independent variables for the Bolsover data set, the resulting regression equation (Equation 7.4) can be criticised since the small negative intercept (-1.3) could not be interpreted in physical terms.

$$TSP = 0.052 \pm 0.01\ Fe + 0.0054 \pm 0.0007\ SO_4^{-2} + 0.0069 \pm 0.004\ Na - 1.3$$

. . . .Equation 7.4

For the case of Wells, all the regression coefficients are calculated to be statistically significant. The regression equation for Wells is represented by Equation 7.5.

$$TSP = 1.2 \pm 0.4\ Mn + 0.0032 \pm 0.0018\ Na + 0.000091 \pm 0.00037\ SO_4^{-2} + 17.9$$

. . . .Equation 7.5

The regression constant obtained in Equations 7.3 and 7.5 is interpreted as a contibution from an unidentified source i.e. a source which has no tracer, possibly the contribution of an organic source. All the regression coefficients, except for Mg in the Lincoln equation are significant at the 95% level. The percentage contributions from identified sources to each site are presented in Table 7.7. These were obtained by multiplying the regression coefficients, shown in Equations 7.3 to 7.5, by the mean concentration of element or ion in the TSP, with the product of this operation consequently divided by the TSP mean concentration (Equation 5.13). The unexplained fraction of the TSP was determined by dividing the regression constant by the mean TSP concentration. Secondarily derived particulate matter was the main contributor to TSP at Lincoln (41%) and Bolsover (60%), whereas the unidentified fraction of TSP contributed the largest fraction at Wells. This fraction may represent either an organic or crustal component. Considering the relatively small TSP mass concentration collected at Wells

Table 7.7 Percentage contribution of individual sources to each receptor site determined by PCA/MR.

Site		Source 1	Source 2	Source 3	Unidentified fraction
Lincoln	Tracer used in MR	NH_4^+	Ca	Mg	
	Inferred source	SPM	Crustal	Soil	
	Percentage Contribution	41	26	6	27
Bolsover	Tracer used in MR	SO_4^{2-}	Fe	Na	
	Inferred source	SPM	Crustal	Sea	
	Percentage Contribution	60	29	12	-1
Wells	Tracer used in MR	Mn	Na	SO_4^{2-}	
	Inferred source	Soil	Seasalt	SPM	
	Percentage Contribution	25	10	14	51

Key: SPM is secondary particulate matter

(35.0 μg m^{-3}), the importance of this unidentified source may be accentuated.

7.3.3 Regression on absolute principal component scores (RAPCS)

Both the statistical background and a worked example, illustrating how the RAPCS method determines the mass contribution from a contributing source, were described in Sections 5.4.2.4 and 5.5.3, respectively.

7.3.3.1 Rotated principal component loading matrices for the RAPCS model

The number of components chosen to represent the contributing sources were selected using the same criteria as used previously for the PCA/MR method, that is, only those

components with eigenvalues greater than 1.0. Hence the RAPCS method also uses three components to construct a receptor model at each sampling site.

Also presented in Table 7.6 were estimates of the communalities, determined by summing the squared factor loading for variable. The communality provides an estimate of the ability of the model to reproduce each variable. For example, the communalities determined for the secondary particulate matter ions, such as NH_4^+ and SO_4^{2-}, at each site are high, whereas the communalities for copper at each site were the lowest obtained. The elements or ions with high loadings, as for the PCA/MR method, will aid identification of each contributing source. Loadings with values of 0.80 or greater (with the exception of Mg at Lincoln) were used to identify the sources. The inferred sources from the association of elements and ions with each principal component are shown in Table 7.8. Each of these variables with high loadings were shown previously in Section 7.3.1 to be prominent members of the associated clusters of correlation coefficients, hence the loading of a variable onto a principal component provides confirmatory evidence of association.

Table 7.8 Sources inferred to be contributing to collected particulate matter, using RAPCS.

	PC Number	Trace metal or ion with high loadings	Possible inferred source from element with high loading
Lincoln	1	NH_4^+, NO_3^-, SO_4^{2-} and TSP	Secondary particulate matter
	2	Fe, Ca.	Crustal/metal source
	3	Cl^-, Mg	Sea-salt/soil
Bolsover	1	Fe, Cd, Pb, Mn, Cu	Originating from castle roof
	2	NH_4^+, NO_3^-, SO_4^{2-}	Secondary particulate matter
	3	Mg, Ca, Na	Soil, crustal, sea
Wells	1	Fe, Mn	Soil, crustal
	2	Mg, Na	Sea salt
	3	NH_4^+, SO_4^{2-}	Secondary particulate matter

7.3.3.2 Mass contribution and source profiles determined using RAPCS at Lincoln Cathedral

Forty particulate samples were collected at Lincoln Cathedral (6 during September 1989, 15 during May 1990, 4 during January 1991, 10 during February 1991, 5 during March 1991).

The percentage contributions from each source are presented in Table 7.9. Sources 1 and 2 can be seen to be contributing approximately equal amounts to the collected particulate mass. This result is different to that obtained by the PCA/MR method which estimated that Source 1 contributed approximately twice as much mass as Source 2.

Table 7.9 Estimated mean mass contribution of each source to particulate matter at Lincoln Cathedral.

Source Number	Source Type	Percentage Contribution to Particulate Matter
1	Secondary particulate matter	38.5
2	Crustal and metal mixture	38.6
3	Sea-salt/soil	22.9

The temporal nature of the mass from each contributing source, determined using the RAPCS method, to each collected sample is illustrated by Figure 7.4. The basis to the calculations to determine the mass contribution were discussed in Section 5.4.2.4.

Examination of the individual peak contributions may provide an indication of the specific nature of the source. For example, Source 2 is estimated to be a major contributor to Sample 1 (collected on 5th September 1989) with a contribution of 53.0 $\mu g\ m^{-3}$ towards the total TSP concentration (72.6 $\mu g\ m^{-3}$) in this sample. This could be due to movement of scaffolding that occurred during this period. Similarly renovation work may have been responsible for the high contributions from Source 2 to Samples 9 and 10.

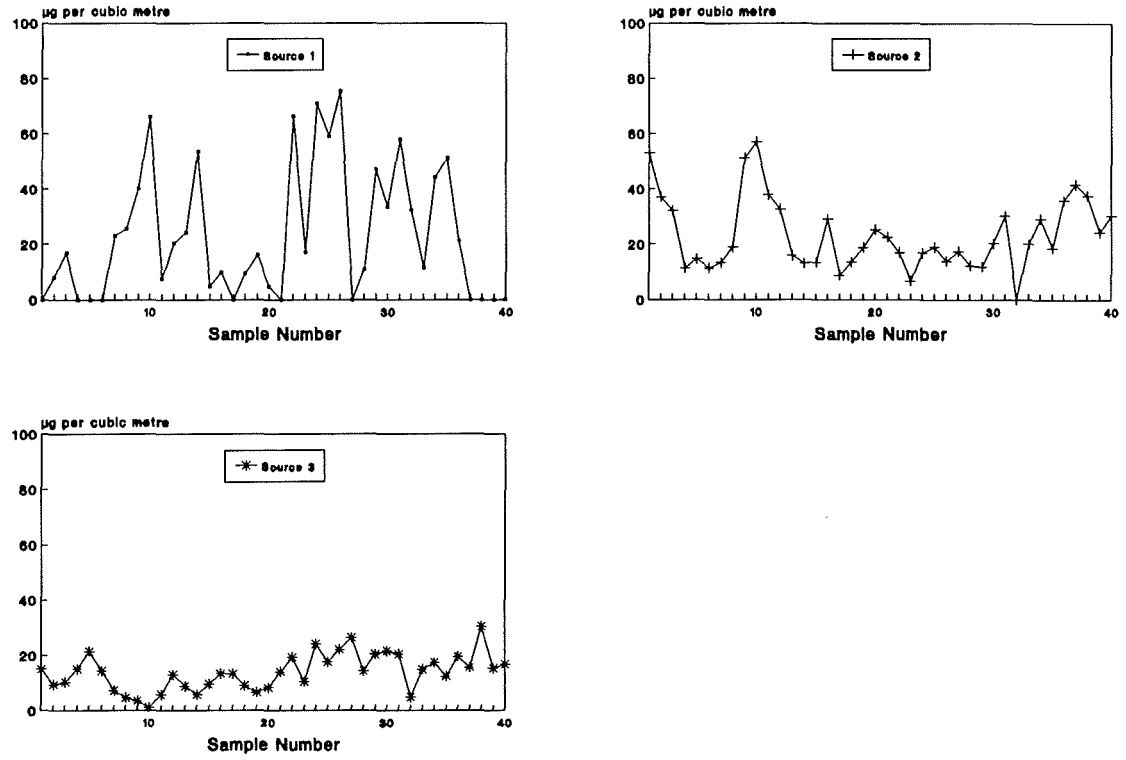

Figure 7.4 Contribution of sources to collected particulate matter samples at Lincoln Cathedral.

A possible reason for the significant contribution from Source 3 (identified previuosly as sea-salt/soil source) to Sample 5 (9th September 1989) may be the increased contribution of a chloride source, suggested by the relatively high chloride concentration measured on this date (5.5 $\mu g\ m^{-3}$). Incineration of waste in the North Sea, as reported by Scorer (1992), could have led to increased atmospheric concentration of Cl^- at Lincoln.

The remaining contributions from Sources 2 and 3 to those samples collected after Sample 10, remained relatively constant. In general, Source 1 appears to fluctuate significantly more than the other two sources. Lowest contributions were observed for Samples 4 to 6 (8th, 9th and 10 th September 1989) and Samples 37 to 40 (18th, 19th, 20th and 22nd March 1991). Whereas a particularly high contribution from Source 1 occurred for samples collected during January and February 1991 (Samples 22 to 35, with the exception of Samples 23, 27, 28 and 33). Further evidence that Source 1 does

consist of secondary particulate matter can be obtained by referring back to Table 6.2 and Figure 6.4, which showed that the relative percentage of the ions characteristic of secondary particulate matter (SO_4^{2-}, NO_3^- and NH_4^+) were relatively high during January and February 1991.

The source profiles, which represent the contribution of each metal or ion, in each source to collected samples, were determined by regressing the absolute principal component scores on to the elemental concentrations (Stage 8, Figure 5.5). The source profiles determined for Lincoln are presented in Table 7.10.

Table 7.10 Source profiles determined for each of the contributing sources at Lincoln Cathedral.

Species	Secondary Particulate Matter	Crustal-Metal	Sea-salt/ soil
SO_4^{2-}	23.97	12.80	7.80
NO_3^-	23.86	13.16	1.74
Cl^-	0.42	--	28.52
NH_4^+	16.45	--	19.19
Na	0.51	0.51	6.82
Ca	0.16	3.76	10.41
Cu	0.07	0.14	0.83
Mg	--	0.51	1.51
Mn	0.02	0.06	0.03
Fe	0.40	1.69	--
Pb	0.07	0.03	0.17

Expressed as a percentage of mass originating from each source.
-- indicates a negative mass has been determined for three source profile.

The profile for Source 1 shows that SO_4^{2-}, NO_3^-, and NH_4^+ account for 64.3% of the mass contribution for this source. However, the proportion of these ions in this source may have been expected to be higher. Unfortunately SO_4^{2-} and NO_3^- were also calculated to make significant contributions to Source 2. In addition, given that Source 2 was identified as a crustal source from the principal component analysis, the calcium contribution is rather low.

The high proportion of chloride and ammonium determined for Source 3 suggests that ammonium chloride aerosol could be making a significant contribution to this primarily sea-salt source. Considering that this source is identified as sea salt, the proportion of

sodium would be expected to be higher. However, this may reflect a major limitation in using the receptor model technique to estimate source profiles, since fluctuations in contributing sources over a time period of nearly two years may not necessarily reproduce accurate source profiles.

7.3.3.3. Mass contribution and source profiles determined using RAPCS at Bolsover

Fifty one samples were collected at Bolsover: 16 during November 1990, 11 during December 1991, 10 during January 1991, 4 during February 1991 and 10 during June 1991. The PCA was performed on 16 variables (As, Cr, Cd, Pb, Fe, Mn, Mg, Cu, Ca, K, Na, NH_4^+, Cl^-, NO_3^-, SO_4^{2-} and TSP). The identification of sources by their high loading on a particular source was shown previously in Table 7.7. The percentage mass contributions from each source are presented in Table 7.11. Unlike the PCA/MR method, no unidentified source was determined. Only Source 1, the mass originating from the castle roof, was estimated to be similar to the contribution determined by the PCA/MR method. Source 2 was estimated to contribute approximately 50% more mass than the PCA/MR method, which would presumably take into account the contribution from the previously unidentified source. The percentage contribution from the Source 3 also increased significantly.

Table 7.11 Estimated mean mass contribution from each source to particulate matter at Bolsover.

Source Number	Source Type	Percentage Contribution to Particulate Matter
1	Originating from Castle Roof	25.6
2	Secondary Particulate Matter	61.3
3	Soil, Crustal and Sea	13.0

The temporal variations in the individual contributions from each source to the 51 collected samples (Figure 7.5) show that Source 1 contributes significantly to Samples 12 and 13 (21st and 22nd November 1990, respectively). Another high contribution was

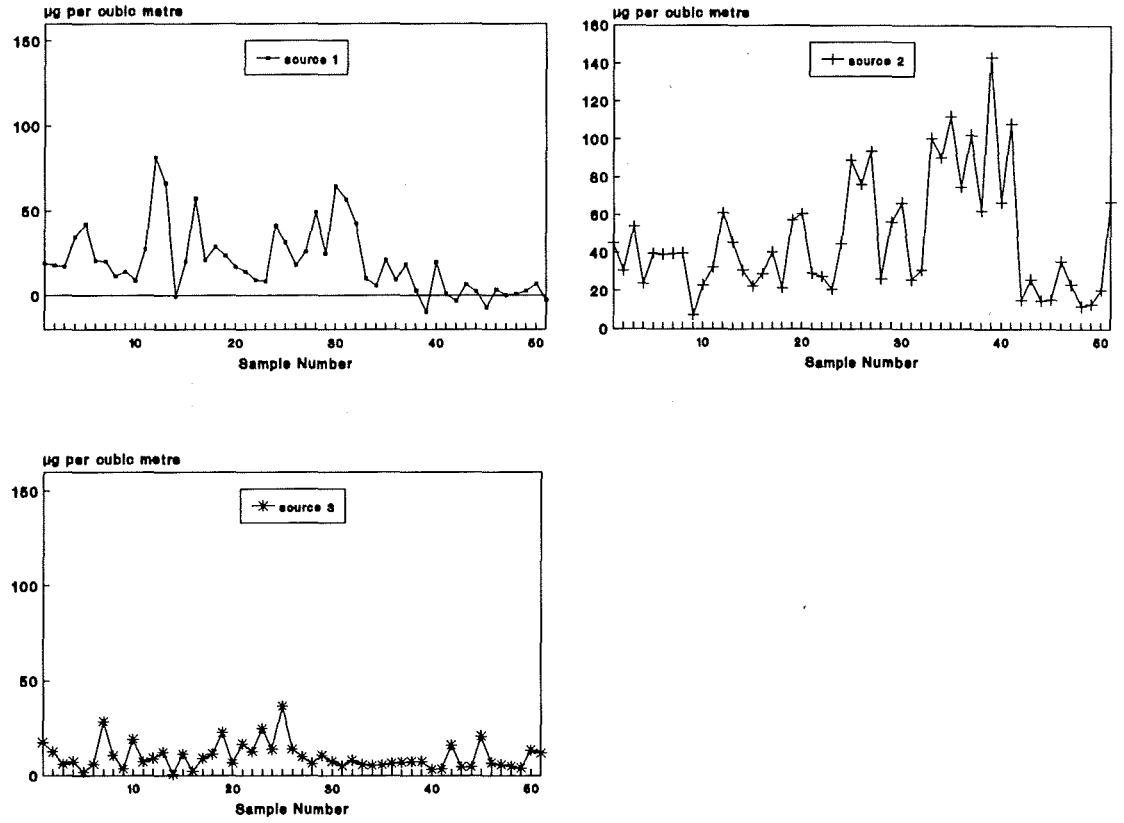

Figure 7.5 Contribution of atmospheric sources to collected matter samples at Bolsover Castle.

estimated for Sample 30 (21st January 1991). Source 1 contributed a relatively minor amount of mass to the remaining samples collected at Bolsover (Samples 32-51), with Samples 14, 39, 42, 45,and 51 estimated to make negative contributions. This indicates a further flaw in the receptor model, since negative mass contributions cannot be explained in physical terms.

Source 2 was the major contributor (61.3%) to the collected particulate matter. The lowest contribution from this source (Sample 9, 16th November 1990) occurred during a period when the meteorological conditions were mild with frequent rain storms to cleanse the air (Weather, 1991). The high contributions observed form Source 2 for Samples 25-27 (14th, 17th and 18th December) could have resulted from the cold foggy conditions that occurred during these dates. The most prominent contribution from Source 2 occurred for Samples 33 to 41 which were collected during the last week of January and the first week of February 1991. This is probably due to the cold

temperatures which occurred during this period resulting in a high levels of emissions from local domestic fuel consumption.

These peaks can also be seen to be present when the other two sources were relatively low indicating the existence of conditions, such as stable cold air, that would favour the build-up of concentrations of secondary pollutants, such as ammonium sulphate, and restrain the turbulent processes required to generate the occurrence of material derived from the soil's surface. Source 3 (identified as a mixture of soil, crustal and sea material) can be seen to be the smallest contributor to the collected mass and appears to be relatively constant. This would suggest that each of the constituent parts of this source made a steady contribution throughout the sampling period and appear not to be affected by meteorological conditions.

The source profiles for particulates sampled at Bolsover Castle are presented in Table 7.12. The four main constituents of Source 2 (SO_4^{2-}, NO_3^-, Cl^- and NH_4^+) together account for 49% of the estimated mass. Source 1 can be seen to be the largest contributor of Cl^-, Ca, Fe, Pb, Cd, Mn and Cr, although the percentage contributions determined were relatively small. Indeed, unlike the non-secondary particulate matter sources estimated at Lincoln by the RAPCS method, the non-secondary particulate sources at Bolsover do not contain significant proportions of the characteristic elements and ions expected in each source, suggesting that the model has limited use in estimating these source contributions.

7.3.3.4 Mass contribution and source profiles determined using RAPCS at Wells Cathedral

Thirty eight samples were collected at Wells during the summer of 1991 (11 during May, 13 during June, 11 during July and 3 during August). The PCA was performed on 13 variables which included Fe, Mn, Mg, Cu, Ca, Al, K, Na, NH_4^+, Cl^-, NO_3^-, SO_4^{2-} and TSP. From the 13×13 correlation matrix, 3 factors were chosen to represent the variation in the data. Although 4 PCs with eigenvalues greater than 1 were obtained in the PCA, the resulting estimated mass contributions produced a large number of negative contributions. Therefore, the analysis was repeated using only three principal

Table 7.12 Source profiles determined for each of the sources at Bolsover Castle.

Species	Originating from Castle Roof	Secondary Particulate Matter	Soil, Crustal and Sea
SO_4^{2-}	2.59	15.97	0.25
NO_3^-	1.02	13.17	–
Cl^-	7.17	6.19	1.74
NH_4^+	3.17	15.11	–
Na	0.53	0.19	1.46
K	–	–	0.94
Ca	1.01	0.03	0.10
Cu	0.10	0.03	0.001
Mg	0.45	0.004	0.31
Mn	0.10	0.004	0.01
Fe	1.43	0.20	0.74
Pb	0.31	0.05	–
Cd	0.007	0.0002	0.0004
Cr	0.02	–	0.0007
As	0.02	0.01	0.002

– indicates a negative mass determined for the source profile.
Expressed as a percentage of mass originating from each source.

components which produced a much lower number of negative contributions. The resulting estimated percentage contributions from each source are presented in Table 7.13.

Table 7.13 Estimated mass contribution from each source to collected particulate matter at Wells.

Source Number	Source Type	Percentage Contribution to Particulate Matter
1	Soil/Crustal	50.0
2	Sea-salt	31.8
3	Secondary Particulate Matter	18.2

The regression on absolute principal component scores method estimated that the soil-crustal source contributed approximately half of the mass of the collected particulate matter at Wells. This is in contrast to the PCA/MR method which estimated that the three sources accounted for 50% of the observed mass concentration, with an unidentified source contributing the remainder. In addition, the RAPCS method

estimates that secondary paticulate matter contributes the lowest mass fraction to the samples collected at this site.

Examination of the temporal trends in individual mass contributions from each source (Figure 7.6) shows that the highest contribution from Source 1 occurred for Sample 7 (22nd May 1991). This was during a particularly warm period when the surface layer of soil in the surrounding countryside may have been loose due to the lack of moisture.

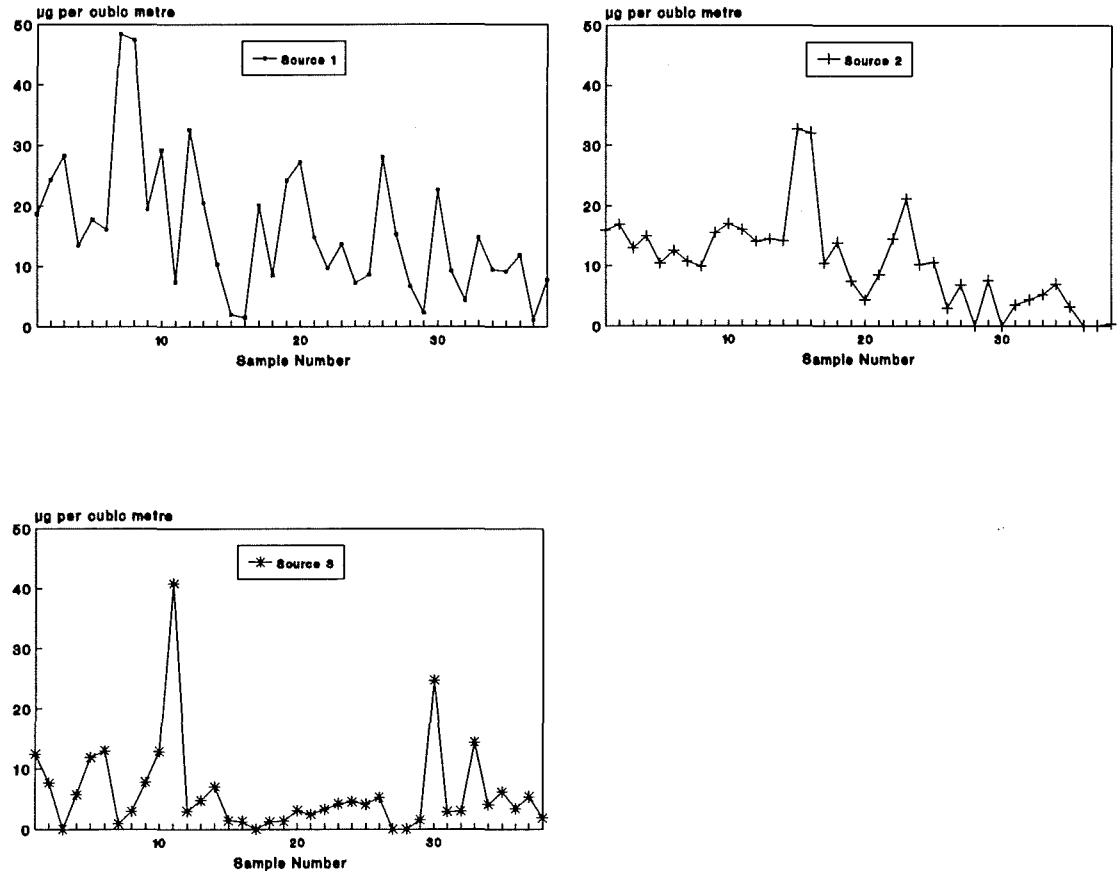

Figure 7.6 Contribution of atmospheric sources to collected particulate matter samples at Wells Cathedral.

The lowest contributions from Source 1 occurred for Samples 15 and 16 (12th and 13th June). This may be explained by the large amount of rainfall that occurred during this week (Weather, 1991), which may have prevented the release of material from the soil's surface. The high contribution from Source 2 (the sea-salt source) on this date may further suggest that the air mass may have originated from the Atlantic carrying in relatively clean air. Further confirmatory evidence of the cleansing effect of rain travelling from the west is suggested by the low contribution from Source 3 (SPM).

The greatest contribution from Source 3 to an individual sample occurs for Sample 11 (30th May 1991), approximately 60% of the TSP (63 $\mu g\ m^{-3}$) was estimated to have originated from this source.

The source profiles determined by the RAPCS method for Wells samples are presented in Table 7.14. The major constituent of Source 1 is nitrate. A speculative suggestion for the high contribution from this source may be the high amounts of nitrate based fertilisers applied to the soil during the spring and early summer months.

Table 7.14 Source profiles determined for each of the sources at Wells Cathedral.

Species	Soil-Crustal	Sea-salt	Secondary Particulate Matter
SO_4^{2-}	5.26	7.46	57.62
NO_3^-	13.63	--	15.59
Cl^-	--	21.72	--
NH_4^+	3.22	--	23.66
Na	1.08	8.73	3.22
K	1.69	4.20	3.15
Ca	4.59	3.39	0.64
Cu	1.05	2.59	0.14
Mg	0.27	1.62	--
Mn	0.04	0.004	0.01
Fe	0.58	0.16	0.17

-- indicates a negative mass has been determined for source profile.
Expressed as a percentage of mass originating from each source.

Both the constituent components of sea-salt and secondary particulate matter sources appear to be more successfully determined than the corresonding sources at Lincoln and Bolsover. For example, approximately 50% of the mass estimated to come from the sea-salt source profile is accounted for, with the expected Na and Cl^- ions making important contributions. Likewise, the characteristic ions of secondary particulate matter NH_4^+, SO_4^{2-} and NO_3^-, together account for 96% of the mass determined to originate from this source.

7.3.4 Target transformation factor analysis (TTFA)

Target transformation factor analysis will establish similar characteristics relating to the

contributing sources to those determined by the regression on absolute component scores described in Section 7.3.3. The background to the method was described previously in Section 5.4.2.2. The computer software program FANTASIA is used to carry out the necessary operations. The TTFA method will calculate the:

- number of contributing sources
- contribution of individual components to each collected sample
- total mass contribution from each source to collected particulate matter
- percentage abundance of each element or ion in each contributing source

A flow diagram showing the necessary procedures has been presented in Figure 5.3. A major difference to the RAPCS method, is that the factor analysis was performed on the correlation matrix showing the association between samples (a Q mode correlation matrix), whereas the RAPCS method performed the PCA on the R mode correlation matrix. Although the FANTASIA program has the potential to perform the factor analysis on both types of correlation matrices, the Q-mode analysis produced a smaller number of negative contributions, which therefore suggested this was the more correct technique for this data set. Consequently, as 40, 51 and 38 samples were collected at Lincoln, Bolsover and Wells, respectively, the factor analysis was performed on correlation matrices with dimensions; 40 $\times$ 40, 51 $\times$ 51 and 38 $\times$ 38, respectively. The factor analysis was performed using FANPART1.

As in the case of the PCA/MR and RAPCS methods, three factors were eventually selected to model the data. Although four factors with eigenvalues greater than one were obtained for Wells and Bolsover (a plot of eigenvalue versus factor number is presented in Figure 7.7), the three factor solution produced a significantly lower number of negative source contributions.

Once the number of factors has been selected (Stage 1, Figure 5.4) the program can then begin to determine the source profiles from the abstract matrix, A_Q (Stage 2, Figure 5.4). This is accomplished using the target transformation routine (FANPART2).

As mentioned in Section 5.4.2.2., the target transformation is an iterative process, which uses the factor loading matrix as the independent variables and the matrices of

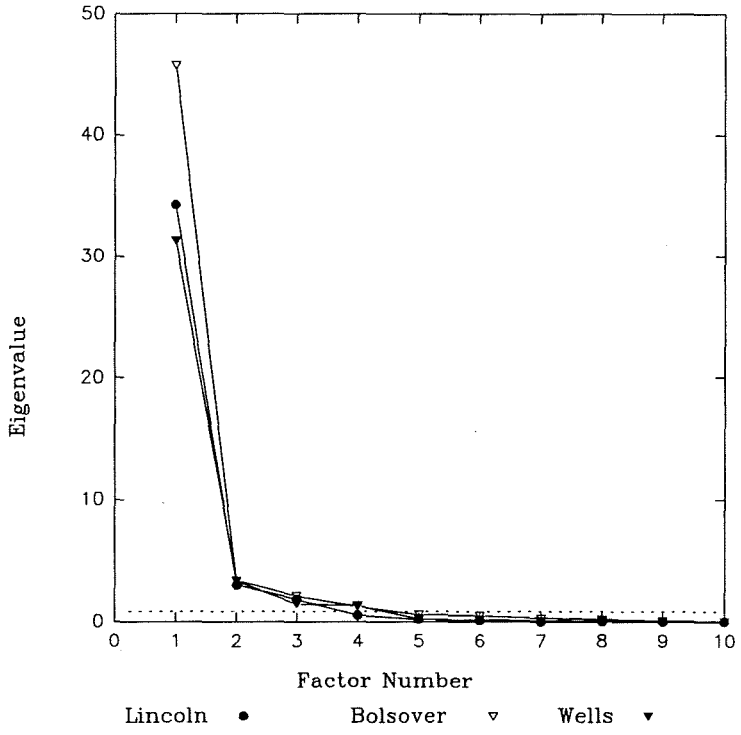

Figure 7.7 Eigenvalues as a function of factor number for FANTASIA analysis.

"test vectors" as the dependent variable. As the number of test vectors will equal the number of elements used in the factor analysis, the factor loading matrix will subsequently be regressed onto this same number of test vectors. That is, if 14 variables were used in the factor analysis, the factor loading matrix will be regressed 14 times onto 14 different test vectors. The iterated test vectors are stored in the file ITER.

Once the iteration has been completed, three profiles, representative of the three contributing sources, are selected. This selection is carried out using the CLUSTER procedure of the FANTASIA program (Stage 3, Figure 5.4). These iterated test vectors are chosen by trial and error, selecting initially those vectors which appear to be most widely spaced in the dendogram (the cluster diagram produced from the CLUSTER routine is shown in Figure 7.8).

Upon selection of three test vectors (B), the program continues again using FANPART2, which subsequently estimates the contribution of each ion or element to

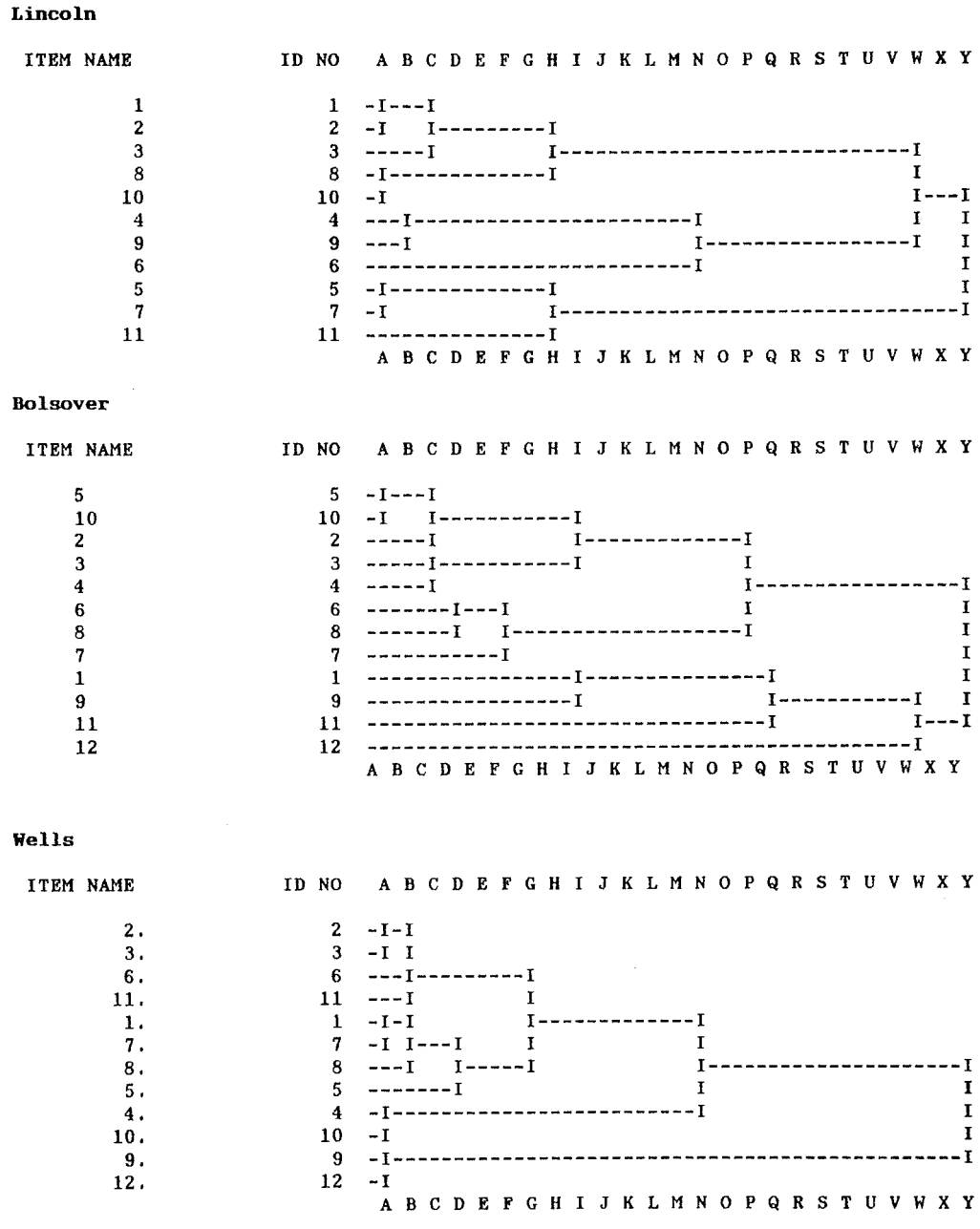

Figure 7.8 Dendograms as aids in the selection of iterated vectors.

the observed TSP mass concentration. These contributions are estimated by multiplying the regression coefficients obtained from the multiple regression analysis (Equation 5.16) by the iterated matrix B. The regression coefficients obtained from the multiple regression analysis (Equation 5.16) are stored in the file LOADMX. The sum of the elements and ions in each source will determine the mass contribution from each source. This represents a major difference to the RAPCS method which calculates the mass contribution from each source by "unstandardising" the principal component scores.

The iterated test vectors and number of negative source contributions finally selected from the dendograms in Figure 7.8 are presented in Table 7.15. The number of negative source contributions were relatively high for at least one of the three sources estimated to contribute to TSP collected at Lincoln and Bolsover. These were the sources labelled 9 and 8 at Lincoln and Bolsover, respectively, which both estimated 16 negative contributions. These sources were labelled using the same labels obtained from the iteration process.

Table 7.15 Number of negative source contributions obtained using the selected iterated test vectors.

Site	No. of samples	**Iterated test vector number selected from dendogram** Number of negative source contributions.		
Lincoln	40	**7** 1	**9** 16	**10** 0
Bolsover	51	**2** 2	**8** 16	**11** 0
Wells	30	**4** 4	**9** 1	**11** 3

The source profiles produced by the FANTASIA method showing the composition of the sources contributing to collected particulate matter are shown in Table 7.16.
These source profiles were determined by multiplying the chosen iterated test vectors by the regression coefficient, obtained when the LOADMX file was regressed onto the TSP mass concentrations. This procedure was carried out using the REGRESS sub-routine.

Table 7.16 Source profiles obtained using FANTASIA. Expressed as percentage of trace metal or ion contained within each contributing sources.

	Lincoln				Bolsover				Wells		
	7 Crustal	9 Sea	10 SPM		2 Soil/sea	8 Castle roof	11 SPM		4 Sea	9 SPM	11 Soil
Pb	0.03	0.07	0.12	Pb	0.11	0.13	0.13	Pb	0.09	0.06	0.07
Fe	0.72	0.65	1.18	Fe	0.75	0.75	0.44	Fe	0.25	0.34	0.44
Mn	0.05	0.04	0.05	Mn	0.06	0.08	0.02	Mn	0.02	0.02	0.03
Mg	1.78	1.31	0.23	Mg	0.65	1.01	0.07	Mg	1.34	0.27	0.37
Cu	1.23	0.32	0.18	Cu	0.08	0.09	0.04	Cu	1.37	0.71	1.57
Ca	4.79	2.33	1.49	Ca	1.31	3.05	0.60	Ca	3.09	0.11	4.75
Na	11.20	2.61	0.01	K	0.62	2.58	0.00	K	3.07	2.21	2.83
NH_4^+	3.53	2.08	12.58	Na	2.29	4.35	0.35	Na	5.05	1.77	3.25
Cl^-	12.71	15.70	2.84	NH_4^+	7.52	2.80	15.74	NH_4^+	0.00	16.65	1.93
NO_3^-	0.01	1.16	23.17	Cl^-	12.97	12.19	3.72	Cl^-	17.78	0.01	0.00
SO_4^{2-}	44.46	0.01	10.96	NO_3^-	1.16	0.01	16.62	NO_3^-	1.96	11.70	13.91
				SO_4^{2-}	0.02	11.26	17.21	SO_4^{2-}	7.96	64.68	1.31

However, the source profiles determined in the FANTASIA program could not be identified directly as originating from a particular source. Identification was only possible by performing a correlation analysis with those source profiles determined by the RAPCS method. The correlation coefficients obtained are presented in Table 7.17.

Table 7.17 Correlation coefficients between source profiles determined by RAPCS method and the FANTASIA method.

	Lincoln				Bolsover				Wells		
Profile labels	7	9	10		2	8	11		4	9	11
Source label*	1	2	3		1	2	3		2	3	1
SPM	0.48	-0.21	**0.92**	Castle	0.91	**0.80**	0.33	Soil	0.21	0.38	**0.85**
Crustal	**0.58**	-0.08	0.91	SPM	0.32	0.44	**0.99**	Sea	**0.97**	0.13	-0.11
Sea	0.25	**0.84**	0.10	Soil/Sea	**0.67**	0.40	0.16	SPM	0.64	**0.99**	0.07

* The numbers used to identify the source profile in FANTASIA are redefined using the labels 1, 2 and 3. This are used to identify the graphical bars in Figures 7.9 to 7.11.

The nature of the FANTASIA sources were deduced from those profiles which had high correlation coefficents with the source profiles determined by the RAPCS method. For example, for the Lincoln source profiles, the FANTASIA source profile labelled 10 had

a high correlation coefficient (0.92) with the SPM source. Source profile 9 was presumed to be a sea-salt source due to the relatively high correlation coefficient (0.84) with the sea-salt source determined using RAPCS. This was chosen despite the observation that the RAPCS crustal source also had a high correlation (0.91) with Source profile 10. However, as Source profile 10 was already identified as SPM, due to an even higher correlation coefficient (0.92), Source profile appeared most appropriately identified as the salt-salt source. Source profile in the FANTASIA was assumed to be a crustal source (r = 0.58). A similar identification method was used to determine those source profiles estimated for samples collected at Bolsover and Lincoln.

a) Source profiles determined by FANTASIA for Lincoln.

Only the components of the secondary particulate matter source appear adequately determined, with NH_4^+, SO_4^{2-} and NO_3^- together accounting for 47% of the source. The contribution of SO_4^{2-} to the crustal source appears unexpectedly high (44%). The anticipated components of both the crustal (Ca and Mg) and sea (Na) sources appear lower than expected.

b) Source profiles determined by FANTASIA for Bolsover

Only the secondary particulate matter source appears to be adequately modelled (49%) at Bolsover. The source identified as a mixture of sea and soil appears to be consist mainly of Na and Cl^- (20%). The source identified as "Castle roof" does not appear to contribute the metals iron and lead that were loaded heavily on to the respective component. Indeed, this source appears to contain relatively high proportions of ions expected in the sea-salt profile.

c) Sources profiles determined by FANTASIA for Wells

As for the RAPCS method, the secondary particulate matter source appears to be determined successfully (93%). A similar large amount of nitrate, as determined by the RAPCS method, appears to originate from the soil source (14%). The sea-salt source profile also contains significant amounts of Na and Cl^-, as previously estimated by the RAPCS method.

To illustrate the output from the FANTASIA program, the estimated contributions from

the three contributing sources to the first four samples collected at Lincoln, Bolsover and Wells, are shown in Figures 7.9, 7.10 and 7.11, respectively. The mass contributions originating from each source are shown in the patterned columns and the actual measured concentrations are shown by the fully-shaded column. As expected, the predicted concentrations of the secondary particulate matter are estimated to contribute most mass to each sample. However, the occurrence of a negative source contribution, for which a source contributes a negative quantity element or major ion, illustrates that the negative source contribution clearly cannot be interpreted as having a physical meaning. This is illustrated for Sample 1, Figure 7.9 for which the Source 1 (sea-salt) is showing a negative source contribution. In addition, Table 7.15 showed that 16 of the 40 collected samples at Lincoln and 16 of the 51 samples collected at Bolsover (castle roof source), were estimated to contribute negative mass concentration, suggesting that a significant proportion of samples at Lincoln and Bolsover have one source that is poorly modelled. The remaining estimated sources contributing to the 11 samples illustrated in Figures 7.9 to 7.11 appear to be more truly modelled in that there are no negative contributions.

In conclusion, the sum of the metal and major ion contributions from each of the three sources will, of course, be expected to equal the respective measured atmospheric concentration in each sample. The degree to which this occurs is dependent on the suitability of the data to be accurately modelled. The suitability of the selected profiles will be apparent by examining the differences in height between the sum of the mass concentrations from the three sources and the actual measured mass concentrations, with the height difference expected to be as small as possible.

A brief examination of the heights of the pattern bars in Figures 7.9 to 7.11 shows that nitrate, in general, is observed to come from the SPM source at Lincoln and Bolsover (in each case labelled Source 3). Whereas, at Wells nitrate comes predominantly from the soil source (labelled Source 1). The sulphate appears to originate predominantly from the SPM source (Source 3) at each sampling site, with Source 1 at Lincoln and Bolsover, the crustal material and soil/sea sources, respectively, also contributing significant amounts.

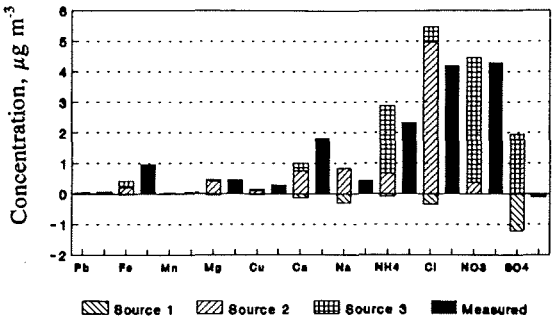

Sample 1. 5th September 1989.

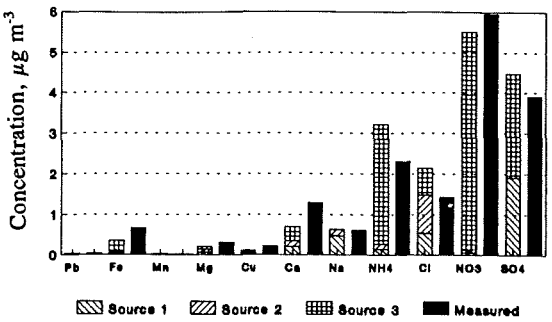

Sample 2. 6th September 1989.

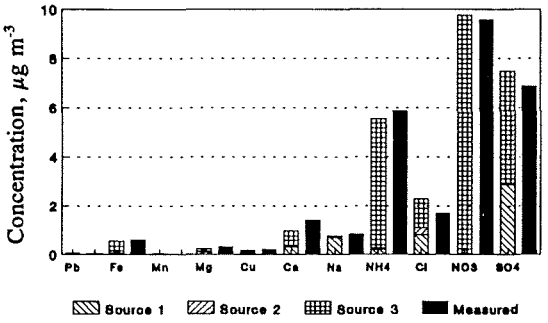

Sample 3. 7th September 1989.

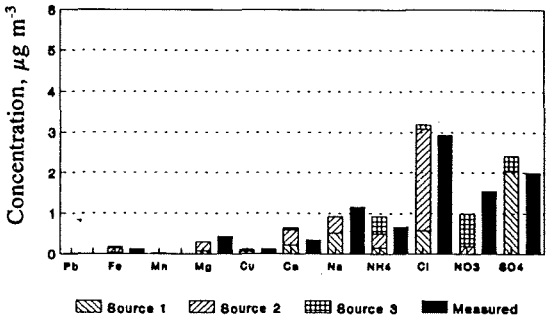

Sample 4. 8th September 1989.

Figure 7.9 Comparing the contribution of ions and metals from each of the determined sources to the actual masses determined for the first four samples collected at Lincoln Cathedral

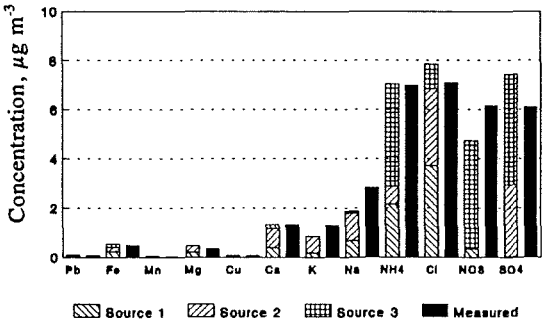

Sample 1. 6th November 1990

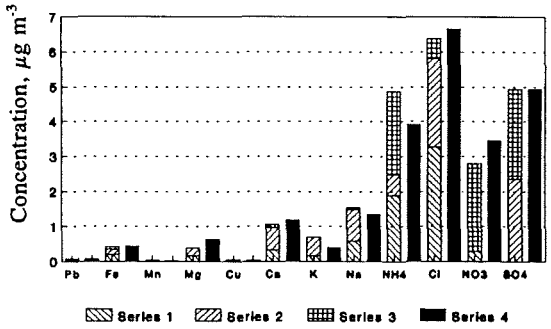

Sample 2. 7th November 1990.

Figure 7.10 Comparing the contribution of ions and metals from each of the determined sources to the actual masses determined for the first four samples collected at Bolsover Castle (continued over)

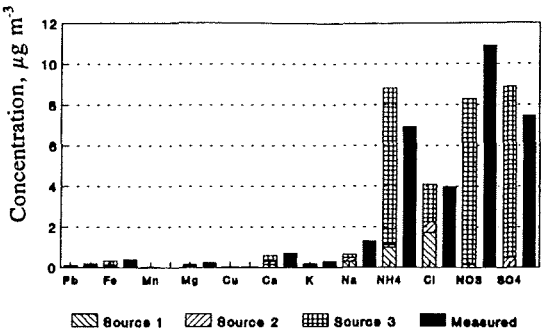

Sample 3. 8th November 1990

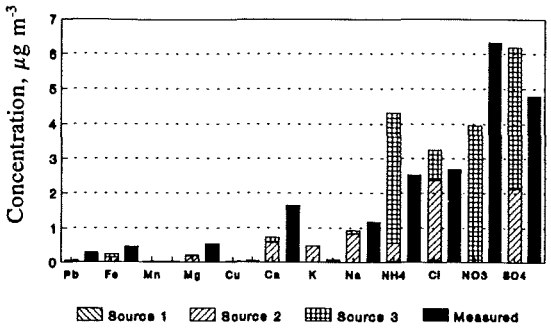

Sample 4. 9th November 1990.

Figure 7.10 Comparing the contribution of ions and metals from each of the determined sources to the actual masses determined for the first four samples collected at Bolsover Castle

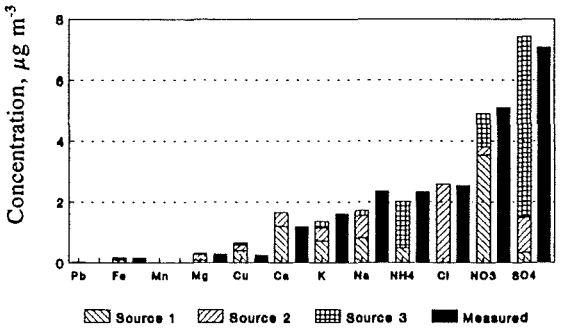

Sample 1. 13th May 1991

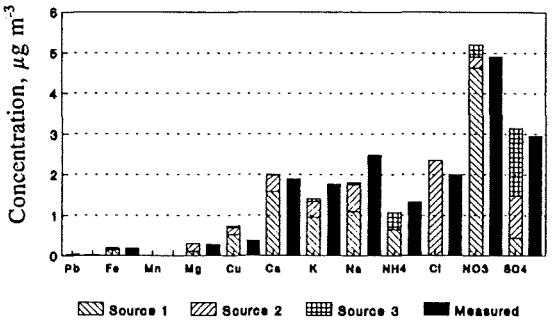

Sample 2. 14th May 1991.

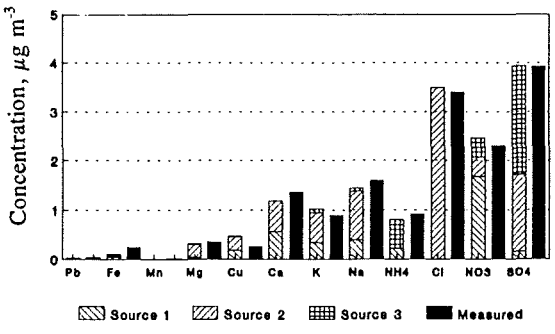

Sample 3. 15th May 1991.

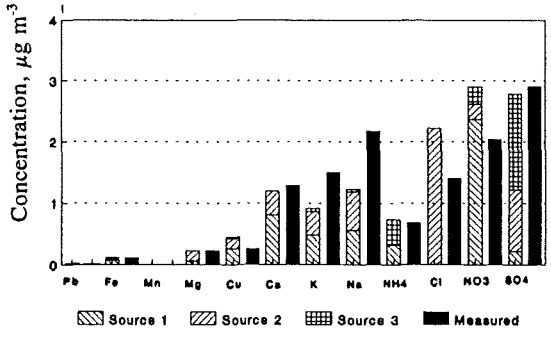

Sample 4. 16th May 1991.

Figure 7.11 Comparing the contribution of ions and metals from each of the determined sources to the actual masses determined for the first four samples collected at Wells Cathedral

7.3.5 Comparison of receptor models

The three receptor models used in this study:

- selection of independent variables using principal component analysis followed by multiple regression (Section 7.3.2)
- regression on absolute factor scores (Section 7.3.3)
- target transformation factor analysis (Section 7.3.4)

were each used to determine the contribution of sources to the collected particulate matter.

The selection of appropriate independent variables from all the measured constituents of TSP using PCA and the subsequent regression of TSP on these variables, required the least manipulation of data, whereas the FANTASIA program was difficult and awkward to use. One difficulty with the FANTASIA program was that a worked example, using aerosol samples, was not provided in the computer manual. The RAPCS method was intermediate between the two in terms of difficulty, and provided an output that could readily be manipulated.

Another disadvantage with the TTFA method was that each of the selected profiles were only identified by comparing the profiles with those obtained by the RAPCS method (Table 7.17). As expected, the mass contributions from the respective sources were also observed to follow the same order of association. For example, using the mass contributions from the respective sources to collected particulate matter at Bolsover, the soil/crustal/sea source contribution derived by RAPCS, was found to be fairly close to that determined by TTFA, with $r = 0.64$, (Diagram A, Figure 7.12). The mass contributions determined by each method for the source castle roof were even more closely associated, with $r = 0.71$ (Diagram B, Figure 7.12). The largest association, as expected, was obtained for the SPM source, $r = 0.94$ (Diagram C, Figure 7.12).

A certain amount of subjectivity occurs in the identification of sources created in a PCA analysis, since identifying a source type, on the basis of high loadings, may be difficult when two or more elements characteristic of different sources are loaded significantly on the same component. An example of this lack of resolution occurred for the PCA analysis of the Bolsover data set; three elements Mg (0.80), Ca (0.77) and Na (0.93)

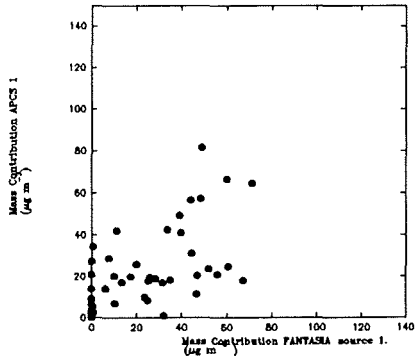

Diagram A. Soil/crustal/sea

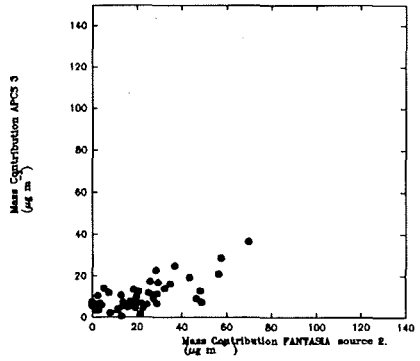

Diagram B. Castle roof

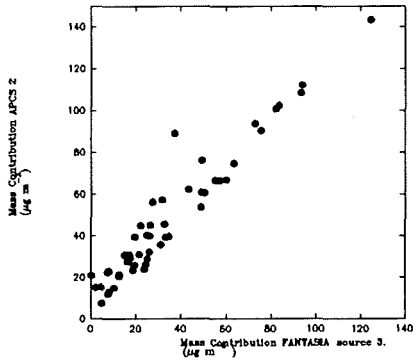

Diagram C. SPM

Figure 7.12 The associations between the mass concentrations determined by the regression on absolute principal components and by FANTASIA.

had high loadings on principal component 3, suggesting contributions from either soil, crustal and sea sources, respectively. Selection of the most representative metal from this source was obviously arbitrary and hence was referred to as a generalised source: soil/sea/crustal.

The estimation of only three sources, on the basis of selecting components with eigenvalues greater than 1.0, contributing to collected particulate matter would obviously suggest other sources were not considered. This is suggested by examining previous utilisation of the receptor modelling technique (Table 7.18). From Table 7.18, two criteria appear to have increased the number of sources which contributed to collected particulate matter:

- increases in the number of collected samples. The receptor models illustrated in Table 7.18 were performed on data sets that contained 130, 70, 332 and 99 samples, significantly greater than the 40, 51 and 38 samples collected at Lincoln, Bolsover and

Table 7.18 Comparison of receptor models to apportion the origin of aerosols

Receptor model	Number of Samples	Number of Sources	Source type (tracer)	Percentage contribution	Reference
FA/MR	130	4 + intercept	Secondary aerosol (SO_4^{2-}) Soil resuspension (Fe) Motor vechicles (Pb) Oil burning (V) Intercept	55 29 8 5 3	Ito *et al.* (1986)
PCA/MR	70	6 + intercept	Soil origin (Al) Traffic emissions (organic carbon) Sea spray (Na) Ammonium salts (SO_4^{2-}) Oil combustion (both Ni and Cr) Intercept	37 18 8 24 1 12	Pio *et al.* (1989)
RAPCS	332	6 + intercept	Soil (Si) Motor vehicles (Pb) Residual oils (V) Refuse burning (Cu) Salt (Cl) Coal related (As) Sulphate (S) Intercept	26 12 9 2 2 27 5 17	Thurston and Spengler (1985)
TTFA	99	5 + unknown	Sulphate (SO_4^{2-}) Fly/ash (Si) Paint (Ti) Refuse (Zn) Motor vehicle (Pb) Unknown	65 11 1 4 15 4	Alpert and Hopke (1981)

Wells, respectively.

- measurement of elements uniquely characterisitic of a particular source. For example, measurement of arsenic and vanadium were used to assess the contribution of coal and oil burning to samples collected by Thurston and Spengler (1985). Alternatively nickel and chromium were used by Pio *et al.* (1989) to identify oil combustion sources. Alpert and Hopke (1981) were able to identify the contribution of paint vapour to their collected particulate samples by measuring the titanium content of collected samples. The lack of sensitivity in the method of instrumental analysis chosen to analyse the trace metals (ICP-AES) obviously hindered the accurate detection of metals such as arsenic and chromium in this study.

Another reason for lack of resolution in the data set, despite the number variables measured ranging from 11 and 16, was that at least four of the major ions measured in

this study (SO_4^{2-}, NO_3^-, Cl^- and NH_4^+) are each predominant constituents of the secondary particulate matter, effectively reducing the number of variables that may have been unique identifiers of contributing sources.

7.3.6 Summary

The three receptor methods used in this study determined that three sources were contributing to the particulate matter collected at each sampling site. However, although each method used principal component analysis or factor analysis and multiple regression analysis as an integral part to the respective technique, slightly different inferences about the nature of the contributing sources were obtained. For example, the PCA/MR method, discussed in Section 7.3.2, estimated that the secondary particulate source contributed approximately 60% of the particulate mass determined at Bolsover.

This was approximately four times the contribution of secondary particulate matter at Wells. However, only 50% of the mass was accounted for at Wells, with the remainder attributed probably to organic material. Secondary particulate matter was the most significant contributor to samples collected at Lincoln, with approximately 25% of the observed TSP concentration attributed to an unknown source.

The mass contributions determined using the regression on absolute principal component scores method (Section 7.3.3) and the target transformation factor analysis (Section 7.3.4) methods totally accounted for the source contributions with no allocation from an unknown source.

The RAPCS method estimated that both the SPM and a crustal/metal sources contributed approximately 40% to the particulate mass concentration at Lincoln. As for the PCA/MR method, 60% of the collected mass at Bolsover was estimated to have originated from SPM. At Wells the soil source was estimated to contribute approximately 50% of the observed mass, with SPM contributing the least mass (18%).

The source profiles, which show the relatively proportion of the constituent parts of each source, were determined using the RAPCS and TTFA methods. However, only

the relative proportion of the secondary particulate matter source was significantly determined. The best source profile was obtained for the SPM source at Wells where NH_4^+, SO_4^{2-} and NO_3^+ together accounted for more than 90% of the particulate mass contribution.

A criticism to the use of receptor models is that the contributing sources were assumed to be constant throughout the sampling period which is an unlikely situation in a constantly changing atmospheric environment.

CHAPTER 8: CONCLUSIONS AND SUGGESTIONS FOR FURTHER RESEARCH

8.1 Deterioration of limestone buildings

The industrialisation which has occurred in the UK during the last two hundred years has resulted in significant increases in the amount of sulphur dioxide, nitrogen oxides and carbon dioxide released into the atmosphere. Early studies which examined the role of atmospheric pollutants in the stone deterioration process (Honeyborne and Price, 1977 and Jaynes and Cooke, 1987) found that deterioration rates were higher in urban areas compared to non-urban areas, with the principal reason for greater decay in the urban area attributed mainly to higher sulphur dioxide concentrations.

Rainfall, or more specifically the hydrogen ions contained within the rainfall, was shown by Lipfert (1989), Baedecker *et al.* (1992) and Webb *et al.* (1992) to be the principal atmospheric agent responsible for bringing about stone decay in relatively non-polluted atmospheres. The Lipfert (1989) and Webb *et al.* (1992) studies each attempted to link the stone deterioration to the amount of pollutants delivered to the stone surface by using a chemical dissolution model. The amount of stone loss, calculated by each model, for a range of concentrations was illustrated in Figures 2.3 and 2.4, respectively. A major difference between the two models was that the Lipfert (1989) model assumed a constant surface recession rate (18 μm m^{-1} incident rainfall), while the Webb *et al.* (1992) model calculated the amount of dissolution due to rainfall by measuring the hydrogen ion concentration in surface runoff.

The presence of atmospheric sulphur dioxide and nitric acid can be seen in both Figures 2.3 and 2.4, to become important at high atmospheric concentrations. For example, the Lipfert model estimated that the concentration must exceed 115 μg m^{-3} to approach the deterioration rate attributed to the natural solubility of limestone in rainfall (the clean rain effect), while the concentration of HNO_3 must exceed 35 μg m^{-3} to have a similar effect. Clearly the role of SO_2 in altering building stones has been significantly reduced compared to concentrations experienced several decades ago. However, as nitrogen oxide concentrations are expected to decrease (QUARG, 1993), the role of nitric acid

in future stone deterioration processes cannot be determined with confidence. Likewise, uncertainities in future acid aerosol concentrations make their evaluation in the stone deterioration process equally uncertain.

Recent increases in the amounts of nitrogen dioxide released into the atmosphere have also prompted laboratory studies, such as those carried out by Haneff *et al.* (1992), to investigate the role played by the gas in the deterioration process. From the various regimes examined including dry and wet deposition both with and without ozone, only dry conditions in the presence of ozone (10 ppmv) exceeded the deterioration experienced for SO_2 under similar conditions for two of the four stone types examined. This reversal in the typical order of reactivity ($SO_2 > NO_2$), was attributed to the formation of gypsum on the stones, which, having a relatively small porous structure, impeded further sulphur dioxide deposition. In conclusion, extrapolation of such detailed laboratory work to the ambient atmosphere suggested that NO_2 and NO play relatively minor roles in the alteration of limestone materials.

Investigations into the stone deterioration hence have concentrated on exposure techniques which attempt to measure deterioration as a function of either a physical property of the stone, such as weight change, or a change in the chemistry of water that flows over the exposed surface. A future research project could examine in detail the microprocess that occur on the stone surface. Such microprocesses that would provide valuable insight into the overall deterioration process include:

- expansion of material, such as water freezing or hydrating gypsum crystallisation, in stone pores, and assessing the forces generated
- migration of deterioration products into the actual body of the stone

This knowledge would assist the continuing development of resins and coatings that ideally can be applied to a building surface to prevent deterioration. Materials that may be used include, natural and synthetic waxes, vinyl polymers, acrylic resins, silicones and epoxy resins (Amoroso and Fassina, 1983). However, as these materials too are subjected to degrading influences, such as ultra-violet light, developmental research is continuing into preparation of a perfect conserving material.

8.2 Deposition of sulphur and nitrogen

The primary purpose of this study was to measure the deposition fluxes of both sulphur and nitrogen onto historic monuments by the following deposition pathways,

- dry deposition of particulate matter
- dry deposition of gases
- wet deposition, resulting from the presence of each element in deposited rainfall

Compared to those exposure simulations presented in Section 2.4.2.2, sulphate and nitrate dry deposition fluxes are significantly lower than those demonstrated to cause alteration. For example, Haneff *et al.* (1992) used a sulphate deposition flux of 16×10^{-3} $\mu g\ cm^{-2}\ s^{-1}$ to investigate weight loss from stone tablets, whereas in this study estimated dry deposition fluxes (Table 6.12) ranged from 2.2×10^{-6} $\mu g\ cm^{-2}\ s^{-1}$ during June 1991 at Wells to 45×10^{-6} $\mu g\ cm^{-2}\ s^{-1}$ during January 1991 at Bolsover.

The high wet deposition flux for sulphate (19×10^{-6} $\mu g\ cm^{-2}\ s^{-1}$) during June 1991 at Wells was approximately an order of magnitude less than the wet deposition flux used by Haneff *et al.* (1992) to produce significant weight loss during a laboratory based exposure study (Table 2.10). The amount of nitrate deposited during July 1991 (21×10^{-6} $\mu g\ cm^{-2}\ s^{-1}$) was proportionally closer to that in the laboratory study (80×10^{-6} $\mu g\ cm^{-2}\ s^{-1}$). However, as hydrogen ions were shown in Chapter 2 to be the most important constituent of rainfall deposited onto a limestone surface, knowledge regarding the amount of sulphate and nitrate co-deposited may not necessarily provide beneficial information relating to the alteration of the stone's surface.

Determining the role that sulphur and nitrogen specifically play in the deterioration process is difficult. For example, a physical damage function for sulphur and nitrogen, as sulphate and nitrate, respectively, like that described previously for the case of H^+, would obviously seek to determine stone deterioration in terms of amount of each species deposited. Each species would be expected to combine with calcium ions to form calcium sulphate or calcium nitrate, which depending on the micrometeorological conditions, form a matrix of deterioration products which may consist of anhydrous

salts. These anhydrous salts may, on the addition of water, dissolve and migrate into pores and capillaries where they can expand, when water evaporates. Alternatively the products may be washed away. Inevitably, a great many difficulties exist with this proposed scheme, since the availability of calcium ion is inextricably linked to the presence of H^+.

Finally, perhaps the most effective way of reducing stone deterioration rates is to dramatically reduce the amount of pollutants entering the atmosphere, this would require changes in how energy is obtained in this country. Obviously given the importance of energy production from combustion processes, this idea is unrealistic.

8.3 Interaction between sulphur and nitrogen in the aqueous, gaseous and particulate phases

After release from their respective sources, and before deposition to the building surface, sulphur dioxide and the nitrogen oxides, NO_2 and NO, may be further oxidised to sulphate and nitrate. The mechanisms by which these conversions take place were discussed in Chapter 3. The oxidation of sulphur dioxide was shown to occur in either the gaseous or aqueous phases. Nitrogen dioxide was shown to be oxidised mainly in the gas phase to nitric acid (which at high concentrations is expected to act as a corrosive agent) or peroxyacetylnitrate (an important component of photochemical smog).

Particulate sulphate and sulphur dioxide concentrations were found to be statistically related during winter time, whereas no corresponding relationship was found during the summer time (Section 6.2.3.1). The former observation was attributed to sulphate and sulphur being emitted together. The lack of a statistical relationship between the sulphur in the gaseous and particulate phases, during the summer time was probably due to a significant proportion of the sulphur already existing in the oxidised (VI) state. This observation is to be expected since higher photochemical oxidant concentrations are present during the summer months.

Assessing the amount of sulphate formed in both the homogeneous and heterogeneous

phases, would provide a major and useful undertaking. In the homogeneous phase, this could involve measuring all the major oxidants: $OH^{\cdot}$, H_2O_2, O_3, and the concentrations of SO_2 and SO_4^{2-}, over small time intervals and observing if patterns in the concentrations of each species are present. Similarly in the aqueous phase, the simultaneous measurement of oxidants in water droplets, along with sulphur in the fourth and sixth oxidation states, may provide insight in to the relative oxidation pathways. A similar operation could be conducted for the formation of nitrate, but this would be an even more extensive operation given the greater number of possible intermediatory products involved.

The amount of sulphur in precipitation originating from sulphur in both the particulate matter and gaseous forms was estimated using a multiple regression model. For those twenty nine events for which the simultaneous measurement of sulphur in the aqueous, particulate and gaseous phases occurred, approximately eighty percent of the sulphur in precipitation was found to have originated from sulphur dioxide (Section 6.4.2). This causal relationship between sulphur in the aqueous and gaseous phases would suggest that sulphur dioxide concentrations should be taken into account when determining washout ratios.

8.4 Receptor modelling

The three receptor modelling techniques:

- regression of TSP on elements selected using principal component analysis (PCA/MR)
- regression on absolute principal component scores (RAPCS)
- FANTASIA, a designated computer software package for apportioning the origin of aerosols,

were each employed in an attempt to determine information about contributing pollution sources. As each employed the same mathematical techniques; principal component analysis and multiple regression analysis, similar results, such as the number and identity of sources and to a certain extent, the amount of material from each source, were obtained.

Principal component analysis of correlation matrices was found to yield only three sources, much less than the expected number contributing in the rapidly changing atmosphere. This was a consequence of the limited number of tracers used. Greater source resolution would be obtained by using organic materials characteristic of organic sources, such as the polyaromatic hydrocarbon pyrene which is characteristic of incomplete diesel combustion. Alternatively lead, although decreasing in atmospheric concentration, could be used as an atmospheric tracer for ignition system automobiles. Unfortunately, the low sensitivity of the ICP-AES prevented the use of lead in this study. Despite the lack of source resolution, the receptor models employed in this project have identified sources such as secondarily formed particulate matter, sea-salt and crustal matter which do contribute to particulate matter.

The three receptor models varied greatly in their ease of use and initial accessability to a non-statistician, with the PCA/MR method being the simplest and the FANTASIA method the most difficult. A natural advancement in the use of receptor models would be to write an interactive computer software package that would allow, perhaps with graphical display, the rapid assessment of output.

In addition, each receptor model employed in this study was of limited use as a pollution monitoring device since actual information regarding the nature of the pollution sources could only be obtained after the collected particulate samples had been analysed in the laboratory. A way of alleviating this disadvantage is to use those gaseous pollutants measured within a relatively short time period, as input data into a receptor model designed to immediately identify potential pollutant sources. Such gases could include those measured in current monitoring programmes, such as CO, SO_2, O_3, PM_{10} and NO_2 measured routinely in the Enhanced Urban Network or a range of organic chemical measured by several local authorities in the United Kingdom using differential optical absorption spectroscopy.

REFERENCES

Adams F, Van Craen Van Espan (1980) The elemental composition of atmospheric aerosol particles at Chacaltaya, Bolivia. *Atmospheric Environment* **23** 893.

Adams F.C. and Van Borm (1989) Characterisation of individual particles in the Antwerp aerosol *Atmospheric Environment* **23** 1139-1151.

Alpert D.J. and Hopke P.K. (1980) A quantitative determination of source in the Boston urban aerosol *Atmospheric Environment* **23** 1137-1146.

Alpert D.J. Hopke P.K. (1981) A Determination of the sources of airborne particles as collected during the regional air pollution study *Atmospheric Environment* **15** 657-687

Altshuller A.P. (1979) Model predictions of the rates of the homogeneous oxidation of sulphur dioxide to sulphate in the troposphere *Atmospheric Environment* **13** 1653-1661

Altshuller A.P. (1980) Seasonal and episodic trends in sulphate concentrations (1963-1978) in the Eastern United States *Environmental Science and Technology* **14** 1337-1349

Amoroso G.G. and Fassina V. (1983) *Stone Decay and Conservation. Atmospheric Pollution, Consolidation and Protection.* Materials Science Monographs, 11. Elsevier

Baedecker P.A., Reddy M.M., Reinmann K.J. and Sciammarella (1992) Effects of the acidic deposition of the erosion of carbonate stone - Experimental results from the U.S. National Acid Precipitation Assessment Program (NAPAP) *Atmospheric Environment* **26B** 147-158

Baeyens W. and Dedeurwaerder H. (1991) Particulate trace metals above the Southern Bight of the North Sea-I. Analytical procedures and average aerosol concentrations *Atmospheric Environment* **25A** 293-304

Balls P.W. (1989) Trace metal and major ion composition of precipitation at a North Sea coastal site *Atmospheric Environment* **23** 2751-2759

Barrie L.A. (1981) The prediction of rain acidity and SO_2 scavenging in Eastern North America. *Atmospheric Environment* **15** 31-41.

Barrie L.A. (1985) Scavenging ratios, wet deposition, and in-cloud oxidation: an application to the oxidies of sulphur and nitrogen *Journal of Geophysical Research* **90** 5789-5799

Barrie L.A. and Neustadter J. (1985) The dependence of sulphate scavenging ratio on meteorological variables. In the proceedings of the Fourth International Conference (29th November to 3rd December) pp. 203-211 Elsevier.

Beilke S. and Gravenhorst G. (1978) Heterogeneous SO_2-oxidation in the droplet phase *Atmospheric Environment* **12** 231-239

Boss C.B. and Fredman K.J. (1989) *Concepts, Instrumentation, and Techniques in Inductively Coupled Atomic Emission Spectometry* The Perkin-Elmer Corporation

Bowens H.J.M. (1979) *Environmental Chemistry of the elements* Academic Press, London

Braun R.C. and Wilson M.J.G. (1970) The removal of atmospheric sulphur by building stones *Atmospheric Environment* **4** 371-378.

Brimblecombe P. (1986) Air - Composition and Chemistry *Cambridge Environmental Chemistry Series* Cambridge University Press

Building Effects Review Group Report (BERG) (1989) The effects of acid deposition on buildings and building surfaces in the United Kingdom, HMSO.

Butler T.J. and Likens G.E. (1991) The impact of changing regional emissions on precipitation chemistry *Atmospheric Environment* **25A** 305-315

Butlin R.N., Coote A.T., Devenish M., Hughes I.S.C., Hutchens C.M., Irwin J.G., Lloyd G.O., Massey S.W., Webb A.H. and Yates T.J.S Preliminary results from the analysis of stone tablets from the National Material Exposure Programme (NEMP) *Atmospheric Environment* **26B** 189-198

Cadle S.H., Muhlbaier Dasch J. and Mulawa P.A. (1985) Atmospheric concentrations and the deposition velocity to snow of nitric acid, sulphur dioxide and various particulate species *Atmospheric Environment* **19** 1819-1827

Calvert J.G. and McQuigg (1975) The computer simulation of the rates and mechanisms of photochemical smog formation. In *Chemical Kinetics Data for the Upper and Lower Atmospheres, International Journal of Chemical Kinetics Symposium* **1** pp.113-163.

Calvert J.G., Su F., Bottenheim J.W. and Strauz O.P. (1978) Mechanism of the homogeneous oxidation of sulphur dioxide in the troposphere *Atmospheric Environment* **12** 197-226

Carroll J.D. and McInnes G. (1988) *Multi-element and sulphate in particulate surveys: summary of the eighth year's results (1984-84)* Stevenage: Warren Spring Laboratory, 1988 Report LR 655 (AP) M

Camuffo D., Del Monte M., Sabbioni C. and Vittori O. (1982) Wetting, deterioration and visual features of stone surfaces in an urban area *Atmospheric Environment* **16** 2253-2259

Chan W.H. and Chung D.H.S. (1986) Regional-scale precipitation of SO_2, SO_4^{2-}, NO_3^- and HNO_3 *Atmospheric Environment* 1397-1402

Cheng R.J. and Show-Mei Leu (1987) Deterioration of marble structures: the role of acid rain *Analytical Chemistry* **59** 104.

Cheng M.D., Hopke P.K., Landsberger S. and Barrie L.A. (1991) Distribution

characteristic of trace elements and ionic species of aerosol collected at Canadian High Arctic *Atmospheric Environment* **25A** 2903-2909

Cho S., Chang Y.S. and Carmichael G.R. (1989) An evaluation of the effect of reductions in ambient levels of primary pollutants on sulphate and nitrate wet deposition *Atmospheric Environment* **23** 1009-1031.

Clarke A.G., Willison M.J. and Zeki E.M. (1984) A comparison of urban and rural aerosol composition using dichotomous samplers *Atmospheric Environment* **18** 1767-1775.

Clarke A.G., Lambert D.R. and Willison M.J. (1990) Trends in particulate deposition and precipitation chemistry at Leeds (U.K.) 1907-1987 *Atmospheric Environment* **24B** 159-169

Clarke A.G. Radojevic M. (1987) Oxidation of SO_2 in rainwater and its role in acid rain chemistry *Atmospheric Environment* **21** 1115-1123.

Clarke P.A., Fisher B.E.A. and Scriven R.A. (1987) The wet deposition of sulphate and its relationship to sulphur dioxide emissions *Atmospheric Environment* **21** 1125-1131

Cox R.A. and Penkett S.A. (1971) Photo-oxidation of atmospheric SO_2 *Nature* **229** 486-488

Cox R.A. (1984) Atmospheric chemistry: a review of progress in the past decade *Journal of Photochemistry* **25** 43-48

Cullis C.F. and Hirschler M.M. (1980) Atmospheric sulphur: natural and man-made sources *Atmospheric Environment* 1263-1278

Damschen D.E. and Martin L.B. (1983) Aqueous aerosol oxidation of nitrous acid by O_2, O_3 and H_2O_2 *Atmospheric Environment* **17** 2005-2011

De Santis F. and Allegrini I. (1992) Heterogeneous reactions of SO_2 and NO_2 on carbonaceous surfaces *Atmospheric Environment* **26A** 3061-3064

Del Monte M., Sabbioni C. and Vittori O. (1981) Airborne carbon particles and marble deterioration *Atmospheric Environment* **15** 645-652.

Del Monte M., Sabbioni C. and Vittori O. (1984) Urban stone sulphation and oil-fired carbonaceous particles *Science of the Total Environment* **36** 369-376.

Del Monte M. and Sabbioni C. (1986) Chemical and biological weathering of an historical building: Reggio Emilia Cathedral *Science of the Total Environment* **50** 165-182.

Delopoulou P. and Sikiotis D. (1992) A comparison of the corrosive action on Pentelic marble of nitrates and sulphates with the action of nitrogen oxides and sulphur dioxide *Atmospheric Environment* **26B** 183-188

Digest of Environmental Protection and Water Statistics, (1993) HMSO

Dignon J. (1992) NO_x and SO_x emissions from fossil fuels: a global distribution *Atmospheric Environment* **26A** 1157-1163

Draper N.R. and Smith H. (1981) *Applied Regression Analysis* Wiley Series in Probability and Mathematical Statistics

Eggleton A.E.J. and Cox R.A. (1978) Homogeneous oxidation of sulphur compounds in the atmosphere *Atmospheric Environment* **12** 227-230

Eggleston S., Hackman M.P., Heyes C.A., Irwin J.G., Timmis R.J. and Williams M.L. (1992) Trends in urban air pollution in the United Kingdom during recent decades *Atmospheric Environment* **26B** 227-239

Erisman J.W., De Leeuw F.A. and Van Aalst R.M. (1989) Deposition of the most acidifying components in the Netherlands during the period 1980-1986 *Atmospheric Environment* **23** 1051-1062

Fassina V., Lazzarini L. and Biscontin G. (1976) Effects of atmospheric pollutants on the composition of black crusts deposited on Venetian marbles and stones. In the Proceedings of the Second International Symposium on the Deterioration of Building Stones, Athens, September 27th to October 1st, 1976. NTU, Athens pp. 201-211

Feddema J.J. and Meierding T.C. (1987) Marble weathering and air pollution in Philadelphia *Atmospheric Environment* **21** 143-157.

Fergusson (1982) *Inorganic Chemistry and the Earth. Chemical Resources, Their Extraction, Use and Environmental Impact.* Pergamon Series on Environmental Science, Volume Six.

Fisher B.E.A. (1975) The long range transport of sulphur dioxide. *Atmospheric Environment* **9** 1063-1070

Fisher B.E.A. (1978) The calculation of long-term sulphur deposition in Europe. *Atmospheric Environment* **12** 489-501

Fisher B.E.A. (1984) The long range transport of air pollutants - some thoughts on the state of modelling *Atmospheric Environment* **18** 553-562.

Fisher B.E.A. (1982) Deposition of sulphur and the acidity of precipitation over Ireland. *Atmospheric Environment* **16** 2725-2734.

Fowler D. (1978) Dry deposition of SO_2 on agriculture crops *Atmospheric Environment* **12** 369-373.

Francis W. and Peters W.C. (1980) *Fuels and Fuel Technology* Second Edition Pergamon Press

Friedlander S.K. (1973) Chemical element balances and identification of air pollution

sources *Environmental Science and Technology* **7** 235-237

Fung C.S., Misra P.K., Bloxam R. and Wong S. (1991) A numerical experiment on the relative importance of H_2O_2 and O_3 in aqueous conversion of SO_2 to SO_4^{2-} *Atmospheric Environment* **25A** 411-423

Galloway J.M.and Likens G. (1981) Acid precipitation: the importance of nitric acid *Atmospheric Environment* **15** 1081-1085

Garland J.A. (1974) Deposition of gaseous sulphur dioxide to the ground *Atmospheric Environment* **8** 75-79.

Garland J.A. and Branson J.R. (1976) The mixing height and mass balance of SO_2 in the atmosphere above G.B. *Atmospheric Environment* **10** 353-362.

Garland J.A. (1977) The dry deposition of sulphur dioxide to land and water surfaces *Proceedings of the Royal Society, London* **A 345** 245-268.

Garland J.A. and Branson J.R. (1977) The deposition of sulphur dioxide to pine forest assessed by a radioactive tracer method *Tellus* **29** 445-454

Garland J.A. (1978) Dry and wet removal of sulphur from the atmosphere *Atmospheric Environment* **12** 349-362.

Gauri K.L. and Holden G.C. (1981) Pollutant effects on stone monuments *Environmental Science and Technology* **15** 386-390

Gay A.J., Humphrey P., van Duin P.J. and Henderson D.K. (1989) A study of some trace elements on coal fly-ash particles by secondary ion mass spectroscopy (SIMS) Netherlands organisation for applied scientific research. TNO-Report. Report number 89/008b

Georgii H-W, Jost D. and Vitze W. Konzentration und Grössenverteilung des sulphate aerosols in der unteren und mittleren troposphäre. Berichte des Institutes für Meteorologie und Geophysik der Universität Frankfurt/MaineNr. 23

Girardet F. and Furlan V. (1989) The ratio between the dry deposition of sulphur by aerosol and gas on vertical stone surfaces. In the proceedings of the European Symposium *Science. Technology and European Cultural Heritage* Bologna. pp. 350-353. Published in 1991 by Butterworth-Heinemann Limited. Editors Baer N.S., Sabbioni C. and Sors A.I.

Golterman H.L., Clymo R.S. and Ohnstad M.A.M. (1984) Methods for Physical and Chemical analysis of Fresh Waters *IBP Handbook* **No. 8**. Second Edition Blackwell Scientific Publications

Goodman R.A. *Introduction to Rock Mechanics.* Second Edition. John Wiley and Sons

Gorden G.E., Pierson W.R., Daisey J.M. Cooper J.A. Watson J.G. and Cass G.R. (1984) Considerations for design of source apportionment studies *Atmospheric*

Environment **18** 1567-1582

Greenwood N.N. and Earnshaw A. (1984) *The Chemistry of the Elements* Pergamon Press

Grigić I., Hudnik V., Bizak M. and Levec J. (1992) Aqueous S(IV) oxidation -II. Synergistic effects *Atmospheric Environment* **26A** 571-577

Hackman M.P., Timmis R.J. and Walker C.A. (1992) Studies of past and present concentrations of sulphur dioxide in Lincoln from measurements and dispersion modelling LR 732 (AP) Warren Spring Laboratory, Stevenage

Hales J.M. (1978) Wet removal of sulphur compounds from the atmosphere *Atmospheric Environment* **12** 389-399.

Hales J.M. and Dana M.T. (1979) Regional-scale deposition of sulphur dioxide by precipitation scavenging *Atmospheric Environment* **13** 1121-1132

Haneff S.J., Johnson J.B., Dickinson C., Thompson G.E. and Wood G.C. (1992) Effect of dry deposition of NO_x and SO_2 gaseous pollutants on the degradation of calcareous building stones *Atmospheric Environment* **26A** 2963-2974

Harman H.H. (1976) *Modern Factor Analysis* Third Edition. The University of Chicago Press

Harrison R.M. and McCartney H.A. (1980) Ambient air quality at a costal site in rural NW.England *Atmospheric Environment* **14** 233-244

Harrison R.M. and Pio C.A. (1983) Size-differentiated composition of inorganic atmospheric aerosols of both marine and polluted continental origin *Atmospheric Environment* **17** 1733-1738.

Harrison R.M. and Pio C.A. (1983) A comparative study of the ionic composition of rainwater and atmospheric aerosols:implications for the mechanism of acidification of rainwater *Atmospheric Environment* **17** 2539-2534.

Harrison R.M. and Perry R. (1986) *Handbook of Air Pollution Analysis* 2nd Edition. Chapman and Hall Limited

Harrison R.M., Rapsomanikis S. and Turnbull A. (1989) Land surface exchange in a chemically-reactive system;surface fluxes of HNO_3, HCl and NH_3 *Atmospheric Environment* 1795-1800

Harrison R.M. (1990) *Pollution: Causes, Effects and Control* Second Edition, Royal Society of Chemistry

Harrison R.M. and Allen A.G. (1990) Measurements of atmospheric HNO_3, HCl, and associated species on a small network in Eastern England *Atmospheric Environment* **24A** 369-376.

Harrison R.M. and Kitto A.B.N. (1992) Nitrous and nitric acid measurements at sites in south-east England *Atmospheric Environment* **26A** 235-241

Harrison R.M., Nedwell D.B. and Shabbeer M.T. (1992) Factors influencing the atmospheric flux reduced sulphur compounds from inter-tidal areas *Atmospheric Environment* **26A** 2381-2387

Heaton C.A. (1986) *The Chemical Industry* Blackie and Sons Limited.

Heaton R.W., Rahn K.A and Lowenthal D.H. (1990) Determination of trace elements, including regional tracers, in Rhode Island precipitation *Atmospheric Environment* **24A** 147-153

Hegg D.A. and Hobbs P.V. (1981) Cloud water chemistry and the production of sulphates in clouds *Atmospheric Environment* **15** 1597-1604

Hegg D.A., Hobbs P.V. and Radke L.F. Measurements of the scavenging of sulphate and nitrate in clouds *Atmospheric Environment* **18** 1939-1946

Heikes B.G. and Thompson A.M. (1983) Effects of heterogenenous processes on NO_3, HONO, HNO_3 chemistry in the troposphere *Journal of Geophysical Research* **88** C15 10,883-10895

Heikes B.G., Kok G.L., Walega J.G. and Lazrus A.L. (1987) H_2O_2, O_3 and SO_2 measurements in the lower troposphere over the Eastern United States *Journal of Geophysical Research* **92** D1 915-931

Henry R.C. (1987) Current factor analysis models are ill-posed *Atmospheric Environment* **21** 1815-1820

Henry R.C. (1992) Dealing with near collinearity in chemical mass balance receptor models *Atmospheric Environment* **26A** 933-938

Hessley P.K, Reasoner J.W. and Riley J.T. (1982) *Coal Science. An Introduction to Chemistry, Technology and Utilisation* John Wiley and Sons Limited

Hewitt C.N. and Harrison R.M. (1985) Tropospheric concentrations of the hydroxyl radical *Atmospheric Environment* **19** 545-554.

Hidy G.M. and Countess R. (1984) Combined analysis of air quality and precipitation chemistry. pp. 37-62. In *Deposition Both Wet and Dry* Edited by Hicks B.B. Acid Precipitation Series Volume 4 Ann Arbor Science. Butterworth Publishers.

Hilst G.R. and Chapman E.G. (1990) Source-receptor relationships for wet SO_4^{2-} and NO_3^- production *Atmospheric Environment* **24A** 1889-1901

Hinds W.C. (1982) *Aerosol Technology - Properties, Behaviour, and Measurement of aribornes paricles* John Wiley and Sons

Hitzberger R., Horvath H., Pimminger M. and H.Puxbaum (1985) Variability of rural aerosols under stable weather conditions *Atmospheric Environment* **19** 159-164.

Hollander W. (1990) Proposed performance criteria for samplers of total suspended

particulate matter *Atmospheric Environment* **24A** 173-177

Honeyborne D.B. and Price C.A. (1977) Air pollution and the decay of limestone buildings, BRE Note 117/77

Hopke P.K., Gladney E.S., Gordon G.E., Zoller W.H. and Jones A.G. (1976) The use of multivariate analysis to identify selected elements in the Boston aerosol *Atmospheric Environment* **10** 1015-1025

Hopke P.K. (1985) A Comparison of R and Q modes in target transformation factor analysis for resolving environmental data (a Discussion) *Atmospheric Environment* **19** 1549-1553

Hopke P.K., Alpert D.J. and Roscoe B.A. (1983) Fantasia - A program for target transformation factor analysis to apportion sources in environmental samples *Computers and Chemistry* **7** 149-155

Hopke P.K. (1984) *Receptor modelling in Environmental Chemistry* Wiley

Hopke P.K. and Dharmavaram S. (1986) Recent improvements to Fantasia, a target transformation factor analysis program *Computers and Chemistry* **10** 163-164

Hopke P.K. (1989a) FANTASIA. Factor analysis to apportion sources in aerosols. *User's Manual*

Hopke P.K. (1989b) Target Transformation factor analysis as aerosol mass apportionment method: a review and sensitivity study *Atmospheric Environment* **22** 1777-1792

Huebert B.J. and Lazrus A.L. (1979) Tropospheric measurements of nitric acid vapour and particulate nitrate. In *Nitrogeneous Air Pollutants-Chemical and Biological Implications*. Edited by Grosjean D. Ann Arbor Science. Butterworth Publishers.

Husain L. (1984) Mn/V ratio as a tracer of aerosol transport *Atmospheric Environment* **18** 1059-1071.

Husain L. and Dutkiewicz V.A. (1990) A long-term (1975-1988) study of atmospheric SO_4^{2-}: Regional contributions and concentration trends *Atmospheric Environment* **24A** 1175-1187

Hutchinson A.J., Johnson J.B. Thompson G.E., Wood G.C., Sage P.W. and Cooke M.J. (1992) Stone degradation due to dry deposition of HCl and SO_2 in a laboratory-based exposure chamber *Atmospheric Environment* **26A** 2785-2793

Hutchinson A.J., Johnson J.B. Thompson G.E., Wood G.C., Sage P.W. and Cooke M.J. (1992) The role of fly-ash particulate material and oxide catalysts in stone degradation *Atmospheric Environment* **26A** 2795-2803

Hwang C.S., Severin K.G. and Hopke P.K. (1984) A comparison of R- and Q- modes in target transformation factor analysis for resolving environmental data *Atmospheric*

Environment **18** 345-352.

Ibrahim M., Barrie L.A. and Fanaki F. (1983) An experimental and theoretical investigation of the dry deposition of particles to snow, pine trees and artifical collector *Atmospheric Environment* **17** 781-788

Ibusuki T., Ohsawa M. and Takeuchi K. (1990) Metal ion catalysed oxidations of SO_2 in the presence of trace H_2O_2 in aqueous solution under environmental conditions *Atmospheric Environment* **24A** 1325-1330.

Irwin J.G. and Williams M.L. (1988) Acid Rain: Chemistry and Transport *Environmental Pollution* **50** 29-59

Ito K., Kneip P.J. and Lioy P.J. (1987) The effects of number of sample and random error on the factor analysis/multiple regression method *Atmospheric Environment* **20** 1433-1440

Jacob P., Taveres T.M., Rocha V.C. and Klockow D. (1990) Atmospheric H_2O_2 field measurements in a tropical environment: Bahia, Brazil *Atmospheric Environment* **24A** 377-382.

Jaffrezo J-L. and Colin J-L. (1988) Rain-aerosol coupling in an urban area: scavenging ratio measurement and identification of some transfer processes *Atmospheric Environment* **22** 929-935

Jaffrezo J., Colin J-L and Gros J-M (1990) Some physical factors influencing scavenging ratios *Atmospheric Environment* **24A** 3073-3083

Jaynes S.M. and Cooke R.U. (1987) Stone weathering in south-east England *Atmospheric Environment* **21** 1601-1622.

Johansson L.-G., Lindqvist O. and Mangio R.E. (1988) Corrosion of calcareous stones in humid air containing SO_2 and NO_2. In *Air Pollution and Conservation - Safeguarding our Architectural Heritage* Edited by Rosvall J. Elsevier.

Johnson J.B., Haneff S.J., Hepburn B.J. Hutchinson A.J., Thompson G.E. amd Wood G.C. (1990) Laboratory exposure systems to simulate atmospheric degradation of building stone under dry and wet deposition conditions *Atmospheric Environment* **24A** 2585-2592

Johnson R.A. and Wichern D.W. (1988) *Applied Multivariate Statistical Analysis* Second Edition, Prentice-Hall International Editions

Joranger E. and Semb A. (1989) Major ions and scavenging of sulphate in the Norwegian Arctic *Atmospheric Environment* **23** 2463-2469

Judeikis H.S. and Stewart T.B. (1976) Laboratory measurement of SO_2 deposition velocities on selected building materials and soils. *Atmospheric Environment* **10** 769-776.

Kaplan W. (1981) *Advanced Mathematics for Engineers* Addison-Wesley Publishing Company

Katsoulis B.D. and Whelpdale D.M. (1990) Atmospheric sulphur and nitrogen budgets for Southeast Europe *Atmospheric Environment* **24A** 2959-2970

Keiding K., Jensen F.P. and Heidam N.Z. (1986) Absolute modelling of urban aerosol elemental composition by factor analysis *Analytica Chimica Acta* **181** 79-85

Keiding K., Pedersen J. and Jensen F.P (1988) A comparison of two procedures for modelling of absolute source contributions in urban air *Atmospheric Environment* **22** 763-767

Keller G.J., Spengler J.D., Koutrakis P., Allen G.A., Raizenne M. and Stern B. (1990) Transported acid aerosols measured in Southern Ontario *Atmospheric Environment* **24A** 2935-2950

Kirk-Ohmer (1982) *Encyclopedia of Chemical Technology* Third Edition Volume 17. John Wiley and Sons Limited.

Kleinman M.T., Pasterneck B.S., Eisenbud M. and Kneip T.J. (1980) Identifying and estimating the relative importance of sources of airborne particulates *Environmental Science and Technology* **14** 62-65

Kok G.L. (1980) Measurements of hydrogen peroxide in rainwater *Atmospheric Environment* **14** 653-656

Koutrakis P., Wolfson J.M. and Spengler J.D. (1988) An improved method for measuring aerosol strong acidity: results from a nine-month study in St.Louis, Missouri and Kingston, Tennessee *Atmospheric Environment* **22** 1576-162.

Kowalczyk G.S., Choquette C.E. and Gorden G.E.(1978) Chemical element balances and identification of air pollution sources in Washington D.C. *Atmospheric Environment* **12** 1143-1153.

Kowalczyk G.S., Gordon G.E. and Rheingrover S.W. (1982) Identification of atmospheric particulate sources in Washington, using chemical element balances *Environment Science and Technology* **16** 79-90 1982

Kozłowski R., Hejda A., Cęckiewicz and Haber J. (1992) Influence of water contained in porous limestone on corrosion *Atmospheric Environment* **26A** 3241-3248

Kraft J. and Van Eldik R (1989) The possible role of iron (III)-sulphur(IV) complexes in the catalysed autoxidation of sulphur(IV)-oxides. A mechanistic investigation. *Atmospheric Environment* **23** 2709-2713.

Kunen S.E., Lazrus A.L, Kok G.L. and Heikes B.G (1983) Aqueous oxidation of SO_2 by hydrogen peroxide *Journal of Geophysical Research* **88** C6 3671-3674

Lagrange J., Pallares C., Wenger G. and Lagrange P. (1993) Electrolyte effects on

aqueous atmospheric oxidation of sulphur dioxide by hydrogen peroxide *Atmospheric Environment* **27A** 129-137

Levine S.Z. and Schwartz S.E. (1982) In-cloud and below-cloud scavenging of nitric acid vapour *Atmospheric Environment* **16** 1725-1734

Leaderer B.P., Tanner R.L. and Holford T.R. (1982) Diurnal variations,chemical composition and relation to meteorological variables of the summer aerosol in the New York Subregion *Atmospheric Environment* **16** 2075-2087.

Lee R.E., Caldwell J., Akland G.G. and Fankhauser R. (1974) The distribution and transport of airborne particulate matter and inorganic components in Great Britain *Atmospheric Environment* **8** 1095-1109

Lee Y-N and Lind J.A. (1986) Kinetics of aqueous-phase oxidation on nitrogen (III) by hydrogen peroxide *Journal of Geophysical Research* **91** D2 2793-2800

Lee D.S. and Longhurst J.W.S. (1992) A statistical intercomparison between "urban" and "rural" precipitation data from Greater Manchester and two nearby secondary national network sites in the United Kingdom *Atmospheric Environment* **26A** 2869-2883

Levine S.Z. and Schwartz S.E. (1982) In-cloud and below-cloud scavenging of nitric acid vapour *Atmospheric Environment* **16**1725-1734

Leyson L., Roekens E.J., Storms H. and Van Grieken R.E. (1987) Classification of suspended particles in deposition samples and run-off water samples from a limestone cathedral *Atmospheric Environment* **21** 2425-2433.

Leyson L., Roekens E.J. Komy and Van Griekan R.E. (1987) A study of the weathering of an historical building *Analytica Chimica Acta.* **195** 247-255.

Leyson L., Roekens E. and Van Grieken R. (1989) Air-pollution-induced chemical decay of a sandy-limestone cathedral in Belgium *Science of the Total Environment* **78** 263-287

Lide D.R. (1990) *The Chemical Rubber Company* Seventy first Edition

Liberti A., Brocco D. and Possanzini M. (1978) Adsorption and oxidation of sulphur dioxide on particles *Atmospheric Environment* **12** 255-261.

Linberg S.E. and Lovett G.M. (1992) Deposition and forest canopy interactions of airborne sulphur: results from the integrated forest study *Atmospheric Environment* **26A** 1477-1492

Lipfert F.W. (1989) Atmospheric damage to calcerous stones; comparison and reconciliation of recent experimental research findings *Atmospheric Environment* **23** 415-429

Lipfert F.W., Morris S.C. and Wyzga R.E. (1989) Acid aerosol: The next criteria air pollutant? *Environmental Science and Technology* **23** 1316-1322

Maahs H.G. (1983) Measurements of the oxidation rate of sulphur (IV) by ozone in aqueous solution and their relevance to SO_2 conversion in nonurban tropospheric clouds *Atmospheric Environment* **17** 341-345

Maenhaut W. and Cornille P. (1989) Trace element composition and origin of the atmospheric aerosol in the Norwegian arctic *Atmospheric Environment* **23** 2551-1569 1551-2569.

Mamame Y and Dzubay T.G. (1986) Characteristics of individual particles at a rural site in the Eastern United States *Journal of Air Pollution Control Association* **36** 906-911

Mansfield F. (1980) Regional Air Pollution Study-Effects of airborne of sulphur pollutants on materials, EPA-600/4-80-007, US Environmental Protection Agency, Research Triangle Park

Martin L.R and Damschen D.E. (1981) Aqueous oxidation of sulphur dioxide by hydrogen peroxide at low pH *Atmospheric Environment* **15** 1615-1621

McArdle J.V. and Hoffman M.R. (1983) Kinetics and mechanism of the oxidation of aquated sulphur dioxide by hydrogen peroxide at low pH *Journal of Physical Chemistry* **87** 5425-5429

McElroy W.J. (1986) Sources of hydrogen peroxide in rainwater *Atmospheric Environment* **20** 427-438

McFarland M. (1979) Nitric oxide measurements in the Equatorial Pacific region *Geophysical Research Letters* **6** 605-608

McGee E.S. and Mossotti V.G (1992) Gypsum accumulation on carbonate stone *Atmospheric Environment* **26B** 249-253

McInnes G. *Multi-element and sulphate in particulate survey: summary and analysis of five years' results (1976-1981)* Stevenage: Warren Spring Laboratory, 1982 Report LR 435 (AP)

McMahon T.A. and Denison P.J. (1979) Empirical atmospheric deposition parameters - a survey *Atmospheric Environment* **13** 571-585

McRae G.J. and Russell A.G. (1984) Dry deposition of nitrogen-containing Species. In *Deposition Both Wet and Dry*. pp. 153-194 Edited by Hicks B.B. Acid Precipitation Series Volume 4 Ann Arbor Science. Butterworth Publishers.

Meagher J.F., Olszyna K.J., Weatherford F.P. and Mohnen V.A. (1990) The availability of H_2O_2 amd O_3 for aqueous phase oxidation of SO_2. The question of linearity. *Atmospheric Environment* **24A** 1825-1829

Middleton P, Kiang C.S. and Mohnen V.A. (1980) Theoretical estimates of the relative importance of various urban sulphate aerosol production mechanisms *Atmospheric Environment* **14** 463-472

Migon C. and Caccia J-L. (1990) Separation of anthropogenic and natural emissions of particulate heavy metals in the western Mediterranean atmosphere *Atmospheric Environment* **24A** 399-405.

Millar M.S., Friedlander S.K. and Hidy G.M. (1972) A chemical element balance for the Pasadena aerosol *Journal of Colloid and Interface Science* **30** 165-176

Miller J.C. and Miller J.N. (1984) Statistics for Analytical Chemistry *Ellis Horwood Series in Analytical Chemistry* John Wiley and Sons.

Moller D. (1984) Estimation of the global man-made sulphur emission *Atmospheric Environment* **18** 19-27.

Morandi M.T., Daisey J.M.and Lioy P.J. (1988) Development of a modified factor analysis/multiple regression to apportion suspended particulate matter in a complex airshed *Atmospheric Environment* **21** 1821-1831

Neter J., Wasserman W. and Whitmore G.A. (1988) *Applied Statistics* Third Edition Allyn and Bacon, Inc.

Nicholson K.W.(1987) Deposition of Caesium to surfaces of buildings *Radiation Protection Dosimetry* **21** 37-42.

Nicholson K.W.(1988a) The dry deposition of small particles: a review of experimental measurements *Atmospheric Environment* **22** 2653-2666.

Nicholson K.W. (1988b) The deposition of radioactive particulate material onto buildings *Air Pollution and its Application (VI)* Edited by Han van Dop, Plenum Publishing Corporation

Nicholson K.W. and Davies T.D. (1987) Field measurements of the dry deposition of particulate sulphate *Atmospheric Environment* **21** 1561-1571

Nicholson K.W. and Davies T.D. (1988) The dry deposition of sulphur dioxide at a rural site *Atmospheric Environment* **22** 2885-2889

Nicholson K.W. and Davies T.D. (1990) Sulphate in atmospheric particulate at five sites in Norwich (U.K.): use of national survey archive filters *Atmospheric Environment* **24B** 329-334.

Novakov T., Chang S.G. and Harker A.B. (1974) Sulphates as pollution particles: catalytic formation on carbon (soot) particles *Science* 30th October

O'Brien P.F., Cooper T.P. and Jeffrey D.W. (1992) Measurement of stone decay rates at remote locations using ion exchange resins *Environmental Technology* **13** 485-491

Okamoto S., Hayashi M., Nakajima M., Kainsuma Y. and Shinozama (1990) A factor analysis-multiple regression model for apportionment of suspended particulate matter *Atmospheric Environment* **24A** 2089-2097.

Organisation for Economic Cooperation and Development (OECD) (1991) Paris

Ottley C.J. and Harrison R.M. (1992) The spatial distribution and particle size of some inorganic nitrogen, sulphur and chlorine species over the North Sea *Atmospheric Environment* **26A** 1689-1699

Owers M.J. and Powell A.W. (1974) Deposition velocity of sulphur dioxide on land and water using a ^{35}S tracer method *Atmospheric Environment* **8** 63-67.

Palmes E.D., Gunnison A.F., DiMattio J. and Tomczyk C. (1976) Personal sampler for nitrogen dioxide *Journal of American Industrial Hygiene Association* **37** 570-577

Parekh P.P. and Husain L. (1981) Trace element concentrations in summer aerosols at rural sites in New York State and their possible sources *Atmospheric Environment* **15** 1717-1725

Parekh P.P., Ghauri B. and Husain L. (1989) Identification of pollution sources of anomalously enriched elements *Atmospheric Environment* **23** 1435-1442.

Parekh P.P. (1990) A study of manganese from anthropogenic emissions at a rural site in the Eastern United States *Atmospheric Environment* **24A** 415-421.

Payrissat M. and Beilke S. (1975) Laboratory measurements of the uptake of sulphur dioxide by different European soils *Atmospheric Environment* **9** 211-217.

Penkett S.A., Jones B.M.R. and Eggleton A.E.J. (1979) A study of SO_2 oxidation in stored water rainwater samples *Atmospheric Environment* **13** 139-147.

Penkett S.A., Jones B.M.R., Brice A. and Eggleton A.E.J. (1979) The importance of atmospheric ozone and hydrogen peroxide in oxidising sulphur dioxide in cloud and rainwater *Atmospheric Environment* **13** 123-137

Pio C.A. PhD Thesis 1981. University of Lancaster

Pio C.A., Nunes T.V., Borrego C.S. and Martins J.G. (1990) Assessment of air pollution sources in an industrial atmosphere using principal component and multilinear regression analysis *The Science of the Total Environment* **80** 279-292.

PORG (1990) *Oxides of Nitrogen in the United Kingdom* The Second Report of the United Kingdom Photochemical Oxidants Review Group. Department of the Environment.

QUARG (1993) *Urban Air Quality in the United Kingdom* The First Report of the Quality of Urban Air Review Group. Department of the Environment

Radojevic M., Tyler B.J., Wicks A.J., Gay M.J. and Choularton T.W. (1990) Field studies of the SO_2 /aqueous S(IV) equilibrium in clouds *Atmospheric Environment* **24A** 323-328.

RGAR (1987) *Acid Deposition in the United Kingdom* The Second Report of the Review Group on Acid Rain. Warren Spring Laboratory

Robinson E. and Robbins R.C. (1968) *Sources, abundance and fate of gaseous atmospheric pollutants.* Final Report, Project PR 6755. Stanford Research Institute,

Menlo Park, California

Rodhe H., Crutzen P. and Vanderpol A. (1981) Formation of sulfuric and nitric acid in the atmosphere during long range transport *Tellus* **33** 132-141.

Roekens E., Komy Z., Leyson L., Veny P. and Van Grieken R. (1988) Chemistry of precipitation near a limestone building *Atmospheric Environment* **22**

Roekens E., Bleyen C. and Van Grieken R. (1989) Sulphite and sulphate concentrations in weathering products of sandy limestone and in deposition samples *Environmental Pollution* **57** 289-298

Santachiara G., Prodi F. and Vivarelli F. (1989) Absorption of sulphur dioxide on monodisperse water droplets and catalytic activity of carbon particles *Atmospheric Environment* **23** 1775-1782.

Savoie D.L., Prospero J.M. and Nees R.T (1987) Washout ratios of nitrate, non-sea salt sulphate and sea salt on Virginia Key, Florida and on America Samoa *Atmospheric Environment* **21** 103-112

Saxena P. and Seigneur C. (1987) On the oxidation of SO_2 to sulphate in atmospheric aerosols *Atmospheric Environment* **21** 807-812.

Schaffer R.J. (1932) The weathering of natural building stones. *DSIR Building Research Special Report* **18**

Scheider W.A., Snyder W.R. and Clark B. (1980) Deposition of nutrients and major ions by precipitation in south-central Ontario *Water, Soil and Air Pollution* **12** 171-185

Scire J.S. and Venatram A. (1985) The contribution of in-cloud oxidation of SO_2 to wet scavenging of sulphur in convective clouds *Atmospheric Environment* **19** 637-650

Scorer R.S. (1992) Deposition of concentrated pollution at large distances *Atmospheric Environment* **26A** 793-803

Scott B.C. (1978) Parameterisation of sulphate removal by precipitation *Journal of Applied Meterology* **17** 1375-1389

Semb A. (1978) Sulphur emissions in Europe *Atmospheric Environment* **12** 455-460.

Sharp A.D., Trudgill S.T., Cooke R.U., Price C.A., Crabtree R.W., Pickles A.M. and Smith D.I. (1982) Weathering of the balustrade on St. Paul's Cathedral, *Earth Surface Processes and Landforms* **7** 387-389

Shepherd J.G. (1974) Measurements of the direct deposition of sulphur dioxide onto grass and water by the profile method *Atmospheric Environment* **8** 69-74.

Simpson D., Davies S., Gooriah B.D. and McInnes G. (1987) Pollution levels in the United Kingdom during 14-22 January 1985 *Atmospheric Environment* **21** 2495-2503

Sisterson D.L. and Shannon J.D. (1990) A comparison of urban and suburban precipitation chemistry *Atmospheric Environment* **24B** 389-394

Smith F.B. (1985) Further perspectives on acid rain. Is there proportionality between emissions and depositions? A key question in the acid rain debate. In the Proceedings of the National Society for Clean Air. 52nd Annual Conference. 14th to 17th October 1985, Scarborough.

Smith F.B. and Hunt R.D. (1978) Meteorological aspects of the transport of pollution over long distances *Atmospheric Environment* **12** 461-477

Smith R.A. (1872) *The Beginnings of a Chemical Climatology*, Longman, London

Söderlund R. and Roswell T. (1982) The Natural Environment and Biogeochemical Cycles from *The Handbook of Environmental Chemistry* Edited by Huntzinger O. Volume 1 Part B. Springer-Verleg Berlin

Spicer C.W. (1977) Photochemical atmospheric pollutants derived from nitrogen dioxides *Atmospheric Environment* **11** 1089-1095

Stedman D.H., and Jackson J.O. (1975) The photostationary state in photochemical smog. In the Preoceedings of the Symposium on *Chemical Reaction Kinetics data for the Lower and Upper Atmosphere*, Edited by Benson J. John Wiley. New York

Stevens R.K., Dzubay T.G., Lewis C.W., and Shaw R.W. (1984) Source apportionment methods applied to the determination of the origin of ambient aerosols that affect the visibility in forested areas *Atmospheric Environment* **18** 261-272

Summers P.W., Bowersox Van C. and Stensland G.J. (1986) The geographical distribution and temporal variations of acidic deposition in Eastern North America *Water, Air and Soil Pollution* **31** 523-535

Szepesi D.J. and Fekete K.E. (1987) Background levels of air and precipitation quality for Europe *Atmospheric Environment* **21** 1623-1630

Tombach I (1982) Conservation of Historic Stone Buildings and Monuments (Measurement of local climatological and air pollution factors affecting stone decay) (1982) National Research Council Report 1982. **14** pp 197-207

Thurston G.D. and Spengler J.D. (1985) A quantatitive assessment of source contributions to inhalable particulate matter pollution in Metropolitian Boston *Atmospheric Environment* **19** 9-25

Trudgill S.T., Viles H.A., Cooke R.U., Inkpen R.J. Heathwaite A.L. and Houston J. (1991) Trends in stone weathering and atmospheric pollution at St.Paul's Cathedral, London, 1980-1990 *Atmospheric Environment* **24A** 1991

Van Borm W.A., Adams F.C. and Maenhaut W. (1989) Characterisation of individual particles in the Antwerp aerosol *Atmospheric Environment* **23** 1139-1151

Waldman J.M., Chris Liang S.-K., Lioy P.J., Thurston G.D. and Lippman M. (1991) Measurements of sulphate aerosol and its acidity in the SO_2 source region of Chestnut Ridge, PA. *Atmospheric Environment* **25A** 1327-1333

Walsh (1990) *Global Warming. The Greenpeace Report* Pages 260-295 Edited by Leggett J.

Weather, 1991. Monthly Weather Log published by the *Royal Meteorological Society*

Webb A.H., Bawden R.J, Busby A.K and Hopkins J.N. (1992) Studies on the effects of air pollution on limestone degradation in Great Britain *Atmospheric Environment* **26B** 165-181

Weisweiler W.K. and Schwarz B.U. (1990) Nature of ammonium containing particles in an urban site in Germany *Atmospheric Environment* **24B** 107-114

Wesley M.L., Hicks B.B., Dannevik W.P., Frisella S. and Husar R.B.(1977) An eddy-correlation measurement of particulate deposition from the atmosphere *Atmospheric Environment* **11** 561-563.

Willison M.J., Clarke A.G. and Zeki E.M. (1985) Seasonal variations in atmospheric aerosol concentration at urban and rural sites in Northern England *Atmospheric Environment* **19** 1081-1089.

Yaaqub R.R., Davies T.D., Jickells T.D. and Miller J.M. (1991) Trace elements in daily collected aerosols at a site in Southeast England *Atmospheric Environment* **25A** 985-996

Zemba S.G., Golomb D. and Fay J.A. (1988) Wet sulphate and nitrate deposition patterns in Eastern North America *Atmospheric Environment* **22** 2751-2761

Appendix A

Errors in the determination of metal concentration.

The recovery values for samples collected during June 1991 at Wells (presented in Table 4.10) indicate that typically 10% of each metal, with the exception of lead, was not removed in the extraction process. This represents a systematic error in the method. The standard deviation (4%) associated with these values can be considered as the random error. Assuming a constant air volume through the filter, this combination of systematic and random errors provides an estimate of 14% as the total error for atmospheric mass concentrations.

Appendix B

Artifact sulphate and nitrate formation on atmospheric particulate filters

Artifact sulphate and nitrate will form on filter media when there is an interaction between the respective precursor gases and the filter. Artifact sulphate will arise from the passage of SO_2 (Coutant, 1977 and Appel *et al.*, 1984) or H_2SO_4 (Klockow *et al.*, 1979) through the filter. Nitrate will form from HNO_3 (Appel *et al.*, 1984). Nitrogen dioxide will produce negligible nitrate formation (Spicer and Schumacher, 1979).

Coutant (1977) demonstrated sulphate formation was dependent mainly on filter pH, sampling time and relative humidity. The role played by filter pH was shown by Appel *et al.* (1984). Significant artifact sulphate formation (10 to 20%) was found to occur on a selection of glass fibre filters with high pH values (9.9 to 10.1). However, as the pH of the GFA and GMW 810 filter papers in this study were determined as 7.2 and 8.0, respectively, lesser amounts of artifact sulphate were probably formed. Accurate determination of the extent of artifact formation would require parallel sampling with a non reactive filter medium, such as Teflon.

References

Appel B.R., Towika Y, Haik M. and Kothny E.L. (1984) Artifact particulate sulphate and nitrate formation on filter media *Atmospheric Environment* **18** 409-416

Coutant R.W. (1977) The effect of environment variables on collection of atmospheric particulate matter *Environmental Science and Technology* **11** 874-878

Klockow D., Jablonski B. and Nießner R. (1979) Possible artifacts in the filter sampling of atmospheric sulphuric acid and acidic sulphates *Atmospheric Environment* **13** 1665-1676

Spicer C.W. and Schumacher P.M. (1979) Particulate nitrate: Laboratory and field studies of major sampling interferences *Atmospheric Environment* **13** 543-552